FLOW PATTERN-BASED TRANSPORT PROCESSES OF GAS-NON-NEWTONIAN FLOW IN HELICAL COIL

ANIL KUMAR THANDLAM

FLOW PATTERN-BASED TRANSPORT PROCESSES OF GAS-NON-NEWTONIAN FLOW IN HELICAL COIL

THESIS

Submitted in Partial Fulfillment of the Requirements for the Degree of

Doctor of Philosophy
in
Engineering
by

Anil Kumar Thandlam

Roll No.: 10610718

Under the supervision of

Dr. Subrata Kumar Majumder

And

Dr. Tapas Kumar Mandal

DEPARTMENT OF CHEMICAL ENGINEERING

INDIAN INSTITUTE OF TECHNOLOGY GUWAHATI

GUWAHATI-781039, INDIA

May, 2015

Dedicated to my family

INDIAN INSTITUTE OF TECHNOLOGY GUWAHATI
GUWAHATI - 781039, ASSAM, INDIA

DEPARTMENT OF CHEMICAL ENGINEERING

CERTIFICATE

This is to certify that the thesis entitled "***Flow Pattern-Based Transport Processes of Gas-Non-Newtonian Flow in Helical Coil***" submitted by **Anil Kumar Thandlam** in fulfillment of the requirement of the *Degree of Doctor of Philosophy in Engineering*, is a record of bonafide research work carried out by him, in the Department of Chemical Engineering, Indian Institute of Technology, Guwahati, under my guidance and supervision. The work documented in this thesis has not been submitted to any other University or Institute for the award of any degree or diploma. In my opinion, the thesis has reached the standard fulfilling the requirements of the Ph. D. degree as prescribed in the regulations of this institute.

Dr. Subrata Kumar Majumder
Associate Professor
Department of chemical Engineering
Indian institute of Technology Guwahati
Guwahati-781039, India.

Dr. Tapas Kumar Mandal
Associate Professor
Department of chemical Engineering
Indian institute of Technology Guwahati
Guwahati-781039, India.

ACKNOWLEDGEMENTS

I would like to express my gratitude to all those who helped me in different ways in completing this research work within the time span of four years, directly or indirectly. First and foremost, I would like to express my deep felt gratitude to my supervisor, **Dr. Subrata Kumar Majumder and Dr. Tapas Kumar Mandal** for providing me continuous inspiration and guidance throughout the entire course of work. In addition, their philosophical guidance has built up a momentum inside me. Their uncompromising approach to complete the experimental part, data analysis, writing manuscripts as well as thesis within the stipulated time period helped me a lot in completing my research work. The numerous brain storming sessions during the project meetings with him were very useful in enriching my analytical power. I also remain indebted for their understanding, support and caring during the times when I was really down and depressed due to personal problems. I also thank almighty for making me to feel fortunate to work under their great stewardship.

I wish to acknowledge my respectful thanks to **Dr. V.S. Mohalkar**, former HOD and **Prof. Bishnupada Mandal** present HOD, Department of Chemical Engineering, for extending all the necessary facilities for carrying out my research work. I am also grateful to all the professors in the department for their sincere cooperation.

I must also thank my doctoral committee members **Prof. G. Pugazhenthi, Prof. Pallab Ghosh** of the Department of Chemical Engineering and **Dr. Chandramohan Somayaji** of the Department of Mechanical Engineering, for their valuable suggestions and contribution towards my research work.

I wish to thank all the non-teaching staff of our department for the help received from them.

I would like to thank my co-researchers and friends Mr. Sivaiah (Late), Mr. Rajeev Parmar, Mr. Bharath Kumar, Mr. Fahad M.K, Mr. Chiranjib Das, Mr. Venkatesh Rao, Mr. Arindam and Mr. Medithi Vikas for their enormous help and support during research work. I am thankful to all my departmental friends, seniors and juniors for their support and good wishes.

I would also like to thank my family who have not only supported me in the completion of my Ph.D. but also have stood by me throughout my life. They have patiently supported me at all instances in my research work.

I am indebted to my wife Lalasa whose constant encouragement, suggestion, patience and motivation, made me to achieve this endeavor in a peaceful and cheerful manner. She transformed all the odds into reality.

Date: 04th May, 2015

Place: IIT Guwahati

Anil Kumar Thandlam

CURRICULUM VITAE

Name	**ANIL KUMAR THANDLAM**
Date of birth	**06-02-1984**

Education Qualifications:

Degree	*University/Institute*	*Year of Passing*
Bachelor of Engineering in Chemical Engineering	Arulmigu Meenakshi Amman College of Engineering, Kanchipuram	2006
Master of Technology in Computer Aided Chemical Engineering	Andhra University, Visakhapatnam	2008
Research Scholar in Chemical Engineering	Indian Institute of Technology, Guwahati	2016

A. Research Papers in Journal:

- Thandlam A.K., Raju. G.M.J., Sarma, G.V.S., Ramesh, K.V., 2009. Mass transfer at the confining wall of helically coiled circular tubes with gas–liquid flow and fluidized beds. Chem. Eng. J. 153, 114–119.
- Thandlam A. K., Mandal, T.K., Majumder, S.K., 2014. Frictional pressure drop in vertical coil reactor (HCR) based on flow regime. J. Eng. Appl. Sci. 9 (4), 97-101.
- Thandlam A.K., Mandal, T.K., Majumder, S.K., 2015. Flow pattern transition, frictional pressure drop, and holdup of gas non-Newtonian fluid flow in helical tube. Asia-Pacific J. Chem. Eng. 10, 422-437.

- Thandlam, A.K., Tyouharia, A and Majumder, S.K., 2016. Frictional Pressure Drop of Gas-liquid-solid Mixture in Helical Coil, Elixir Chem. Engg. 92, 38927-38932.

B. Manuscript under review

- Thandlam. A.K., Majumder S.K. and Mandal T.K. Dynamic interaction model to analyse hydrodynamics of gas-non-Newtonian-liquid plug and slug flow in vertical helical coil pipe (VHCP). Int. J. fluid Mech. Res. (Manuscript No. FMR-13627), (under review)
- Thandlam A.K., Mandal, T.K., Majumder, S.K., Flow Pattern based Degree of Mixing and Mass Transfer in Helical Coil Reactor (HCR). Asia-Pacific J. Chem. Eng. (under review).
- Thandlam, A.K., Mandal, T.K., Majumder, S.K., Flow Pattern-based Mass Transfer and Frictional Drag of Gas-Non-Newtonian Liquid Flow in Helical Coil: Two- and Three-phase Systems, Heat mass transfer (Manuscript No. HAMT-D-15-00314), (under review).

C. Research Papers in Conferences:

- Thandlam A. K., Mandal, T.K., Majumder, S.K., Experimental investigation of flow patterns and pressure drop for air-water two phase flow in vertical helical circular tube, Proceedings of International Conference on Chemical and Bioprocess Engineering-INDIA (ICCBPE-IN, 2013), November 16-17, 2013, NIT Warangal, A.P. India Page 22.

ABSTRACT

Helical coiled tubing service is one of the fastest growing technology in chemical, petrochemical, food and pharmaceutical industries. The devices of various unit operations and unit processes can be made compact using helical coiled tubes. The helical coils also improve the performance of equipment like heat exchangers, coil steam generators, boilers, evaporators, reverse osmosis units, nuclear reactors, etc. due to its inherent secondary flow generation capability. Curvature of the helical coils helps in generating the centrifugal forces acting at right angles to the main flow, resulting secondary flow occurred in planes perpendicular to the curved central axis of pipe. In a coiled tube there was a pressure gradient across the tube to balance the centrifugal force on the fluid due to its curved path. Secondary flow increases the turbulence leading to greater heat and mass transfer coefficients. The behavior of two-phase gas-liquid flow through curved tubes was practically much more complex than single phase flow. In two-phase flow through curved tubes, the heavier phase, which is accountable to a larger centrifugal force, moves away from the center of curvature, whereas the lighter phase flows toward the center of the curvature.

Based on the present status of research, this work was undertaken with the following objectives:

(i) Study the flow pattern and its map in helical coil. Model to predict the flow pattern transitions.

(ii) Study the two-phase frictional pressure drop in helical coil. Development of mechanistic model based on the plug/slug formation, drag at interface and wettability effect of the Newtonian and non-Newtonian fluids.

(iii) Study the flow pattern-based dispersion characteristic of two-phase flow in vertical helical coil. Development of model to interpret the flow pattern-based dispersion coefficient.

(iv) Study the convective heat transfer of two-phase gas-non-Newtonian flow in vertical helical coil. Development of correlation to interpret the heat transfer performance in the helical coil.

(v) Study the flow pattern-based confined liquid-wall mass transfer in gas-non-Newtonian liquid flow condition in helical coil. Development of a flow pattern-based correlation for mass transfer coefficient.

In the present study, experiments have conducted to study the hydrodynamics of air-non-Newtonian flow (Sodium Carboxy Methyl Cellulose) in vertically helical coil. Three different flow patterns namely plug flow, slug flow and stratified flow were observed from the experimental study. The plug flow appeared with the higher liquid Reynolds number and with lower gas Reynolds number. With further increasing of gas flow rate, plugs were converted to slug flow as the length of gas bubble becomes equal or more than the tube diameter. Similarly the stratified flow observed with lower liquid Reynolds number and higher gas Reynolds number. Interestingly, stratified flow in case of non- Newtonian fluid (SCMC solution) occupies a larger domain of the flow pattern map compare to the Newtonian fluid. With increasing coil diameter plug and stratified flow domain was changed but there was no change in slug flow. For a small change in pitch difference, plug flow was resulted without any change in slug and stratified flow. It was noticed that the plug, slug and stratified pattern transitions shifted by changing of liquid concentrations at a particular geometrical variable. Correlations for flow pattern transitions were developed for two-phase air-non-Newtonian liquid in vertically helical coil. Probabilistic neural network (PNN) was

successfully developed for two-phase helical coil system to predict the flow patterns and their transition boundaries.

Extensive experimental studies have been carried out to investigate the effect of gas holdup and pressure drop characteristics of two-phase air-non-Newtonian flow in helical coil. The two-phase pressure drop increases with the increase in ratio of the tube to coil diameter. There was no change in two-phase pressure drop when increasing pitch difference. If coil diameter was increased the two-phase friction factor decreases. The friction factor decreases with the increase in wettability. A mechanistic model was developed to interpret the flow pattern based frictional pressure drop based on energy balance. Increasing liquid velocity, coil diameter and pitch difference at a particular gas velocity, the gas holdup was decreased. Both gas holdup and frictional pressure drop depend on the liquid concentrations of non-Newtonian liquid and the geometrical variables. Correlation model was proposed for flow pattern based holdup and friction factor of air-non-Newtonian fluids.

Next an attempt was made to investigate the effect of various dynamic and geometrical variables on mixing characteristics in helical coil reactor based on flow pattern. The mixing characteristics were estimated by the residence time distribution method. The effects of various parameters on the dispersion coefficient were enunciated based on the flow patterns of the flow in the helical coil reactor. Base on the experimental data a correlations were proposed to predict the flow pattern-based intensity of mixing by dimensional analysis.

Helical coils are widely used as heat exchangers and have multiple applications in various industries because of their unique properties such as large heat transfer areas, compactness, and promotion of a good mixing of the fluids, resulting enhancement of heat and mass transfer. In this work the heat transfer characteristic of air-water system and air-SCMC (non-Newtonian liquid) system in helical coil has been studied. It was observed thatvwith increasing concentration of SCMC, the heat transfer coefficient in the helical coil system increases significantly. A correlation model was also developed to interpret the heat transfer performance in the helical coil.

Finally an attempt has been made to investigate the flow pattern-based mass transfer and drag phenomena of two-phase (gas-liquid) and three-phase (gas-liquid-solid) flow influencing the mass transfer phenomena in vertical helically coiled tube with various geometrical conditions. The effects of various parameters on the mass transfer coefficient were enunciated based on the flow patterns of the flow in the helical coil reactor. The mass transfer coefficient was estimated using limiting current technique. Mass transfer coefficient has strongly influenced by gas holdup. With non-Newtonian fluid the mass transfer coefficient decreases with increasing the liquid viscosity (SCMC concentration). For a given set of conditions the rate of mass transfer coefficient in helical coil decreases with increasing pitch length. In three-phase flow system mass transfer increases with decreasing the particle diameter. It was observed that the mass transfer coefficient increases with decreasing tube diameter and coil diameter. Variations in mass transfer with gas and liquid flow rate were related to flow patterns. Plug flow results the lower mass transfer coefficient compared to stratified flow. Slug flow results in mass transfer rates fairly independent of gas superficial velocity. Correlations were developed for mass transfer coefficient based on flow patterns. The correlation was based on the law of the wall similarity which can be expressed by the Colburn J-factor. A correlation has also been developed to relate the dispersion coefficient and the mass transfer coefficient.

CONTENTS

Page No.

LIST OF FIGURES

Chapter-4

Chapter-5

Chapter-6

LIST OF TABLES

CHAPTER-1

BACKGROUND AND FORMULATION OF RESEARCH

In this chapter, an introduction to helical coil and its applications in different fields of engineering are enunciated. The scope and significance of research in the field are explained. The research formulation and its significance based on scope is highlighted.

1.1 Introduction

Helical coiled tubing service is one of the fastest growing technology in oilfield industries, compact heat exchangers, chemical industries, petroleum industries, food industries and pharmaceuticals. They are of great importance to the chemical engineering process because of their unique properties such as large heat transfer areas, they are compact, and above all, their geometry promotes a good mixing of the fluids, which results in increase in the heat and mass transfer coefficients. Helical coils consist of the curved surfaces in which the curvature helps in generating the centrifugal forces acting at right angle to the main flow resulting secondary flow occurred in planes perpendicular to the curved central axis of pipe. In a coiled tube there must be a pressure gradient across the pipe to balance the centrifugal force on the fluid due to its curved path and the pressure being highest at the outer wall side of the tube and least at the inner wall of the tube. Therefore a secondary flow occurs in which the fluid near the top and bottom walls of the pipe moves inside near the centre of curvature of the central axis and the fluid near the central plane moves outside. Secondary flow produces the vortices to increase the turbulence leading to greater heat and mass transfer coefficients. The flow through curved tubes is commonly occurred in human body in blood flow system and industrial piping network. The helical coiled tubes in chemical and allied industries are used in compact heat exchangers, coil steam generators, boilers, evaporators, reverse osmosis units, nuclear reactors, fluid mixing units and waste heat recovery units, in power production units, cooling systems of electric generators etc. One of the main important applications is phase separators in petroleum industries. In case of two-phase flow in helical coil, the heavier density phase is subjected to a larger centrifugal force and this force causes the liquid to move away from the centre of the curvature. This has many important applications in petroleum industry, such as sand is often carried from oil wells in adding to oil-water mixtures and natural gas streams. Most of the reported studies in coiled flow were aimed at estimating pressure drop and friction factor. A comprehensive review of these studies was provided by Ali (2001). However, studies on using helically coiled tubes for hydrodynamics, residence time distribution (RTD), heat and mass transfer with non-Newtonian fluids are sparse. Hence there is a scope to investigate the effects of various dynamic and geometric variables on hydrodynamics, RTD, heat and mass transfer with non-Newtonian fluids in multi-phase flow system in helically coiled tubes.

1.2 Curved coils (or) Tubes

The helically coiled tube is one of the different types of smooth space curve. There are five different types of curved tubes such as: (a) helical coil, (b) bend tube, (c) serpentine tube, (d) Spiral tube, (e) Twisted tubes. Schematic diagrams of different types of curved tubes are shown in Figure 1.1. The different components of a helical coil are shown in Figure 1.2. The main difference between the flows through a helical coil with respect to the flow through a straight pipe is the presence of secondary flows resulting from the imbalance between centrifugal force, directed to the outward, and pressure force, acts on the fluid. The secondary flow consists of counter-rotating structures. The secondary flows in the curved ducts are usually called as Dean vortices.

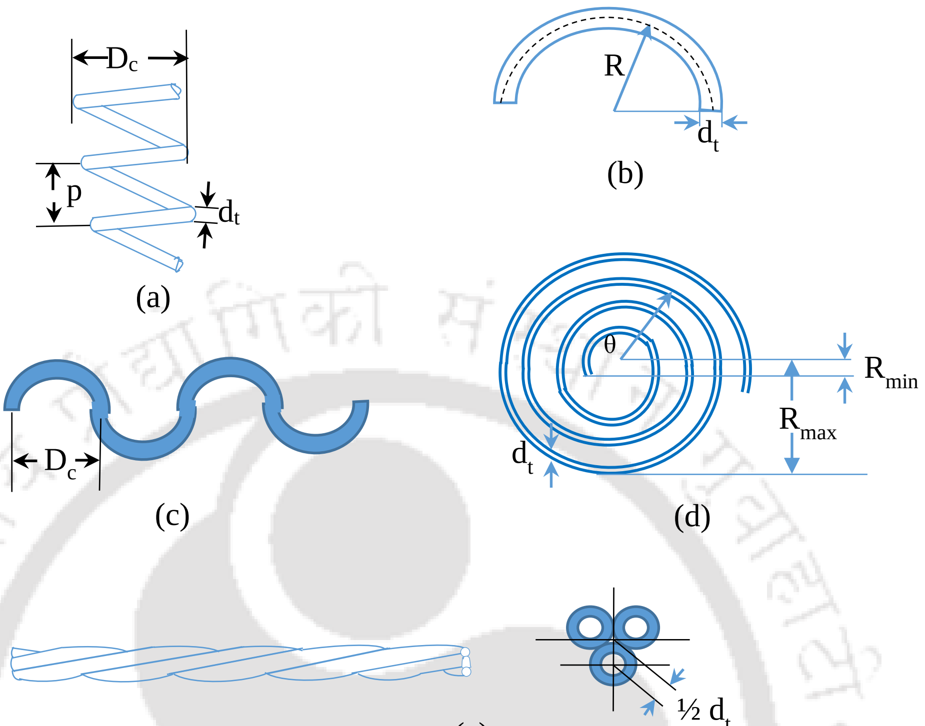

Figure 1.1: Different types of coiled tube geometry. (a) helical coil, (b) bend tube, (c) serpentine tube, (d) spiral tube and (e) twisted tubes

In helical coil the generation of secondary flow due to unstable centrifugal forces enhances cross sectional mixing to improve heat and mass-transfer coefficient. The secondary flow in a circular cross-section, the axial velocity contours of the secondary flow in a circulated cross section is shown in Figure 1.3. The secondary flow pattern consists of two vortices perpendicular to the axial flow direction. Vashisth et al. (2008) showed the secondary flow pattern in helical coil as shown in Figure 1.4. The working principle of helical coil and reasons for its advantage over straight tube is well described by Vashisth et al. (2008). The advantages are: (a) generation of secondary flow due to unbalanced centrifugal forces, (b) enhanced cross-sectional mixing, (c) reduction in axial dispersion, (d) improved heat-transfer coefficient and (e) improved mass-transfer coefficient.

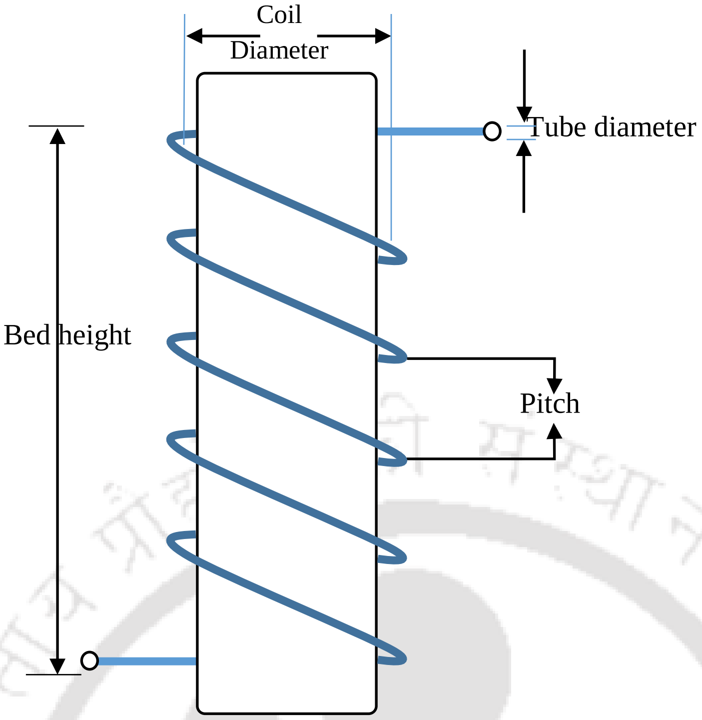

Figure 1.2: Structure of helical coil

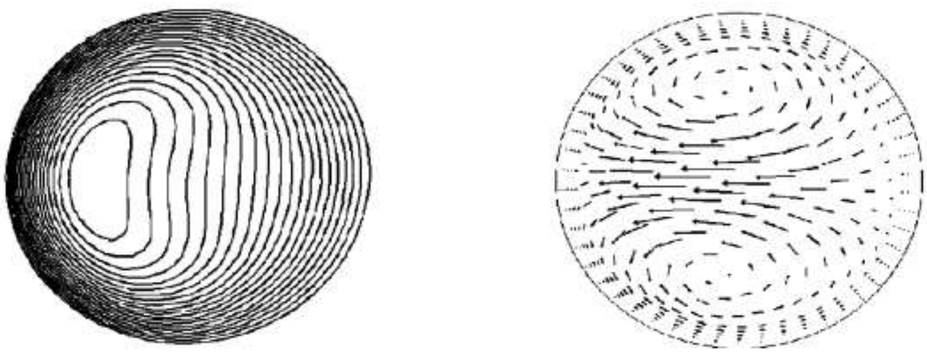

Curved tube of circular cross section Axial velocity contours

Figure 1.3: Velocity streamlines and Dean vortices in curved tube (Vashisth et al., 2008)

The study of fluid flow in helically coiled pipes is important both for engineering applications and scientific interest (Soh and Berger, 1984; Vashisth et al., 2008; Berger et al., 1983). There are many industrial processes require curved ducts to satisfy space and geometric requirements: heat exchangers, chemical reactors, exhaust gas ducts of engines, evaporators, condensers, storage tanks and piping systems.

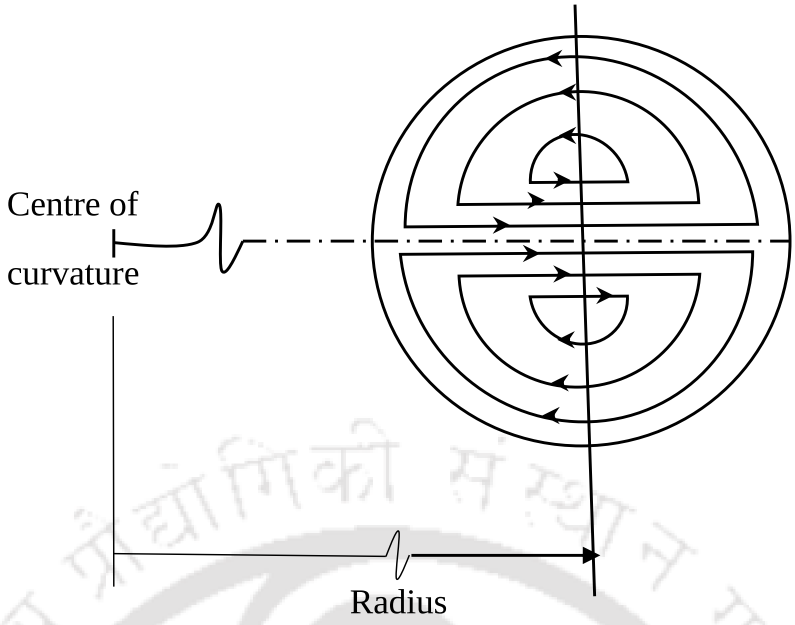

Figure 1.4: Secondary flow pattern

Flow in curved pipes is also important in bioengineering applications. The various applications of helical coil reported in the literature are mentioned as follows:

- Nuclear engineering, polymerisation and cryogenics (Kasturi and Stepanek, 1972).
- Coiled tube reactors could be operated advantageously for diffusion controlled reactions (Stepanek and Kasturi, 1972).
- Advantageous configuration for carrying out chemical reactions (Hewitt and Boure, 1973).
- Curved flow passages can be used to improve mass transfer rates, such as in membrane blood oxygenators, in kidney dialysis devices, and reverse osmosis units (Xin et al., 1997).
- Non-Newtonian fluids in helical coil are often encountered in processing industries such as rayon, plastics, foods, dye-stuffs, and pharmaceuticals (Chhabra and Richardson, 1999).

- Understanding of hydrodynamics of coil flow is also important for the designing of various biomedical appliances such as blood oxygenators, reverse osmosis equipments, etc., and for the comprehension of the nature of cardio- vascular and kidney flows (Vashisth et al., 2008).

- The swirling flow produced by helical ribs has the beneficial effect of forcing the liquid to the tube wall and carrying the vapour to the tube centre. There is, however, very limited information on the conditions under which the desired swirling flow is obtained (Weisman et al., 1994).

- Cross-sectional mixing of fluid elements takes place which results in the increased heat and mass transfer coefficients and thus makes curved conduits useful for heat exchangers and diffusion equipment (Vashisth et al., 2008)

- Frictional losses in the fluid stream are enhanced. Though this increase in pressure drop is disadvantageous in requiring larger power for maintaining flow rate in other applications of curved channel geometries, this effect makes coiled capillary tubes useful for the precision viscometry of gases, as the increased pressure drop can be measured accurately (Ali, 2001).

- The axial dispersion of the solute particles in the flow decreases. This gives rise to better RTD distribution for coils as chemical reactors (Ali and Zaidi, 1980)

- Curved pipe flows are of importance in the research of biological fluid mechanics and the chemical transport process (Mujawar and Rao, 1978)

- The coil is a suitable device for boiling in the absence of gravity (Ali et al., 1968)

- It also has attractive features as a chemical reactor where large volumes of vapour react with a liquid accompanied by a high heat of reaction, such as chlorination reactions (Ali et al., 1968).

- It provides efficient contact and excellent heat transfer in coil tube heat exchanger (Ali et al., 1968)

1.3 Hydrodynamics in helical coil

The study of fluids in motion and different forces affecting the movement of fluids is called hydrodynamics. It refers how energy and forces interact with fluids, including gas and liquids. The hydrodynamic studies are: Pressure drop, holdup, flow pattern and its map, etc. The brief description of some hydrodynamic characteristics are given below.

1.3.1 Flow Pattern

Different types of flow patterns are observed in helically coiled tube which are described as follows:

Bubbly flow: Typically occurring at very high liquid velocities and low gas velocities, this flow regime is characterized by the presence of fast rising bubbles with a diameter equal to or less than the capillary diameter. The bubbles are often spherical or spherical-like in shape.

Taylor flow regime: Also known as the slug flow regime. Taylor flow consists of gas bubbles with lengths greater than the tube diameter that move along the capillary separated from each other by liquid slugs. Depending on the gas and liquid flow rates and properties, the bubbles often have hemispherical-like tops and bottoms.

Slug flow: This is a transition regime that occurs between bubbly and Taylor flows. Like in Taylor flow, bubble slugs, separated from one another by liquid slugs. However, in the slug-bubbly regime, small bubbles are present in the liquid slugs, something not observed for Taylor flow. The transition from Taylor flow to slug-bubbly flow occurs by increasing the liquid flow rate.

Churn flow regime: Churn flow occurs at very high gas velocities. It consists of very long gas bubbles and relatively small liquid slugs. Due to the high gas velocity, a wave or ripple motion is often observed at the bubble tail. Further increase in gas flow rate results in annular flow.

Annular flow: At excessively high gas velocities and very low liquid velocities, annular flow results. In this case a continuous gas phase is present in the central core of the capillary with the liquid phase which is displaced to form an annulus between the capillary wall and the gas phase.

Dispersed flow: Dispersed flow is characterized by the flow where one phase is dispersed in the other continuous phase. This flow configuration is observed in all types (gas-liquid, gas-solid, liquid-liquid and liquid-solid)

There are various methods are available to identify the regime transition. However following two methods are widely used in case of helically coiled system.:

Visual observation: Traditionally, flow regimes have been defined according to visual observations performed by viewing the flow through transparent pipe/tube. The majority of all the reported data in literature have been obtained in this manner. Although visual observation provides some information on the flow patterns, it is often difficult to identify the flow regime transitions without quantitative measurements, even in transparent pipe/tube, due to the relatively opaque nature of multiphase flow. At very high phase velocity due to intense in interaction of the phases, it is difficult to pinpoint the exact transition velocity by visual observation. It is admitted, however, that ambiguities regarding the exact nature of flow patterns may exist in the interpretation of such visual observations. In this connection, still pictures by high speed photography can be employed as a useful aid. Even though such pictures may give a clear view of flow at a certain moment of time. The interpretation regarding the flow regime may be arbitrary or somewhat subjective, depending on the observer. The difficulty of obtaining a clear view of the central parts of the flow cross section by high speed photography is due to the light diffraction at all gas-liquid interfaces which, in some cases, would make the clear observations limited to only a layer of the mixture near the pipe/tube walls. However, in spite of the limitation, the direct visual observation approach has been used for its simplicity and inexpensiveness. It certainly has its everlasting merit as the best tool for simple experiments.

Evolution of global hydrodynamic parameter: The global hydrodynamic parameter (pressure drop and holdup) displays the prevailing flow patterns varying with the regimes. This fact has generally been utilized to identify flow regime transition point. Typically, the global hydrodynamics have been quantified based on overall gas holdup (it is defined as the percentage by volume of the gas in the two or three phase mixture in the system). The overall gas holdup increases with an increase in superficial gas velocity (the velocity of fluid moving through a tube, defined as the volumetric flow rate of that fluid divided by the cross-sectional area of the tube) linearly ($\varepsilon_g \propto u_{sg}^{0.8-1}$) at low gas velocity but due to an intense nonlinear interaction of phases at high gas velocities, the relationship between overall gas holdup and superficial gas velocity deviates from linearity and it obeys $\varepsilon_g \propto u_{sg}^{0.4-0.6}$. Hence, the change in slope of the gas holdup curve can be identified as a regime transition point. Sometimes, gas holdup shows an S-shaped curve, depending upon operating and design conditions (Shaikh and Dahhan, 2005) in two-phase flow system. In such cases, the superficial gas velocity at which maximum gas holdup attained is identified as the transition velocity. However, when the change in slope is gradual or the gas holdup curve does not show a maximum in gas holdup, it is difficult to identify the transition point. In such cases, the Zuber and Findlay (1965) drift flux method can be used extensively. They argued that gas holdup in two-phase flow depends on two phenomena: the gas rises locally relative to liquid due to phase density differences, and the gas holdup and velocity distribution across the diameter causes gas to concentrate in a faster or slower region of flow, thereby affecting the average gas holdup and flow pattern. The following drift-flux model of Zuber and Findlay (1965) is applicable to describe the flow regime criteria:

$$u_{sg} / \varepsilon_g = C_o (u_{sg} + u_{sl}) - V_d \tag{1.1}$$

C_0 is a distribution parameter and is a measure of the interaction of the holdup and velocity distribution according to flow pattern. The detailed literature on flow patterns is given in chapter 2.

1.3.2 Pressure drop

The concept of pressure is central to understanding how fluids behave within themselves and also how fluids interact with surfaces. The pressure drop in the straight tube is less than the coils for small Reynolds numbers, but at higher flow rates coils have lesser resistance to flow than straight tubes. This is probably due to the effect of flow pattern change in the presence of secondary flow in coils. (Ali and Zaidl, 1979). To calculate the two-phase pressure drop and holdup in a coiled tube, the most widely used correlations are based on Lockhart-Martinelli (L-M) parameters (Lockhart–Martinelli parameters for liquid and gas, ϕ_{sl}, ϕ_{sg} are defined as: $\phi_l^2 = \Delta P_{f,tp} / \Delta P_{f,l}$, $\phi_g^2 = \Delta P_{f,tp} / \Delta P_{f,g}$ where ΔP_{tp} is the two-phase frictional pressure drop (N/m^2), $\Delta P_{f,g}$ is the single gas phase frictional pressure drop (N/m^2) and $\Delta P_{f,l}$ is the single liquid phase frictional pressure drop (N/m^2)). Most of the researchers used the Lockhart-Martinelli (L-M) method to correlate their experimental data on two-phase frictional pressure drop and holdup while others modified the Lockhart-Martinelli parameters to fit their experimental data. A summary of correlations and related parameters observed from the literature is shown in Table 3.1 described in chapter 3.

A comprehensive review of pressure drop studies for flow through helical coils has been made by Ali (2001). By denoting the friction factors for straight tube as f_s and coiled tubes as f_c, the ratio f_c/f_s have been defined. This friction factor ratio is called as coiling effect factor, *C*. Most of the correlations for laminar flow through the helically coiled tubes were made based on f_c/f_s. For turbulent flow, f_c and curvature ratio, $\lambda = d_t/D_c$ were used. Most correlations employed Dean Number (*De*) as characterizing dimensionless group. De is the product of Reynolds number (*Re*) and square root of curvature ratio, λ.

$$De = \mathrm{Re}\sqrt{d_t / D_e} \tag{1.2}$$

The flow in helical pipe is controlled by three parameters: *Re*, *De* and *Tn*. *Tn* is called Torsion number which is defined as 2τ Re. τ is called as torsion defined as.

$$\tau = \frac{p}{R^2 + p^2} \tag{1.3}$$

where p is a pitch (space between coils) and R is a coil radius. Some investigations accounted for pitch effect by defining helical number (*He*)

$$He = \mathrm{Re}\left[\frac{d_t / D_e}{1 + (p / \pi D_e)^2}\right] \tag{1.4}$$

where De is equivalent coil diameter, which is expressed as

$$D_{eq} = \sqrt{\frac{p^2 + (\pi / D_c)^2}{\pi}} = \frac{L_c}{n\pi} \tag{1.5}$$

1.3.3 Void fraction (or) holdup of phase

The void fraction of phase is the fraction of the channel volume that is occupied by the phase. It is one of the main parameter to describe the hydrodynamics in multiphase flows. The gas holdup is generally estimated by the following methods:

Phase Isolation method: Phase isolation method is the easiest method to measure the gas holdup. The holdup at different flow rates is measured by quick closing valve technique in a helically coiled tube. The quick-closing valves regulate simultaneous closing of the two valves to trap the flowing mixture instantaneously. Once the system reaches steady state at particular flow rate of two fluids, the flowing mixture is arrested by closing valves in the test section instantaneously. The liquid amount after isolation is used to calculate the gas holdup as per the following equation:

$$\varepsilon_g = \frac{v_T - v_L}{v_T} \tag{1.6}$$

where, ε_g is the gas holdup, V_L is the volume of water, V_T is the total volume of fluid mixture.

Electrical conductivity method: The gas holdup can also be calculated by measuring the electrical conductivity of the liquid. The gas holdup can be related to the conductivity of liquid gas mixture and conductivity of liquids as (Maxwell, 1892)

$$\varepsilon_g = 2\left(\frac{E_L - E_m}{2E_L - E_m}\right) \tag{1.7}$$

where E_L and E_m are the electrical conductivities of liquid and gas-liquid mixture. The electrical conductivity can be measured by two grid electrodes covering the cross section of the column. The detail of the literature on pressure drop and holdup is given in chapter 3.

1.3.4 Mixing characteristics in helical coil

In most of the process industries, mixing is an important and a common operation because it is the homogeneousness of desired degree to increase the heat and mass transfer for the system which enduring chemical change. Compared to straight tubes, tubes with bends provide advantages of compactness, higher heat and mass transfer coefficients and reduced axial dispersion due to intense mixing of the phases. Dispersion theory is concerned with the dispersion of a solute in a flowing liquid due to the combined action of a non-uniform velocity profile and molecular diffusion. Additional complexities arise when flow instabilities are introduced using Dean Vortices, where lateral mixing due to molecular diffusion is augmented by the convective secondary motion. Many studies aimed at providing an efficient method of mixing by reducing axial dispersion in coiled tubes (Koutsky and Adler 1964; Saxena and Nigam; 1979; Saxena and Nigam 1981; Saxena and Nigam, 1983). Leclerc et al. (1987) reported an almost curvature independent change in dispersion in coiled tubes of different curvature ratios. They found that dispersion increases as $(N_{Re}/N_{Re,c})^{2/3}NSc$ at low fluid velocities and decreases as $(N_{Re,c}^{1/6}/(NRe/NRe,c)^{4/5}N_{Sc}^{0.08})$ at higher velocities. The helical coils have been used for measuring diffusion coefficients assuming that coiling does not influence dispersion at low values of the Dean number, a point which needs experimental verification (Trivedi and Vasudeva, 1975). The centrifugal force on fluid elements moving with different axial velocities in a curved tube results in secondary flow in the plane of tube cross-section. This secondary flow field directs to the increased pressure drop, higher heat and mass transfer coefficients and narrowed residence time distributions (RTD) (Trivedi and Vasudeva, 1975). The details of the literature on mixing characteristics is given in chapter 4.

1.3.5 Heat transfer in helical coil

Helical coils are extensively used in compact heat exchangers, heat exchanger networks, heating or cooling coils in the piping systems, intake in aircrafts, fluid amplifiers, coil steam generators, refrigerators, nuclear reactors, thermosyphons, other heat transfer equipment involving phase change, chemical plants as well as in food and drug industries. One of the main advantage in the use of helical coiled tubes as chemical reactors or heat exchangers lies in the fact that considerable length of tubing may be contained in a space saving configuration, which can easily be placed in a temperature- controlled environment. The heat transfer enhancement is facilitated in coiled tube heat exchangers without undue increase in pressure drop (Ali et al., 1968). Rajasekharan et al. (1970) reported that heat transfer coefficient for non-Newtonian fluids in coiled pipes compared to straight tube were higher due to the curvature ratio and flow behaviour index. Sethumadhavan and Rao (1983) presented the experimental investigations of heat transfer in a helical-wire-coil inserted tubes and concluded that thermal performance of the helical tubes is significant compared to straight tube. Kozo and Yoshiyuki (1988) studied a theoretical and experimental work which is carried out on the effect of the secondary flow on heat transfer from a uniformly heated helically coiled tube to fully developed laminar flow. In theoretical analysis the centrifugal and buoyancy forces were considered. They reported that the secondary flow effects on heat transfer due to the centrifugal and the buoyant forces. They reported the approximation equation for Nusselt number to represent the heat transfer phenomena as:

$$\frac{Nu}{Nu_0}=1+\left[\left(\frac{Nu_c}{Nu_0}-1\right)^4+\left(\frac{Nu_b}{Nu_0}-1\right)^4\right]^{1/4} \tag{1.8}$$

Acharya et al. (2001) analyzed the phenomenon of steady heat transfer augmentation due to chaotic particle paths in steady, laminar flow through helical coil tubes. Performance of two different coils, one with regular mixing and the other with chaotic mixing were analyzed and compared numerically and experimentally. They reported that the augmentation mechanism is attributed to the breaking of an interior boundary layer and the degree of convective mixing across this layer in the helical coil. Devanahalli et al. (2004) carried out experimental investigation of the natural convection heat transfer from outer wall of the helical coiled tubes. Correlations of outside Nusselt number was made with Rayleigh number using different characteristic lengths. A model to predict the outlet temperature of the fluid flowing through the helically coiled tube has been developed. Numerical and experimental investigations of a tube-in-tube helically coiled heat exchanger have also been carried out by Kumar et al. (2008). The details of the literature about heat transfer is given in chapter 5. The summary of heat transfer in helical coil is shown in Table 5.1.

1.3.6 Mass transfer in helical coil

The coiled tubes are widely used for mass-transfer operations, like membrane separation processes of reverse osmosis, ultra-microfiltration, gas permeation, and chromatography. The mass-transfer improvement is induced by complex hydrodynamic phenomena involving the centrifugal force (Vashisth et al. 2008). The studies on mass transfer in helically coiled tube is very scanty. Hameed and Muhammed (2003) experimentally determined the mass-transfer coefficients for thin films of liquid falling in case of straight and coiled tubes for the absorption of carbondioxide (CO_2) into liquid films of distilled water, ethyl alcohol (96.25%), or ethylene glycol of 12 or 5.2%. They reported a higher mass-transfer coefficient in the helical liquid film. Sujatha et al. (2003) also reported higher mass transfer coefficient in the presence of spiral coil promoters in batch fluidized beds. They found that the mass transfer coefficient increased with increasing flow rate and particle diameter, but increasing pitch of the coil has decreased the mass transfer coefficient. With increase in solids fraction ($1-\varepsilon_s$) up to 20%, mass transfer coefficient is increased and remain nearly constant. It was improved up to 16-fold over the smooth tube coefficient. The detailed study of the ammonia-water vapour rectification process in absorption systems using a helical coil rectifier was carried out by Seara et al. (2003). They showed that the vapour mass transfer coefficient has the most significant effect on the rectifier length (number of turns); while the other heat and mass transfer coefficients have no substantial effect. Thandlam et al. (2009) did an experiment on mass transfer coefficient in helically circular tube and they observed about 10% improvement in mass transfer coefficient in helical coils in the presence of fluidizing solids in comparison with homogeneous flow. In case of two-phase flow, the mass transfer coefficient is found to be double in comparison with homogeneous flow through coils, when the gas velocity is 0.5 m/s. They also reported that the mass transfer coefficient is found to be independent of p/D_c ratio in two-phase flow system. Kumar et al. (2011) did an experiment of helically coiled circular tube for mass transfer coefficient in packed bed. Similarly they did those experiments in empty coils. They found mass transfer coefficient 2 to 2.5 times in helical coils in comparison with straight tube. The more details of literature on mass transfer in helical coil is given in chapter 6.

1.4 Scope of work

From the literature it is very clear that still there is a large gap in various areas of helical coils. The effect of operating variables on gas holdup is limited to non-Newtonian fluids. Studies on variation of holdup and flow regimes in different geometries of helical coils are not available in literature. Researches on mixing are not remarkable till now. There is also lack of research on mass transfer mechanism and the parameter affecting the mass transfer coefficient. Based on the background, the scope of the work in helical coils are pointed as:

(i) Study the flow pattern and its map in helical coil. Model to predict the flow pattern transitions.

(ii) Study the two-phase frictional pressure drop in helical coil. Development of mechanistic model based on the plug/slug formation, drag at interface and wettability effect of the Newtonian and non-Newtonian fluids.

(iii) Study the holdup characteristics of fluid flow in helical coil system.

(iv) Study the flow pattern-based dispersion characteristic of two-phase flow in vertical helical coil. Development of model to interpret the flow pattern-based dispersion coefficient.

(v) Study the convective heat transfer of two-phase gas-non-Newtonian flow in vertical helical coil. Development of correlation to interpret the heat transfer performance in the helical coil.

(vi) Study the flow pattern-based confined liquid-wall mass transfer in gas-non-Newtonian liquid flow condition in helical coil. Development of a flow pattern-based correlation for mass transfer coefficient.

1.5 Formulation and outline of the work

Based on various scopes of studies, the following research work were formulated for the present study:

1. Flow pattern and its transition of gas-non-Newtonian two-phase flow in vertical helical coil tube. The work is described in chapter 2.
2. Gas holdup and frictional pressure drop characteristics of gas-non-Newtonian two-phase flow in vertical helical coil tube. The work is described in chapter 3.
3. Mixing characteristics of gas-non-Newtonian two-phase flow in vertical helical coil tube. The work is described in chapter 4.
4. Heat transfer characteristics of gas-non-Newtonian two-phase flow in vertical helical coil tube. The work is described in chapter 5.
5. Convective mass transfer characteristics of gas-non-Newtonian two-phase flow in vertical helical coil tube. The work is described in chapter 6.

1.6 Significance of formulated research work

Now-a-days, helical coil is hence gaining importance as a simple intensified and inexpensive means of achieving gas-liquid or gas-liquid-solid reactor. In literature, significant research has been reported to understand the properties of non-Newtonian fluids like thermodynamics, stability, thermal conductivity, thermal diffusively, viscosity and convective heat transfer coefficient. Apart from gas-Newtonian liquid reaction, there are lots of reactions with gas-non-Newtonian liquid which are executed in the chemical and biochemical industries. Literature shows that there are limited works on air-non-Newtonian liquid two-phase flow through helical coils as compared to air-Newtonian fluids. The behaviour of two phase flow in helical system shows a different behaviour than vertical and horizontal systems. Hydrodynamics studies help to understand the flow patterns, flow behaviour holdup and pressure drop of fluid in the helical system. The residence time of gas bubbles in helical system is more than vertical system. Reactions requiring high residence time can be well handle in helical system. The studies helps to understand the residence time distribution of liquid and the dispersion characteristics of system. Heat transfer coefficient is key parameter in design of gas-liquid contactor. Heat transfer characteristics help to optimise the rate of heat input and output to the reactor. A detailed study of heat transfer is required in helical system to understand and quantify the heat transfer for optimization of the operation and minimize the capital cost. From the literature review mass transfer coefficient in helical system is more than the straight tube. In order to achieve a high degree of mass transfer efficiency, all the parameters affecting mass transfer characteristics has to be studied in detailed.

Nomenclature

d_t	Diameter of tube (m)
D_c	Diameter of coil (m)
De	Dean Number $\left(= \mathrm{Re}\sqrt{d_t / D_c}\right)$ (-)
D_{eq}	Equivalent diameter ($L_c/n\pi$) (m)
He	Helical number $\left(= \mathrm{Re}\,[(d_t / D_c)/\{1+(p/\pi D_c)^2\}]^{0.5}\right)$ (-)
N_{NU}	Nusselt number (hd/k) (-)
Nu_b	Nusselt number (hd/k) in case where the buoyancy force alone acts (-)

Nu_c	Nusselt number (hd/k) in case where the centrifugal force alone acts (-)
Nu_o	Nusselt number (hd/k) for Poiseuille flow (an incompressible and Newtonian fluid in laminar flow flowing through a long cylindrical tube of constant cross section) (-)
N_{sc}	Schmidt number ($=\mu/\rho D_m$) (-)
p	Pitch (m)
Re	Reynolds Number ($=d_t U_l \rho/\mu$) (-)
u_{sl}	Superficial liquid velocity ($=Q_l/A$) (m/s)
u_{sg}	Superficial gas velocity ($=Q_g/A$) (m/s)
V_d	Drift flux velocity (m/s)

Greek Letters

ρ	Density (kg/m^3)
λ	Curvature ratio (d_t/D_c)
μ_l	Viscosity of the liquid (kg/m.s)
μ_g	Viscosity of the gas (kg/m.s)
μ_{eff}	Effective viscosity (kg/m.s)
τ	Shear stress (N/m^2)
τ_n	Torsion number (2τRe)
ε_g	Gas holdup (-)
θ	Contact angle (degree)

Subscripts

c	Coil
f	Frictional
g	Gas
l	Liquid

t	Tube

Reference

- Acharya, N., Sen, M., Chang, H.C., 2001. Analysis of heat transfer enhancement in coiled-tube heat exchangers. Int. J. Heat Mass Transfer 44, 3189-3199.
- Ali, O., Kenneth, J.B., Crain jr, B., 1968. Forced convection boiling inside helically-coiled tubes. Int. J. Heat Mass Transfer 11, 1779-1793.
- Ali, S., 2001. Pressure drop correlations for flow through regular helical coil tubes. Fluid Dyn. Res. 28, 295–310.
- Ali, S., Zaidl, A.H., 1979. Head loss and critical Reynolds numbers for flow in ascending equiangular spiral tube coils. Ind. Eng. Chem. Proc. Des. Dev. 18, 349 – 353.
- Ali, S., Zaidi, A.H., 1980. Pressure drop and stability of flow in negative logarithmic spiral tube coils. Ind. Eng. Chem. Proc. Des. Dev. 19, 75 – 80.
- Berger, S.A., Talbot, L., Yao, L.S., 1983. Flow in curved pipes. Ann. Rev. Fluid Mech. 15, 461-512.
- Chhabra, R.P., Richardson, J.F., 1999. Non-Newtonian Flow: Fundamentals and Engineering Applications. Elsevier Science.
- Devanahalli, G.P., Timothy, J.R., Vijaya Raghavan, G.S., 2004. Natural convection heat transfer from helical coiled tubes. Int. J. Therm. Sci. 43, 359–365.
- Hameed, M.S., Muhammed, S., 2003. Mass transfer into liquid falling film in straight and helically coiled tubes. Int. J. Heat Mass Transfer 46, 1715-1724.
- Hewitt, G.F., Boure, J.A., 1973. Some Recent Results and Development in Gas-Liquid Flow: A Review. Int. J. Multiphase Flow 1, 139-171.
- Kasturi, G., Stepanek, J.B., 1972. Two-Phase flow - I. Pressure drop and void fraction measurements in co-current gas-liquid flow in coil. Chem. Eng. Sci. 27, 1871–1880.

- Koutsky, J.A., Adler, R.J., 1964. Minimization of axial dispersion by use of secondary flow in helical tubes. Can. J. Chem. Eng. 42, 239-246.
- Kozo, F., Yoshiyuki, A., 1988. Laminar heat transfer in a helically coiled tube. Int. J. Heat Mass Transfer 31, 387-396.
- Kumar, R.H., Ramesh, K.V., Sarma, G.V.S., Raju, G.M.J., 2011. Mass transfer at the confining wall of helically coiled circular tubes in the absence and presence of packed solids, Int. Commun. Heat Mass Transfer 38, 319–323.
- Kumar, V., Faizee, B., Mridha, M., Nigam, K.D.P., 2008. Numerical studies on a tube-in-tube helically coiled heat exchanger. Chem. Eng. Proc. 47, 2287-2295.
- Leclerc, D.F., Smith, C.J., Clifford, Toren, E.C., 1987.Axial dispersion in coiled tubular reactors: The effect of curvature at low Dean Numbers. Analytica Chimica Acta 184, 173-185.
- Maxwell, J.C., 1892. A treatise of electricity and magnetism. 3rd edition, Oxford University press, London, 1, 435 -449.
- Mujawar, B.A., Rao, M.R., 1978. Flow of Non- Newtonian fluids through helical coils. Ind. Eng. Chem. Proc. Des. Dev. 17, 22–27.
- Rajasekharan, S., Kubair, V.G., Kuloor, N.R., 1970. Heat transfer to Non-Newtonian fluids in coiled pipes in laminar flow. Int. J. Heat Mass Transfer 13, 1583-1594.
- Saxena, A. K., Nigam, K.P.D., 1981. Axial dispersion in laminar flow of polymer solutions through coiled tubes. J. Appl. Polym. Sci. 26, 3475-3486.
- Saxena, A.K., Nigam, K.D.P. 1979. On RTD in coiled tube. Chem. Eng. Sci. 34, 425-426.
- Saxena, A.K., Nigam, K.P.D., 1983. Laminar dispersion in helically coiled tubes of square cross section. Can. J. Chem. Eng. 61, 53-57.

- Seara, J.F., Sieres, J., Vazquez, M., 2003. Heat and mass transfer analysis of a helical coil rectifier in an ammonia-water absorption system. Int. J. Therm. Sci. 42, 783-794.
- Sethumadhavan, R., Rao, M.R., 1983. Turbulent Flow Heat Transfer and Fluid Friction in Helical-Wire-Coil-Inserted Tubes. Int. J. Heat Mass 26, 12, 1833-1845.
- Shaikh, A., Al-Dahhan, M., 2005. Characterization of the hydrodynamic flow regime in bubble columns via computed tomography. Flow Meas. Instrum. 16, 91-98.
- Soh, W.Y., Berger, S.A., 1984. Laminar entrance flow in curved pipe. J. Fluid Mech. 148,109-135.
- Stepanek, J.B., Kasturi, G., 1972. Two-phase flow- II. Parameters for void fraction and pressure drop correlations. Chem. Eng. Sci.27, 1881–1891.
- Sujatha, V., Rajendra Prasad, P., Bhaskara Sarma, C., Jagannadha Raju, G.J.V., 2003. Studies on ionic mass transfer with insert helical tape promoters in batch fluidized beds. Ind. J. Chem. Tech. 10, 694-700.
- Thandlam A.K., Raju. G.M.J., Sarma, G.V.S., Ramesh, K.V., 2009. Mass transfer at the confining wall of helically coiled circular tubes with gas–liquid flow and fluidized beds. Chem. Eng. J. 153, 114–119.
- Trivedi, R.N., Vasudeva, K., 1975. Axial dispersion in laminar flow in helical coils. Chem. Eng. Sci. 30, 317-325.
- Vashisth, S., Kumar, V., Nigam, K.D.P., 2008. A review on potential applications of curved geometries in process industry. Ind. Eng. Chem. Res. 47, 3291–3337.
- Weisman, J., Lan, J., Disimile, P., 1994. Two-phase (air-water) flow patterns and pressure drop in the presence of helical wire ribs. Int. J. Multiphase Flow 20, 885–899.

- Xin, R.C., Awwad, A., Dong, Z.F., Ebadian, M.A., 1997. An experimental study of single-phase and two-phase flow pressure drop in annular helicoidal pipes. Int. J. Heat Fluid Flow 18, 482-488.
- Zuber, N., Findlay, J.A., 1965. Average volumetric concentration in two-phase flow systems. J. Heat Trans. 87(4), 453-68.

CHAPTER-2

FLOW PATTERN AND ITS TRANSITIONS

This chapter investigates the flow pattern of co-current upward two-phase flow in a vertical helical coil tube with Newtonian and non-Newtonian fluids. The effects of the different geometrical properties of helical coil on flow patterns have been enunciated. Based on the experimental data a correlation was proposed to predict the transitions of flow patterns (*i.e., plug-slug flow and slug-stratified flow*) *by dimensional analysis. Probabilistic Neural Network* (*PNN*) *model has also been developed to predict the flow patterns of two-phase flow.*

2.1. Introduction

The devices of various unit operations and unit processes can be made compact using helical coiled tubes. The helical coils also improve the performance of equipment due to its inherent secondary flow generation capability (Vashisth et al., 2008). In three-phase gas-liquid-solid flow, coil system has an important applications in petroleum industry to separate the sand particles in oil-gas-sand and water. This secondary flow arises due to the centrifugal force acting over the fluid body/mass while it crosses a curved path. Gas-liquid two-phase flow is much more complicated than the single flow under such condition. The centrifugal force compels the heavier fluid to move away from the centre of curvature and lighter one flow towards the centre of curvature (Biswas and Das, 2008). Therefore, hydrodynamics of two-phase flow in a helical coil are different from that in a straight pipe. Various authors showed that there is a change of flow pattern of gas-liquid flow in the helical coil depending on the geometry of the coil and physical properties of the system. Past work shows that the separated flow patterns (stratified and annular) occupy a major area of the flow pattern maps

(Biswas and Das, 2008; Rippel et al., 1966; Banerjee et al., 1969; Akagawa et al., 1971; Mujawar and Rao, 1981; Saxena et al., 1990; Vashisth and Nigam, 2007; Banerjee et al., 1967). They identified annular and stratified flow patterns for air-water flow in helical tube and compared their experimental results (vertical, helical and horizontal two-phase flow) with theoretically predicted values. Rippel et al. (1966) performed the experiments in a two-phase flow with different gases (air, helium and Freon-12) and liquids (water and 2-propanol) to generate flow pattern, for scaling up of devices. They also developed three empirical correlations for three different flow patterns. The hydrodynamics of such flow (flow pattern, pressure drop, and holdup) is highly influenced by tube diameter, coil diameter, helix angle and liquid properties (like density, viscosity and interfacial tension). Whalley (1980) studied adiabatic air-water flow through helical coil and found out transition boundary between annular and stratified flow. Mujawar and Rao (1981) also reported that the trends of the flow pattern in helical coil were similar to the straight horizontal tube. They did not interpret the flow patterns and its maps with non-Newtonian liquids. Saxena et al. (1990) observed that there is a similar flow patterns between the helical coil and inclined tubes. In their study, the tube inclination and tube curvature shows similar effect to the flow patterns. To increase the mixing efficiency and compactness of a device, Vashisth and Nigam (2007) introduced a new concept of helical coil termed as coiled flow inverter (CFI) and bagged a patent on it. They observed various flow patterns such as stratified, slug, plug, wavy and churn flow for two-phase flows. Several researches have focused in this field and published their works mainly with gas-Newtonian liquids. The helical coil system is also important as a compact helical reactor to execute the gas-liquid reaction with intense mixing. The reaction performance may be significant in the helical coil due to its absence of back mixing. In this chapter it has been focused on the hydrodynamics like flow patterns and its transition in helical coil with two- and three-phase systems with Newtonian and non-Newtonian liquid and effects of various geometrical parameters like tube diameter, coil diameter, pitch difference and physical properties of liquid on it. The prediction of the flow pattern transitions is done by probability neural network and correlation models.

2.2. Theoretical background

2.2.1. Analysis to predict flow patterns by using Probabilistic Neural Network (PNN)

The artificial neural networks (ANN) are used for engineering purposes, such as pattern recognition, forecasting, classification, optimization function, approximation, vector quantization and data compression (Basheer and Hajmeer, 2000). It is an alternative tool to solve many complex and nonlinear problems. Feed forward back-propagation (FFBP), generalized regression neural networks (GRNN), radial basis network (RBN), probabilistic neural network (PNN) and support vector machine (SVM) are some common types of the artificial neural networks. Probabilistic neural network is a special type of artificial neural network. The selection of probabilistic neural network for the present study is for its accuracy in prediction, swiftness and ease in operation. Probabilistic neural networks have the big advantage that the prediction algorithm works with only few training samples and they are very flexible and new information can be added immediately with almost no retraining (Basheer and Hajmeer, 2000). Probabilistic neural network is a feed forward neural network based on Bayes-Parzen classification theory which was first introduced by Specht (1990). Specht (1990) showed that the Bayes-Parzen classifier could be broken up into a large number of simple processes implemented in a multilayer neural network, each of which could be run independently. Bayes theorem is used for conditional probability whereas Parzen's method is for estimating the probability density function (PDF) of random variables. Hajmeer and Basheer (2002) gave a detailed description of Bayes-Parzen theory. To explain Bayes' theorem, let us consider a set of sample, X = [x_1, x_2,..., x_p] obtained from any samples belonging to the number of different classes (*1, 2, ..., k,..., K*). If probability of a sample belongs to the k^{th} class is h_k, the value associated for misclassification of that sample is c_k and the true probability density function of all classes $f_1(x)$, $f_2(x)$,..., $f_k(x)$ are known, then the Bayes theorem classifies any unknown sample into i^{th} class if

$$h_i C_i f_i(x) \geq h_j C_j f_j(x), \text{ for all classes } j \neq i \qquad (2.1)$$

The misclassification refers to the information bias arising from the experimental error. The probability density function $f_k(x)$ corresponds to the concentration of class *k* samples around the unknown sample. Classification can be estimated from Bayes strategy if the probability density $f_k(x)$ of a sample is known (Basheer and Hajmeer, 2000; Hajmeer and Basheer, 2002). In most of the cases it is known and a Gaussian distribution is assumed to get classification. If there is a large deviation between assumed distribution and the true distribution samples, then it results in high scale misclassification of samples. This misclassification can be minimized by introducing the concept of multivariate probability density function (PDF) estimator for each class from the set of training data itself. The multivariate PDF combines all the features of any random scattered variables. Cacoullos (1966) extended Parzen's (1962) univariate PDF method to multivariate PDF. The multivariate PDF estimator, $g(x)$ is expressed as:

$$g_k(x_1, x_x, ..., x_p) = \frac{1}{n\sigma_1\sigma_2...\sigma_p} \times \sum_{i=1}^{n} W\left(\frac{x_1 - x_{1,i}}{\sigma_1}, \frac{x_2 - x_{2,i}}{\sigma_2}, ..., \frac{x_p - x_{p,i}}{\sigma_p}\right) \qquad (2.2)$$

where σ_1, σ_2,..., and σ_p are the smoothing parameters representing standard deviation (also called window or kernel width) around the mean of *p* random variables x_1, x_2,...,x_p, *W* is the activation function (Specht, 1990; Masters, 1995) and *n* is the total number of training samples. If all the smoothing parameters are assumed equal (i.e., $\sigma_1 = \sigma_2 = \sigma_3 = ... = \sigma_p = \sigma$), and using shaped Gaussian function for *W*, a reduced form of Eq. (2.2) results:

$$g_k(x) = \frac{1}{(2\pi)^{p/2} n\sigma^p} \sum_{i=1}^{n} \exp\left(\frac{\|x - x_i\|^2}{2\sigma^2} \right) \tag{2.3}$$

where x is the vector of scattered variables and x_i is the i^{th} training vector and σ is the smoothing parameter. Eq. (2.3) represents the average of the multivariate distributions where each distribution is cantered at one distinct training sample. The general structure of a probabilistic neural network has been given in Figure 2.1.

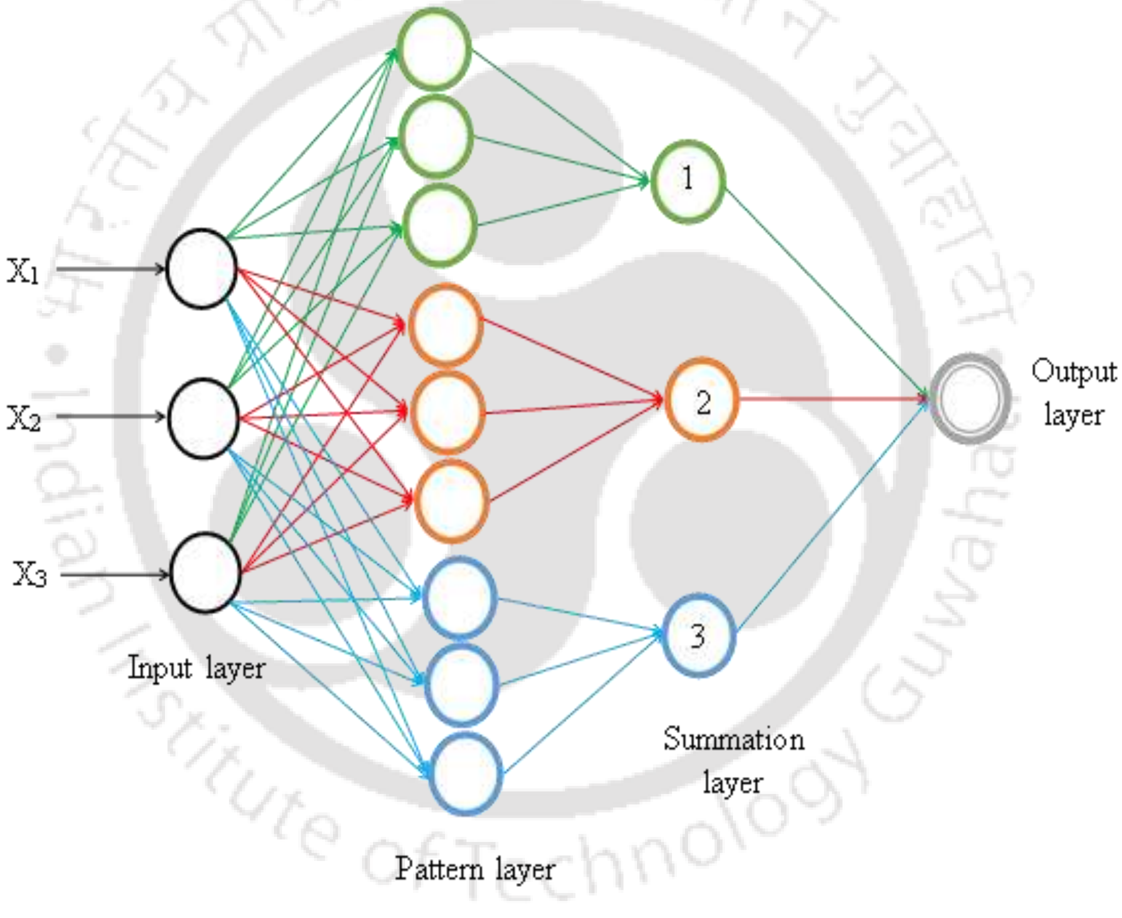

Figure 2.1: Block diagram of Probabilistic Neural Network (PNN architecture).

The Figure 2.1 has a simple network architecture with four layers namely input layer (containing input nodes), hidden layer (containing hidden nodes), pattern layer (containing class nodes) and output layer (containing decision nodes). The input layer does not perform any computational or arithmetic operations and simply distributes the inputs to each neuron in hidden layer. The hidden layer consists of neurons that are equal to the total number of training variables. The hidden layer computes Euclidean distances between the each random variable and the training sample that represented by the hidden layer and then processed through a Gaussian activation function as

$$\psi_i(x) = \exp\left(-\frac{\|x - x_i\|}{2\sigma^2}\right) \tag{2.4}$$

where x is the vector of random variables and x_i is the i^{th} training vector. The class layer computes the summation and gives out arithmetic mean of the output of hidden layer for each class, H_k. The output layer classifies any random variable by comparing the output of class layer for each class and then following the Bayes' classification theorem as,

$$H_k(x) = \arg\max\{g_k(x)\} \tag{2.5}$$

2.3. Experimental

The schematic of an experimental setup is shown in Figure 2.2. It comprises of a vertical helical coil (H) twisted on a column, centrifugal pump (Pm) to deliver liquid, one compressor (C) for pumping air, one storage tank (S) and one separator (S). The experiments were carried out with air, water and Sodium Carboxy Methyl Cellulose (SCMC) as a non-Newtonian liquid. SCMC were prepared in a tank and pumped by the centrifugal pump (Pm) through the pre-calibrated rotameters (make: Five Stars Ltd., Mumbai) R_{L1} (6.94×10^{-05} - 6.67×10^{-04} m^3/s) and R_{L2} (1.67×10^{-05} - 3.33×10^{-04} m^3/s). Air was pumped into the test section of helical coil by using compressor (C). The air flow rate were measured by the gas rotameter (R_G) ranging from 1.67×10^{-05} to 1.67×10^{-04} m^3/s.

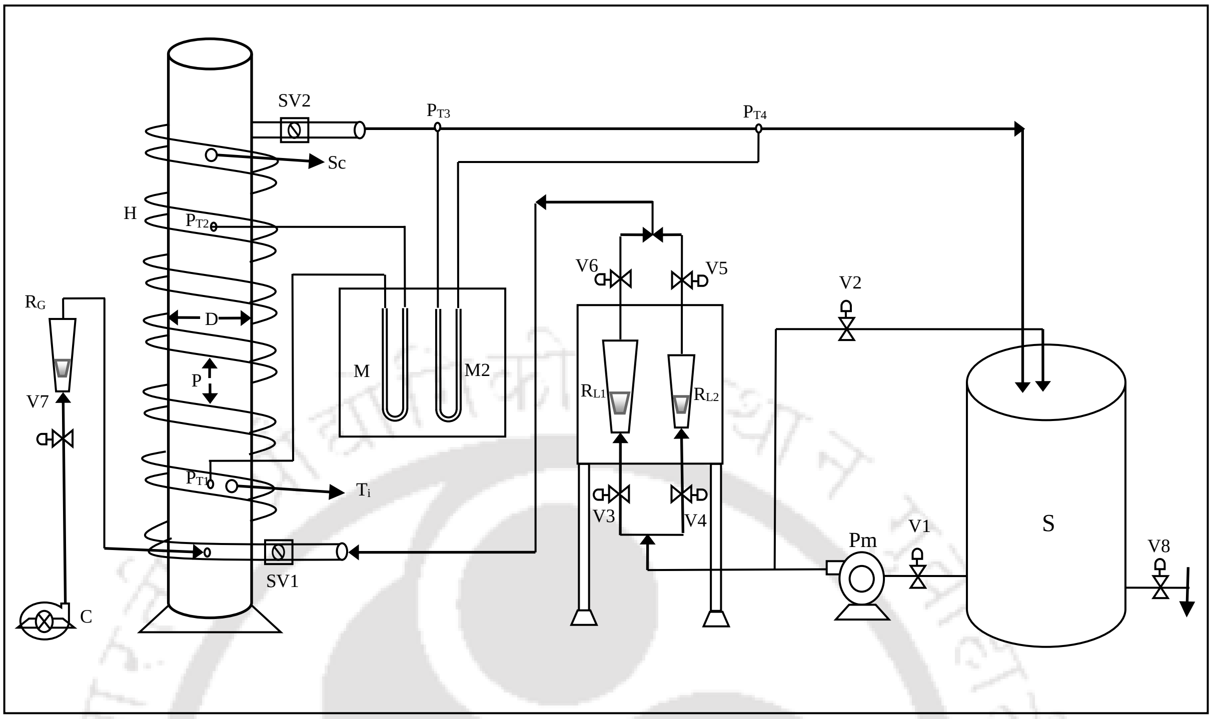

Figure 2.2: Schematic diagram of the experimental system.

Legends- C: Compressor, D: Diameter of the coil, H: Helical coil, M1, M2: U-tube Manometers, P: Pitch, Pm: Pump, P_{T1} – P_{T4}: Pressure taps, R_{L1}, R_{L2}: Liquid Rotameter, R_G: Gas Rotameter, Sc: Sample collector, SV1, SV2: Solenoid valves, S: Storage tank, T_i: Tracer input, V1 – V8: Valves.

Flow patterns were carefully observed at every set of flow rates (air and liquid). A snapshot of the same was taken by a digital camera (Model: SONY Cyber-short DSC-Hx10V, Sony Electronics Inc., Japan, pixel resolution: 18200000 pixels, shutter speed: 1/1600 sec, CMOS sensor with enhanced image processing, mega pixel: 18.2 (4896×3672) with 16X optical and 32X clear zoom, lens magnification: 4.28 – 68048 mm) to identify the flow patterns at steady state flow condition. The flow is illuminated by a sheet of light, then photographs were taken as a multiple image or as a video. Each experiment was repeated thrice to check its reproducibility and it was found above 98%. Pressure drop across vertical helical coil (P_{T1} and P_{T2}) and horizontal straight tube (P_{T3} and P_{T4}) were also measured by two U-tube manometers (M1 and M2). The gas holdup at different flow conditions is measured by quick closing valve (Solenoid Valve). For this, two quick closing valves SV1 and SV2 are placed at the two ends of the test section (Figure 2.2). The experiments were carried out with three sets of helical coiled tubes of diameter 0.009, 0.015, 0.02 m. Each set of helical coil is arranged in three different pitches (pitch differences (p/D_c): 0.5, 1 and 1.5). The tubes are made up of transparent and flexible polyethylene pipe for better visualization and getting desired pitch arrangement. The present experiment was performed within the operating ranges of the liquid flow rates of 3.33×10^{-05} - 5.00×10^{-04} m^3/s and the air flow rates of 1.67×10^{-05} - 1.00×10^{-04} m^3/s. At steady state operation, the experimental data for flow patterns, for different operating conditions of two-phase (air-SCMC) flow in the vertical helical coil were noted.

2.3.1. Physical properties of the slurry system

The physical properties of the fluid (air, water and SCMC) used for the present study is are shown in Table 2.1. The density of liquid was measured by gravity bottle and the surface tension by tensiometer (Model: K9-MK1, Make: KRÜSS GmbH Co., Hamburg, Germany). The rheological properties of SCMC solutions were measured by rheometer (Model: Haake Rheostress 1, Make: Thermo Electron Co., Karlsruhe, Germany). The apparent viscosity of SCMC solution was calculated by (Chhabra and Richardson 1999)

$$\mu_{eff} = K(8U/d_t)^{n-1}\left(\frac{3n+1}{4n}\right)^n \tag{2.6}$$

where d_t is internal diameter of tube, U is the average velocity of liquid, K is consistency coefficient, and n is flow behaviour index. For the slurry system, the average sizes of the particles were taken as 2.21 μm (zinc oxide), 19.39 μm (kieselguhr), and 96.0 μm (aluminum oxide). The physical properties of the slurry are shown in Table 2.2. The sizes of the particles were measured by using laser particle size analyzer (Model: APA 2000, Make: Malvern Instruments Ltd., Malvern, U.K.).

Table 2.1: Physical properties of the system at 25 ± 1°C.

System	Concentration (kg/m^3)	Flow behaviour index (n)	Consistency index K (Pa s)	Density ρ_l (kg/m^3)	Surface tension σ_l (N/m)
Water	-	-*	-	999.70	0.0710
Air	-	-**	-	1.1850	-
SCMC-1	0.5	0.9532	0.01801	1000.55	0.0747
SCMC-2	1.0	0.9099	0.02552	1000.83	0.0694
SCMC-3	1.5	0.8701	0.03617	1001.69	0.0683
SCMC-4	2.0	0.8338	0.05126	1001.96	0.0662
SCMC-5	2.5	0.8010	0.07266	1002.01	0.0657
SCMC-6	3.0	0.7717	0.10299	1002.03	0.0645

*viscosity of water: 0.797×10^{-3} kg/m.s, ** viscosity of air: 1.863×10^{-5} kg/m.s

The density of the slurry was calculated as per following equation (Abulnaga, 2002):

$$\rho_m = \frac{100}{(C_w / \rho_s) + [(100 - C_w) / \rho_l]} \tag{2.7}$$

where ρ_m is a density of slurry mixture, C_w is solid concentration by weight (%), ρ_s is a density of solid particles in mixture and ρ_l is a density of liquid phase in mixture. The effective viscosity and density of slurry were calculated by using Thomas correlations (Abulnaga, 2002) which are given as:

$$(\mu_{ls}/\rho_{ls}) = (\mu_l/\rho_{ls})\left[1 + 2.5(C_c/\rho_p) + 10.05(C_c/\rho_p)^2 + 2.73\times10^{-3}\exp(16.6(C_c/\rho_p))\right] \quad (2.8)$$

$$\rho_{ls} = \rho_l + C_c(1 - (\rho_l/\rho_p)) \quad (2.9)$$

where ρ_{ls} is a density of slurry, ρ_p is a density of particle and μ_{ls} is a slurry viscosity.

Table 2.2: Physical properties of the liquid-solid slurry measured at 25 ± 1 ^{0}C

Particles	Diameter (μm)	Concentration (wt %)	Density (kg/m^3)	Viscosity × 10^3 (kg/m-s)	Surface Tension (N/m)
Kieselguhr	19.00	5.000	990.418	1.041	0.072
Kieselguhr	19.00	10.00	981.137	1.084	0.072
Kieselguhr	19.00	15.00	971.855	1.131	0.073
Zinc oxide	2.210	10.00	981.562	1.126	0.072
Aluminum oxide	96.00	10.00	981.124	1.064	0.072

2.3.2. Particle size distribution

Aqueous slurry of hydrophilic neutral Zinc oxide, Kieselguhr and Aluminum oxide are used for the experiment. In a gas-liquid-solid slurry system, the particles are used usually smaller than 100 micron. In such cases, the spatial profile of the solid concentration is almost uniform. In the present study the average size of the particles are taken 2.2, 19 and 96 μm which are measured by laser particle size analyser. The particle size distribution of the Zinc oxide, Kieselguhr and Aluminium oxide are shown in Figure 2.3, 2.4 and 2.5 respectively.

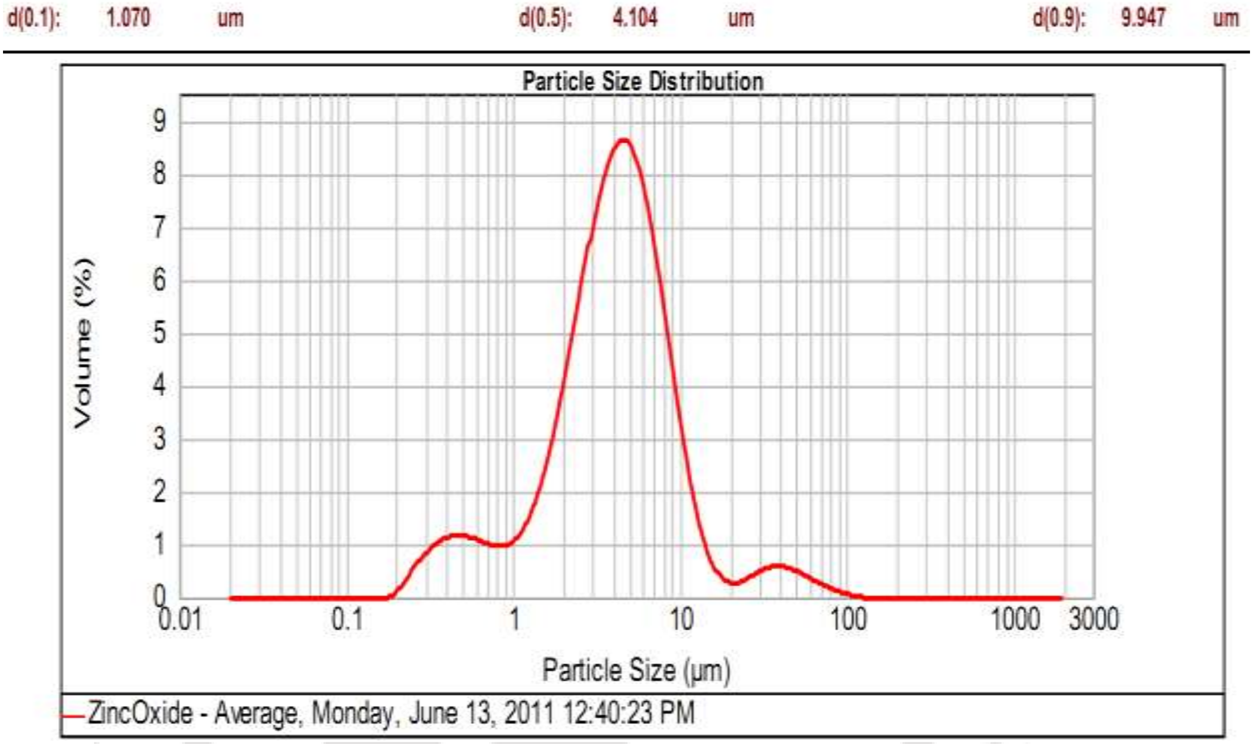

Figure 2.3: Particle size distribution of zinc oxide particles

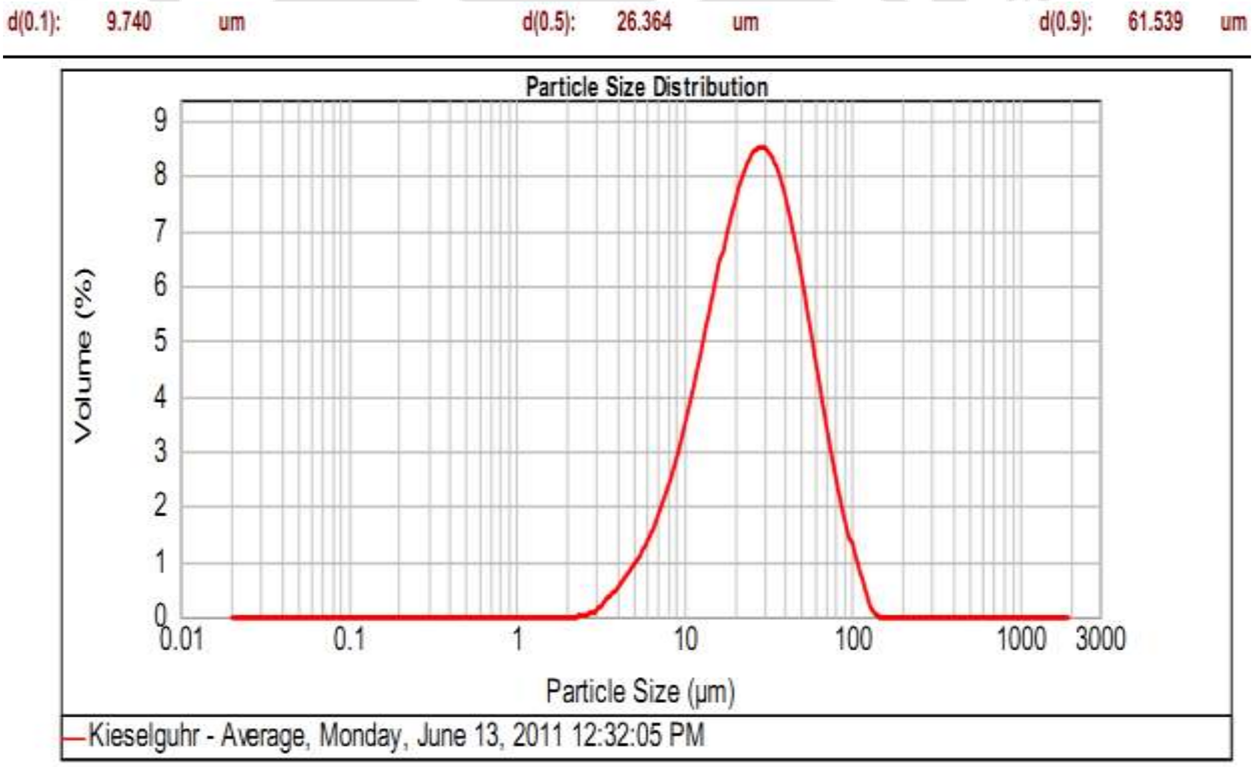

Figure 2.4: Particle size distribution of Kieselguhr particles

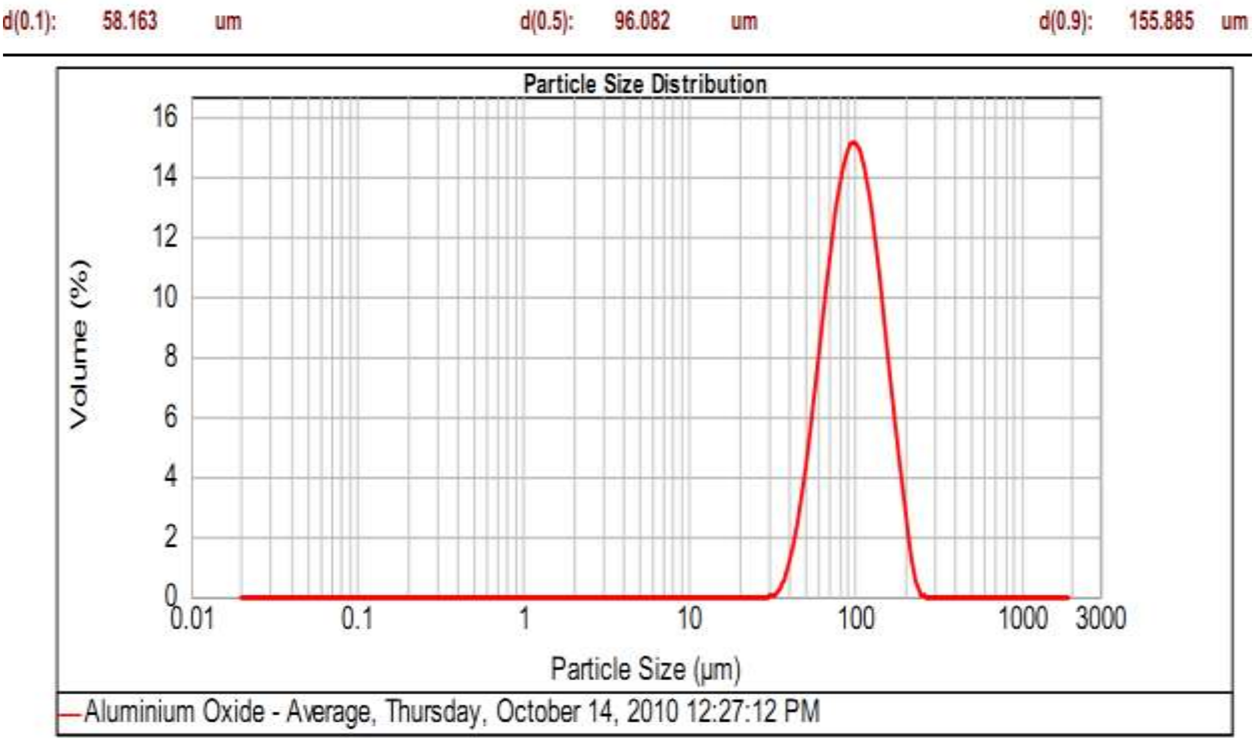

Figure 2.5: Particle size distribution of aluminum oxide particle

2.3.3. Uncertainty analysis

In the present study, experiments were repeated five to six times, and the results obtained in these experiment were averaged. The advantage of the taking the average value is that the variations caused by various influences tend to be nullified. Using the average value, the standard deviation (STDEV) and standard uncertainty (*U*) of the repeated experiments were calculated. In the present study the mean ($\bar{x}$) and standard deviation (STDEV) of the repeated experiments were calculated respectively as

$$\bar{x} = \frac{1}{N}\sum_{i=1}^{N} x_i \qquad (2.10)$$

$$STDEV = \sqrt{\frac{\sum_{i=1}^{N}(x_i - \bar{x})^2}{N-1}} \qquad (2.11)$$

The standard uncertainty (*U*) of the mean value was estimated by

$$U = \frac{STDEV}{\sqrt{N}} \tag{2.12}$$

The typical range of the means, standard deviations, and uncertainties of the flow patterns within a range of operating variables are reported in Table 2.3. Each value of superficial velocities in 1st column corresponds to the mean of 6 data points (i.e., N = 6). Relative uncertainty is calculated from standard uncertainty and mean value of the corresponding data set.

Table 2.3. Typical uncertainties of the flow patterns at constant tube diameter (d_t = 0.015 m) and coil diameter (D_c = 0.0117 m)

U_{sl} (m)	U_{sg} (m)	SCMC (kg/m^3)	N	Flow patterns	Range of STDEV (x10^{-3})	Range of uncertainty (x10^{-3})	Range of relative uncertainty %
0.566-1.132	0.094	1.0	6.0	Pug flow	4.176-2.137	0.875-1.705	0.302-0.077
0.189-1.132	0.189	1.0	6.0	Slug flow	3.142-3.445	1.284-1.412	0.124-0.683
0.189-0.566	0.283	1.0	6.0	Stratified flow	3.085-4.541	1.265-1.854	0.327-0.668

2.4. Results and discussion

2.4.1. Flow pattern in two-phase system

Three flow patterns plug flow (P), slug flow (S) and stratified flow (ST) were observed from the present experiment. A typical snapshot and sketch of different flow patterns are shown in Figure 2.6 at constant SCMC concentration of 3.0 kg/m^3 as a representative results. All the experiments and analysis were carried out under the following ranges of different dimensionless numbers: curvature ratio: $3.75 \le D_c/d_t \le 22.22$; Reynolds number: $62.15 \le Re_m \le 3913.58$; $74.60 \le Re_l \le 2364.53$; $69.60 \le Re_g \le 621.22$; Dean Number: $26.71 \le De_l \le 857.53$; $22.01 \le De_g \le 215.19$. The entire ranges of different flow patterns have been represented in the form of flow pattern maps as shown in Figure 2.7. Figure 2.7 shows the flow patterns observed at three different tube diameters at constant coil diameter of 0.117 m, and pitch difference of 1.0 for non-Newtonian fluid (SCMC - 3.00 Kg/m^3). The firm line represents the transition line between plug to slug flow (P-S) and dashed line represents the transition line between slugs to stratified flow (S-ST).

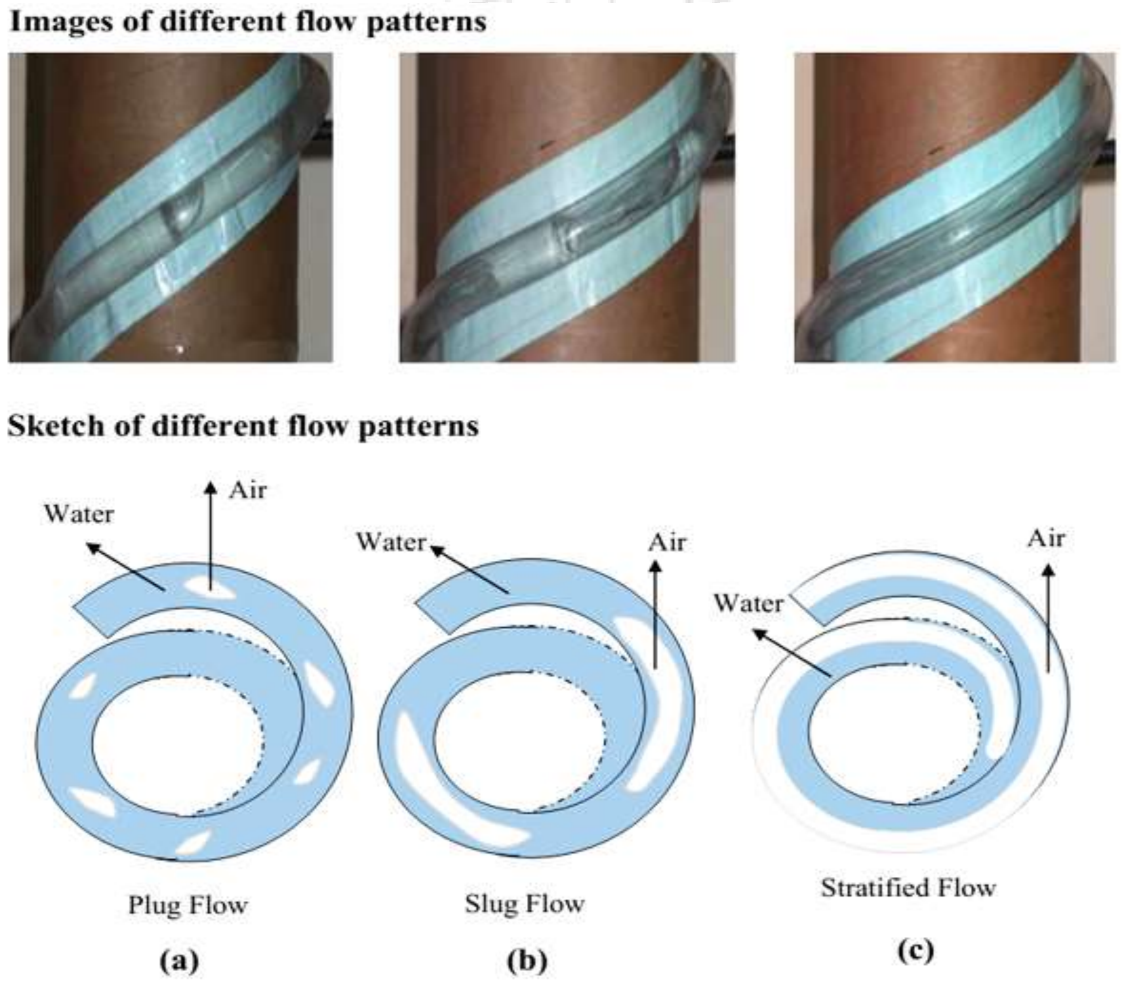

Figure 2.6: Observed flow patterns in vertical helical coil tube at d_t = 0.015 m, D_c = 0.117 m, p/D_c = 1.0 and SCMC - 3.0 kg/m^3**.** (a) Plug flow at U_{SL} = 0.755, U_{Sg} = 0.094 (m/s), (b) slug flow at U_{SL} = 0.566, U_{Sg} = 0.189 (m/s) and (c) stratified flow at U_{SL} = 0.189, U_{Sg} = 0.377. (m/s)

It was noticed that as the tube diameter increases, the ranges of plug flow were increased, whereas region of stratified flow was decreased with the increasing tube diameter (Figure 2.7 (a)). Similarly range of slug flow reduced as shown in Figure 2.7 (b and c). The plug flow appeared with the higher liquid Reynolds number ($Re_l \geq 939.53$) and with lower gas Reynolds number ($Re_g \leq 70.25$). At higher liquid flow rate, small bubbles were formed due to higher momentum transfer though the coil. These bubbles started to coalesce as it moved up. After a few turns the bubbles became larger in size and appeared as a plug flow.

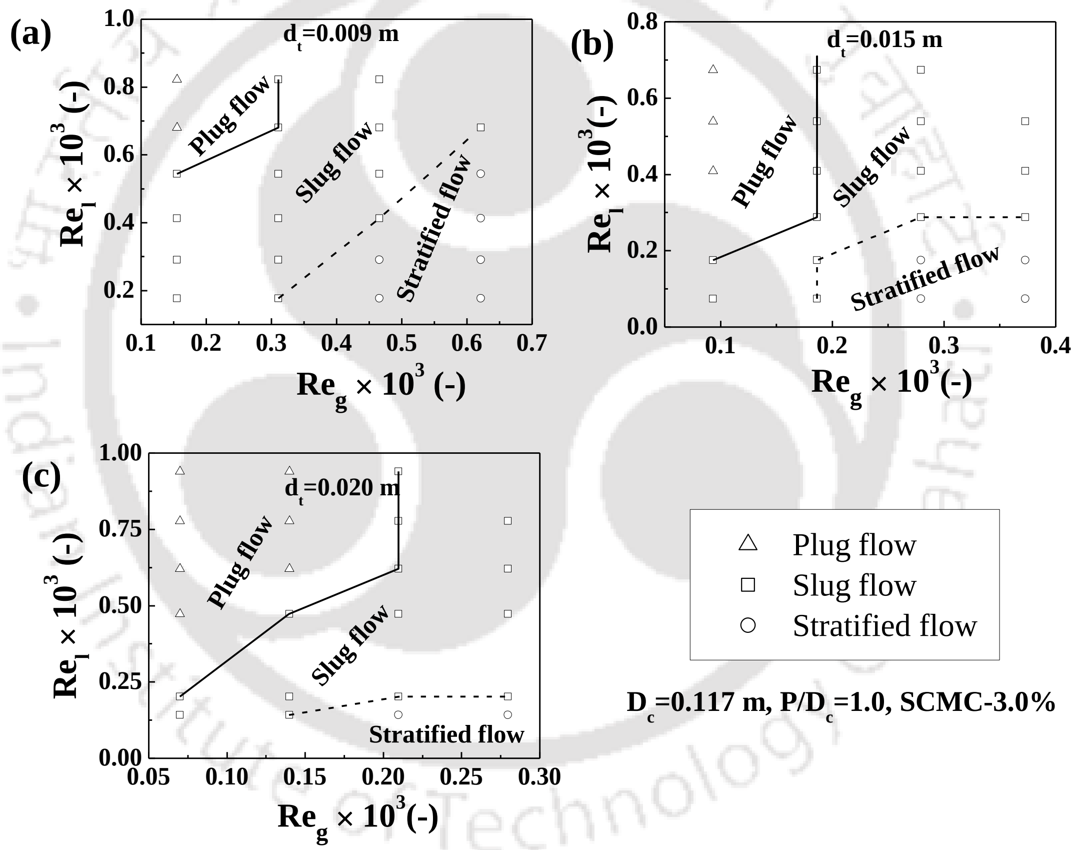

Figure 2.7: Effect of tube diameter on flow regime of two-phase air-non-Newtonian fluid at constant coil diameter and pitch difference.

These flow patterns are mainly surface and buoyancy force dominated flow. With further increasing of gas flow rate, liquid bridge between two successive plugs decreased and these plugs were converted to slug flow as the length of gas bubble becomes equal or more than the tube diameter. The plug flow is defined as when the bubble diameter is less than tube diameter.

Similarly the stratified flow observed with lower liquid Reynolds number ($Re_l \leq 70.56$) and higher air Reynolds number ($Re_g \geq 621.54$) as liquid bridge completely disappeared and gas formed a continuous stream on top of liquid layer due to buoyancy. Interestingly, stratified flow in case of non- Newtonian fluid (SCMC solution) occupies a larger region of the flow pattern map compared to the Newtonian fluid. The effect of coil diameter on flow regime at constant tube diameter, SCMC concentration, and pitch difference is shown in Figure 2.8.

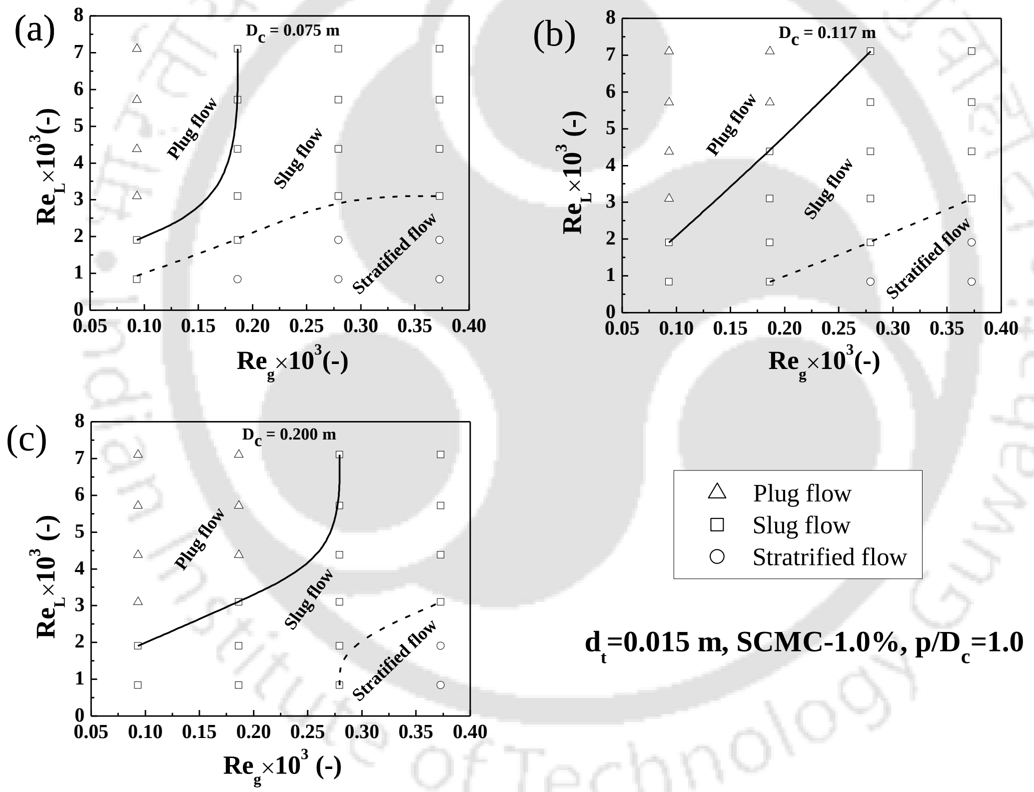

Figure 2.8: Effect of coil diameter (D_c) on flow regime of non-Newtonian fluids at constant tube diameter d_t = 0.015 m, SCMC- concentration = 1.0 kg/m^3 and pitch difference (p/D_c). =1.0.

The plug flow appears at higher liquid ($Re_l \geq 1233.99$) and lower gas Reynolds number ($Re_g \leq 150.15$) while stratified flow observed with lower liquid ($Re_l \leq 315.104$) and higher gas

Reynolds number ($Re_g \geq 311.781$). It was observed that with increasing coil diameter, the range of plug flow increased and the stratified flow decreased, whereas slug flow got effected when the changes of plug and stratified flow happened. As the coil diameter was changed the centrifugal force was changed, because the centrifugal force depends on the curvature of the coil. From the experiment it was clear that with change in pitch difference there was no significant change in slug flow and the stratified flow, whereas a small change was observed in case of plug flow as shown in Figure 2.9.

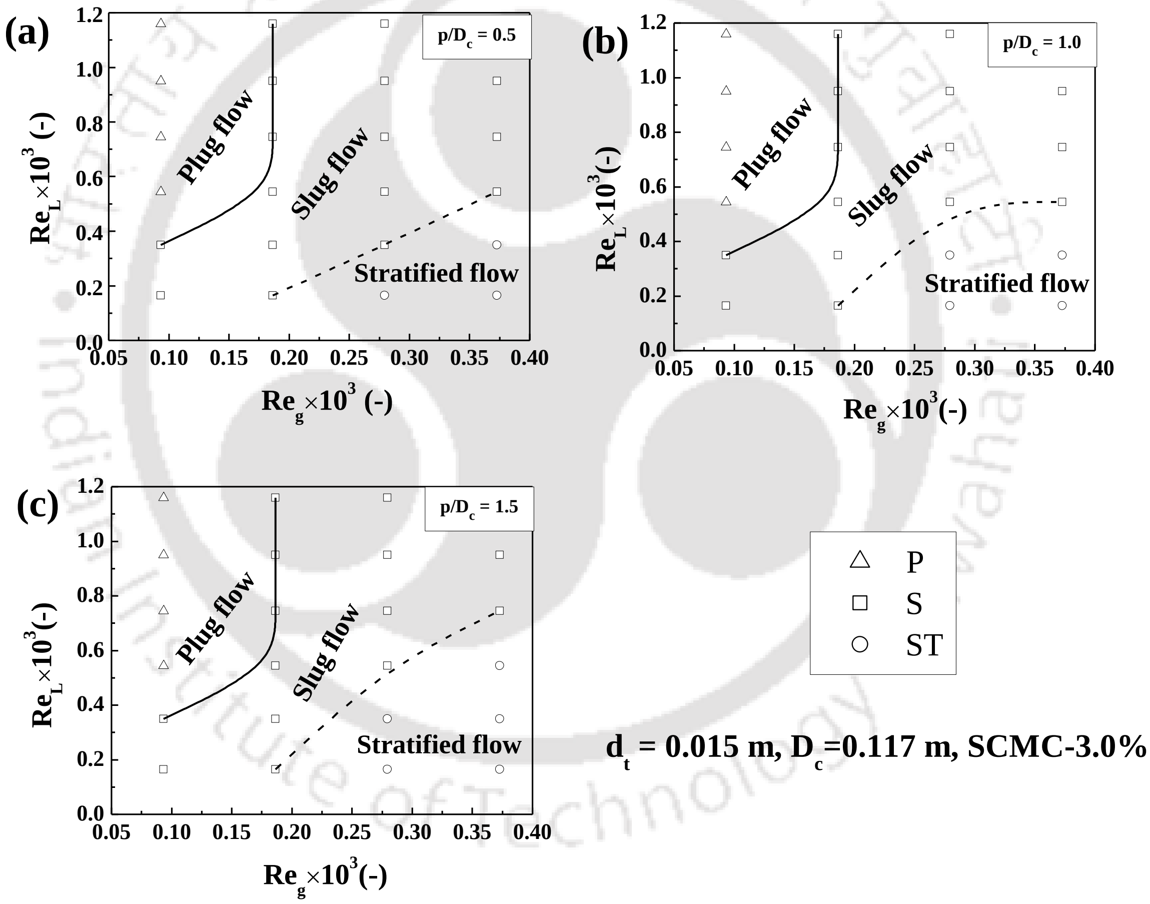

Figure 2.9: Effect of tube pitch difference (p/D_c) on flow regime at constant tube diameter d_t = 0.015 m, D_c = 0.117 m and SCMC concentration = 1.0 kg/m^3

The effect of liquid concentration on flow regime with constant tube diameter (d_t = 0.015 m), coil diameter (D_c = 0.117 m) and pitch difference (p/D_c = 1.0) is shown in Figure 2.10. The range of the liquid Reynolds number for three liquid concentrations are $0.075 \leq Re_l \times 10^3 \leq 1.159$ (for SCMC - 1.0 kg/m^3 is $0.164 \leq Re_l \times 10^3 \leq 1.159$, for SCMC - 2.0 kg/m^3 is $0.114 \leq Re_l \times 10^3 \leq 0.923$ and for SCMC-3.0 kg/m^3 is $0.075 \leq Re_l \times 10^3 \leq 0.674$) while for gas Reynolds number is $0.069 \leq Re_g \times 10^3 \leq 0.621$. With increasing liquid concentration, the transitions of flow patterns were also happened to change. With increasing liquid concentration, the viscosity changed the momentum transfer between the phases and at constant coil diameter the centrifugal force was less effective at higher concentration of SCMC. This caused to change the transition of flow patterns.

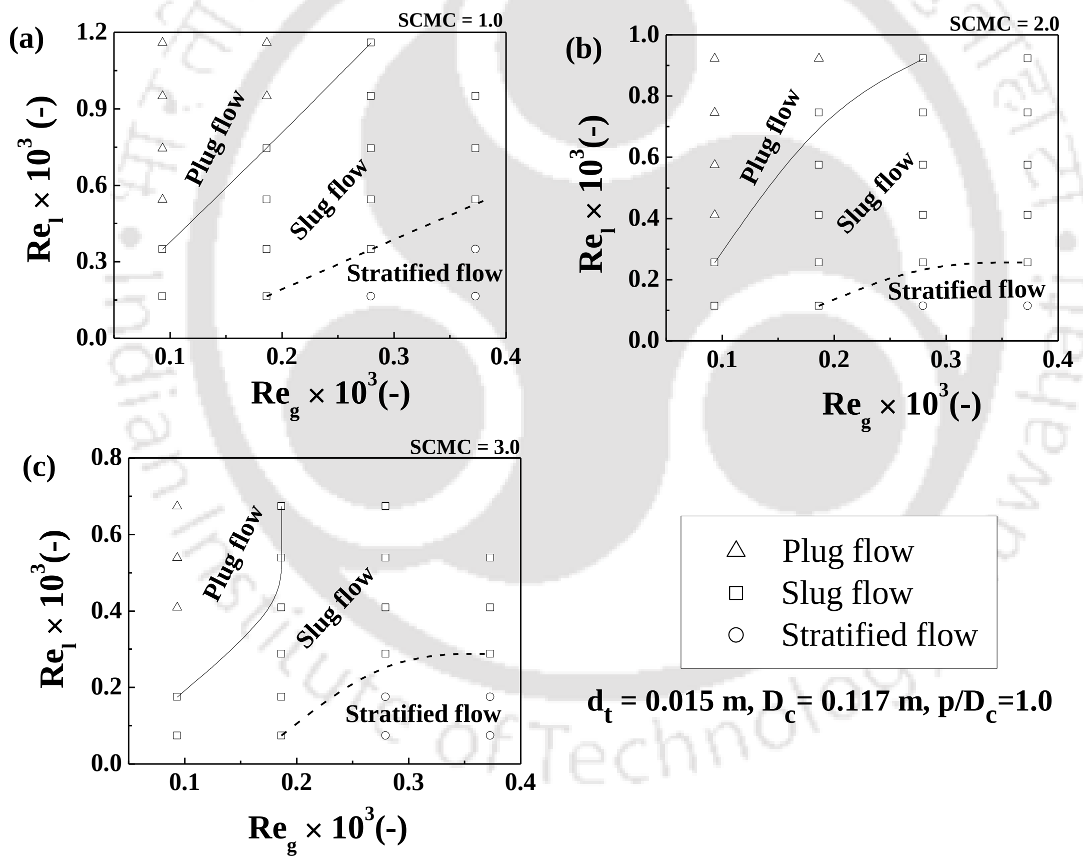

Figure 2.10: Effect of SCMC concentration on flow regime at constant tube diameter d_t = 0.015 m, D_c = 0.117 m and p/D_c = 1.0.

2.4.2. Flow pattern in three-phase system

From the present range of study, there three flow patterns such as plug flow (P), slug flow (S) and stratified flow (ST) were also observed in three-phase system. Typical snapshots of different flow patterns in helical coil from the present experiment are shown in Figure 2.11. The plug flow was seen at the higher liquid Reynolds number ($Re_l \geq 7108.02$) and at lower gas Reynolds number ($Re_g \leq 93.18$). At high liquid flow rate, small bubbles were seen to form due to higher momentum transfer though the coil which starts to coalesce as it moved up. After a few turns the bubbles became larger in size due to coalescence and appeared as a plug flow.

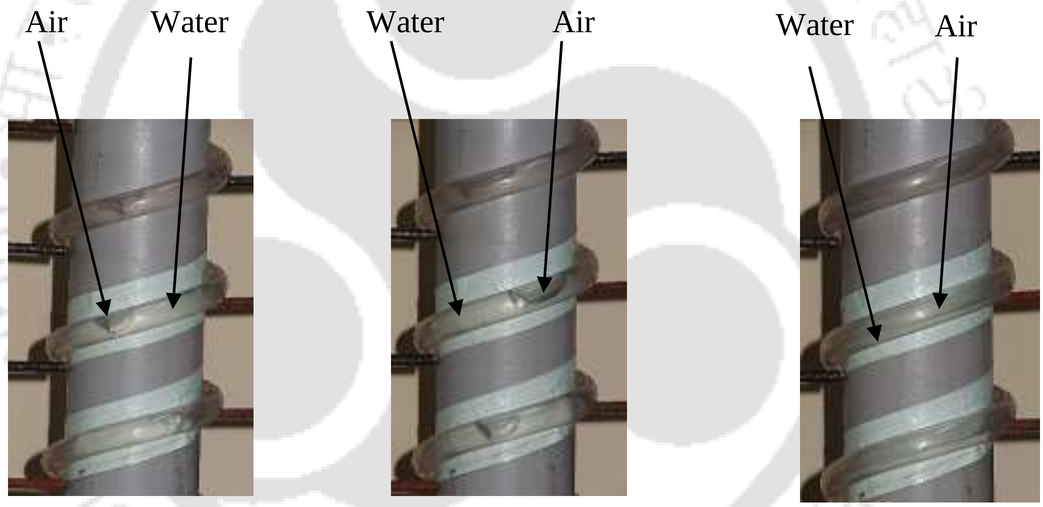

Plug flow   Slug flow   Stratified flow

Figure 2.11: Observed flow patterns in vertical helical coil tube at $d_t = 0.015$ m, $D_c = 0.075$ m, $p/D_c = 1.0$ and SCMC - 1.0 Kg/m^3 with 5 wt% slurry of kieselghur**.** Plug flow at $U_{Sl} = 0.755$, $U_{Sg} = 0.094$ (m/s), slug flow at $U_{Sl} = 0.377$, $U_{Sg} = 0.189$ (m/s) and stratified flow at $U_{Sl} = 0.189$, $U_{Sg} = 0.283$ (m/s).

These flow patterns were mainly surface and buoyancy force dominated flow. With further increasing of gas flow rate ($U_{sg} \geq 0.189$ m/s), liquid bridge between two successive plugs decreased and these plugs were converted to slug flow as the length of gas bubble becomes equal or more than the tube diameter. As the tube diameter increased ($d_t \geq 0.009$ m), the domain of plug flow was increased, whereas that of stratified flow was decreased with increasing tube diameter. The stratified flow observed with lower slurry Reynolds number ($Re_{sl} \leq 833.85$) and higher gas Reynolds number ($Re_g \geq 372.73$) as liquid bridge completely disappeared and gas formed a continuous stream on top of liquid layer due to buoyancy. The stratified flow in case of non-Newtonian fluid (SCMC solution) occupies a larger region of the flow pattern map compared to the Newtonian fluid for same slurry concentration. It was observed that with increasing coil diameter, the domain of plug flow increased and the stratified flow decreased, whereas slug flow gets effected when the change of plug and stratified flow were happened. A typical flow pattern map is shown in Figure 2.12.

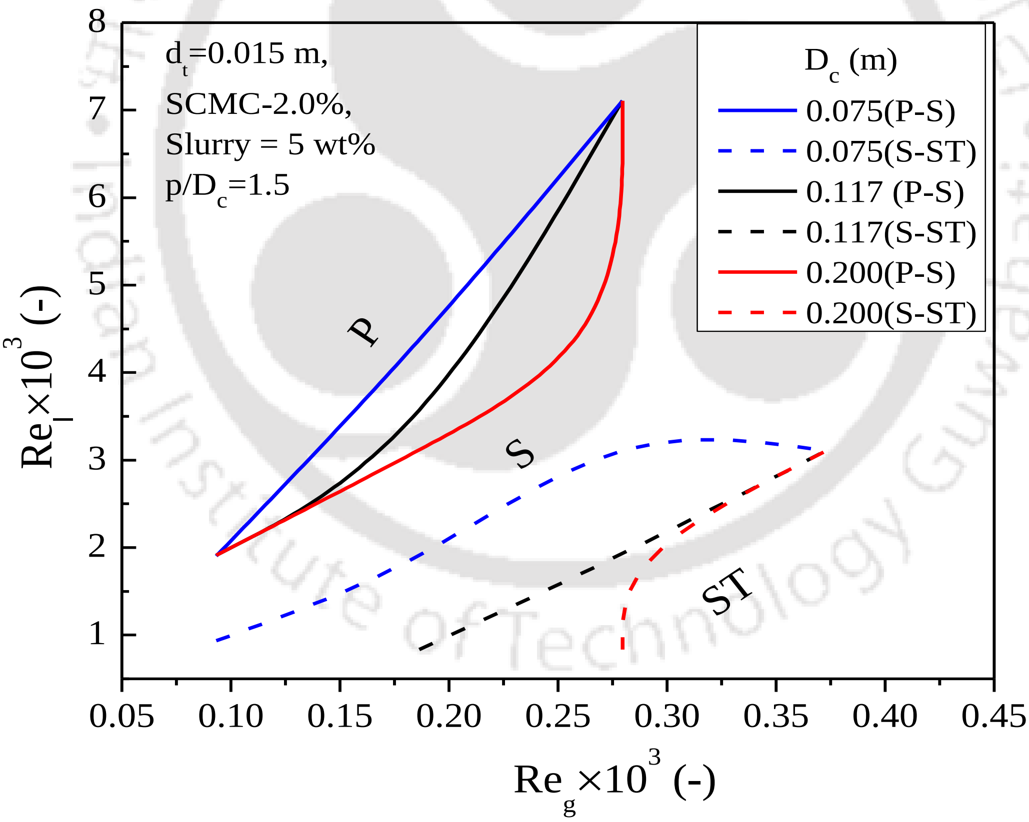

Figure 2.12: Effect of coil diameter on flow transitions of two-phase air-nonNewtonianfluid at constant coil diameter and pitch difference at 5wt% slurry. (P) plug flow, (S) slug flow, (ST) stratified flow, (P-S) plug to slug and (S-ST) slug to stratified flow.

Figure 2.12 shows the flow patterns observed at three different coil diameters at constant tube diameter (d_t = 0.015 m), SCMC (2.0 kg/m^3) and pitch difference (1.5). The lines represents the transition between plug to slug (P-S) and slug to stratified flow (S-ST). With increasing the coil diameter the transitions of flow patterns decreases. It was observed that by increasing coil diameter the range of plug flow and stratified flow were changed, but slug flow does not have any significant change as observed in non-slurry system. Figure 2.13 shows that the flow patterns observed at three different slurry concentrations at constant tube diameter (d_t = 0.009 m), coil diameter (D_c = 0.075 m), and pitch difference (p/D_c = 1.0).

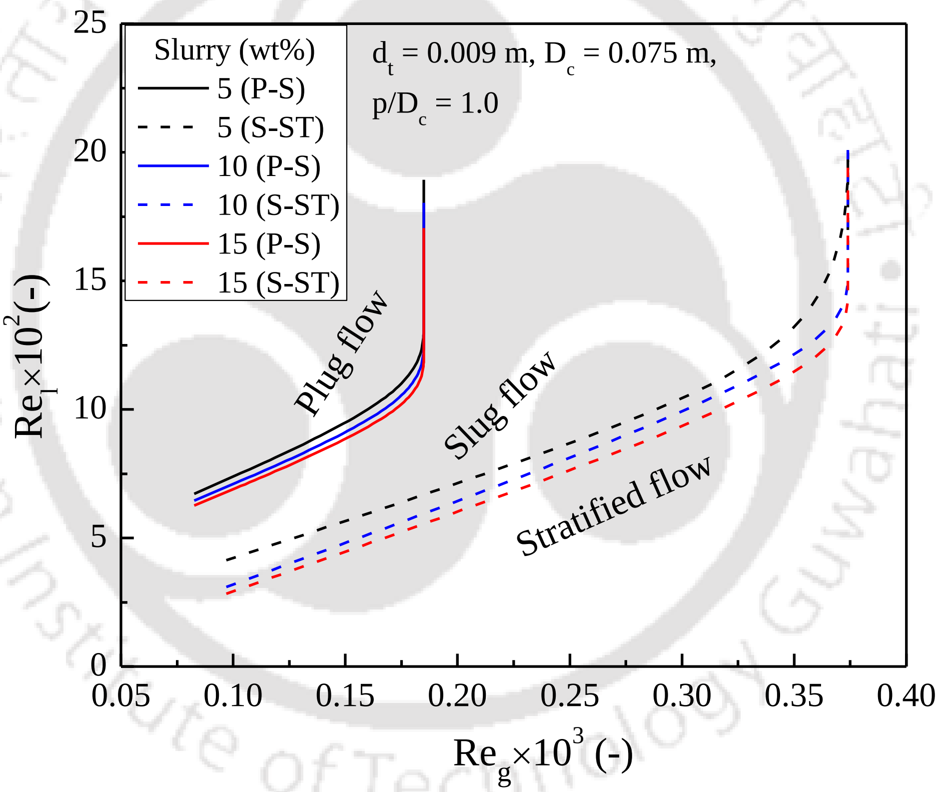

Figure 2.13: Effect of slurry on flow transitions of three phase flow at constant tube diameter, coil diameter and pitch difference. (P-S) plug to slug and (S-ST) slug to stratified flow.

The range of slurry Reynolds number was from $3.649 \leq Re_{sl} \times 10^2 \leq 21.546$ while for gas Reynolds number it was from $0.093 \leq Re_g \times 10^3 \leq 0.372$. The straight line represents the transition line between plug flow to slug flow and dashed line represents the transition between slugs to stratified flow. With increasing the slurry concentration a small change of flow patterns were observed.

2.4.3. Prediction of flow pattern transition

2.4.3.1. Analysis to predict the flow pattern transition by empirical correlation model

With the present experimental data, flow patterns occurs in two transitions, i.e., plug-slug flow and slug-stratified flow. The general simple empirical correlation to predict the flow pattern transition was developed with the different operating variables by regression analysis with experimental data as shown in Eqs. (2.13) and (2.14) as follows:

For the transition of plug to slug flow

$$\mathrm{Re}_l = 1.678\,\mathrm{Re}_g^{1.136}\left(\frac{D_c}{d_t}\right)^{-0.127}\left(\frac{L_p}{d_t}\right)^{-0.022}\left(\frac{L_t}{d_t}\right)^{0.082} \tag{2.13}$$

For the transition of slug to stratified flow

$$\mathrm{Re}_l = 0.009\,\mathrm{Re}_g^{1.563}\left(\frac{D_c}{d_t}\right)^{0.085}\left(\frac{L_p}{d_t}\right)^{-0.078}\left(\frac{L_t}{d_t}\right)^{0.317} \tag{2.14}$$

The parity plots of flow pattern transition with the experimental data are shown in Figures 2.6-2.8 by line profiles. The correlation coefficients, standard error of the correlations were found to be 0.967, 0.066 for plug to slug transition and 0.992, 0.077 for the transition of slug to stratified flow.

2.4.2.2. Prediction of flow pattern map by PNN model

A PNN has been trained by using the inbuilt function of MATLAB R2010a. For this purpose, total 598 data points were selected. 478 out of 598 data points has been used for training

(80%) and 120 data (20%) were used in test. During the PNN training, the selection of an optimum value of spread constant (smoothing parameter, σ) is very important as the shape of Gaussian function is totally influenced by this constant. The spread constant were chosen for a network that gives the minimum prediction error in training and test period. Some of the algorithms like genetic algorithm and trial error method (Hajmeer and Basheer 2002; Mao et al., 2000; Sharma et al., 2006) are used to find out the optimum spread constant. The spread constant (σ) was found by using trial and error method in the present study as it involves simple operation process. The optimum value of spread constant selected during training process has been used in testing steps to check the accuracy of the trained PNN and this spread constant has been used to predict the unknown data. Figure 2.14a shows the variation of regression constant with spread values for a set of 478 training data points.

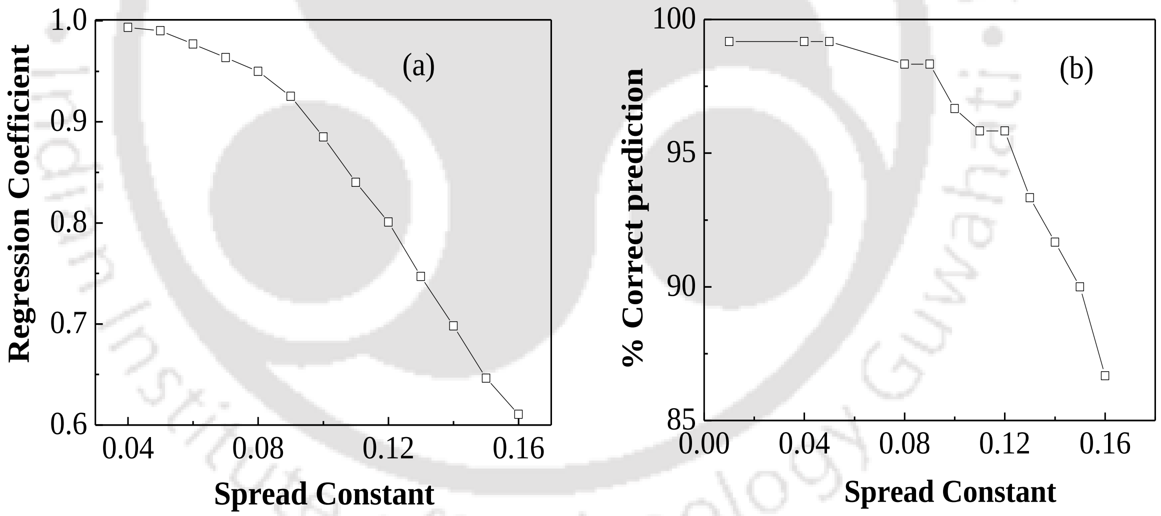

Figure 2.14: Selection of spread constant and regression constant for helical coil tube with different tube diameters: (a) variation of % regression constant with spread constant and (b) variation of % accuracy in prediction with spread constant.

Figure 2.14b shows variation of average percentage accuracy in the prediction with different spread values for the same set of data. From these two figures, it can be concluded that the trained PNN gives maximum average percentage accuracy in prediction (Figure 2.14b) at a spread constant value of 0.04 with regression coefficient of 0.993. The percentage accuracies in prediction for different flow patterns were found to be 100% for both plug and stratified flow and 98.75% for slug flow. Figure 2.15 shows the predicted flow pattern map and the experimental transition boundaries of different flow patterns. There is only one mismatching point and encircled it in the Figure 2.15a.

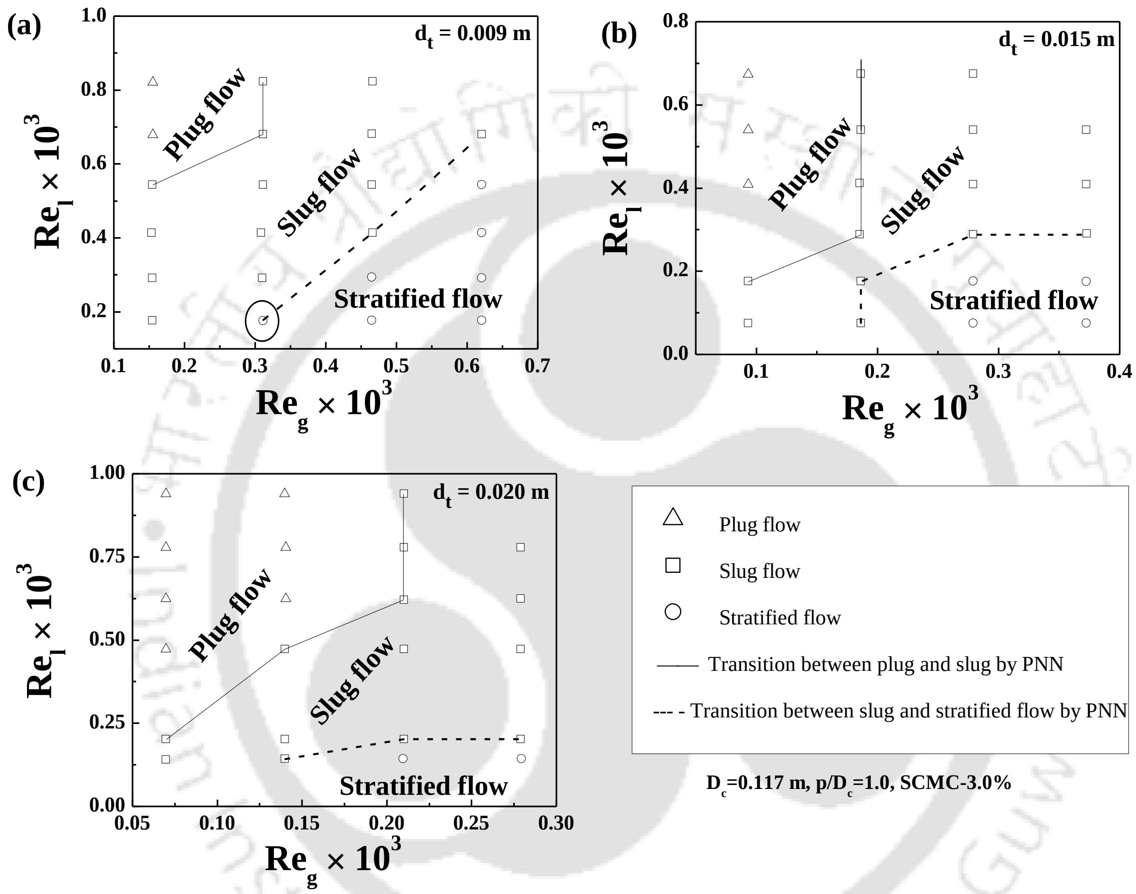

Figure 2.15: Comparison of PNN predicted flow pattern map with experimental data at three different tube diameter.

The PNN prediction achieves altogether 99.3% accuracy (average % accuracy of all three flow patterns). The accuracy of prediction strongly depends on the number of data points used in the PNN training. Finally PNN had predicted successfully with the flow pattern maps with the good accuracy $0.015 \leq d_t \leq 0.020$ m, whereas $d_t \leq 0.009$ m shows less accuracy compared to other tube diameters.

2.5. Conclusions

The flow patterns and their transitions of air-non-Newtonian two-phase flow in vertically helical coil tubes with various geometrical variables have been experimentally investigated. The experiments were conducted with three different tube diameters, coil diameters, pitch differences and liquid concentrations. Three different types of flow patterns namely plug, slug and stratified flow were observed from present experimental study. The flow patterns of two-phase air-non-Newtonian that were not similar compared to air-Newtonian at a particular conditions. In both cases slug flow appeared as intermittent region. With increasing coil diameter, plug and stratified flow was affected but there was no change in slug flow. When a small pitch difference increased, plug flow is resulted without any change in slug and stratified flow. The flow pattern transitions among the plug, slug and stratified pattern shifted by changing liquid concentrations at a particular geometrical variables. Probabilistic neural network (PNN) was successfully developed for two-phase helical coil system to predict the flow patterns and their transition boundaries. Correlation model was also proposed for flow pattern transitions of air-non-Newtonian fluids which may be useful for further understanding of multiphase flow in helical pipe and their installation in industry.

Nomenclature

A_t	Area of tube (m)
d_t	Tube diameter (m)
D_c	Coil diameter (m)
De	Dean Number $\left(= \mathrm{Re}\sqrt{d_t / D_c}\right)$ (-)
L_p	Pitch length (m)
L_t	Tube length (m)
p/D_c	Pitch difference (-)

Re Reynolds number for non-Newtonian $\left(= \left(\frac{d_t^n U_{sl}^{2-n} \rho_l}{8^{n-1} K} \right) \left(\frac{4n}{3n+1} \right)^n \right)$ (-)

SCMC Sodium Carboxymethyl cellulose

U_{sg} Gas superficial velocity (m/s)

U_{sl} Liquid superficial velocity (m/s)

Greek Letters

ρ Density (kg/m^3)

μ Viscosity (kg/m.s)

σ Surface tension (N/m)

Subscripts

c Coil

g Gas

l Liquid

m Mixture

References

- Abulnaga, B., 2002. Slurry systems handbook, McGraw-Hill Handbooks, New York.
- Akagawa, K., Sakaguchi, T., Ueda, M., 1971. Study on a gas-liquid two-phase flow in helically coiled tubes. Bulletin JSME 14, 564-571.
- Banerjee, S., Rhodes, E., Scott, D.S., 1967. Film inversion of co-current two-phase flow in helical coils. AlChE J. 13, 189-191.
- Banerjee, S., Rhodes, E., Scott, D.S., 1969. Studies on co-current gas-liquid flow in helically coiled tubes I. flow patterns, pressure drop and holdup. Can. J. Chem. Eng. 47, 445–453.

- Basheer, I.A., Hajmeer, M., 2000. Artificial neural networks: fundamentals, computing, design, and application. J. Microbiol. Methods 43, 3-31.
- Biswas, A.B., Das, S.K., 2008. Two-phase frictional pressure drop of gas–non-Newtonian liquid flow through helical coils in vertical orientation. Chem. Eng. Proc. 47, 816–826.
- Cacoullos, T., 1966. Estimation of a Multivariate Density. Ann. Inst. Stat. Math. 18, 179-189.
- Chhabra, R.P., Richardson, J.F., 1999. Non-Newtonian Flow: Fundamentals and Engineering Applications. Elsevier Science.
- Ellahi, R., 2013. The effects of MHD and temperature dependent viscosity on the flow of non-Newtonian nano-fluid in a pipe: Analytical solutions. Applied Math. Inf. Sci. 37, 1451-1457.
- Ellahi, R., 2014. The Thermodynamics, Stability, Applications and Techniques of Differential Type: A Review. Rev. Theor. Sci. 2, 116-123.
- Hajmeer, M., Basheer, I., 2002. A probabilistic neural network approach for modelling and classification of bacterial growth/no-growth data. J. Microbiol. Methods 51, 217-226.
- Mao, K.Z., Tan, K.C., Ser, W., 2000. Probabilistic neural-network structure determination for pattern classification. IEEE T. Neural Network. 11, 1009-1016.
- Masters, T., 1995. Advanced algorithms for neural networks: a C++ sourcebook. John Wiley & Sons, Inc. New York, NY, USA.
- Mujawar, B.A., Rao, M.R., 1981. Gas–non-Newtonian liquid two-phase flow in helical coils. Ind. Eng. Chem. Proc. Des. Dev. 20, 391–397.
- Parzen, E., 1962. On Estimation of a Probability Density Function and Mode. Ann. Math. Stat. 33, 1065-1076.

- Ripple, G. R., Eidt, C.M., Jordan, H.B., 1966. Two-phase flow in a coiled tube. Pressure drop, Holdup, and Liquid phase axial mixing. Ind. Eng. Chem. Proc. Des. Dev. 5, 32-39.
- Saxena, A.K., Schumpe, A., Nigam, K.D.P., Deckwer, W.D., 1990. Flow regimes, hold-up and pressure drop for two phase flow in helical coils. Can. J. Chem. Eng. 68, 553–559.
- Sharma, H., Das, G., Samanta, A.N., 2006. ANN-based prediction of two-phase gas-liquid flow patterns in a circular conduit. AlChE Journal 52, 3018-3028.
- Specht, D.F., 1990. Probabilistic Neural Networks. Neural Networks 3, 109-118.
- Thandlam, A.K., Mandal, T.K., Majumder, S.K., 2015. Flow pattern transition, frictional pressure drop, and holdup of gas non-Newtonian fluid flow in helical tube, Asia Pac. J. Chem. Eng. 10, 422-437.
- Vashisth, S., Nigam, K.D.P., 2007. Experimental investigation of pressure drop during two-phase flow in a coiled flow inverter. Ind. Eng. Chem. Res. 46, 5043-5050.
- Vashisth, S., Kumar, V., Nigam, K.D.P., 2008. A review on potential applications of curved geometries in process industry. Ind. Eng. Chem. Res. 47, 3291–3337.
- Whalley, P.B., 1980. Air-water two-phase flow in a helically coiled tube. Int. J. Multiphase flow 6, 345–356.
- Zeeshan, A., Ellahi, R., 2013. Series Solutions for Nonlinear Partial Differential Equations with Slip Boundary Conditions for non-Newtonian MHD Fluid in Porous Space. Applied Math. Inf. Sci. 7, 257-265.

CHAPTER-3

GAS HOLDUP AND PRESSURE DROP CHARACTERISTICS

In this chapter gas holdup and pressure drop characteristics in two and three-phase system in helical coil are investigated with Newtonian and non-Newtonian systems. The interfacial shear stress in helical coil with air-Newtonian and non-Newtonian liquid has been analyzed by developing a dynamic interaction model. The model equation has been developed based on the flow regimes, drag at interface and the wettability effect of the liquid. Also the intensity factor of friction pressure of two-phase flow in the helical coil is analyzed and correlated with the dynamic, geometric and physical variables.

3.1. Introduction

Pressure drop and holdup are important parameters for design of a process unit. The knowledge of pressure drop gives the pattern of energy dissipation, helps in modeling the system and forms the basis of assessment of performance of the equipment. In order to predict the two-phase pressure drop and holdup in a coiled tube, the most widely used correlations are based on Lockhart-Martinelli (L-M) parameter (Lockhart and Martinelli 1949). Most of the researchers used the L-M method to correlate their experimental data on two-phase holdup while others modified the L-M parameters to fit their experimental data. Ripple et al. (1966) carried out experimental work on coiled tubes and observed that pressure drop for such systems satisfied the L-M correlation. They found that the in-situ gas holdup (ε_g) was in good agreement with that predicted by the L-M curve, at higher valves of X, but it was found that ε_g values were higher at lower values of X. They attributed this difference to the downward flow orientation in the coiled tubes. They also pointed out that the liquid holdup was influenced by liquid properties rather than gas properties. Xin et al. (1996) observed that two-phase pressure drop and holdup depend not only on the L-M parameter but also on the flow rates. They found good agreement between the holdup data and the L-M correlation. Banerjee et al. (1969) investigated the gas-liquid flow through transparent coils with different tube diameters, coil diameters, and helix angles. They concluded that Baker's plots (Baker 1954) adequately predicted the flow patterns and reported that their experimental values of liquid holdup ε_l agreed with those predicted by the L-M curve within ± 30%. They modified the L-M correlation to satisfy their experimental data on holdup. Kasturi and Stepanek (1972) proposed correlations for holdup and pressure drop in terms of different conditions (air- water, air-corn-sugar-water, air-glycerol-water and air-butanol-water) that could account more fundamentally for the complex behavior of the two-phase flow than the simple correlation by using Lockhart-Martinelli (Lockhart-Martinelli 1949) and Dukler's (Dukler et al., 1964) correlation. Holdup results were compared with Hughmark's correlation. They found that L-M correlation fitted better than Dukler's correlation but observed a systematic displacement of the curves for the various systems with the L-M plot. The curve for the most viscous corn sugar solution-air system was the lowest in the set of curves and the curve for the butanol-water-air system was highest. The same applied for the Hughmark's correlation for the holdup. They intuitively thought that the L-M parameter could be modified to take into account the effects of viscosity and holdup. Further, Kasturi and Stepanek (1972) proposed correlations for pressure drop and holdup in terms of new parameters that could account more fundamentally for the complex behavior of the two-phase flow than the simple correlation in terms of L-M parameters. Akagawa et al. (1971) also used the Hughmark (Hughmark 1962) correlation to correlate the gas holdup. Ali and Seshadri (1971) reported that the pressure drop is very high in the helical coil tube when compared to Archimedean spiral tube because of the compactness of the helical coil. On the other hand due to compactness of helical coil tube heat transfer rate is enhanced. Mujawar and Rao (1978) established a new dimensionless number and given an appropriate correlations for friction factor in coiled tubes in laminar conditions. Ali and Zaidl (1979) found that the pressure drop in the straight tube is less than both the coils for small Reynolds numbers whereas for higher flow rates, coils have lesser resistance to flow than straight tubes. Mishra and Gupta (1979a) studied the effect of coil diameter, pitch, and tube diameter on the frictional loss for Newtonian fluids, covering a wide range of variables and presented the pressure drop data in laminar and turbulent region. Ali and Zaidi (1980) carried out hydrodynamics studies for steady Newtonian fluid flow in a spiral coils. They found that the pressure drop of negative logarithmic spiral coil shows a higher resistance to flow. Mujawar and Rao (1981) pointed out that if the flow patterns were specified for two phase flow then the pressure drop could be successfully correlated by Lockhart-Martinelli method. Rangacharyulu and Davis (1984) carried out experimental work on helical coil tubes to study pressure drop and holdup for a system of air-liquid co-current upward flow and presented a new correlation for the two-phase frictional pressure drop. Saxena et al. (1990) conducted experiments to study the holdup for co-current upward and downward flow in coiled tubes. They found close similarities between the flow patterns in coiled tubes and those of inclined tubes reported by Spedding et al. (1982). Weisman et al. (1994) performed experiments on pressure drops in single and double helically ribbed circular tubes. They showed that swirling annular flow resulted at low qualities once a minimum liquid velocity is exceeded. Yamamoto et al. (1994) studied theoretically the effect of curvature, Dean Number and torsion on the flow in a helical pipe of circular cross-section and solved the equations numerically by applying the spectral method. They reported that the friction factor at a large curvature first increases from that of a toroidal pipe and then decreases to that of a straight pipe with increasing torsion. Xin et al. (1996) showed that the pressure drop of the two-phase flow in vertical helicoidally pipes depends on both Lockhart-Martinelli parameter and the flow rates which were represented by the superficial Reynolds number of water for low flow rates in small ratio of coil diameter to pipe diameter. Chen and Guo (1999) investigated the three-phase, oil-air-water flow in helical coils to study the effect of flow rate and liquid properties. They reported that the flow characteristics can be classified into more than four flow patterns and also suggested flow regime maps and correlation for pressure drop. Biswas and Das (2006) conducted an experiment to study the two-phase friction factor and holdup for Newtonian and non-Newtonian fluid flow through helical coil. They noted that the effect of helix angle ($0 - 12^0$) in liquid holdup is negligible. Mandal and Das (2003) studied the two-phase pressure drop and holdup for gas-Newtonian liquid flow through vertical helical coils. A summary of correlations and related parameters observed from the literature review is shown in Table 3.1.

Formulation of analysis tool, simulation of the systems behavior depends on different flow regimes, pressure drop etc. as a function of fluid properties. Especially the effect of change of apparent flow viscosity of non-Newtonian liquid on hydrodynamics and flow conditions are very important in industryy to reproduce the flow phenomena. It is required to study the hydrodynamic behavior of the gas-non-Newtonian liquid in a device before installation for industrial applications. The aim of the present study is to examine the effects of fluid flow on pressure gradient and holdup in two-phase, air-non-Newtonian liquid flow in vertical helical coil. Also the studies involve the analysis of friction factor of air-non-Newtonian liquid two-phase flow in helical coil. From the literature review, it is seen that correlations based on experiments exist for predicting the pressure drop, but none of these approaches have taken into account the contacting mechanism between the phases, effect of bubble formation, phase interaction due to movement of bubbles and the wettability effect on pressure drop in helical coil system and also with non-Newtonian system. A model is formulated based on mechanical energy balance within the framework of dynamic interaction of the phases. The model includes the effect of bubble formation, phase interaction or slip due to movement of gas as slug, friction at the wall of the conduit and the wettability effect of liquid on the pressure drop.

3.2. Theory of frictional pressure drop

Conservation of momentum principles for a mass of fluid flowing in an inclined pipe of constant cross-sectional area yields the following equation for single phase flow

$$\frac{dp}{dL} = \rho g + \left(\frac{dp}{dL}\right)_f + \left(\frac{dp}{dL}\right)_{rad} \tag{3.1}$$

The first term on the right side of Eq. (3.1) is the component of the pressure gradient due to hydrostatic head. The second term, $(dp/dL)_f$ is the pressure gradient due to viscous shear or friction loss. When fluid flows through a curved tube, it experiences a positive pressure gradient due to radial acceleration arising in the radial direction due to the centrifugal force, which can be written as (Vashishth et al., 2008)

$$(\Delta p)_{rad} = \frac{2\rho U^2 d}{D} \tag{3.2}$$

Mishra and Gupta (1979b) concluded from their experimental work that the effect of pitch on the friction factor can be eliminated if the coil diameter D is replaced by the diameter of curvature D_c given by

$$D_c = D\left[1+\left(\frac{b}{2\pi D}\right)^2\right] \tag{3.3}$$

Incorporating D_c instead of D in the mathematical definition of Dean number (the Dean number is defined as Re $(d/D)^{0.5}$, a significant number for identifying the dominating force between inertia and viscous force of flow in a curved tube) results a new number, referred to as the helical coil number, *He*, which can be expressed as

$$He_n = \mathrm{Re}_n\left(\frac{d_t}{D_c}\right)^{0.5} = D_e\left[1+\left(\frac{b}{2\pi D_c}\right)^2\right]^{-0.5} \tag{3.4}$$

As the pitch increases for the same coil curvature, the centrifugal force decreases at the same flow rate thus weakening the secondary flow field, and ultimately straight tube behavior is appeared (Lin and Tarbell 1980; Yamamoto et al., 1995; Vashisth et al., 2008). Applying a force balance to a differential element of a pipe, the wall shear stress can be expressed as,

$$\tau_w = \frac{d}{4}\left(\frac{dp}{dL}\right)_f \tag{3.5}$$

Viscous shear occurs primarily at the pipe wall. The friction factor is a dimensionless group representing the pressure loss due to friction and is defined as the ratio of wall shear stress (τ_w) to kinetic energy per unit volume which represents the relative importance of wall shear stress to the total energy losses. The Fanning friction factor is expressed as

$$f = \frac{2\tau_w}{\rho U^2} \tag{3.6}$$

Eqs. (3.5) and (3.6) yields

$$\left(\frac{dp}{dL}\right)_f = \frac{2 f\rho U^2}{d} \tag{3.7}$$

It is well known that friction factors have been successfully correlated for single-phase flow with two dimensionless groups called Reynolds number and relative roughness. For gas-liquid two-phase flow through a pipe, Eq. (3.1) becomes

$$\frac{dp}{dL} = g\rho_m + \frac{2 f_{2\phi}\rho_m u_m{}^2}{d} + \frac{2\rho_m u_m^2 d}{D} \tag{3.8}$$

where the subscript *m* refers to the mixture of gas and liquid. Normally mixture properties such as density and viscosity are calculated as weighted averages of the individual phase properties with input fraction or holdup of the phases as weighting factors. For mixture, density, $\rho_m = \alpha_g \rho_g + \alpha_l \rho_l$. The mixture velocity is defined as the sum of the superficial velocities of individual phases as $u_m = u_{sg} + u_{sl}$.

3.3. Experimental

The schematic of the experimental setup used in the present investigation are given in Figure. 2.2 in Chapter 2. The equipment and apparatus consisted of a cylindrical storage tank (S), centrifugal pump (P_m) for circulating the fluid, two rotameters (make: Five Stars Ltd., Mumbai) of different ranges R_{L1} and R_{L2} for measuring the flow rate of the fluid, and U-tube manometer (U) to measure the pressure difference across the helically coiled tube. Valves (V_1 to V_8) were used to control the flow rate of the liquid. The storage tank was of 100 liters capacity, the bottom side of the tank was connected to the suction side of the pump (P_m) through a globe valve (V_1). Another globe valve (V_8) was provided at the bottom of the storage tank to facilitate the periodic cleaning. Through the compressor, air was passed to the inlet of the tube. The discharge end of the pump was divided into two lines, one directly connected to rotameters (R_{L1}& R_{L2}) and the other to a by-pass line.

Table 3.1: Summary of work on two-phase hydrodynamics in helical coil reported in literature

Author	Parameters	Working Fluid	Correlation	Remarks
Mujawar and Rao (1981)	d_t = 1.21 cm; D_c = 17.4, 25.4, 61, 121 cm; p = 1.9, 2.6, 5.7, 13.6 cm; n = 2, 4, 6, 8; L_c = 262, 437, 480, 770 cm	Air-water, Helium, Sodium alginate (0.3-0.5%), SCMC (0.5-1.0%).	$\phi_l^2 = 1 + \frac{C}{X} + \frac{1}{X^2}$, $\phi_{G_c} = 1.85/(E_g)^{4.60}$, $\left(\frac{\Delta p}{\Delta L}\right)_{tp} = \left(\frac{\Delta p}{\Delta L}\right)_{sg} + C(n')(C_L)^b \frac{\rho_g V_{sg}^2}{g_c d}$ X is the Lockhart –Martinelli parameter ϕ is the pressure drop multiplier	Given a correlations for holdup and frictional pressure drop
Rangacharyulu and Davies (1984)	d_t = 11, 13 mm; Q_G = 1 - 10 m^3/s; Q_L = 0.04 - 0.75 m^3/s; 18.48< D_c/d_t < 23.4	Air - water, Air- glycerol, Air-Isobutyl alcohol	$\phi_g^2 - 1 = 0.05\,\mathrm{Re}_l (d_i/D_c)^{1/2} (u_t/C_o)^{-0.68} \left((g\mu_l^4)/(\rho_l\sigma_l^3)\right)^{0.18} (R_i/R_c)^{3.66}$ $C_0 = (\frac{R_g}{\rho_g} + \frac{R_l}{\rho_l})/(\frac{R_g}{\rho_g} C_g^2 + \frac{R_l}{\rho_l} C_l^2)$ C_0 is the stratified speed of sound, (m/hr)	Done pressure drop and holdup by using Lockhart and Martinelli

Hart et al. (1988)	d_t = 14.66 ± 0.04 mm; d_o = 17.66 ± 0.04 mm; n = 7, 8, 10, 11, 12, 13; L_c = 17 m	Air - Water	$f_c = f_s\left(1+\left[\frac{0.090De^{1.5}}{(70+De)}\right]\right),\ 0 \le \mathrm{Re} \le \mathrm{Re}_{crit}$ Re_{crit} = Critical Reynolds number	Friction factor for a pressure drop
Awwad et al. (1995)	d_t = 12.7, 19.1 25.4, 38.1 mm; D_C = 330, 340, 350, 360, 640, 650, 660 mm; α : 0.5 – 200; n = 4 - 14	Air -water	$\phi_L / \left[1+\frac{X}{C[F_d]^n}+\frac{1}{X^2}\right]\left(1+\frac{12}{X}+\frac{1}{X^2}\right)^{1/2}$ $F_d = Fr\left(\frac{d_t}{D_c}\right)^{0.1} = \frac{U_l^2}{gd_t}\left(\frac{d_t}{D_c}\right)^{0.1}$ X is the Lockhart –Martinelli parameter	Given correlation for pressure drop and holdup
Xin et al. (1996)	d_t = 12.7, 19.1, 25.4, 38.1 mm; D_c = 305, 609 mm	Air - water	$\phi_L / \left[1+\frac{20}{X}+\frac{1}{X^2}\right]^{\frac{1}{2}} = 1+\frac{X}{65.45F_d^{0.6}}$, for $F_d \le 0.1$ $\phi_L / \left[1+\frac{20}{X}+\frac{1}{X^2}\right]^{\frac{1}{2}} = 1+\frac{X}{434.8F_d^{1.7}}$, for $F_d > 0.1$ $F_d = F_r\left[\frac{d}{D}\right]^{1/2}(1+\tan\beta)^{0.2}$	Produced correlation for pressure drop and holdup

Chen and Guo (1999)	d_t = 39 mm; D_c = 265, 522.5 mm; L_c : 4320, 6760 mm	Oil- air - water	$\phi_L^2 = f(\theta)\left(1+\frac{C}{X}+\frac{1}{X^2}\right)$, where $\phi_L^2 = \frac{(dP)_{tp}}{(dL)_l}$, $X^2 = \frac{(dP)_{ll}}{(dL)_{\lg}}$ X is the Lockhart –Martinelli parameter	Given a correlation for holdup
Ali (2001)	d_t = 0.603, 0.464 cm D_c = 1.6225, 22.448 cm; p = 1,5 cm L_C =223.8, 112.3, 111.5, 226.3, 113.2, 426, 213 cm; n = 3, 6	Air - water	$EuG_{rhc} = 21.88\,\mathrm{Re}^{-0.9}$, $\mathrm{Re} \le 500$ $EuG_{rhc} = 5.25\,\mathrm{Re}^{-2/3}$, $500 \le \mathrm{Re} \le 6300$ $EuG_{rhc} = 0.56\,\mathrm{Re}^{-2/5}$, $6300 \le \mathrm{Re} \le 10{,}000$ $EuG_{rhc} = 0.09\,\mathrm{Re}^{-1/5}$, $\mathrm{Re} \ge 10{,}000$ where $G_{rhc} = 0.85\,\mathrm{e}0.15/\mathrm{Lc}$	Given correlation for pressure drop in single phase and multi-phase flow
Mandal and Das (2003)	di = 0.01, 0.013 m; Dc = 0.131 - 0.222 m; Θ = 0, 4, 8, 12; n = 12, 13, 15, 16, 19, 20	Water, 1% Amyl alcohol, 30% Glycerin	$\Delta P_{ftp} = \Delta P_{tp} - \frac{M_l + M_g}{Q_l + Q_g} hg$	Produced correlation for Pressure drop

Biswas and Das (2006)	d_t = 9.33, 9.7, 12 mm; D_c = 176, 178, 216, 266 mm;	Air - CMC	$\Delta P_{fl}^{'} = \left[(\mu_{eff})_{wtp} / (\mu_{eff})_{wl}\right] \Delta P_{fl}$	Given correlation for pressure drop
Gupta et al. (2011)	d_t = 4.5, 6.5, 7.94, 9.53, 12.01 mm; L_c = 3.98,5 m; D_c = 114.3, 266.85, 323.1, 462, 655 mm; p = 40, 60, 100, 200, 300 mm	Air - water	$f_c = f_s(1+0.903 N_{Gn}^{0.227})$, for $N_{Gn} \le 70$ $f_c = f_s(1+0.525 N_{Gn}^{0.516})$, for $N_{Gn} \ge 70$ where $f_c = f_s(1+aN_{Gn}^{b})$, $f_s = 16/N_{\mathrm{Re}}$ $N_{Gn} = N_{\mathrm{Re}} \times \delta = N_{\mathrm{Re}} \left\{ \dfrac{\pi^2 (D_c/d_t)}{\left[\pi^2 (D_c/d_t)\right]^2 + (p/d_t)^2} \right\}$ NGn = Germano number	Developed correlation for coil and the straight tube

The by-pass was provided with a globe valve V_2 to control the flow through rotameters. Two more valves V_3 and V_4 were provided at the inlet of rotameters to operate the rotameters either separately or in combination. Two solenoid valves were fixed in the inlet (entrance) and another one in outlet (Exit). Solenoid valves (SV1 and SV2) (Techno company) are of range of maximum 10 kg/cm^2). The helical coils were made using transparent thick-walled polyethylene tube. Two pressure taps (P_{T1} and P_{T2}) at the beginning and end of the coil were provided to measure pressure drop across the coil. These taps were connected to the limbs of a U-tube manometer (M1). One more U-tube manometer (M2) is used for measuring the pressure drop in horizontal side which is connected to the pressure taps (P_{T3} and P_{T4}) in horizontal tube at its outlet. One more tap is created for collecting fluid for holdup. Compressor (C) is connected to the gas rotameter (R_G), and this gas rotameter connected the inlet tube for two phase flow. Water and the air are sent to the inlet of the coil tube and with the second coil onwards it gets constant flows of air and water. The background of the test section consists of graph sheet to know the size of the bubble/drop flowing through the test section. The equivalent bubble diameter which is observed in the coil is measured by the image analysis software (Digimizer) from air gap length observed in test section. Water and air are pumped into the test section of helical coil by using centrifugal pump (for water) and compressor (for Air). The flow rate of water is measured through pre-calibrated rotameters R_{L1} and R_{L2}. The flow rate of air is measured through the gas pre-calibrated rotameter. Holdup at different flow rates is measured by quick closing valve technique. The quick closing valves (Solenoid valves) SV1and SV2 in the setup are placed at the two ends of the test section. These quick closing valves (Solenoid valves) are arranged in the entry of the coil and exit of the coil. There is electrically adjustment for simultaneous closing of the two valves to trap the flowing mixture instantaneously. Once the system reaches steady state at particular flow rate of two fluids, the flowing mixture is arrested by closing these two valves in the test section instantaneously. By knowing the volume of liquids, gas holdup is calculated from the following equation

$$\varepsilon_g = \frac{v_T - v_L}{v_T} \tag{3.9}$$

where, ε_g = gas holdup, v_L = volume of water, v_T = total volume of gas liquid mixture. Physical properties of the systems are given in Table 2.1 in chapter 2. The uncertainty of the experimental data is shown in Table 3.2.

Table 3.2: Typical uncertainties of the gas holdup at constant tube diameter (d_t = 0.015 m), coil diameter (D_c = 0.117 m)

U_{sl} (m/s)	U_{sg} (m/s)	Range of mean*	N	Range of STDEV* ($\times 10^{-3}$)	Range of uncertainty* ($\times 10^{-3}$)	Range of relative uncertainty* %
0.189-1.132	0.094	0.438 - 0.601	6.0	4.415-5.432	1.802- 2.217	0.299 - 0.507
0.189-1.132	0.189	0.452 - 0.667	6.0	2.486-4.236	1.014-1.735	0.225 - 0.261
0.189-1.132	0.283	0.467 - 0.713	6.0	2.817-4.035	1.652-7.411	0.355 - 1.089
0.189-1.132	0.377	0.503 - 0.748	6.0	4.023- 4.681	1.645-1.917	0.256 - 0.328

* The theory to calculate the values is given in chapter 2 in equations (2.10 – 2.12)

Each value of gas holdup in 3rd column corresponds to the mean of 6 data points (i.e., N=6). Relative uncertainty is calculated from standard uncertainty and mean value of the corresponding data set.

3.4. Results and discussion

The influence of the holdup and pressure on transport phenomena in a gas–non-Newtonian liquid system is a strong incentive in helical coil reactor. In fact, reported studies on transport phenomena under pressure in different gas–liquid contactors diverge. In the following section the effects of different operating variables on the pressure drop and holdup have been discussed based on the present study.

3.4.1. Variations of the two-phase pressure drop

3.4.1.1. Effect of flow rate and concentration of SCMC on two-phase pressure drop

The variation of pressure drop with the change in concentration of the non-Newtonian liquid (SCMC) is shown in Figure 3.1. It is clear from the graph that the two-phase frictional pressure drop per unit length of coil increases with increasing liquid viscosity. The liquid has a retarding effect as its viscosity increases, and also the slip is expected to be higher in a viscous liquid. Hence, the two-phase pressure drop per unit length of coil increases with increasing liquid viscosity.

It was found that as Reynolds number increased, the friction factors decreased and were much higher than the friction factors calculated from standard correlations available for laminar (Metzner and Reed 1955) and turbulent (Dodge and Metzner 1959) flow of non-Newtonian fluids in straight pipes. But the difference in friction factors for straight and coiled pipes is not significant when the flow in turbulent, whereas the difference is appreciable in the case of laminar flow owing to the higher contribution of centrifugal forces towards total pressure drop values. In the case of turbulent flow, the suppressed motion of secondary flows by dominating inertia force is responsible for smaller difference in friction factors between curved and straight pipes. Moreover, the onset of turbulences delayed in all the coils owing to the fact that transverse motions of turbulent flow are suppressed by centrifugal forces.

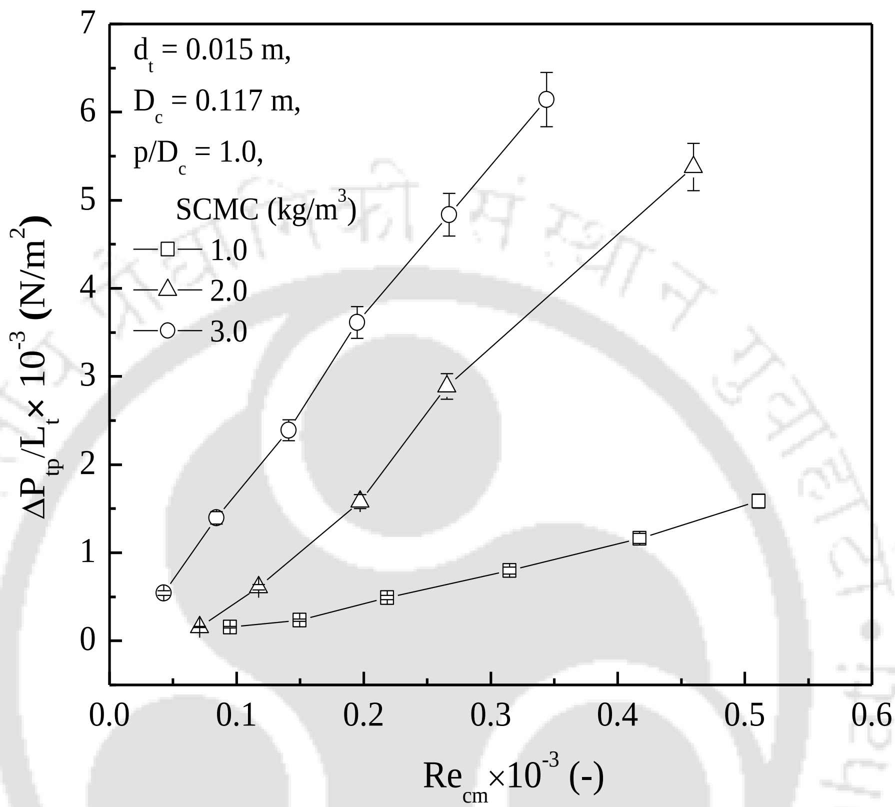

Figure 3.1: Variation of the pressure drop with coil Reynolds number at different SCMC solutions

3.4.1.2. Effect of tube to coil diameter ratio on two-phase pressure drop

As the coil diameter deceased, the tube to coil diameter ratio increased which results in increase in pressure drop as shown in Figure 3.2. This is because of increase in frictional resistance due to more centrifugal action on the wall of the tube. The secondary flow generation also contributed the increase in interfacial stress which resists to flow with high pressure. This action is relatively lower in the laminar flow. As the flow rate increases, the centrifugal action predominates over the hydrostatic pressure which may contribute more pressure gradient relative to laminar flow.

3.4.1.3. Effect of pitch length to coil diameter ratio on two-phase pressure drop

To identify the effect of pitch length on two-phase frictional pressure drop in laminar region, various lengths of pitch were selected. It was observed from the experimental results that the effect of pitch length is significant at moderate to high Reynolds number (Re_n) in the laminar region while at low Reynolds number the effect is negligible as shown in Figure 3.3 for various concentrations of SCMC solution ranging from 0.5% to 3% as per present experiment. Xin et al. (1996) concluded that the helix angle had some effect on the frictional pressure drop whereas Banerjee et al. (1969) observed that the two-phase frictional pressure drop was independent of helix angle in the laminar region which is a function of pitch length.

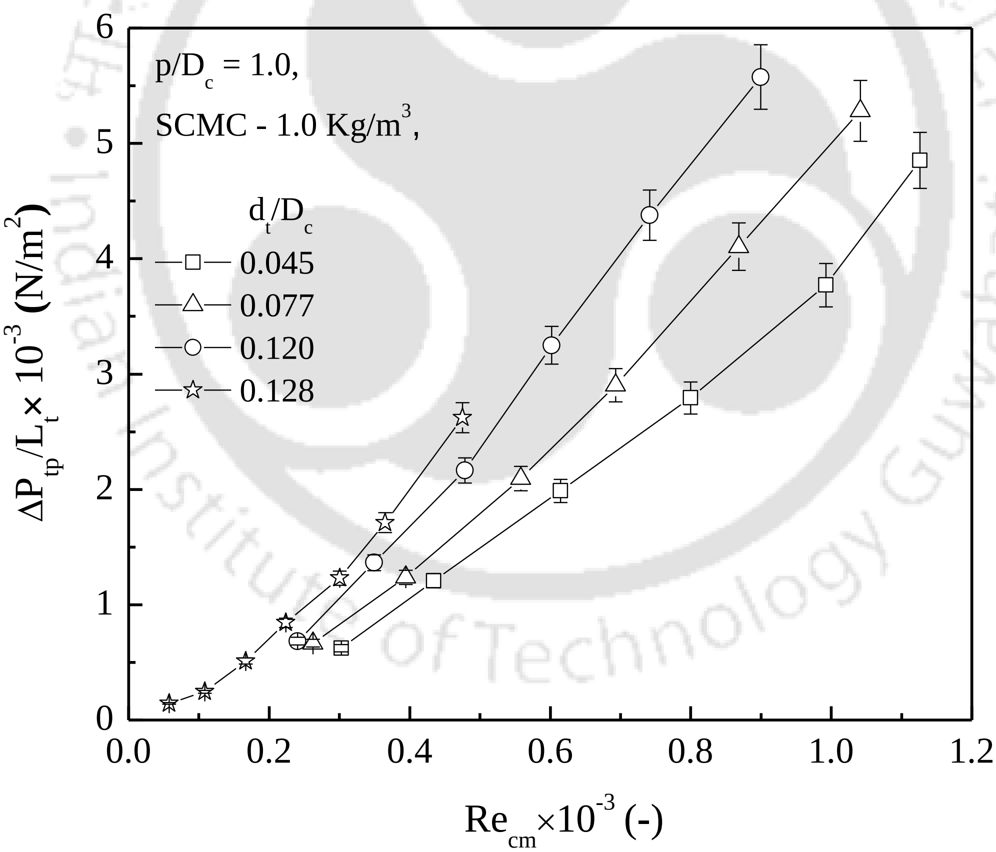

Figure 3.2: Variation of the pressure drop with tube to coil diameter

3.4.1.4. Effect of bubble size and phase interaction on two-phase pressure drop

The bubble formation is one of the decisive criteria to raise in pressure drop in the coil tube. At lower coil diameter, since the centrifugal action is higher, the more interfacial energy distributed in the motion of the liquid to generate the more smaller bubble tends to change the flow pattern from bubble flow to plug flow. The energy distributed to form the plug flow is inversely related to the size of the gas bubble as $E_b = (6A_t G\sigma)/(d_b \rho_g)$. The equivalent bubble diameter is a function of mixture Reynolds number ($d_{be} = \mathrm{Re}_m^{-0.002}$). As the Reynolds number increases the bubble diameter decreases which results in the formation of plug flow pattern in the helical coil. This is due to the more momentum transfer between the phases to break the interface of the phases and formation of smaller bubble. For slug flow, it was found opposite in nature. This is due to elongation of the gas slug for dominating the wall shear stress to the curvature effect.

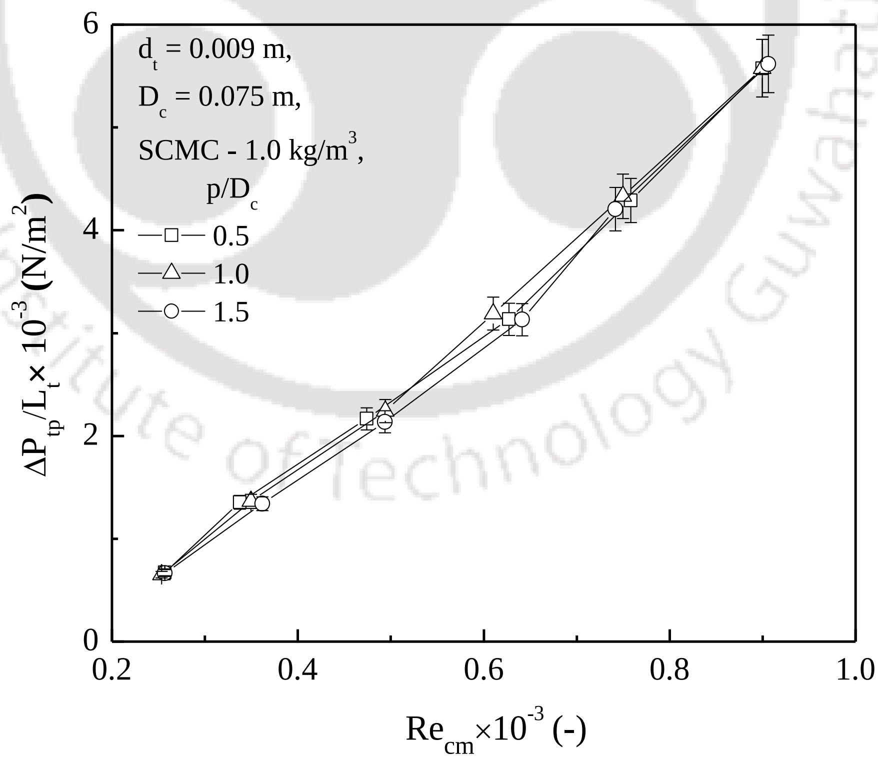

Figure 3.3: Variations of pressure drop with pitch to coil diameter

3.4.2. Variations of the three-phase pressure drop

Variation of frictional pressure drop with slurry flow rate is shown in Figure 3.4. It was observed that frictional pressure drop for three-phase system increased with increase in slurry flow rate. It was also observed that frictional pressure drop for three-phase system increased with increase in gas flow rate.

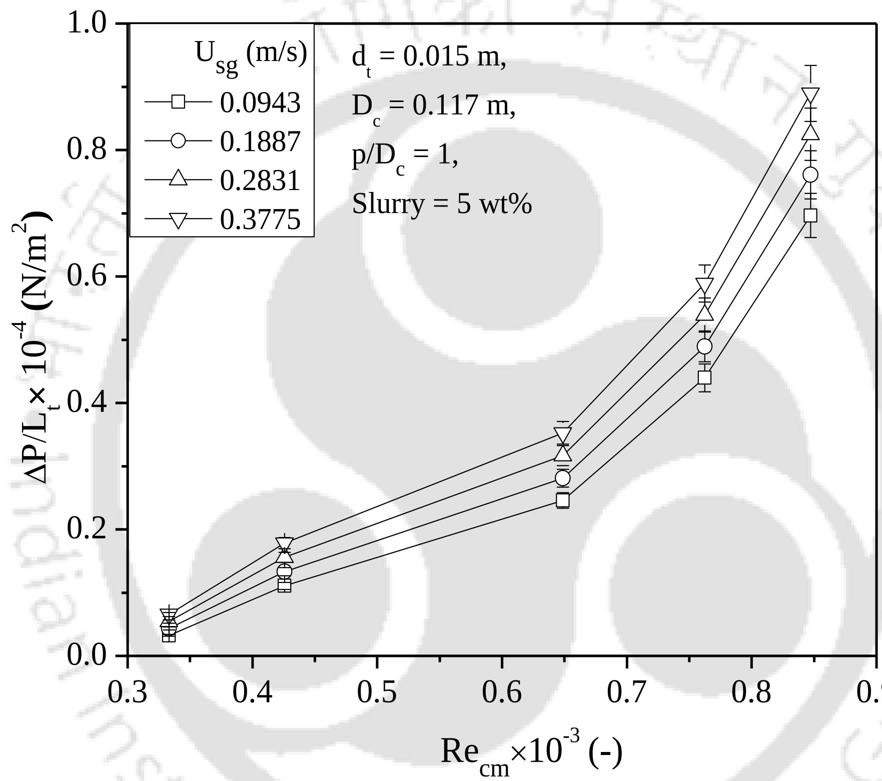

Figure 3.4: Variation of frictional pressure drop with slurry flow rate

The variation of frictional pressure drop for three-phase system is shown in Figure 3.5. From the figure it is observed that three-phase frictional pressure drop decreases with increase in pitch at constant gas and slurry flow rates. The variation of frictional pressure drop for three-phase system with Kieselguhr concentration is shown in Figure 3.6. The frictional pressure drop increases with increase in Kieselguhr concentration at constant gas flow rate and constant slurry flow rate due to increase in viscosity with concentration.

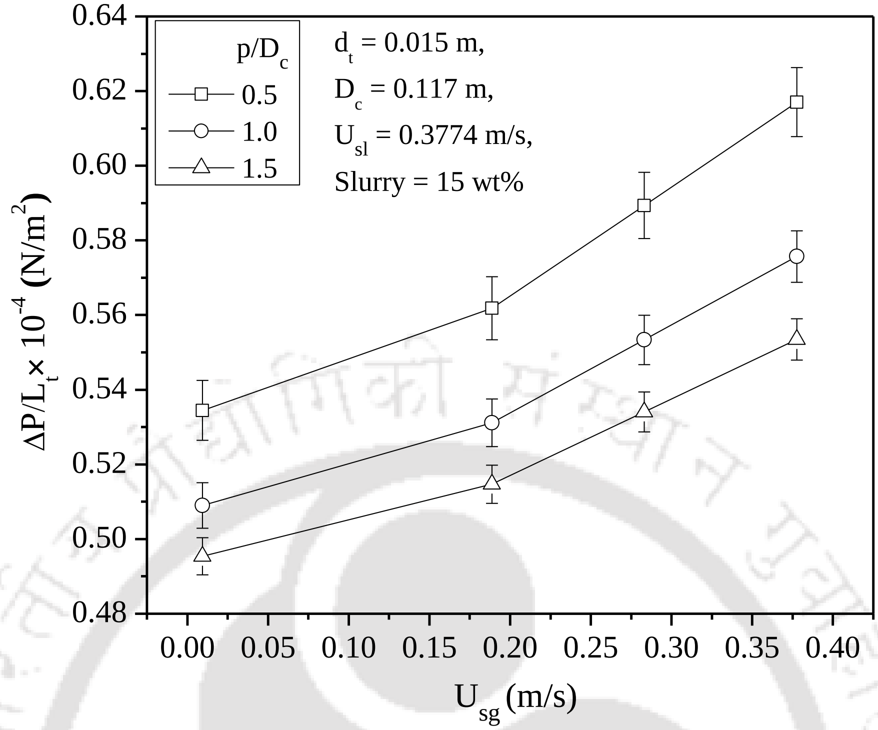

Figure 3.5: Variation of frictional pressure drop with pitch

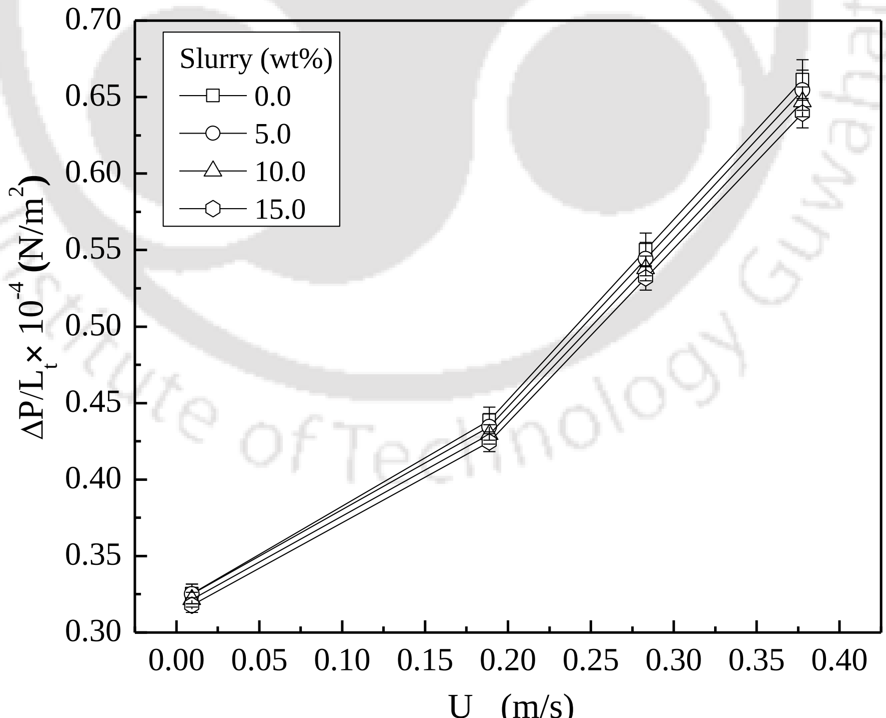

Figure 3.6: Variation of frictional pressure drop with kieselguhr concentration

3.4.3. Gas holdup and its analysis

Figure 3.7 shows the effect of gas flow rate on gas hold-up for different Newtonian and non-Newtonian fluids at a constant tube diameter, coil diameter, pitch difference and liquid concentration. It was observed that at constant liquid flow rate when gas flow rate increases, the gas holdup also increases. Comparing gas holdup on Newtonian and non-Newtonian fluids, non-Newtonian having much effect as shown in Figure 3.7. By decreasing liquid velocity at constant gas flow rate, gas holdup increases in both Newtonian and non-Newtonian fluids. With increasing the coil diameter at the same length of the tube, number of turns will get decrease. Gas holdup depends on number of turns. When number of turns decreases the gas holdup decreases. Centrifugal force is mainly depends on curvature of the tube, with increasing pitch difference the curvature of the tube was decreased. It was also observed that the gas holdup decreased as the slurry concentration increased. The gas hold up data was analyzed by Bankoff's principle (Bankoff 1960). As per Bankoff's principle, the gas holdup is related to the liquid to gas density ratio and the gas mass fraction which can be expressed as

$$\varepsilon_g \propto \left[1-\frac{\rho_g}{\rho_l}\left(1-\frac{1}{x}\right)\right]^{-1} \tag{3.10}$$

where x is the gas mass quality which is defined as the gas mass flow rate upon total gas-liquid mass flow rate. The proportionality constant is called Bankoff's parameter K. The parameter was found to be dependent on the experimental conditions. In the present case of helical coil system, the parameter was estimated by the regression analysis of the experimental values of gas holdup by incorporating the dimensional analysis of wide range of the operating variables. The final correlations for gas holdup at different flow patterns can be represented as:

$$\varepsilon_g / \psi = \lambda \left(\frac{\mu_m}{\rho_m U_m d_t} \right)^a \left(\frac{\sigma_L}{\rho_m U_m d_t^2} \right)^b \left(\frac{D_c}{d_t} \right)^c \left(\frac{L_p}{d_t} \right)^d \left(\frac{L_t}{d_t} \right)^e \tag{3.11}$$

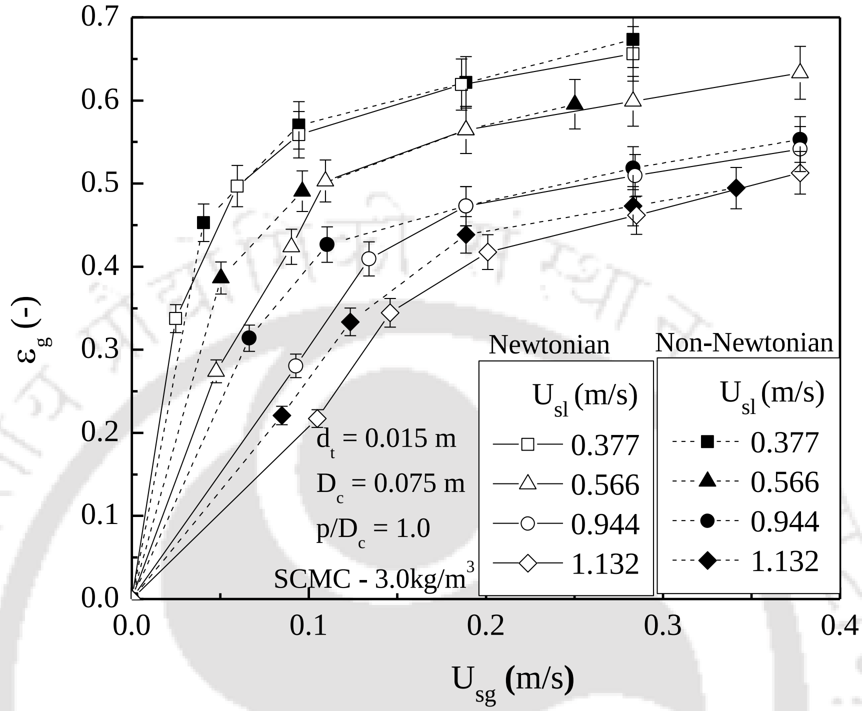

Figure 3.7: Effect of fluid flow rate on gas holdup

where $\psi = \left[1 - \frac{\rho_g}{\rho_l} \left(1 - \frac{1}{x} \right) \right]$. The values of the parameters (λ and a to e) in the equation with the correlation coefficients and standard error for different flow pattern are shown in tabular format in Table 3.3. The details of regression analysis is shown in Appendix –I.

3.4.4. Frictional pressure drop and its analysis

It was observed from the experimental results that the two-phase frictional pressure drop per unit length of coil depends on the different gas velocities, SCMC concentrations, tube diameter, coil diameter and pitch difference, as shown in Figure 3.8. The frictional pressure drop increases with increasing gas velocities (Figure 3.8(a)). Similarly with increasing liquid velocity the pressure drop increases. It was observed that when the coil diameter increase for various gas velocities the pressure drop is decreased as shown in Figure 3.8(b). As the coil diameter increases with the same length of the tube, the numbers of turns decreased. When number of turns decreased the curvature effect decreases. At any particular coil diameter the centrifugal force acting on the liquid phase are higher than the gas phase. The centrifugal force depends on number of turns in the coil tube. Number of turns increase the centrifugal force. Increasing tube diameter frictional pressure drop increased at various constant variables as shown in Figure 3.8(c). Increasing the pitch difference the coiling effect decreased, which results the decrease in slip effect. Increasing pitch difference for liquid velocity the frictional pressure drop is decreased as shown in Figure 3.8d).

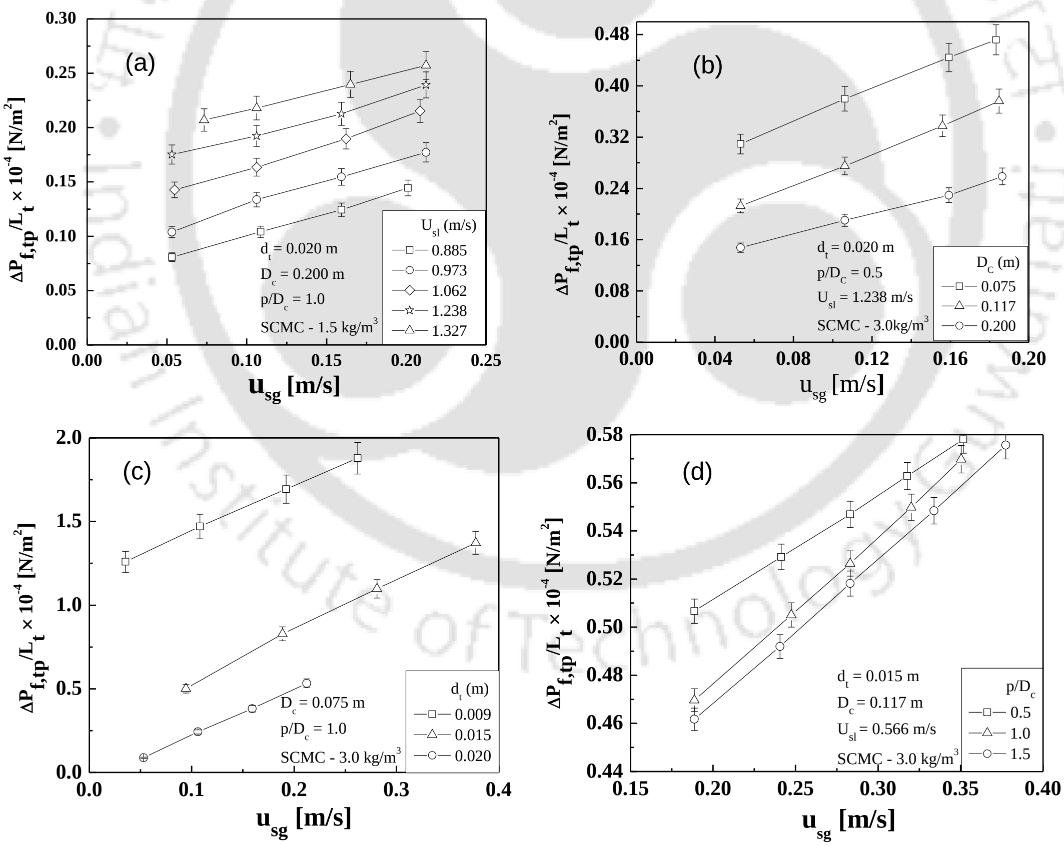

Figure 3.8: Effect of different variables ((a) superficial liquid velocity, (b) coil diameter, (c) tube diameter and (d) pitch difference) on frictional pressure drop

Table 3.3: The parameter of correlations (Eq. (3.11)) for holdup (α_g / ψ)

Flow patterns	λ	a	b	c	d	e	R^2	SE
Plug Flow	52.116	0.214	0.146	-0.590	-0.066	0.062	0.984	0.052
Slug Flow	5.652	0.137	-0.055	-0.307	-0.066	0.074	0.957	0.044
Stratified flow	7.336	0.143	-0.055	0.012	-0.020	-0.171	0.904	0.034

3.4.4.1. Analysis of frictional pressure drop by Lockhart–Martinelli (L-M) model

In order to predict the two-phase frictional pressure drop and holdup in a coiled tube, the most widely used correlations are based on Lockhart-Martinelli (L-M) parameter. Most of the researchers used the L-M method to correlate their experimental data for two-phase frictional pressure drop and holdup while others developed a modified expression for L-M parameters to fit their experimental data (Kasturi and Stepanek 1972; Stepanek and Kasturi. 1972; Mujawar and Rao 1981; Rangacharyulu and Davies 1984; Saxena et al., 1990; Xin et al., 1996; Xin et al., 1997; Bandaru and Chhabra 2002). The Lockhart–Martinelli correlation is a recognized tool to describe the two-phase pressure drop in different flow process system. It has also been used with proper modification in flow through channels (Azbel and Kemp-Pritchard 1981). As per Lockhart–Martinelli model, the Lockhart–Martinelli parameters for liquid and gas, ϕ_{sl}, ϕ_{sg} and X are defined as follows:

$$\phi_l^2 = \Delta P_{f,tp} / \Delta P_{f,l} \tag{3.12}$$

$$\phi_g^2 = \Delta P_{f,tp} / \Delta P_{f,g} \tag{3.13}$$

and

$$X = \frac{\phi_g}{\phi_l} = \sqrt{\left(\frac{\Delta P_{f,l}}{\Delta P_{f,g}}\right)} \tag{3.14}$$

The single phase frictional pressure drop in coil ΔP_{fc} over a distance of *ΔL* of the pipe can be evaluated by the Eq. (3.15)

$$\Delta P_{fc} = \frac{2 f_c \rho U^2 \Delta L}{d_t} \tag{3.15}$$

In the laminar flow range ($10 < He_n < 3000$), the friction factor for non-Newtonian liquid can be calculated as (Mishra and Gupta 1979a)

$$f_c = f_s\{1 + 0.033(\log_{10} He_n)^4\} \tag{3.16}$$

and for turbulent flow of non-Newtonian liquid in the range of $4500 < Re_n < 10^5$, $6.7 < D_c/d_t < 346$ and $0 < p/D_c < 25.4$

$$f_c = 0.0791\, He_n^{-0.25} + 0.0075\,(d_t / D_c)^{0.50} \tag{3.17}$$

where

$$He_n = \mathrm{Re}_n\ [(d_t / D_c)/\{1 + (p/\pi D_c)^2\}]^{0.5} \tag{3.18}$$

The onset of laminar and turbulent flow conditions followed in the helical coil tube is derived and is shown in Appendix-II. From the values of the friction factor the calculated frictional pressure drop can be obtained from Eq. (3.15). From each experimental value of the total pressure gradient ($\Delta P/\Delta L_t$), an experimental frictional pressure gradient can be obtained by Eq. (3.1). The single phase friction factor was calculated for laminar and turbulent flow in a hydraulically smooth helical coil tube from Eqs. (3.16) and (3.17) respectively. Various authors expressed the Lockhart–Martinelli parameters in terms of not only gas or liquid flow rate, it was also expressed in terms of different geometric variables and physical properties. Based on the

Lockhart-Martinelli concept, in the present study, the parameters, ϕ_l and ϕ_g have been correlated by incorporating the effect of different geometric variables like coil diameter, tube diameter and pitch length and the physical properties of the fluid by dimensional analysis as:

$$\phi_l^2 = f(X) = \lambda'\left(\mathrm{Re}_s\left(1-\frac{8d_t}{\pi D_c}\right)\right)^{a'}\left(\frac{\sigma_L}{\rho_m U_m^2 d_t^2}\right)^{b'}\left(\frac{D_c}{d_t}\right)^{c'}\left(\frac{L_p}{d_t}\right)^{d'}\left(\frac{L_t}{d_t}\right)^{e'}(X)^{f'} \tag{3.19}$$

$$\phi_g^2 = f(X) = \lambda'\left(\mathrm{Re}_s\left(1-\frac{8d_t}{\pi D_c}\right)\right)^{a'}\left(\frac{\sigma_L}{\rho_m U_m^2 d_t^2}\right)^{b'}\left(\frac{D_c}{d_t}\right)^{c'}\left(\frac{L_p}{d_t}\right)^{d'}\left(\frac{L_t}{d_t}\right)^{e'}(X)^{f'+2} \tag{3.20}$$

The values of constants with correlation coefficient (R^2) and the standard error (SE) of Eq. (3.19) for different flow patterns are shown in Table 3.4. The predicted values of two-phase frictional pressure drop can then be calculated as:

$$\Delta P_{fc,tp} / \Delta L = \phi_l^2 (\Delta P_{fc,l} / \Delta L) \tag{3.21}$$

A typical comparison between the predicted values by the proposed modified Lockhart-Martinelli parameter and the experimental data of the present system is shown in Figure 3.9.

For slurry system

$$\Phi_{ls}^2 = 5.82\times10^6(\mathrm{Re}_{ls})^{-1.018}(\mathrm{Re}_g)^{0.644}\left(\frac{\sigma_{ls} d_t \rho_{ls}}{\mu_{ls}^2}\right)^{-0.241} X^{0.639}\beta \tag{3.22}$$

$$\beta = \left(\frac{D_c}{d_t}\right)^{-0.063}\left(\frac{L_p}{d_t}\right)^{0.091}\left(\frac{h_b}{d_t}\right)^{-0.017}\left(\frac{L_t}{d_t}\right)^{-0.020}\left(\frac{C_c}{\rho_{ls}}\right)^{0.032}\left(\frac{\mu_g}{\mu_{ls}}\right)^{2.024} \tag{3.23}$$

The correlation coefficient (R^2) and the standard error of Eq. (3.22) were found to be 0.931 and 0.062, respectively.

Table 3.4: The parameters for Eq. (3.19) of liquid multiplier (ϕ_l^2) of air-non-Newtonian two-phase flow in helical coil

Flow patterns	λ′	a′	b′	c′	d′	e′	f′	R^2	SE	Range (Re_{cm})
Plug flow	7.34×10^2	-1.606	-1.469	1.045	0.017	1.005	-1.676	0.998	0.053	199-3152
Slug flow	27.424	-1.209	-1.078	0.740	-0.011	0.569	-0.727	0.978	0.053	65-3855
Stratified flow	9.918	-1.268	-1.138	0.409	0.041	0.629	-0.397	0.967	0.043	83-1848

3.4.4.2. Analysis of three-phase frictional pressure drop using Davis Correlation

Davis extended the applicability of Lockhart-Martinelli's correlation to the vertical flow through modification of the parameter X by incorporating the Froude number (Fr), to account the effect of gravity and velocity. The modified parameter, X_{mod} is expressed as:

$$X_{\mathrm{mod}} = 0.19 Fr^{0.185} X \tag{3.24}$$

where the Froude Number is Fr = U_m^2/gD_c. By dimensional analysis and fitting the experimental data, following correlations were obtained:

$$\Phi^2_{ls,Devis} = 1.94 \times 10^7 (\mathrm{Re}_{ls})^{-2.965} (\mathrm{Re}_g)^{1.200} \left(\frac{\sigma_{ls} d_t \rho_{ls}}{\mu^2_{ls}} \right)^{0.625} X_{\mathrm{mod}}{}^{2.027} \beta' \tag{3.25}$$

$$\beta' = \left(\frac{d_c}{d_t}\right)^{0.037} \left(\frac{L_p}{d_t}\right)^{0.446} \left(\frac{h_b}{d_t}\right)^{-0.203} \left(\frac{L_t}{d_t}\right)^{-0.047} \left(\frac{C_c}{\rho_{ls}}\right)^{0.021} \left(\frac{\mu_g}{\mu_{ls}}\right)^{2.077} \tag{3.26}$$

The correlation coefficient (R^2) and the standard error of Eq. (3.25) were calculated and were found to be 0.985 and 0.031 respectively. The calculated values of $\Phi^2_{ls,Devis}$ using Eq. (3.25) have been plotted against the experimental values which are shown in Figure 3.10. The correlation was not as good as that is developed based on the concept of L-M method.

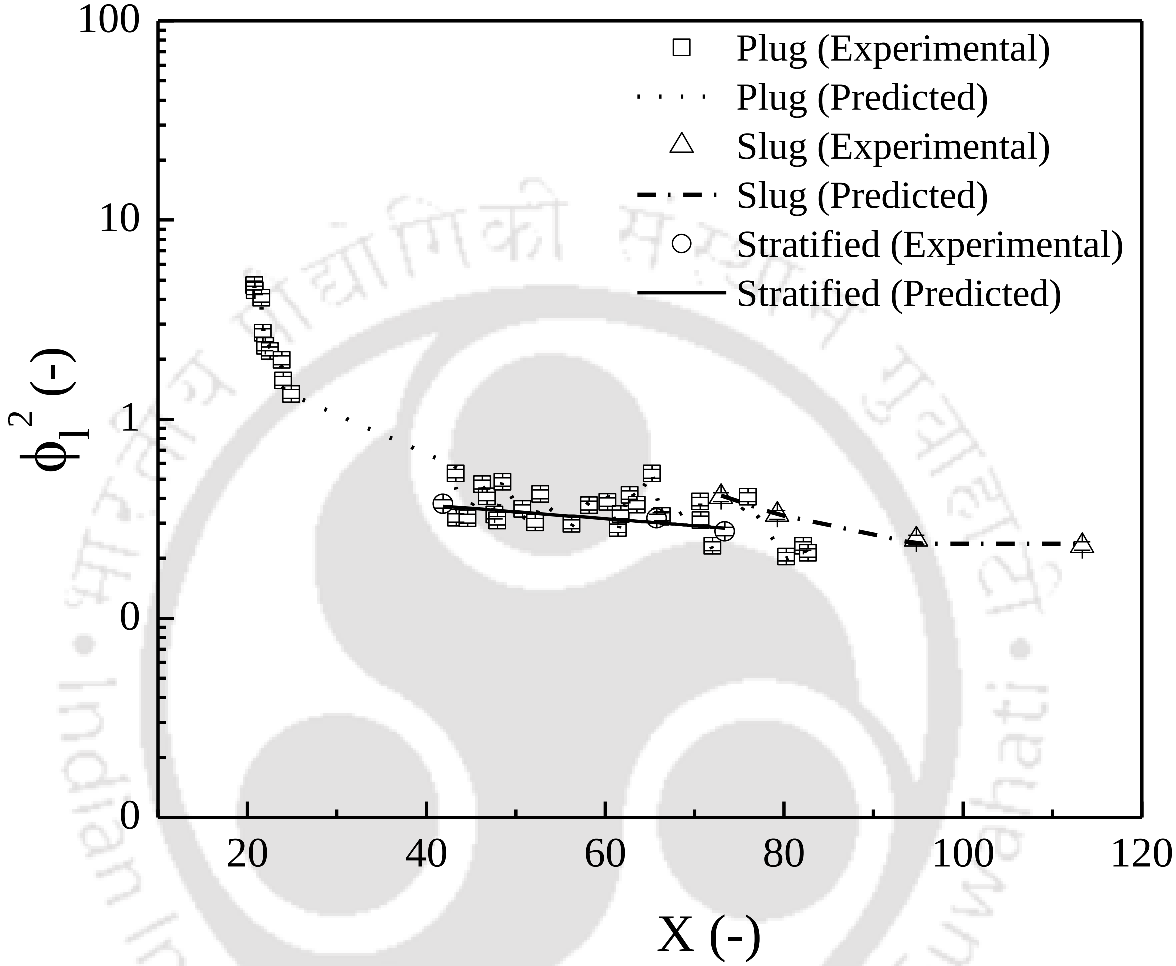

Figure 3.9: Comparing experimental and predicted of liquid phase multiplier versus Lockhart - Martinelli parameter (X). For plug flow: D_c/d_t = 10.00 m, L_p/d_t = 10.00 m, L_t/d_t = 58.50 m, for slug flow: D_c/d_t = 13.00 m, L_p/d_t = 13.00 m, L_t/d_t = 275.55 m, for stratified flow: D_c/d_t = 8.30 m, L_p/d_t = 12.50 m, L_t/d_t = 275.55 m.

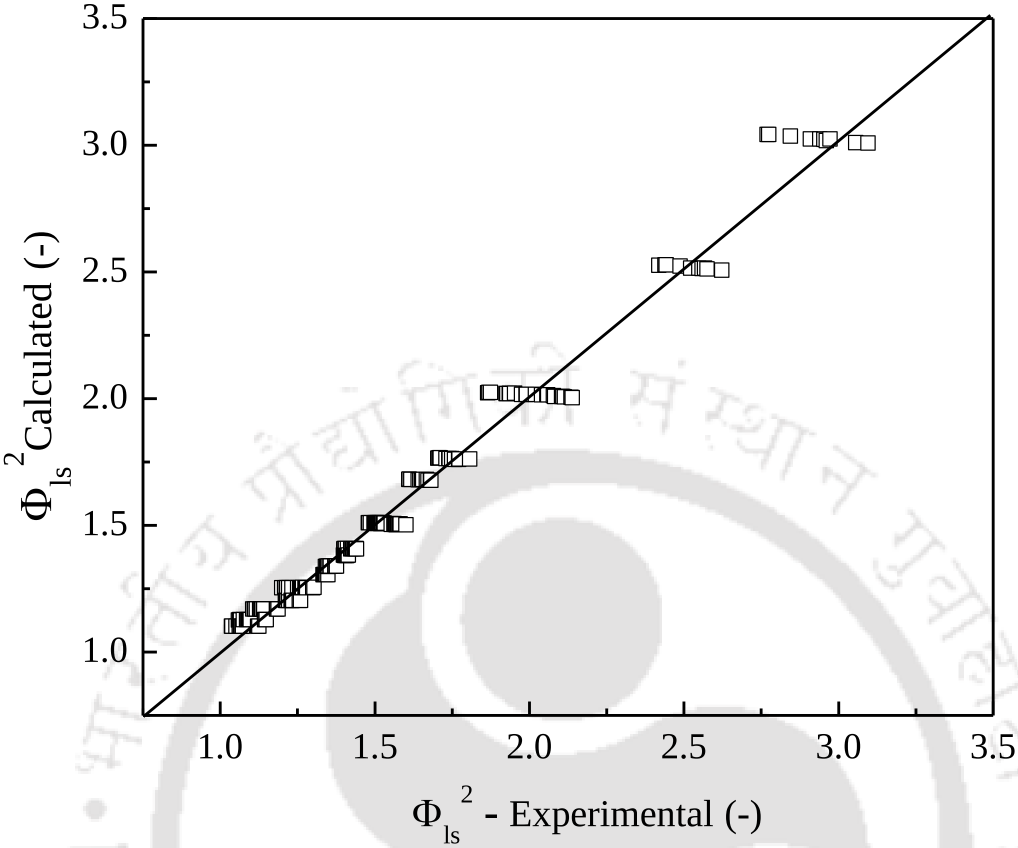

Figure 3.10: Comparison between experimental and calculated $\Phi^2_{ls,Davis}$

3.4.4.3. Prediction of friction factor at different flow patterns by correlation model

A general correlation to predict the two-phase friction factor was also developed with the operating variables as shown in Eq. (3.27) for different flow patterns.

$$f_{c,tp} = \lambda''\left(\mathrm{Re}_s\left(1-\frac{8d_t}{\pi D_c}\right)\right)^{a''}\left(\frac{\sigma_L}{\rho_m U_m^2\ d_t^2}\right)^{b''}\left(\frac{D_c}{d_t}\right)^{c''}\left(\frac{L_p}{d_t}\right)^{d''}\left(\frac{L_t}{d_t}\right)^{e''} \tag{3.27}$$

The parameters (λ'', a'' to e'') in the Eq. (3.27) with the correlation coefficients and standard error are shown in in Table 3.5. The two-phase friction factor with the Reynolds number at different flow conditions was compared with the predicted values calculated by correlation, as shown in Figure 3.11.

Table 3.5: The parameters for Eq. (3.27) of friction factor ($f_{c,tp}$) of air-non-Newtonian two-phase flow in helical coil.

Flow patterns	λ″	a″	b″	c″	d″	e″	R^2	SE	Range (Re_{cm})
Plug flow	2.21×10^5	-3.685	-1.476	1.517	0.023	0.432	0.997	0.061	179-2887
Slug flow	19.582	-1.758	-0.792	0.761	-0.024	-0.005	0.991	0.059	62-2911
Stratified flow	5.363	-1.893	-1.028	0.377	0.045	0.365	0.993	0.059	83-1848

3.4.4.4. Analysis of frictional pressure drop by Mechanistic model development

Energy Balance Equation:

The mechanical energy balance of two-phase flow in the vertical helical coil can be written as

$$-\Delta P_{tp}\varepsilon_g A_t U_{sg} + g\Delta Z A_t \varepsilon_g \rho_g U_{sg} + E_g = 0 \tag{3.28}$$

In Eq. (3.28), the first term is "energy due to two-phase pressure", second term is "potential energy" and the third term is "energy dissipation due to friction"

Similarly for the liquid

$$-\Delta P_{tp}(1-\varepsilon_g)A_t U_{sl} + g\Delta Z A_t(1-\varepsilon_g)\rho_l U_{sl} + E_l = 0 \tag{3.29}$$

Adding Eqs. (3.28) and (3.29) one gets

$$-\Delta P_{tp}[(1-\varepsilon_g)U_{sl} + \varepsilon_g U_{sg}] + [(1-\varepsilon_g)\rho_l U_{sl} + \varepsilon_g \rho_g U_{sg}]g\Delta Z + (E_l + E_g)/A_t = 0 \tag{3.30}$$

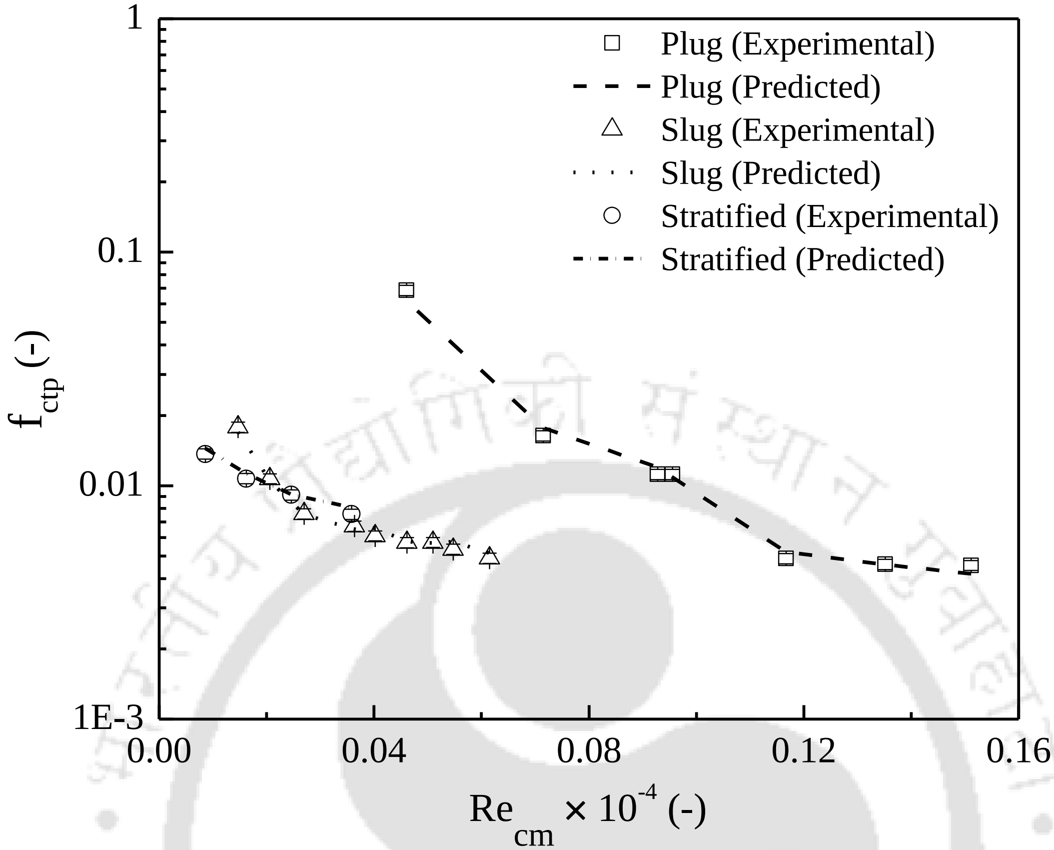

Figure 3.11: A comparison of predicted and experimental two-phase friction factor values. For plug flow: D_c/d_t = 5.85 m, L_p/d_t = 5.85 m, L_t/d_t = 58.50 m; for slug flow: D_c/d_t = 5.00 m, L_p/d_t = 2.50 m, L_t/d_t = 165.33 m; for stratified flow: D_c/d_t = 5.00 m, L_p/d_t = 5.00 m, L_t/d_t = 165.33 m

Total energy dissipation of the two phases is equal to the sum of frictional loss due to each of the phases and the loss due to bubble formation, phase slip and wettability.

An expression for (E_l +E_g) can be obtained as

$$\Delta P_{fl} A_t (1-\varepsilon_g) U_{sl} + \Delta P_{fg} A_t \varepsilon_g U_{sg} + E_b + E_{slip} + E_w = (E_l + E_g) \tag{3.31}$$

where ΔP_{fl} is the frictional pressure loss due to liquid in two-phase flow and ΔP_{fg} is the frictional pressure loss due to gas in two-phase flow. E_b is the rate of energy loss due to bubble formation; E_{slip} is the rate of energy loss due to slip of gas-liquid interface and E_w is the rate energy loss due to wetting of thin liquid layer with the solid wall.

Substituting Eq. (3.31) for ($E_l + E_g$) in Eq. (3.30) one gets

$$\begin{aligned}&\Delta P_{tp}[L/\rho_l + G/\rho_g]\\ &= [L+G]g\Delta Z + \Delta P_{fg} G/\rho_g + \Delta P_{fl} L/\rho_l + [E_b/A_t + E_{slip}/A_t + E_w/A_t]\end{aligned} \tag{3.32}$$

where L and G are the mass flux of liquid and gas respectively which were defined as, $L = (1-\varepsilon_g)U_{sl}\rho_l$ and $G = \varepsilon_g U_{sg}\rho_g$ respectively.

Energy dissipation due to skin friction

To determine the frictional losses due to each gas and liquid phase in two-phase flow in the coil a model can be formulated on the basis of the following assumptions: (i) The friction factor for each phase in two phase flow is a constant multiple, α' of that if only flow of single phase takes place in the coil. (ii) The area of contact of each phase with wall in two-phase flow is α'' times to that of only flow of single phase in the coil. In case of gas phase, the values of α' and α'' depend on number of bubbles coming in contact with the wall of the coil. From these assumptions and from a simple overall momentum balance it follows:

For liquid phase

$$\frac{\Delta P_{fl}(Cross\sec tional\ area)_{tp}}{\Delta P_{fl0}(Cross\sec tional\ area)_{l0}} = \frac{(Wall\ \ shear\ stress)_{tp}}{(Wall\ \ shear\ stress)_{l0}} \times \frac{(Area\ of\ contact\ with\ wall)_{tp}}{(Area\ of\ contact\ with\ wall)_{l0}} \tag{3.33}$$

$$\Rightarrow \frac{\Delta P_{fl} A_t (1-\varepsilon_g)}{\Delta P_{fl0} A_t} = \frac{(0.5 f \rho_l U_{sl}^2)_{tp}}{(0.5 f \rho_l U_{sl}^2)_{l0}} \times \frac{(Area\ of\ contact\ with\ wall)_{tp}}{(Area\ of\ contact\ with\ wall)_{l0}} = \frac{f_{\lg}}{f_{l0}} \cdot \frac{(U_{sl}^2)_{tp}}{(U_{sl}^2)_{l0}} \times \alpha_l''$$

$$\Rightarrow \frac{\Delta P_{fl} A_t (1-\varepsilon_g)}{\Delta P_{fl0} A_t} = \alpha_l' \cdot \frac{1}{(1-\varepsilon_g)^2} . \alpha_l'' = \frac{\alpha_l}{(1-\varepsilon_g)^2} \tag{3.34}$$

$$\Rightarrow \frac{\Delta P_{fl}}{\Delta P_{fl0}} = \frac{\alpha_l}{(1-\varepsilon_g)^3} \tag{3.35}$$

where, the subscripts "*l0*" refers to liquid single phase, "*tp*" refers to liquid-gas two-phase, "*sl*" refers to liquid superficial, $(U_{sl})_{tp} = (U_{sl})_{l0}/(1-\varepsilon_g)$, $\alpha_l = \alpha_l' \alpha_l''$ and cross-sectional area for the flow of liquid in two-phase is equal to ($1-\varepsilon_g$) times the cross-sectional area of the coil. The parameter α_l' is defined as f_{lg}/f_{l0} and α_l'' is defined as (Area of contact)$_{tp}$ / (Area of contact)$_{l0}$. ΔP_{fl0} is the frictional pressure drop due to liquid when only liquid phase flows through the coil. It is assumed that the area of contact of liquid with wall in two-phase flow is the same as the area of contact with wall in single phase liquid flow, i.e. Area of contact)$_{tp}$ = (Area of contact)$_{l0}$. Therefore α_l can be interpreted as α_l' which is defined as f_{tp}/f_{l0}.

Similarly for the gas phase

$$\frac{\Delta P_{fg}}{\Delta P_{fg0}} = \frac{\alpha_g}{\varepsilon_g{}^3} \tag{3.36}$$

where ΔP_{fg0} is the frictional pressure drop due to gas when only gas phase flows through the coil and $\alpha_g = \alpha_g' \alpha_g''$.

Energy dissipation due to phase slip

A bubble imbedded in a flowing fluid is influenced by a number of mechanisms, which act on it through the traction at the gas–liquid interface. The bubbles moving through the fluid experiences pressure forces that affect its motion. The formulation of the pressure force due to phase interaction can be expressed as

$$\Delta P_{\mathrm{FD}} = \frac{1}{8} C_d \rho_l U_s^2 \tag{3.37}$$

where C_d is the drag coefficient, U_s is the slip velocity (difference in velocities between liquids and solids (or gases and liquids) in the flow of two-phase mixtures through a pipe or tube.). The interaction force depends on the size and shape of the bubble and the nature of the gas-liquid interface. The drag coefficient and slip velocity can be calculated as:

$$U_s = \left| \frac{U_{sl}}{1-\varepsilon_g} - \frac{U_{sg}}{\varepsilon_g} \right| \tag{3.38}$$

The drag coefficient C_d can be calculated by using the following empirical correlations (Lain et al., 1999)

$$C_d = \frac{16}{\mathrm{Re}_b}, \qquad \mathrm{Re}_b < 1.5, \tag{3.39a}$$

$$= 14.9\,\mathrm{Re}_b^{-0.78}, \qquad 1.5 < \mathrm{Re}_b < 80, \tag{3.39b}$$

$$= \frac{48}{\mathrm{Re}_b}(1.0 - 2.21\mathrm{Re}_b^{-0.5}), \qquad 80 < \mathrm{Re}_b < 700 \tag{3.39c}$$

where

$$\mathrm{Re}_b = \frac{\rho_l d_b U_s}{\mu_l} \tag{3.40}$$

The rate of energy loss due to slip of the two phases is then calculated by

$$E_{slip} = \Delta P_{\mathrm{FD}} Q_m = \frac{1}{8} C_d \rho_l U_s^2 A_t (G/\rho_g + L/\rho_l) \tag{3.41}$$

Energy dissipation due to formation of gas bubble

To account for dynamic interaction, it is necessary to first calculate the energy loss due to formation of bubbles. The rate of energy loss for the formation of bubbles can be calculated as follows

$$E_b = \left(\frac{G}{\rho_g} A_t \right) \frac{6\sigma}{d_{be}} \tag{3.42}$$

where, d_{be} is the equivalent bubble diameter by comparing the same volume of sphere if the bubbles are not is regular shape.

Energy dissipation due to wettability between liquid and coil wall

Practically there is a very thin layer of liquid film adjacent to the wall and hence no gas was assumed to come in contact with the wall of the coil. This means surface tension between gas and solid coil wall (σ_{sg}) is zero. In this case it is assumed that there is no energy loss due to wettability of gas with the coil wall. But there is of course energy loss due to wettability of liquid with the wall. The rate of energy loss due to wettability of liquid with the wall can be represented as

$$E_w = \frac{\pi d_t U_{sl} \sigma_{sl}}{1-\varepsilon_g} \tag{3.43}$$

The energy loss due to wetting of liquid depends on the dynamic contact angle between liquid and coil wall (Cubaud and Ho 2004). According to Cubaud and Ho (2004), dynamic contact angle (θ) is approximately equal to $Ca^{1/3}$, where Ca is the capillary number which is defined as, $Ca = \mu_l U_s/\sigma_l$. The condition $\theta < 90°$ indicates that the solid is wet by the liquid, and $\theta > 90°$ indicates non-wetting, with the limits $\theta = 0$ and $\theta = 180°$ defining complete wetting and complete non-wetting, respectively. In the present study, the range of capillary number was $0 \geq Ca \geq 0.026$ (for Newtonian) and $0.010 \geq Ca \geq 0.797$ (for Non-Newtonian) degrees, which indicate the coil wall was wet by the liquid.

Determination of Model Parameters

The liquid and gas phase frictional pressure drop can be calculated from Eqs. (3.35) and (3.36) respectively. The parameter α_g in Eq. (3.36) depends on the number of bubbles coming in contact with the wall of the coil. Since there is a thin layer of liquid through the wall of the coil, no bubbles are assumed to come in contact with the wall of the coil. Consequently the area of contact of gas with coil wall in two-phase flow is negligible compared to the area of contact of gas in single gas phase flow and hence the value of α_g can be considered as zero. The single liquid phase pressure drop was calculated using Fanning's equation:

$$\Delta P_{fl0} = 2 f_{cl0}\ \rho_l U_{sl}^2 L_c / d_t \tag{3.44}$$

Similarly for the gas phase, pressure drop was calculated as

$$\Delta P_{fg0} = 2 f_{cg0}\ \rho_g U_{sg}{}^2 L_c / d_t \tag{3.45}$$

In the laminar flow range (10 < He_n < 3000), the friction factor for non-Newtonian liquid can be calculated as (Mishra and Gupta 1979b)

$$f_{c0} = f_{s0}\left(1+\frac{0.033}{(\log_{10} He_n)^{-4}}\right) \tag{3.46}$$

and for turbulent flow of non-Newtonian liquid in the range of 4500 < Re_n < 10^5, 6.7 < D_c/d_t < 346 and 0 < p/D_c < 25.4

$$f_{c0} = \frac{0.0791}{He_n{}^{0.25}} + \frac{0.0075}{\sqrt{(D_c / d_t)}} \tag{3.47}$$

where

$$He_n = \mathrm{Re}_n\left[\frac{(d_t / D_c)}{1+(p/\pi D_c)^2}\right]^{0.5} \tag{3.48}$$

The friction factor for straight tube (f_{s0}) is calculated as

$$f_{s0} = \frac{16}{\mathrm{Re}_n} \quad \text{for laminar flow } (Re_n < 2100) \tag{3.49}$$

$$f_{s0} = \frac{0.079}{n^5 (\mathrm{Re}_n)^{\frac{2.63}{10.5^n}}} \quad \text{for turbulent flow } (Re_n > 4000) \tag{3.50}$$

where Re_n is the Reynolds number for non-Newtonian fluid flow which is defined as

$$\mathrm{Re}_n = \frac{d_c^n U_{sl}^{2-n} \rho}{8^{n-1} K} \left(\frac{4n}{3n+1} \right)^n \tag{3.51}$$

For transition flow, the friction factor for straight pipe, f_{s0} can be deduced from the generalized pressure loss equation as (Desouky and E1-Emam 1989):

$$f_{s0} = 0.125 \left[n^{\sqrt{n}} \left(0.0112 + \frac{1}{\mathrm{Re}_n^{\;0.3185}} \right) \right] \text{ for transition flow } (2100 < Re_n < 4000) \tag{3.52}$$

Substituting the Eqs. (3.35) for ΔP_{fl}, (3.36) for ΔP_{fg}, (3.41) for E_{slip}, (3.42) for E_b and (3.43) for E_w into Eq. (3.32), one can the final equation for ΔP_{tp} as

$$\delta_{tp} = (1-\psi_g) \left[\frac{1}{1-\psi_g} + \lambda \alpha_l + \phi + \kappa + \frac{\psi_g}{1-\psi_g} \Gamma \right] \tag{3.53}$$

In Eq. (3.53), except α_l, all parameters are known. α_l can be obtained from the Eq. (3.54) as

$$\alpha_l = \frac{1}{\lambda} \left[\frac{1}{1-\psi_g} (\delta_{tp} - \Gamma \psi_g - 1) - \phi - \kappa \right] \quad . \tag{3.54}$$

where

$$\delta_{tp} = \frac{\Delta P_{tp}}{[\gamma_g \rho_g + (1-\gamma_g)\rho_l]}; \quad \gamma_g = \frac{G/\rho_g}{[G/\rho_g + L/\rho_l]}; \quad \lambda = \frac{2 f_{cl0} U_{sl}^2 L_t}{g\Delta z (1-\varepsilon_g)^3 d_t}; \quad \phi = \frac{(1/8) C_d U_s^2}{g \Delta z (1-\gamma_g)};$$

$$\Gamma = \frac{6\sigma}{\rho_g g \Delta z d_b}; \; \kappa = \frac{4\sigma / d_t}{\rho_l g \Delta z (1-\varepsilon_g)^2}; \; \psi_g = \frac{\rho_g \gamma_g}{\rho_g \gamma_g + \rho_l (1-\gamma_g)}$$

For gas-liquid stratified flow, the formation of the bubble was not happened. So energy dissipation due to formation of gas slug is considered to be neglected and hence the parameter Γ becomes zero. Therefore for stratified flow the Eq. (3.54) becomes

$$\alpha_l = \frac{1}{\lambda} \left[\frac{1}{1-\psi_g} (\delta_{tp} - 1) - \kappa \right] \tag{3.55}$$

Using the experimental pressure drop and gas hold up, the corresponding values of α_l were calculated for different operating variables from Eq. (3.50). The drag coefficient was calculated by the equation as given by Eq. (3.39). The range of bubble Reynolds number is 260 to 262440. To estimate the value of α_l data for ΔP_{tp} and ε_g for different operating conditions of two-phase (air-SCMC) flow in the helical coil was taken from present experimental results. The correlation for equivalent bubble diameter obtained by dimensional analysis is shown in Eqs. (3.56) and (3.57).

For plug flow

$$d_{be} = 0.048\left(\frac{\mu_m}{\rho_m U_m d_t}\right)^{0.002}\left(\frac{\sigma_L}{\rho_m U_m d_t^2}\right)^{-0.070}\left(\frac{D_c}{d_t}\right)^{0.099}\left(\frac{L_p}{d_t}\right)^{-0.083}\left(\frac{L_t}{d_t}\right)^{-0.202} \quad (3.56)$$

For slug flow

$$d_{be} = 0.068\left(\frac{\mu_m}{\rho_m U_m d_t}\right)^{-0.034}\left(\frac{\sigma_L}{\rho_m U_m d_t^2}\right)^{0.023}\left(\frac{D_c}{d_t}\right)^{0.108}\left(\frac{L_p}{d_t}\right)^{-0.022}\left(\frac{L_t}{d_t}\right)^{-0.231} \quad (3.57)$$

The two-phase frictional pressure drop increases with increasing phase interaction. Table 3.6 shows the values of pressure drop due to bubble formation and phase interaction which contribute to the total pressure drop for typical flow rates of the phases.

This result can be explained by the introduction of slip effect in two-phase flow conditions. Because the liquid density is higher than the gas density and the overall gas flow rate is higher than the liquid flow rate, the centrifugal forces acting on the liquid phase are much higher than those acting on the gas phase at any particular coil diameter. The liquid is accelerated because of the slip existing between the gas and liquid phases.

Table 3.6: Typical values of different contributions to the total frictional pressure drop as predicted by the present model for typical flow rate of phases at constant tube diameter (0.015 m), coil diameter (0.117 m) and pitch difference (1.0)

Systems	Superficial liquid velocity, V_{sl}, [m/s]	Superficial gas velocity, V_{sg}, [m/s]	Contributory components of dimensionless pressure drop, δ_{tp}			
			from wall frictional $(1-\psi_g)\lambda\alpha_l$	from phase interaction $(1-\psi_g)\phi \times 10^5$	from bubble formation $\psi_g \Gamma \times 10^7$	from surface tension change $(1-\psi_g)\kappa \times 10^2$
Air-Water	0.566	0.094	1.462	2.712	1.266	1.116
	0.944	0.189	4.925	4.165	1.928	1.044
	0.755	0.283	3.189	2.440	2.803	1.497
	1.132	0.377	6.904	3.318	2.354	1.021
Air-SCMC-1	0.566	0.094	0.207	0.094	0.071	1.197
	0.944	0.189	1.817	0.112	0.050	0.998
Air-SCMC-2	0.566	0.094	2.541	0.293	0.061	0.952
	0.944	0.189	2.667	0.301	0.046	0.973
Air-SCMC-3	0.755	0.094	8.406	1.151	0.053	1.037
	0.944	0.189	10.978	0.865	0.045	0.927

The gas-phase pressure drop is very small compared to that of the liquid phase, so the net of the two-phase frictional pressure drop decreases. Due to the retarding effect of liquid against centrifugal force as its viscosity increases, the slip is expected to be higher in a viscous liquid. Hence, the two-phase pressure drop per unit length of coil increases with increasing slip effect, i.e. with phase interaction. Surface tension also has a pronounced effect on the two-phase pressure drop per unit length of coil. As the liquid surface tension decreases with higher SCMC concentration, and more bubble is observed than for the air-water two-phase system. This reduces the slip between the phases and had a tendency to retain the gas phase. Because of the continuous changes in the centrifugal forces, the liquid is continuously pushing to the outer wall while the gas phase is at the inside wall. The probable effect of the centrifugal force is greater than the retarding effect of gas phase. As viscosity increases the Reynolds number decreases at constant flow rate of liquid. The interfacial shear stress is inversely proportional to the 1.6th power of Reynolds number which physically signifies the domination of viscous force for the contribution to the interfacial shear stress. For constant viscous flow the interfacial shear stress increases as the Reynolds number increases. This is due to the fact that the bubble liquid interaction increases as the Reynolds number increases due to increase in liquid flow rates. The bubble-liquid interfacial shear stress can also be obtained by balance between the dynamic pressure force exerted on the bubble by the turbulent liquid flow and the resistance forces (surface tension force and the resistance of the liquid phase to bubble deformation, although the latter is usually small). The ratio between surface tension and turbulent fluctuation forces is the Weber number (*We*). So the bubble-liquid interfacial shear stress increases with the increase in surface tension and decreases with increase in bubble diameter. The decrease in bubble diameter increases the interfacial surface area, which results in increase in bubble-liquid interfacial shear stress.

3.4.5. Correlations of friction factor multiplier (α_l)

The factors which affect the two-phase friction factor are (i) system variables, i.e., physical properties of liquid namely, density, ρ_l, effective viscosity, μ_l and surface tension, σ_l and physical properties of air namely, density, ρ_g and viscosity, μ_g , (ii) operating variables namely, liquid and gas flowrates, respectively and gas-liquid mixing height and (iii) geometric variables namely, the diameter of the tube, d_t, and diameter of the coil, D_c and the pitch of the helical coil system. Hence, friction factor multiplier (α_l) may be written as a function of all these variables. By the use of dimensional analysis the functional relationship between (α_l) and the relevant physical and dynamic parameters can be deduced to the following equivalent relationship

$$\alpha_l = \lambda\left(\frac{\mu_m}{\rho_m U_m d_t}\right)^a \left(\frac{\sigma_L}{\rho_m U_m d_t^2}\right)^b \left(\frac{D_c}{d_t}\right)^c \left(\frac{L_p}{d_t}\right)^d \left(\frac{L_t}{d_t}\right)^e \quad (3.58)$$

The multiple linear regression analysis of the 3200 experimental data yielded the different coefficients of Eq. (3.58) for different flow patterns in helical coils which is shown in Table 3.7. The frictional multiplier is to be calculated by Eq. (3.58). A plot of experiment values of α_l and that of α_l calculated from Eq. (3.58) is shown in Figure 3.12.

It shows excellent agreement. The ranges of variations of the different parameters for the present system are: Curvature ratio range: $3.75 \le D_c/d_t \le 2\ 2.22$; Reynolds number range: $62.15 \le Re_m \le 3913.58$, $74.60 \le Re_l \le 2364.53$, $69.60 \le Re_g \le 621.22$; Dean Number range: $26.71 \le De_l \le 857.53$, $22.01 \le De_g \le 215.19$. After knowing the predicting values of frictional multiplier from the correlation Eq. (3.58), one can calculate the two-phase friction factor, f_{tp} from the definition of α_l as follows

$$f_{ctp} = \alpha_l f_{cl0} \quad (3.59)$$

The gas slug-liquid interfacial shear stress depends on the two-phase friction factor, f_{tp} and that can be calculated as

$$\tau_i = \frac{1}{2} f_{ctp} \rho_l V_{sl}^2 \quad (3.60)$$

A typical frictional intensity factor (α_l) is shown in Figure 3.13. The friction factor depends on the intensity factor of shear stress and flow behavior index of non-Newtonian liquid.

Table 3.7: The parameters for correlations (Eq. (3.58)) of frictional multiplier (α_l)

Flow patterns	λ	a	b	c	d	e	R^2	SE
Plug Flow	2.22×10^{08}	3.512	-1.756	-1.911	1.199	1.029	0.998	0.049
Slug Flow	2.46×10^{03}	2.893	-2.233	-0.817	1.019	1.404	0.996	0.054

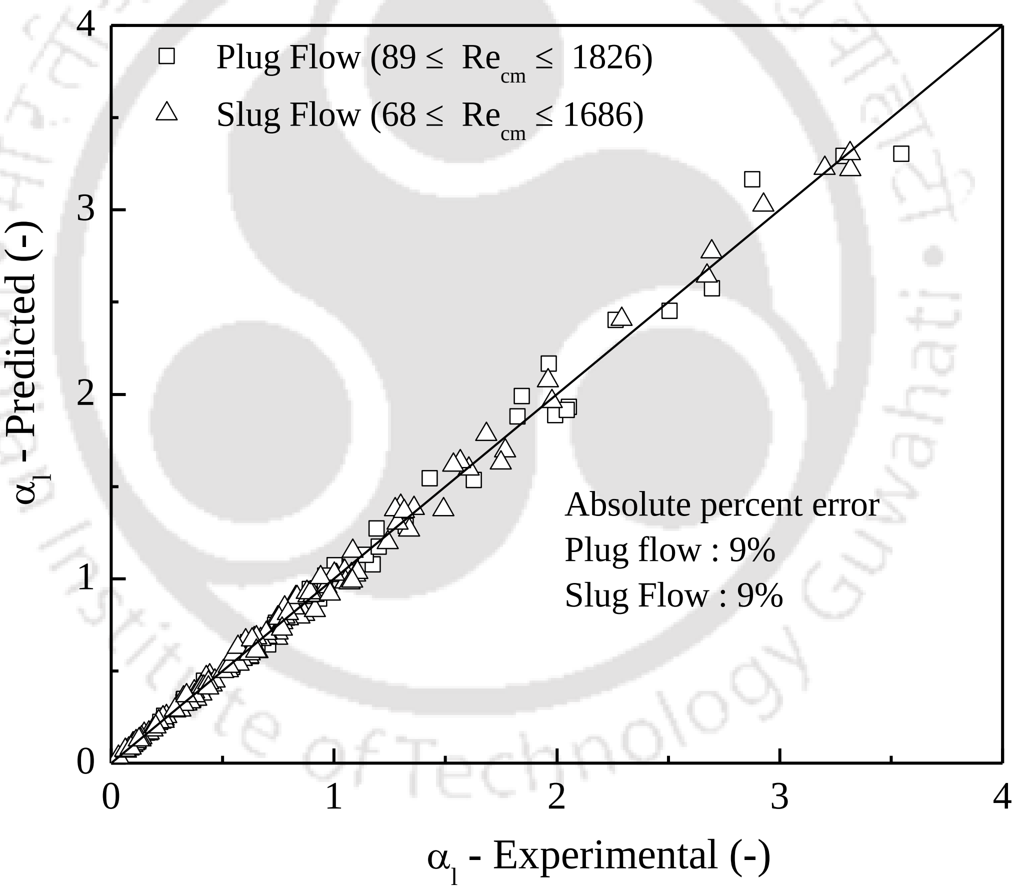

Figure 3.12: Parity plot of experimental and predicted values of frictional multiplier

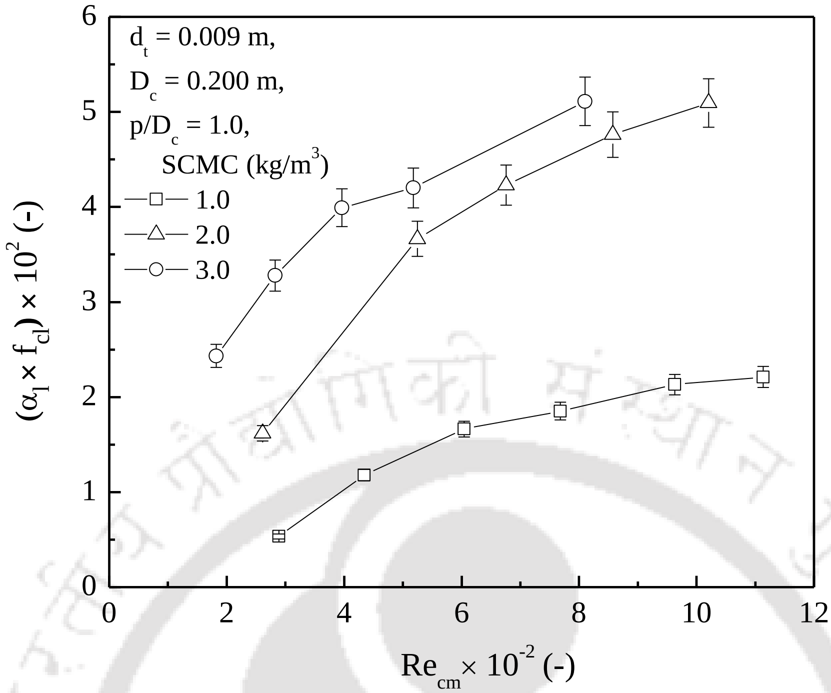

Figure 3.13: Variation of intensity factor with non-Newtonian Reynolds number

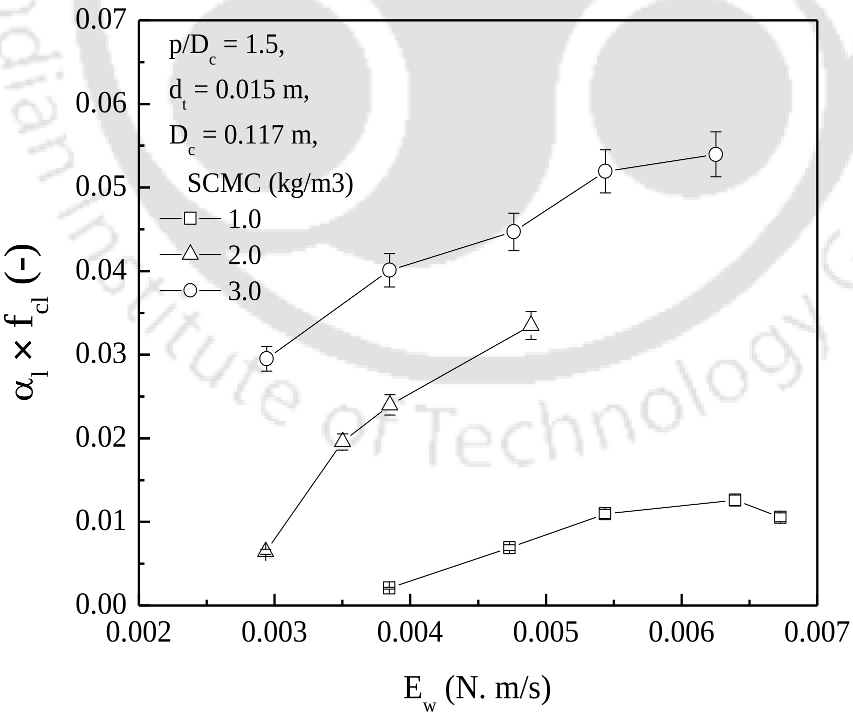

Figure 3.14: Variation of friction factor with the loss of energy due to wettability at different SCMC solutions.

The friction factor can also be represented by the rate of energy loss due to wettability. The friction factor decreases with the increase in wettability. The energy loss due to wettability increases with the increase in surface tension. The surface tension decreases with the increase in concentration of SCMC which leads to increase in loss of energy due to wettability. So as the surface tension increases the friction factor and hence increase in frictional losses. The variation of friction factor with the loss of energy due to wettability is shown in Figure 3.14.

3.5. Conclusions

The characteristics of gas holdup and the frictional pressure drop are investigated. Increase in liquid concentrations two-phase frictional pressure drop increases. Due to viscous effect of non-Newtonian liquid the changes of flow patterns and two-phase frictional pressure drop may occurs. The two-phase pressure drop increases with the increase in ratio of the tube to coil diameter. The ratio of tube to coil diameter changes the generation of secondary flow. There is no change in two-phase pressure drop when increasing pitch difference. The two-phase frictional pressure drop increases due to bubble formation and phase interaction which contribute to the total pressure drop for a particulart flow rate of the phase. The bubble-liquid interfacial shear stress depends on the surface tension and the bubble diameter. The bubble-liquid interfacial shear stress increases with the increase in surface tension and decreases with increase in bubble diameter. The effect of gas holdup is more in non-Newtonian fluids when compared with Newtonian fluids. With decreasing liquid velocity at constant gas flow rate, gas holdup increases in both Newtonian and non-Newtonian fluids. If coil diameter is increased the two-phase friction factor decreases. The energy loss due to wettability increases with the decrease in surface tension. The frictional two-phase pressure drop was analyzed by a mechanistic model based on the plug/slug formation, drag at interface and wettability effect of the Newtonian and non-

Newtonian fluids. The present study may be helpful for further understanding the multiphase flow in curvature system for industrial applications.

Nomenclature

A_t Area of tube (m^2)

C_d Drag coefficient (–)

d_t Tube diameter (m)

d_b Bubble diameter (*m*)

d_{be} Equivalent bubble diameter (m)

D_c Coil diameter (m)

D_m Molecular diffusion coefficient (cm^2/sec)

E_b Rate of energy loss for bubble formation (N m/s)

E_g Rate of energy loss due to gas phase (N m/s)

E_l Rate of energy loss due to liquid phase (N m/s)

E_{slip} Energy loss due to slip (N m/s)

E_w Energy loss due to wettability of liquid (N m/s)

f_{tp} Friction factor of two-phase flow (–)

f_{lo} Friction factor due to single liquid phase (–)

f_{og} Friction factor due to single gas phase (–)

f_{so} Friction factor for straight tube (–)

f_{co} Friction factor for coil tube (–)

g Acceleration due to gravity (m/s^2)

G Gas mass flux (kg/m^2/s)

k Consistency of fluid (Pa.s^n)

L Liquid mass flux (kg/m^2/s)

L_c Coil length (m)

L_p Pitch length (m)

L_t Tube length (m)

n Flow behavior index (–)

p Pitch length (m)

R_c Radius of coil (m)

ΔP_{fg0} Single gas phase frictional pressure drop (N/m^2)

ΔP_{fl0} Single liquid phase frictional pressure drop (N/m^2)

ΔP_{FD} Pressure drop due to phase interaction (N/m^2)

ΔP_{tp} Two-phase frictional pressure drop (N/m^2)

U_{sg} Gas superficial velocity (m/s)

U_{sl} Liquid superficial velocity (m/s)

U_m Mixed velocity (m/s)

U_s Slip velocity (m/s)

Dimensionless groups

C_a Capillary number ($= \mu_l U_s/\sigma_l$) (–)

De Dean Number $\left(= \mathrm{Re}\sqrt{d_t / D_c}\right)$ (–)

Eu Euler number ($=d^{0.85}D_c^{0.85}/L$) (–)

Fr Froude number ($= U_{sl}^2/gd_t$) (–)

G_{rgc} Geometrical number for regular helical coil (-)

He_n Helical number $\left(= \mathrm{Re}\,[(d_t / D_c)/\{1+(p/\pi D_c)^2\}]^{0.5}\right)$ (–)

M Mass flow rate (kg/s)

Q	Flow rate (m^3/s)
Re_n	Reynolds Number ($=d_t U_{sl}\rho/\mu$) (–)
Re_b	Bubble Reynolds number $\left(=\left(\dfrac{\rho_l d_b U_s}{\mu_l}\right)\right)$ (–)
Re_c	Coil Reynolds number $\left(=\mathrm{Re}_s\left(1-\dfrac{8d_t}{\pi D_c}\right)^n\right)$ (–)
Re_{cm}	Coil mixture Reynolds number $\left(=\mathrm{Re}_m\left(1-\dfrac{8d_t}{\pi D_c}\right)^n\right)$ (–)
Re_m	Mixture Reynolds number $\left(=\left(\dfrac{d_t^n U_m^{2-n}\rho_m}{8^{n-1}K}\right)\left(\dfrac{4n}{3n+1}\right)^n\right)$ (–)
Re_s	Non Newtonian Reynolds number for straight tube $\left(=\left(\dfrac{d_t^n U_{sl}^{2-n}\rho_l}{8^{n-1}K}\right)\left(\dfrac{4n}{3n+1}\right)^n\right)$ (–)
We	Weber number ($=\tau_i d_b/\sigma$) (–)

Greek Letters

ρ	Density (kg/m^3)
μ_l	Viscosity of the liquid (kg/m.s)
μ_g	Viscosity of the gas (kg/m.s)
μ_{eff}	Effective viscosity (kg/m.s)
τ	Shear stress (N/m^2)
ε_g	Gas holdup (–)
σ	Surface tension (N/m)
θ	Contact angle (degree)

Φ Wall flux (W/m^2)

α_l Friction factor multiplier (–)

γ_g Dimensionless factor ($=(G/\rho_g)/(G/\rho_g + L/\rho_l)$) (–)

λ Dimensionless parameter ($=(2 f_{cl0} U_{sl}^2 L)/(g\Delta z(1-\varepsilon_g)^3 d_t)$) (–)

ψ_g Dimensionless parameter ($=\rho_g\gamma_g/(\rho_g\gamma_g + \rho_l(1-\gamma_g))$) (–)

Γ Dimensionless parameter ($=6\sigma/(\rho_g g\Delta z d_b)$) (–)

ϕ Dimensionless parameter ($=((1/8)C_d U_s^2)/(g\Delta z(1-\gamma_g))$) (–)

δ_{tp} Dimensionless two-phase pressure drop ($=\Delta P_{tp}/([\gamma_g\rho_g + (1-\gamma_g)\rho_l])$ (–)

κ Dimensionless parameter ($=(4\sigma/d_t)/(\rho_l g\Delta z(1-\varepsilon_g)^2)$) (–)

Subscripts

c	Coil
f	Frictional
g	Gas
i	Interfacial
l	Liquid
m	Mixture
o	Single
s	Superficial
tp	Two-phase
w	Wettabilty

References

- Akagawa, K., Sakaguchi, T., Ueda, M., 1971. Study on a gas-liquid two-phase flow in helically coiled tubes. Bulletin of JSME 14, 564-571.

- Ali, S., Seshadri, C.V., 1971. Pressure drop in Archimedean spiral tubes. Ind. Eng. Chem. Proc. Des. Dev. 10, 328 – 332.
- Ali, S., Zaidl, A.H., 1979. Head loss and critical Reynolds numbers for flow in ascending equiangular spiral tube coils. Ind. Eng. Chem. Proc. Des. Dev. 10, 328 – 332. 18, 349 – 353.
- Ali, S., Zaidi, A.H., 1980. Pressure drop and stability of flow in negative logarithmic spiral tube coils. Ind. Eng. Chem. Proc. Des. Dev. 19, 75 – 80.
- Ali, S., 2001. Pressure drop correlations for flow through regular helical coil tubes. Fluid Dynamics Research 28, 295–310.
- Awwad, A., Xin, R.C., Dong, Z.F., 1995. Measurement and correlation of the pressure-drop in air-water two-phase flow in horizontal helicoidal pipes. Int. J. Multiphase Flow 21, 607-619
- Azbel, D., Kemp-Pritchard, P. 1981. Two-phase flows in chemical engineering. Cambridge University Press, United Kingdom.
- Baker, O., 1954. Simultaneous flow of oil and gas. Oil Gas J. 53, 185-195.
- Bandaru, S.V.S.R.K., Chhabra, R.P., 2002. Pressure drop for single and two-phase flow of non-Newtonian liquids in helical coils. Can. J. Chem. Eng. 80, 315-321.
- Banerjee, S., Rhodes, E., Scott, D.S., 1969. Studies on co-current gas-liquid flow in helically coiled tubes I. flow patterns, pressure drop and holdup. Can. J. Chem. Eng. 47, 445–453.
- Bankoff, S.G., 1960. A variable density single-fluid model for two-phase flow with particular reference to steam-water flow. J. Heat Transfer 82, 265-272.

- Biswas, A.B., Das, S.K., 2006. Holdup characteristics of gas-non-Newtonian liquid flow through helical coils in vertical orientation. Ind. Eng. Chem. Res. 45, 7287-7292.
- Chen, X., Guo, L., 1999. Flow pattern and pressure drop in oil-air-water three phase flow through helically coiled tubes. Int. J. Multiphase Flow 25, 1053 – 1072.
- Cubaud, T., Ho, C., 2004. Transport of bubbles in square micro channels, Phys. Fluids 16, 4575 – 4585.
- Desouky, S.E.D.M., E1-Emam, N.A., 1989. Program designs for pseudo plastic fluids. Oil Gas J. 48–51.
- Dodge, D.W., Metzner, A.B., 1959. Turbulent flow of non-Newtonian systems. AIChE J. 5, 189 – 204.
- Dukler, A.E., Wicks, M., Cleveland, R.G., 1964. Frictional pressure drop in two-phase flow: A. A comparison of existing correlations for pressure loss and holdup. AlChE J. 10, 38-43.
- Gupta, R., Wanchoo, R. K., Jafar Ali, T.R.M., 2011. Laminar flow in helical coils: A parametric study. Ind. Eng. Chem. Res. 50, 1150–1157.
- Hart, J., Ellenberger, J., Hamersma, P.J., 1988. Single and two-phase flow through helically coiled tubes. Chem. Eng. Sci. 43, 775–783.
- Hughmark, G. A., 1962. Holdup in gas-liquid flow. Chem. Eng. Prog. 58, 62-65.
- Kasturi, G., Stepanek, J.B., 1972. Two-Phase flow - I. Pressure drop and void fraction measurements in co-current gas-liquid flow in coil. Chem. Eng. Sci. 27, 1871–1880.
- Lain, S., Broder, D., Sommerfeld, M., 1999. Experimental and numerical studies of the hydrodynamics in a bubble coil. Chem. Eng. Sci. 54, 4913 – 4920.

- Lin, J.Y., Tarbell, J.M., 1980. An experimental and numerical study of periodic flow in a curved tube. J. Fluid Mech. 100, 623-638.
- Lockhart, R.W., Martinelli, R.C., 1949. Proposed correlation of data for isothermal two-phase two component flow in pipes. Chem. Eng. Prog. 45, 39–48.
- Mandal, S.N., Das, S.K., 2003. Gas–liquid flow through helical coils in vertical orientation. Ind. Eng. Chem. Res. 42, 3487–3494.
- Metzner, A.B., Reed, J.C., 1955. Flow of non-Newtonian fluids - correlation of the laminar, transition, and turbulent-flow regions. AIChE J. 1, 434 – 440.
- Mishra, P., Gupta, S. N., 1979b. Momentum-Transfer in Curved Pipes 2. Non-Newtonian Fluids. Ind. Eng. Chem. Proc. Des. Dev. 18, 137-142.
- Mishra, P., Gupta, S.N., 1979a. Momentum transfer in curved pipes 1. Newtonian fluids; 2. Non-Newtonian fluids. Ind. Eng. Chem. Proc. Des. Dev. 18, 130–137.
- Mujawar, B.A., Rao, M.R., 1978. Flow of Non- Newtonian fluids through helical coils. Ind. Eng. Chem. Proc. Des. Dev. 17, 22–27.
- Mujawar, B.A., Rao, M.R., 1981. Gas–non-Newtonian liquid two-phase flow in helical coils. Ind. Eng. Chem. Proc. Des. Dev. 20, 391–397.
- Rangacharyulu K., Davies, G.S., 1984. Pressure drop and holdup studies of air-liquid flow in helical coils. Chem. Eng. J. 29, 41–46.
- Ripple, G. R., Eidt, C.M., Jordan, H.B., 1966. Two-phase flow in a coiled tube. Pressure drop, Holdup, and Liquid phase axial mixing. Ind. Eng. Chem. Proc. Des. Dev. 5, 32-39.
- Saxena, A.K., Schumpe, A., Nigam, K.D.P., Deckwer, W.D., 1990. Flow regimes, hold-up and pressure drop for two phase flow in helical coils. Can. J. Chem. Eng. 68, 553–559.

- Spedding, P.L., Chen, J.J.J., Nguyen, V.T., 1982. Pressure drop in two phase gas-liquid flow in inclined pipes. Int. J. Multiphase Flow 8, 407–431.
- Stepanek, J.B., Kasturi, G., 1972. Two-phase flow- II. Parameters for void fraction and pressure drop correlations. Chem. Eng. Sci. 27, 1881–1891.
- Trivedi, R.N., Vasudeva, K., 1975. Axial dispersion in laminar flow in helical coils. Chem. Eng. Sci. 30, 317-325.
- Vashisth, S., Kumar, V., Nigam, K.D.P., 2008. A review on potential applications of curved geometries in process industry. Ind. Eng. Chem. Res. 47, 3291–3337.
- Weisman, J., Lan, J., Disimile, P., 1994. Two-phase (air-water) flow patterns and pressure drop in the presence of helical wire ribs. Int. J. Multiphase Flow 20, 885–899.
- Whalley, P.B., 1980. Air-water two-phase flow in a helically coiled tube. Int. J. Multiphase flow 6, 345–356.
- Xie, G.D., 1990. Torsion effect on secondary flow in helical pipes. Int. J. Heat Fluid Flow 11, 114-119.
- Xin, R.C., Awwad, A., Dong, Z.F., Ebadian, M.A., 1996. An investigation and comparative study of the pressure drop in air-water two-phase flow in vertical helicoidal pipes. Int. J. Heat Mass Transfer 39, 735–743.
- Xin, R.C., Awwad, A., Dong, Z.F., Ebadian, M.A., 1997. An experimental study of single-phase and two-phase flow pressure drop in annular helicoidal pipes. Int. J. Heat Fluid Flow 18, 482-488.
- Yamamoto, K., Akita, T., Ikeuchi, H., Kita, Y., 1995. Experimental-Study of the Flow in a Helical Circular Tube. Fluid Dyn. Res. 16, 237-249.

- Yamamoto, K., Yanase, S., Yoshida, T., 1994. Torsion effect on the flow in a helical pipe. Fluid Dyn. Res. 14, 259 –273.
- Yanase, S., Goto, N., Yamato, K., 1989. Dual solutions of the flow through a curved tube. Fluid Dyn. Res. 5, 191– 201.

CHAPTER-4

MIXING CHARACTERISTICS

This chapter describes the investigation of the effect of various dynamic and geometrical parameters on mixing characteristics in helical coil tube based on flow pattern. Based on the experimental data a correlations were proposed to predict the flow pattern based intensity of mixing characteristics by dimensional analysis.

4.1. Introduction

Mixing is one of the most common physical operations carried out in the chemical, and petrochemical operations. Knowledge of the magnitude of all these effects is very important in designing heat exchangers and holding tubes for the food industry (Trivedi and Vasudeva, 1975). As an effect of secondary flow, the axial dispersion is reduced and the maximum axial velocity region is shifted toward the outer wall. The axial dispersion could be greatly reduced in a helical tube as compared to that in a straight tube (Koray and Sandeep, 2004; Chhabra and Richardson, 2008). Many authors reported their different studies done on the mixing characteristics by examining axial dispersion coefficient in coiled tubes (Leclerc et al., 1987; Saxena and Nigam, 1979; Saxena and Nigam, 1981; Saxena and Nigam, 1983a; Saxena et al., 1983; Saxena and Nigam, 1983b). Dispersion processes are often investigated, both theoretically and experimentally, using the concept of residence time distribution (RTD). Schonfeld and Hard (2003) proposed a different concept of chaotic mixing which relies on helical flows induced in planar curved channels. In the micro mixers proposed by them, the mixing time was in the range of milliseconds, thus lending towards the fast, mass-transfer-limited reactions. Kumar et al. (2006) studied the mixing is an essential component of nearly all industrial chemical processes, ranging from simple blending to complex multi-phase reaction systems for which reaction rate, yield and selectivity are highly dependent upon mixing performance. Castelain and Legentilhomme (2006) experimentally studied the residence time distribution in a helical system and in a spatially chaotic system. They concluded that axial dispersion is reduced while compared with the helical system. Trivedi and Vasudeva (1975) reported the experimental study of dispersion of solute in helical coils under laminar flow conditions by the tracer method. They covered the range of variables for their experimental as $10 < \lambda < 280$, $10 < N_{Re} < 1600$ and $1.5 \times 10^3 < N_{sc} < 8.7 \times 10^3$. Under these conditions they reported that the coiling tube can decrease axial dispersion under laminar flow conditions. They found that the conditions under which dispersion analyzed can be expected to hold with effective Bodenstein numbers and correlated successfully as a function of N_{De} (Dean number) and N_{sc} (Schmidt number). Jiang et al. (2004) have proposed s-shaped geometry to generate chaotic flows by alternating switching between different flow patterns. However these studies have been performed for planar curved ducts with square cross section and zero pitch. From the literature it is found that in helical coil, studies on flow pattern based mixing characteristics with Newtonian and non-Newtonian fluids is very scanty. The present work shows the mixing characteristics in helical coil using Newtonian and non-Newtonian fluid. A flow pattern based axial dispersion coefficients are predicted by developing the correlation model.

4.2. Theory to analyze mixing characteristics

Normally for the measurement of residence time distribution, the tracer technique is used which involves the injection of tracer material at some location in the helical coil tube and the concentration of the test section is detected as a function of time at one or more downstream positions. The tracer input may be step, impulse, imperfect pulse, sinusoidal (Kramers and

Alberda, 1953; Bennett and Goodridge, 1970). But as per majority of the literature, the investigators have used impulse, pulse or imperfect pulse inputs. The true impulse function is difficult to introduce in most practical cases. Proper precaution should be taken to inject the tracer to ensure good pulse injection. Flow distribution have significant effects on the residence time distribution. Other factors such as reactor channeling dead zones, by passing on the residence time distribution are undesired for proper residence time distribution curve. The non-uniform velocity and method of injection and detection can affect the nature of residence time distribution curve. The position of detection probe can also affect the curve.

4.2.1. Models for analyzing mixing characteristics

The mixing characteristics can be evaluated by different models (differential and stage-wise models) (Kelkar et al., 1983). Axial dispersion model is a simplest and single parameter differential model. From the literature review it is seen that most of the cases the study of liquid phase dispersion coefficient is done by using axial dispersion model. The axial dispersion model characterizes the mixing by a simple one-dimensional Fick's-law-type diffusion equation (Shah, 1979; Majumder et al., 2005).

4.2.1.1. Method for evaluation the axial dispersion coefficient from RTD data

One parameter axial dispersion model is widely used to correlate the RTD data. According to axial dispersion model in addition to transport of tracer material by bulk flow, U_iAC_T, every component in the mixture is transported through any cross section of the reactor at a rate equal to [$-E_zA\,(\partial C_T/\partial Z)$] resulting from molecular and convective diffusion. Therefore the molar flow rate of tracer (F_T) in the coil tube at any position z can be written as

$$F_T = -E_Z A \frac{\partial C_T}{\partial Z} + AU_i C_T \qquad (4.1)$$

Here E_z is the axial dispersion coefficient (m²/sec), *A* is the tube cross-section area (m²), C_T is concentration of tracer at any location *z* in helical coil, U_i is the interstitial or actual velocity of the tracer element in tube. A mole balance on inert tracer under the diffusion mechanisms can be expressed as

$$-\frac{\partial F_T}{\partial Z} = A\frac{\partial C_T}{\partial t} \tag{4.2}$$

Substituting for F_T and dividing by cross-sectional area *A*, the Eq. (4.2) becomes

$$E_Z \frac{\partial^2 C_T}{\partial Z^2} - \frac{\partial (U_i C_T)}{\partial Z} = \frac{\partial C_T}{\partial t} \tag{4.3}$$

After normalizing, the Eq. (4.3) becomes

$$\frac{1}{Pe}\frac{d^2\Psi}{d\lambda^2} - \frac{d\Psi}{d\lambda} = \frac{d\Psi}{d\theta} \tag{4.4}$$

$$Pe = \frac{U_{sl}L}{(1-\varepsilon_g)E_z} \tag{4.5}$$

$$\theta = \frac{U_{sl}t}{(1-\varepsilon_g)L} \tag{4.6}$$

$$\Psi = \frac{C_T}{C_{T_0}} \tag{4.7}$$

$$\lambda = \frac{Z}{L} \tag{4.8}$$

$$U_i = \frac{U_{sl}}{(1-\varepsilon_g)} \tag{4.9}$$

The above equation is a second order ordinary differential equation, which can be easily solved by proper boundary condition. Generally three types of cases arises open-open vessel, closed-closed vessel and closed-open vessel. In the present system, the open open boundary conditions is considered.

Open-open vessel: In an open-open vessel dispersion occurs both upstream and downstream of the test section. A schematic of open-open boundary conditions are shown in Figure 4.1.

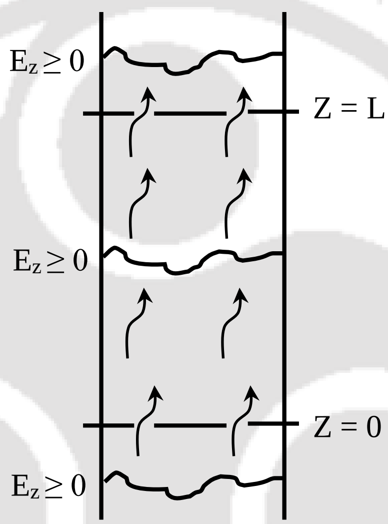

Figure 4.1: Schematic of open-open boundary condition

Boundary conditions: At the plane Z = 0 there is continuity of flux.

So at Z = 0 and t = 0

$$F_T(0^-, t) = F_T(0^+, t) \tag{4.10}$$

$$F_T(0^-, t) = U_i A C_T(0^-, t) \tag{4.11}$$

$$F_T(0^+,t) = -E_Z A\left(\frac{\partial C_T}{\partial Z}\right)_{Z=0^+} + U_i A C_T\left(0^+,t\right) \tag{4.12}$$

$$U_i A C_T(0^+,t) = -E_Z A\left(\frac{\partial C_T}{\partial Z}\right)_{Z=0^+} + U_i A C_T\left(0^+,t\right) \tag{4.13}$$

At Z = L the concentration of tracer is constant not varying with position.

Therefore at Z = L

$$C_T(L^+,t) = C_T(L^-,t) \tag{4.14}$$

$$\frac{\partial C_T}{\partial z} = 0 \tag{4.15}$$

The solution of equation (4.4) for long tubes with open-open boundary condition is given by (Fogler, 2007)

$$\Psi = \frac{C_T}{C_{T0}} = \frac{1}{2\sqrt{\pi\theta / Pe}}\exp\left[\frac{-(1-\theta)^2}{4\theta / Pe}\right] \tag{4.16}$$

By the moment method, the parameters mean residence time (t_m) and the Peclet number (*Pe*) can be estimated from the axial dispersion model. The mean residence time (t_m) and the variance (σ) for an open system are given by

$$t_m = \frac{\sum t_i C_{Ti}}{\sum C_{Ti}} \tag{4.17}$$

$$\sigma^2 = \frac{\sum t_i^{\,2} C_{Ti}}{\sum C_{Ti}} - t_m \tag{4.18}$$

For open-open system the mean residence time (t), Peclet number (*Pe*) and variance (σ) are related as (Fogler, 2007)

$$\frac{\sigma^2}{t^2{}_m} = \frac{2}{Pe} + \frac{8}{Pe^2} \tag{4.19}$$

Variance represents the square of spread of the distribution as passes through the test section.

4.3. Experimental

The schematic of the experimental setup used in the present investigation is shown in Figure 2.2. in chapter 2. Once steady-state was reached and when the flow is fully developed, the tracer, 3 ml of Sodium chloride solution of concentration 1 M (non-reactive with other liquid used in the experiment) was injected at a point below of the coil tube. The volume of tracers used was kept small (~ 10%) in relation to the total volume of the coil tube. The injection was carried out as quickly (2-3 seconds) and smoothly as possible by a syringe operating manually. Liquid was collected in test tubes at every interval at a downstream position of the helical coil tube. The variation of tracer concentration with time was measured by digital conductivity meter (Model: VSI-04 ATC Deluxe, Make: VSI Electronics Pvt. Ltd., Chandigarh, India). The experiments were conducted at four different liquid flow rates (3.33×10^{-5} to 1.33×10^{-4} m^3/s) and four different gas flow rates (1.67×10^{-5} to 6.67×10^{-5} m^3/s) for air-SCMC system of concentrations 0-3.0 kg/m^3. The range of conductivity meter is about 0 - 999 micro Siemens per meter (μ Sm^{-1}). For the calibration of the conductivity meter first of all, the conductivity probe was cleaned by using distilled water, and then different samples of NaCl with tap water ranging from 5 $moles/m^3$ to 35 $moles/m^3$ were prepared. The samples of about 20 ml each were prepared in a beaker in which conductivity probe is inserted and then the reading of the conductivity meter is recorded varying with concentration of samples. The change of conductivity with concentration is shown in Figure 4.2.

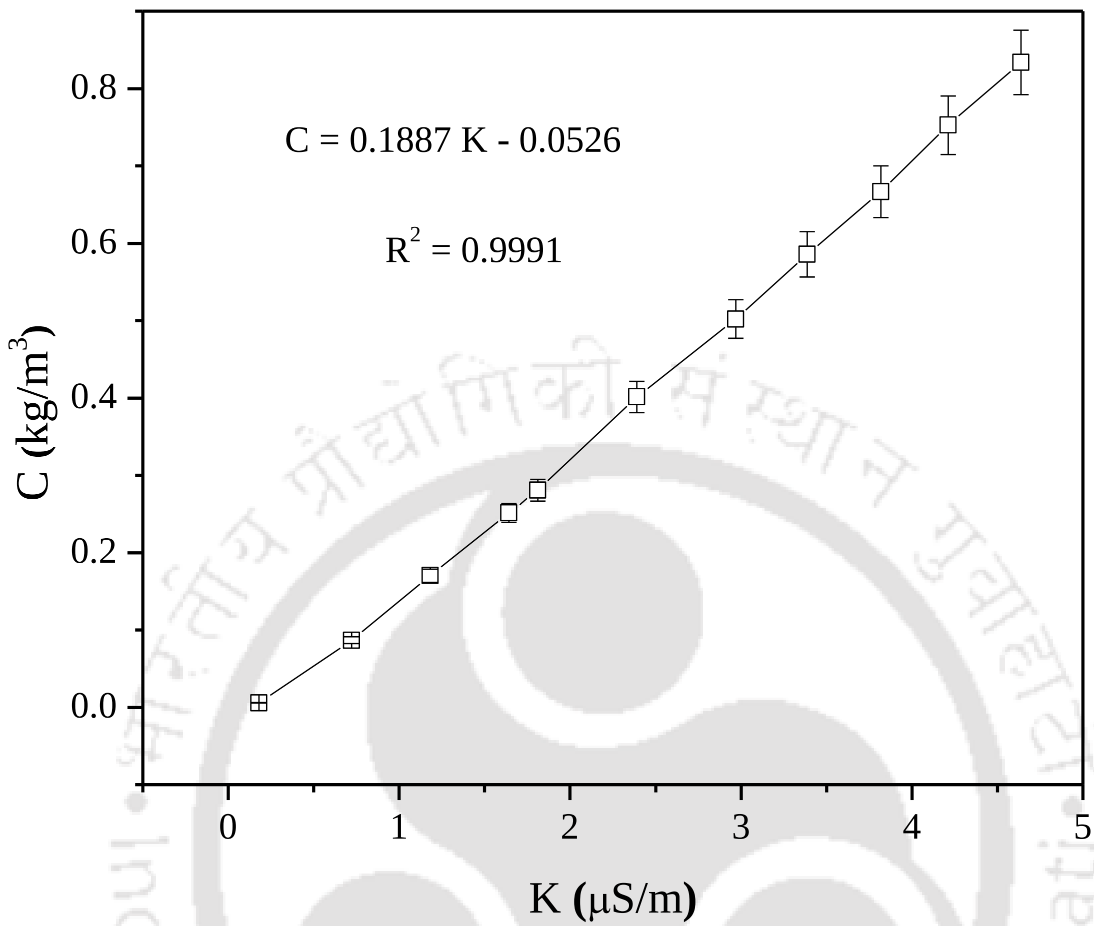

Figure 4.2: Calibration graph for conductivity meter for water

A correlation has been made with the data and can be represented as:

$$C = 0.1887K - 0.0552 \qquad R^2 = 0.9991 \tag{4.20}$$

where C = concentration of tracer, kg/m^3 and K is the conductivity of the solution, μSm^{-1}. As per the equation (Eq. (4.20)) all the conductivity data obtained from experiment were converted to concentration data. For non-Newtonian fluid, three different concentrations of Sodium Carboxy Methyl Cellulose (SCMC) were used and calibrated the conductivity meter for each composition of SCMC solution. The corresponding correlations are represented as follows:

$$C = aK - b \tag{4.21}$$

The values of parameters *a* and *b* (Eq. 4.21) for different SCMC+ NaCl solutions are given in Table 4.1. A graph of conductivity with different SCMC + NaCl concentrations is shown in Figure 4.3. The uncertainty of the experimental data is shown in Table 4.2.

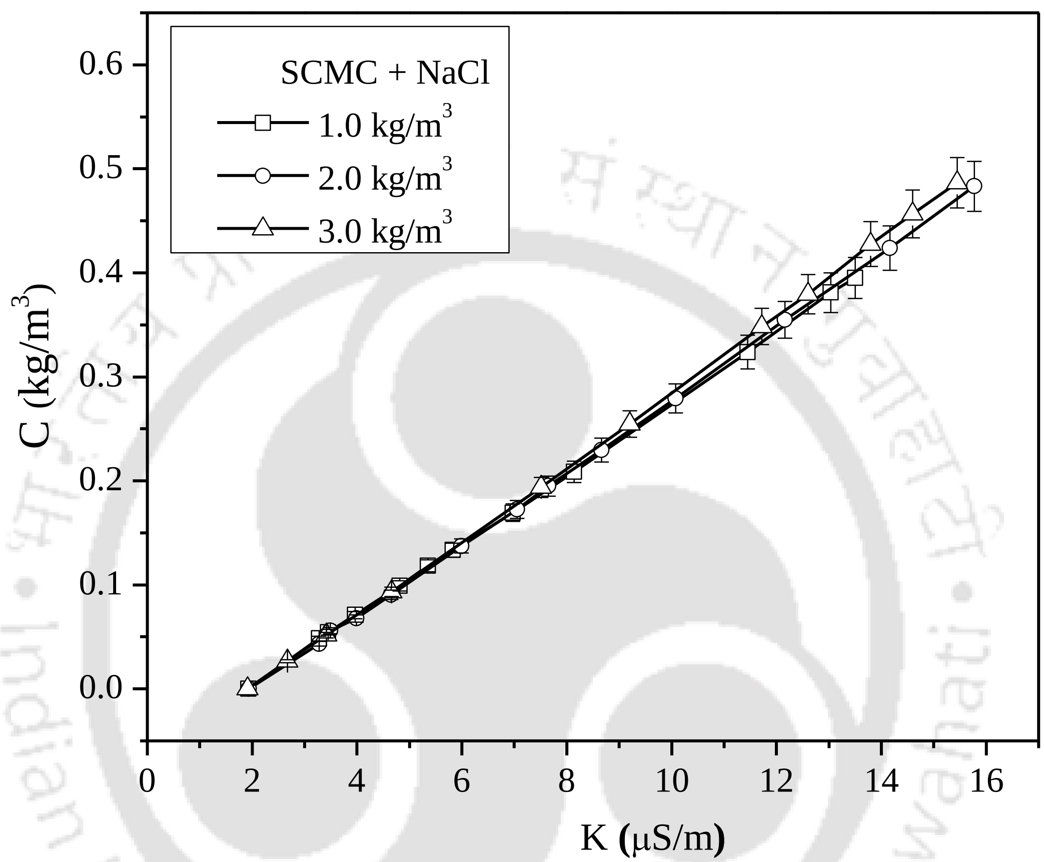

Figure 4.3: Calibration graph for conductivity meter for different SCMC solution

Table 4.1: Calibration parameters for the system measured 25 ± 1°C

System	Parameter a	Parameter b	R^2
SCMC (1.0) + NaCl	0.3421	0.0912	0.991
SCMC (2.0) + NaCl	0.3531	0.1204	0.992
SCMC (3.0) + NaCl	0.3598	0.1293	0.991

Table 4.2: Range of the means, standard deviations, and uncertainties of the dispersion coefficient (E_z) at constant tube diameter (d_t = 0.015 m), coil diameter (D_c = 0.117 m)

U_{sl} (m/s)	U_{sg} (m/s)	SCMC (kg/m^3)	Range of mean* (m^2/s)	N	Range of STDEV* (x 10^{-3})	Range of uncertainty* (x 10^{-3})	Range of relative uncertainty %
0.188 - 0.755	0.094	1.0	0.264 - 0.843	6.0	2.58 - 3.78	1.05 - 1.54	0.125 - 0.588
0.188 - 0.755	0.189	1.0	0.295 - 1.121	6.0	3.82 - 3.83	1.56 - 1.57	0.139 - 0.534
0.188 - 0.755	0.283	1.0	0.465 - 1.182	6.0	2.99 - 4.17	1.22 - 1.71	0.103 - 0.367
0.188 - 0.755	0.377	1.0	0.537 - 1.229	6.0	4.88 - 5.26	1.99 - 2.15	0.371 - 1.829
0.188 - 0.755	0.094	2.0	0.235 - 0.605	6.0	3.25 - 6.05	1.33 - 2.47	0.410 - 0.572
0.188 - 0.755	0.094	3.0	0.201 - 0.513	6.0	3.08 - 3.35	1.26 - 1.37	0.266 - 0.626

* The theory to calculate the values is given in chapter 2 in equations (2.10 – 2.12)

Each value of E_z in 4th column corresponds to the mean of 6 data points (i.e., N=6). Relative uncertainty is calculated from standard uncertainty and mean value of the corresponding data set.

4.4. Results and discussion

4.4.1. Residence time distribution

The experimentation on RTD for mixing phenomena has been done with air -Newtonian liquid (water) and air - Non-Newtonian fluid (SCMC) system. The result has been analyzed with axial dispersion model. A typical parity plot of experimental values with the data obtained by axial dispersion model is shown in Figure 4.4.

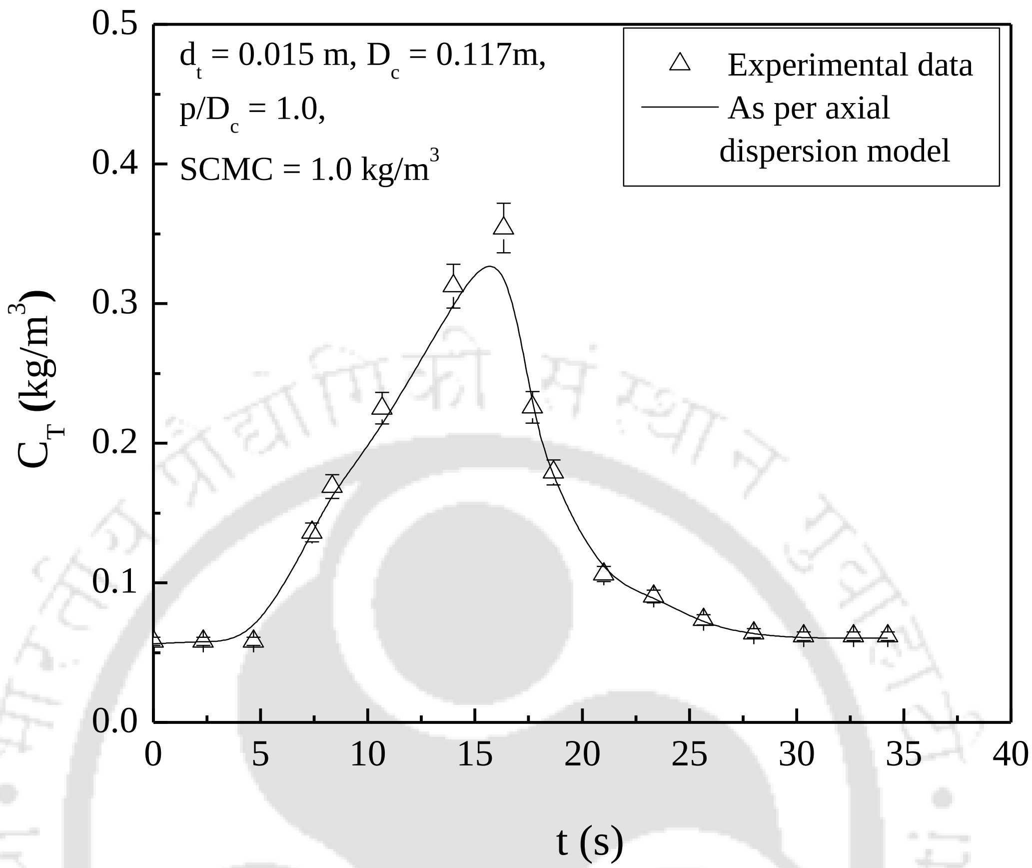

Figure 4.4: Parity plot of RTD curve with axial dispersion model

The axial dispersion model is fitted well where 90% of data are predicted within ±6 % deviation. It was found that the intensity of the mixing in the helical coil depends on different operating variables. The effect of gas velocity on the residence time of tracer particles is shown in Figure 4.5. It was found that just after the injection of tracer, up to a certain time the concentration of the tracer particles was zero of the sample collected. When the tracer particle is injected, the particle of tracer starts to disperse in the coil tube and mixing of tracer particle takes place. Tracer takes some time to respond at exit point. So, the concentration of samples collected from the coil tube have almost zero at the start.

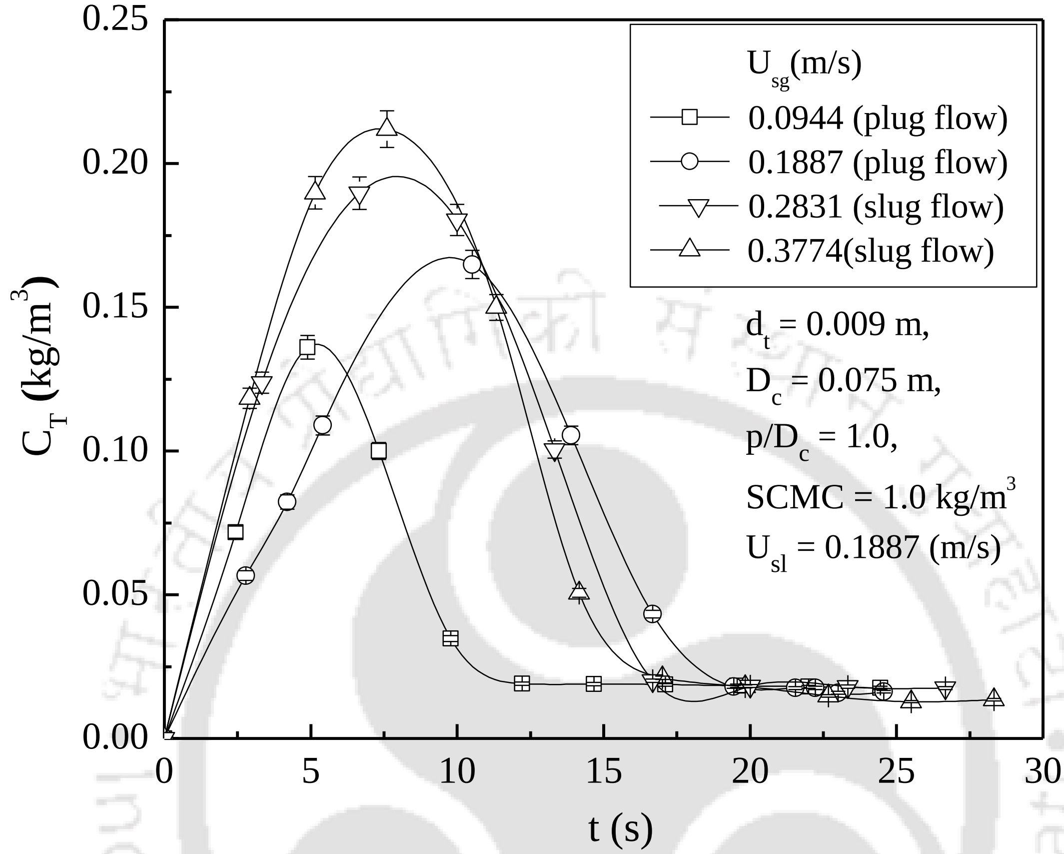

Figure 4.5: Variation of residence time distribution of tracer particle with gas velocity

It was also observed that the residence time of the tracer particle decreases when the gas velocity was increased. This is due to the fact that at high gas velocity the momentum energy in the liquid-gas mixture increases which increases the dispersion and reduces the residence time. The effect of liquid velocity on residence time of tracer particle is shown in Figure 4.6. It was observed that the residence time of the tracer decreased with increasing superficial liquid velocity. At the higher liquid velocity more energy dissipated for the gas-liquid mixture and mixture gets more agitated which enhances the dispersion of the liquid in the helical coil tube. This may result the variation of the RTD with superficial liquid velocity.

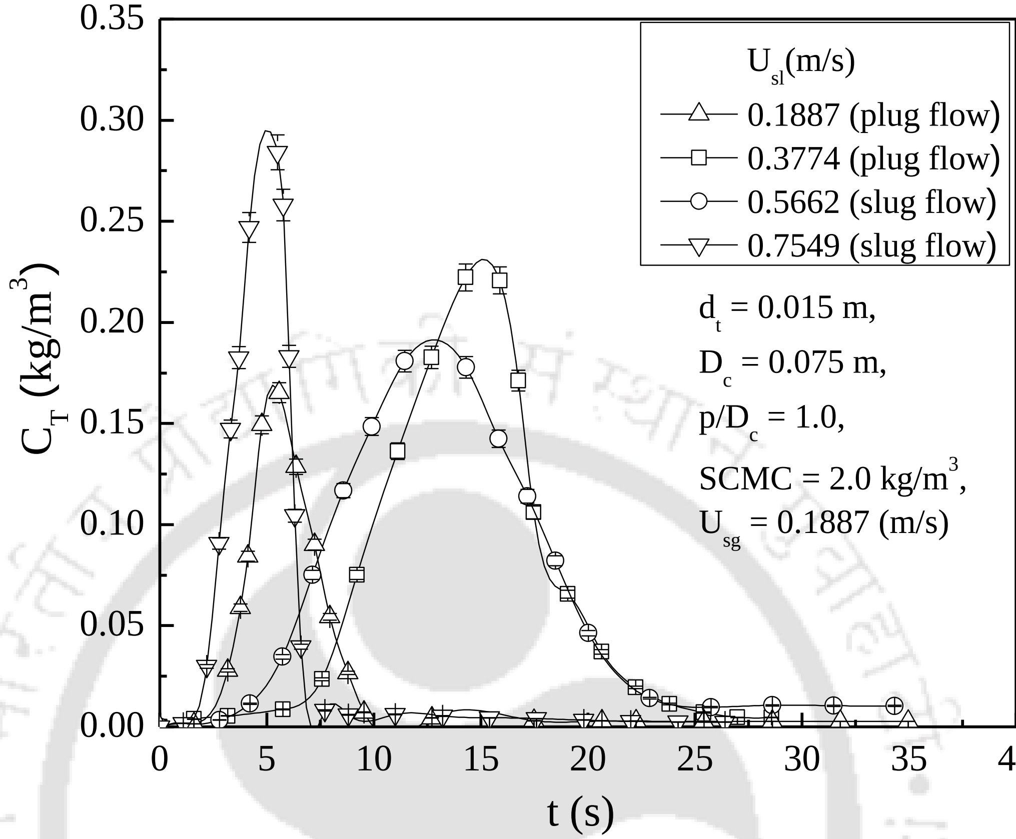

Figure 4.6: Variation of residence time distribution of tracer particle with liquid velocity

The effects of gas superficial velocity on residence time at different superficial liquid velocities are shown in Figure 4.7. It was observed that the residence time of the liquid decreases with increase in gas flow rate. This is due to the increase in axial dispersion with the increase in gas flow rate. The effect of superficial liquid velocity on the mean residence time is shown in Figure 4.8. When liquid flow rate increases the turbulence in the coil tube increase and momentum exchange in the fluid element also increases. The high flow rate of fluid element tends to pass the coil tube very fast hence their residence time in coil tube decreases.

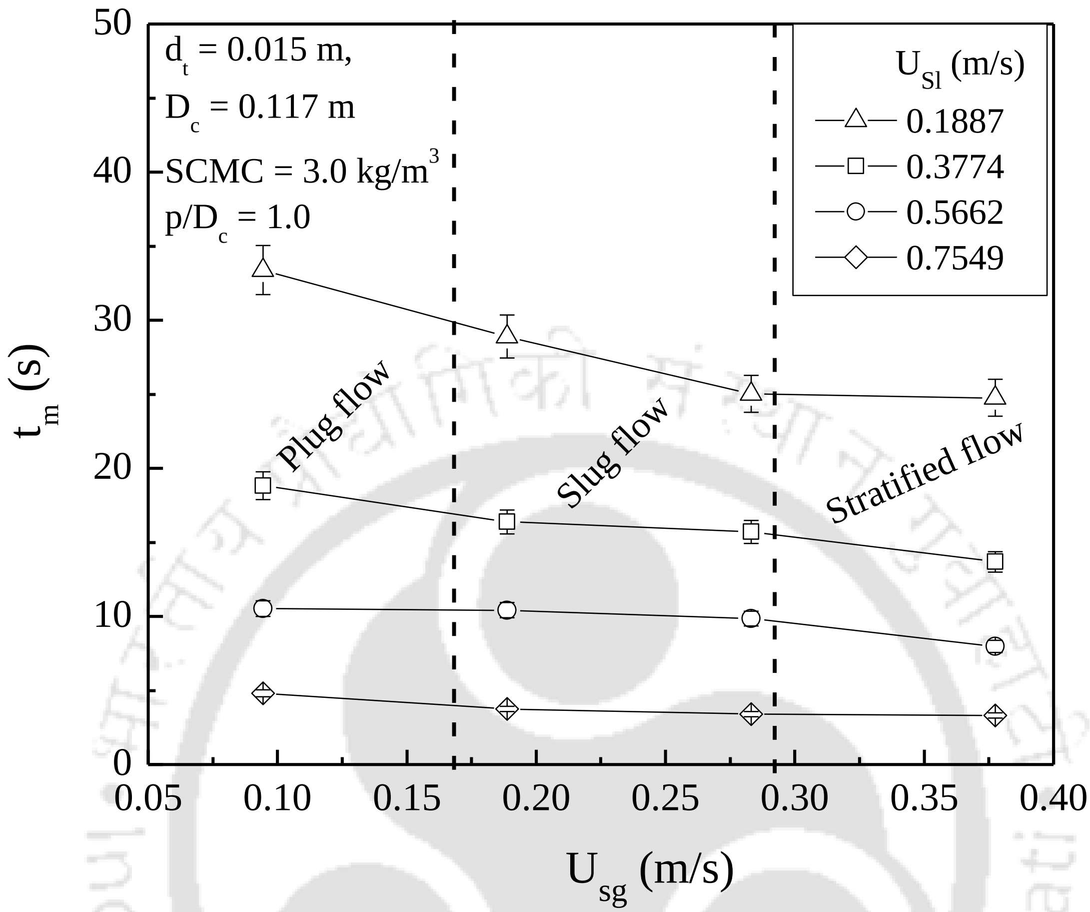

Figure 4.7: Variation of mean residence time with superficial gas velocity for air-SCMC system

It was also observed that the residence time of the liquid at higher superficial gas velocity is less compared to the low superficial gas velocity. At low gas flow rate the residence time decreased mainly due to increase in liquid flow rate. But in case of high gas flow rate, the liquid flow rate as well as gas velocity in the coil tube are increased and both this factors act in the same direction which resulted in the decrease in residence time of the fluid at a faster rate.

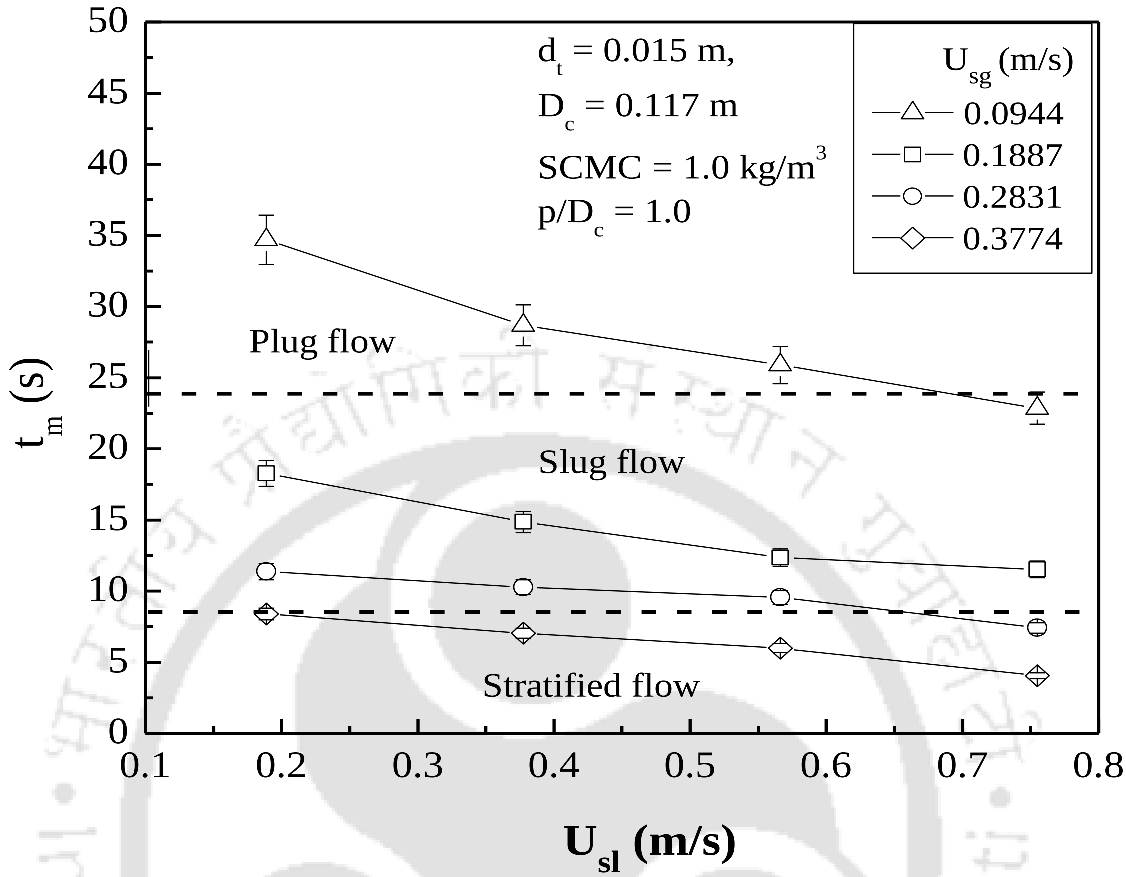

Figure 4.8: Variation of mean residence time with superficial liquid velocity

4.4.2. Effect of superficial velocity on dispersion coefficient

The effect of superficial gas velocity on dispersion coefficient is shown in the Figure 4.9. It is observed that increasing the gas velocity, the dispersion coefficient increases. Increasing in the gas flow rate, the turbulence in the coil tube increases and the flowing fluid tends to deviate more from plug flow and hence the dispersion coefficient increases. From the Figure 4.10 it is also observed that the value of dispersion coefficient is higher at higher liquid flow rate. When the gas flow rate is increased, the value of dispersion coefficient increases at a faster rate with liquid flow rate. At higher liquid velocity, the gas holdup increases which enhances the turbulence of the gas liquid mixture and consequently increases the dispersion.

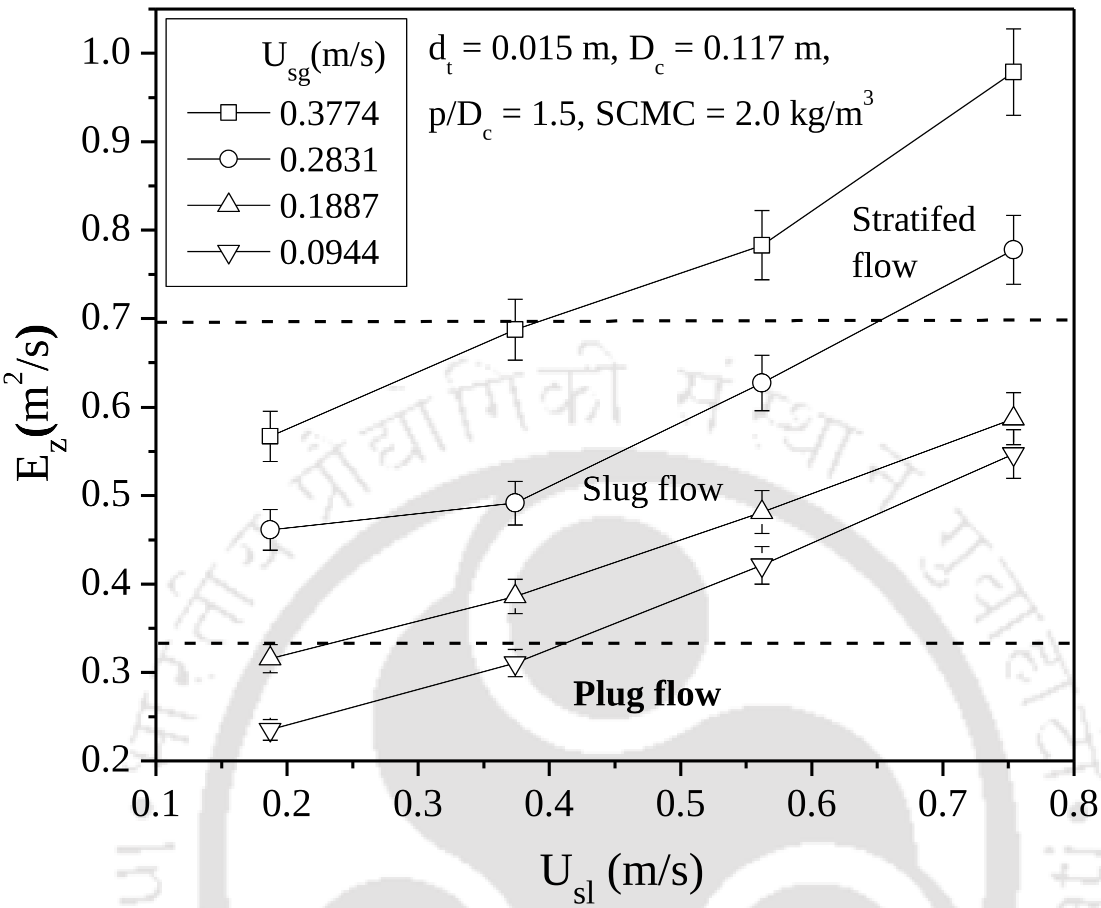

Figure 4.9: Effect of superficial gas velocity on dispersion coefficient

The comparison of dispersion coefficients of air-water system and aqueous SCMC solution-air system is shown in Figure 4.11. It was observed that at same liquid velocity the dispersion of liquid increases as the concentration of SCMC decreases and it was also found that the dispersion coefficient in non-Newtonian fluid is less as compare to Newtonian fluid (water). According to the visual observation, at higher concentration of SCMC the slug flow regime were observed in the coil tube and in slug flow the intensity of disturbance is observed to increase in the coil tube, which results in high kinetic energy transfer inside the coil tube due to which the dispersion coefficient increases. This may be due to the formation of more gas bubble in the tube with decreasing surface tension of SCMC solution.

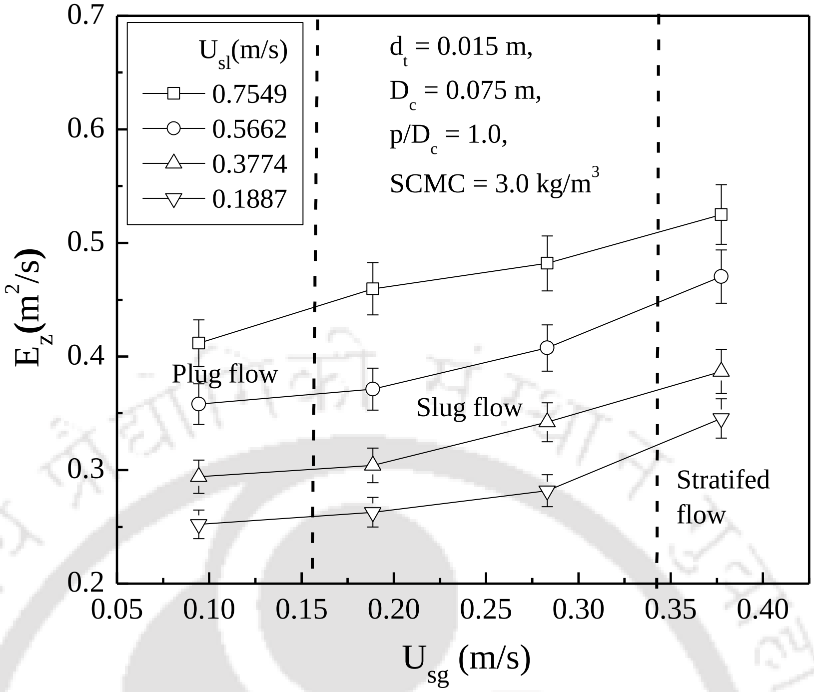

Figure 4.10: Effect of superficial liquid velocity on dispersion coefficient

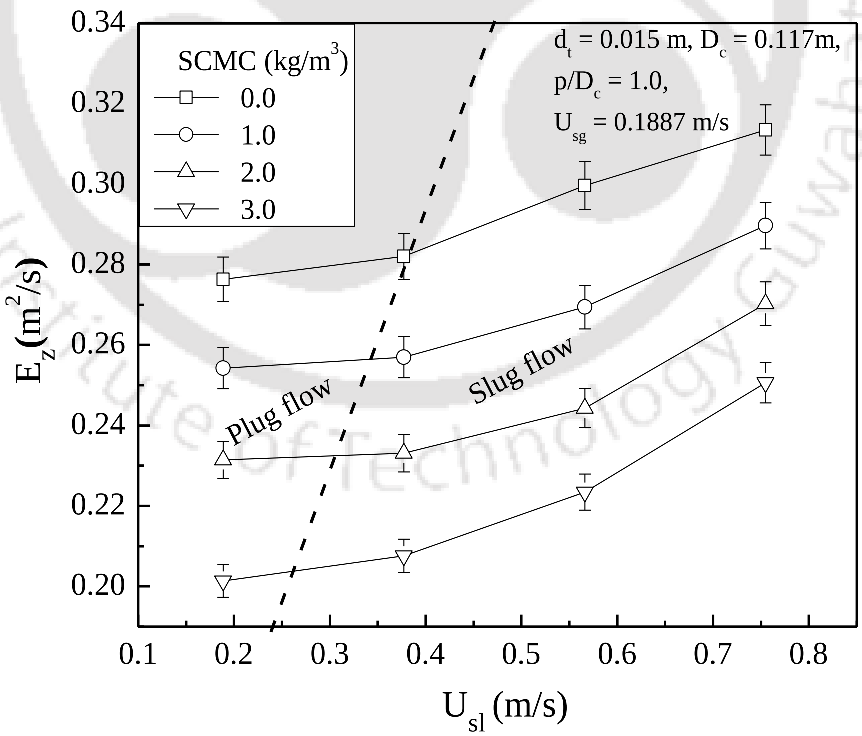

Figure 4.11: Effect of SCMC concentration on dispersion coefficient

4.4.3. Effect of geometrical variables on dispersion coefficient

The effects of geometrical variables on dispersion coefficient are observed under the flow patterns of plug flow and slug flow. The Figure 4.12 shows the variations of dispersion coefficient with superficial liquid velocity for three different tube diameters (0.009, 0.015 and 0.020 m) at constant coil diameter (D_c= 0.117 m), pitch difference (p/D_c = 1.0) and gas superficial velocity (U_{sg} = 0.118 m/s) for non-Newtonian fluid (SCMC = 2.0 kg/m^3).

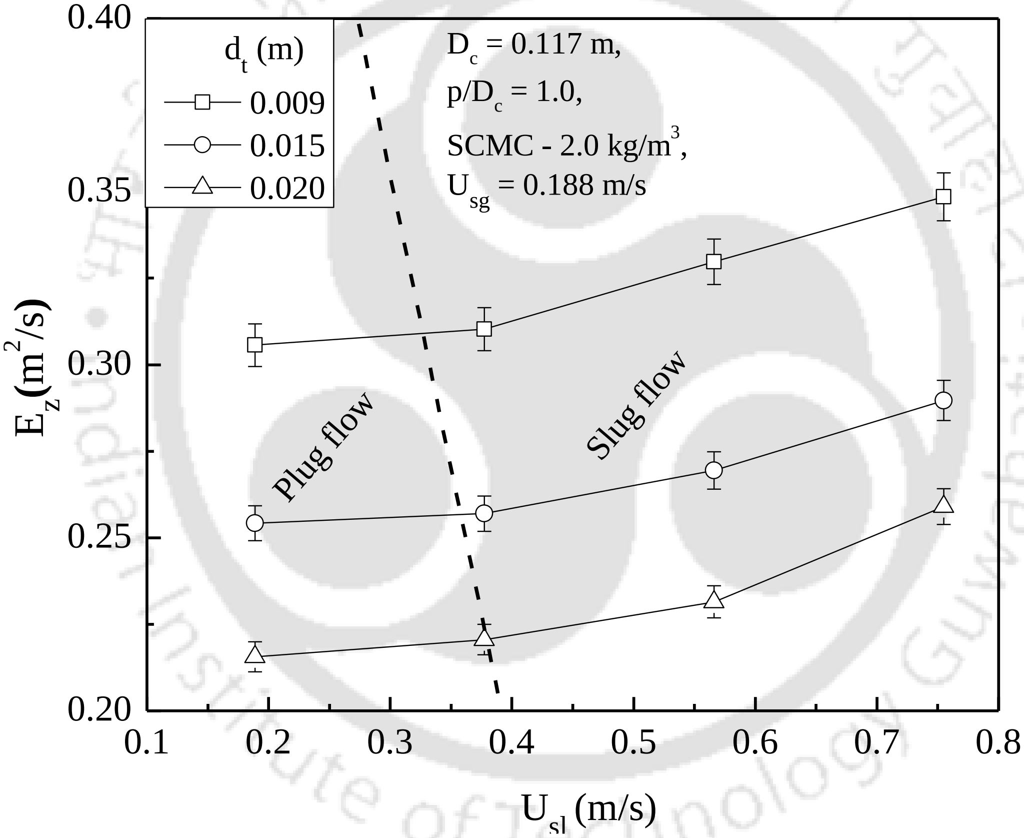

Figure 4.12: Effect of tube diameter on dispersion coefficient

It was observed that the increase in tube diameter, the dispersion coefficient decreased at constant two-phase flow. With increasing tube diameter at a fixed liquid flow rate pressure of the flow decreases, momentum decreases and hence the dispersion coefficient decreases. Figure 4.13 shows that the effect of coil diameter on dispersion coefficient at tube diameter (d_t = 0.015 m), pitch difference (p/D_c = 1.0) gas superficial velocity (U_{sg} = 0.188 m/s) and liquid concentration (SCMC = 1.0 kg /m^3). With increasing coil diameter the dispersion coefficient decreases. While increasing the coil diameter curvature and the number of turns also decreases, which results in decrease in the dispersion coefficient.

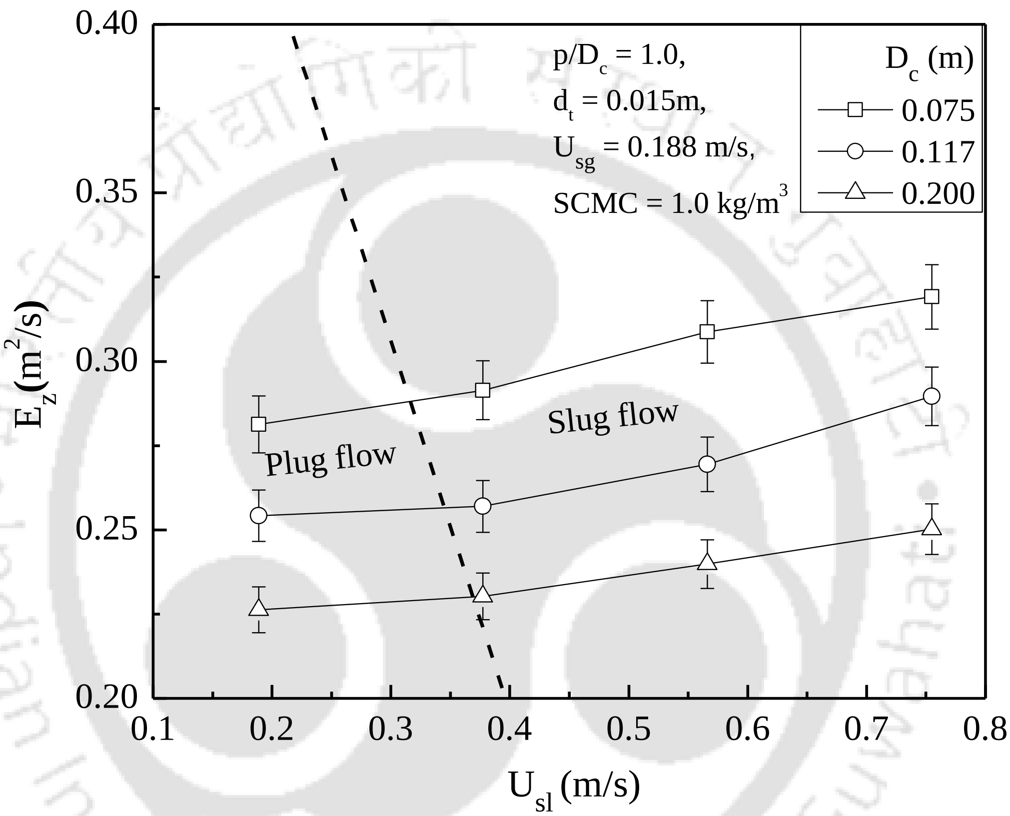

Figure 4.13: Effect of coil diameter on dispersion coefficient

Figure 4.14 shows that effect of pitch difference (p/D_c) on dispersion coefficient at constant tube diameter (d_t = 0.015 m), coil diameter (D_c= 0.117 m), gas superficial velocity (U_{sg} = 0.188 m/s) and liquid concentration (SCMC = 2.0 kg/m^3). The increase in pitch difference, the dispersion coefficient decreases. If pitch distance is becoming high, the curvature effect will decrease. The centrifugal force will decrease with the decrease in curvature which may results in decrease in dispersion coefficient.

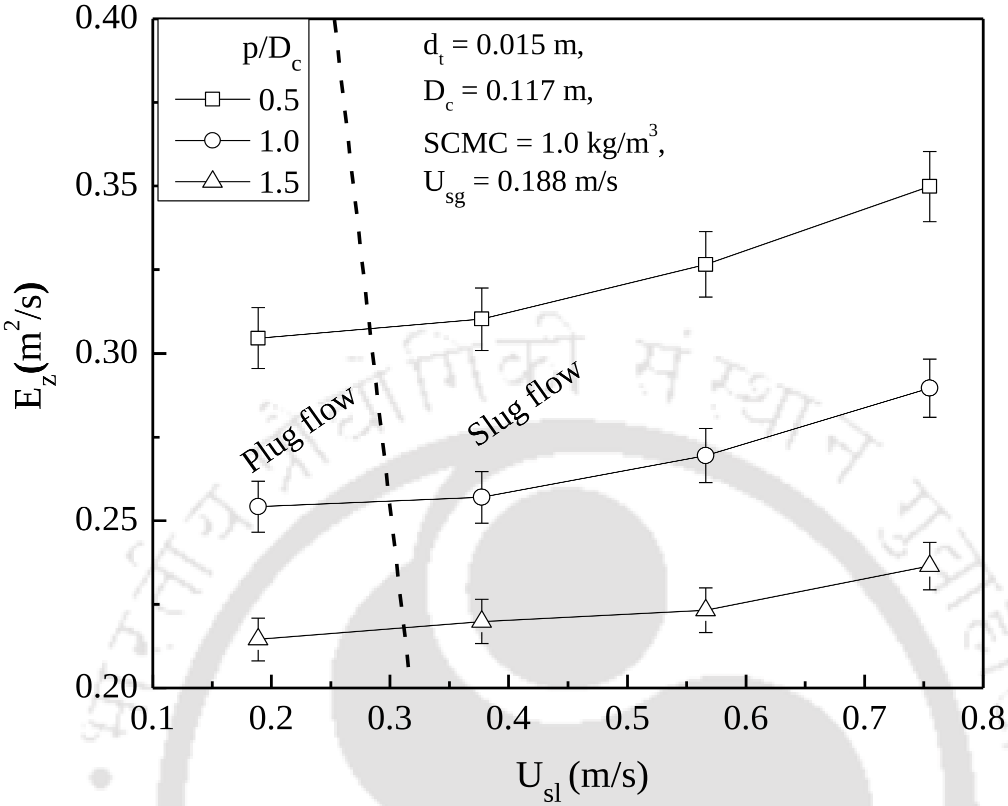

Figure 4.14: Effect of pitch difference on dispersion coefficient

4.4.4. Development of correlation model to predict the intensity of mixing

The axial dispersion coefficient in helical coil system is found to be affected by many parameters such as gas velocity (U_{sg}), liquid velocity (U_{sl}), mixed density (ρ_m), tube diameter (d_t), pitch length (L_p). Hence an attempt has been made to correlate the effect of these variables on dispersion coefficient based on different flow patterns. The correlations can be expressed as

$$Pe = \alpha\left(\frac{\mu_l}{\rho_m U_{sl} d_t}\right)^a \left(\frac{U_{sg}}{U_{sl}}\right)^x \left(\frac{L_p}{D_c}\right)^y \left(\frac{\gamma_l}{\rho_m U_{sl}^2 d_t^2}\right)^z \quad (4.22)$$

where α, a, x, y and z are the constants. By regression analysis with the experimental data, the values of a, x, y and z are obtained. The regression analysis is done by the MS EXCEL Software with "Data analysis tool". The detail principle is shown in Appendix-I. The flow pattern based correlations are given as follows:

For plug flow

$$Pe = 5.126\left(\frac{\mu_l}{\rho_m U_{sl} d_t}\right)^{-0.012}\left(\frac{U_{sg}}{U_{sl}}\right)^{0.051}\left(\frac{L_p}{D_c}\right)^{-0.068}\left(\frac{\gamma_l}{\rho_m U_{sl}^2 d_t^2}\right)^{0.031} \quad (4.23)$$

within the range of variables: $0.00034 \leq \mu_l/(\rho_m U_{sl} d_t) \leq 1.0$, $0.125 \leq U_{sg}/U_{sl} \leq 2.0$, $0.1 \leq L_p/D_c \leq 3.0$ and $0.271 \leq \gamma_l/(\rho_m U_{sl}^2 d_t) \leq 42.792$. The correlation coefficient and standard error were found to 0.938 and 0.028 respectively.

For slug flow

$$Pe = 3.771\left(\frac{\mu_l}{\rho_m U_{sl} d_t}\right)^{-0.057}\left(\frac{U_{sg}}{U_{sl}}\right)^{0.015}\left(\frac{L_p}{D_c}\right)^{-0.030}\left(\frac{\gamma_l}{\rho_m U_{sl}^2 d_t^2}\right)^{0.058} \quad (4.24)$$

within the range of variables: $0.00034 \leq \mu_l/(\rho_m U_{sl} d_t) \leq 1.0$, $0.125 \leq U_{sg}/U_{sl} \leq 2.0$, $0.1 \leq L_p/D_c \leq 3.0$, and $0.5654 \leq \gamma_l/(\rho_m U_{sl}^2 d_t) \leq 35.681$. The correlation coefficient and standard error were found to 0.913 and 0.024 respectively.

For stratified flow

$$Pe = 3.718\left(\frac{\mu_l}{\rho_m U_{sl} d_t}\right)^{-0.102}\left(\frac{U_{sg}}{U_{sl}}\right)^{0.180}\left(\frac{L_p}{D_c}\right)^{-0..001}\left(\frac{\gamma_l}{\rho_m U_{sl}^2 d_t^2}\right)^{-0.073} \quad (4.25)$$

within the range of variables: $0.0009 \leq \mu_l/(\rho_m U_{sl} d_t) \leq 1.0$, $0.125 \leq U_{sg}/U_{sl} \leq 2.0$, $0.1 \leq L_p/D_c \leq 3.0$, $0.581 \leq \gamma_l/(\rho_m U_{sl}^2 d_t) \leq 25.919$. The correlation coefficient and standard error were found to 0.929 and 0.039 respectively. The parity plot of experimental and predicted Peclet number with different flow patterns is shown in Figure 4.15. It was observed that the proposed correlation predicts the intensity of mixing (Peclet number) to a good extent within the range of variables.

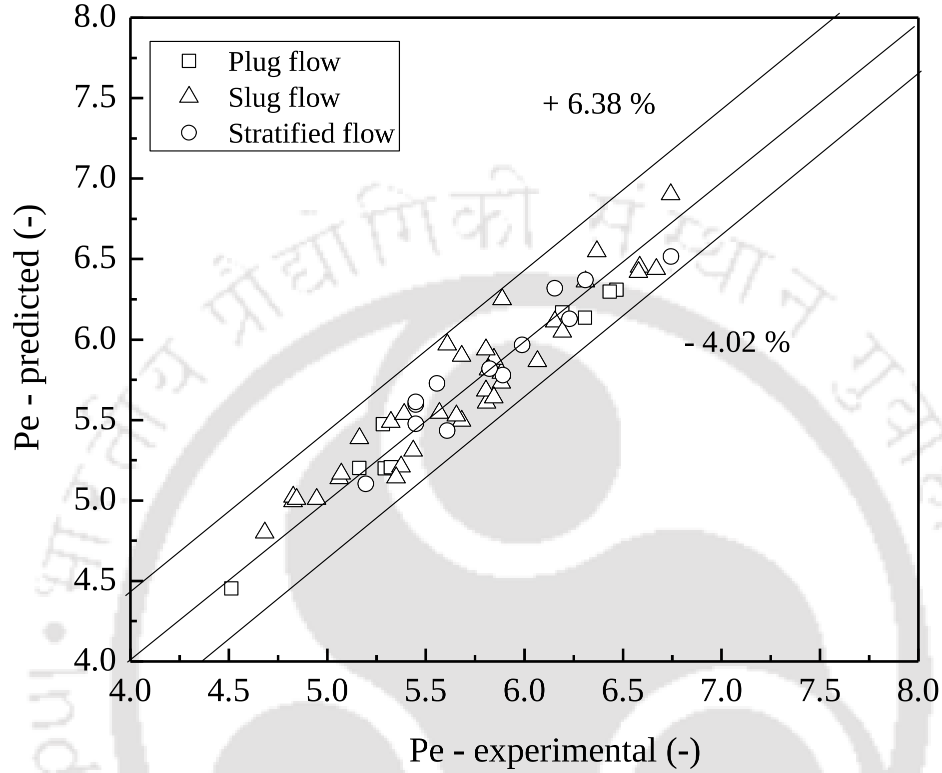

Figure 4.15: Parity plot of experimental and predicted Peclet number

4.5. Conclusion

In the present chapter, an attempt has been made to study the mixing characteristics of two-phase gas-Newtonian and gas-non-Newtonian fluid flow in vertical helical coil system. It is found that the mixing phenomenon in the helical coil system is affected by many variables such as gas flow rate, liquid flow rate, and various geometrical variables. Based on flow patterns, plug flow results the lowest dispersion coefficient whereas stratified flow provides highest dispersion coefficient. Slug flow results in dispersion coefficient fairly independent of gas superficial velocity. The mean residence time of the fluid decreases when the gas flow rate (or) liquid flow rate is increased. The Peclet number of liquid decreases with increasing either gas velocity or liquid velocity. It is observed that the dispersion coefficient increases with the decrease of tube diameter (d_t), coil diameter (D_c), liquid concentration (SCMC) and pitch difference (p/D_c). The developed correlation for a Peclet number with different operating variables based on different flow patterns (plug flow, slug flow and stratified flow) may be useful for scaling up the system for suitable application of the helical coil in mass transfer and heat transfer operations.

Nomenclature

C	Concentration of salt (kg/m^3)
C_T	Tracer concentration (kg/m^3)
C_{T0}	Initial tracer concentration (kg/m^3)
d_t	Tube diameter (m)
D_c	Coil diameter (m)
E_z	Axial dispersion coefficient (m^2/s)
F_T	Volumetric flow rate of tracer (m^3/s)
g	Acceleration due to gravity (m^2/s)
K	Conductivity meter reading (μ S/m)
L	Characteristic length (m)
L_p	Pitch length (m)
n	Flow behavior index (-)
Pe	Peclet number (-)

Re	Reynolds number (-)
t	Time (s)
t_m	Mean residence time (s)
U_i	Interstitial velocity of fluid (m/s)
U_{sl}	Superficial liquid velocity (m/s)
U_{sg}	Superficial gas velocity (m/s)
Z	Any location in vertical axis (m)

Greek letters

Ψ	Dimensionless concentration (C_T/C_{TO})
θ	Dimensionless time (t/t_m)
ρ_L	Liquid density (kg/m^3)
σ	Square root of variance
γ	Surface tension (N/m)
μ_L	Liquid viscosity (kg/m s)

References

- Bennett, A., Goodridge, F., 1970. Hydrodynamic and mass transfer studies in packed absorption columns. Trans. Inst. Chem. Eng. 48, 232-244.
- Castelain, C., Legentilhomme, P., 2006. Residence time distribution of a purely viscous non-Newtonian fluid in helically coiled or spatially chaotic flows. Chem. Eng. J. 120, 181-191.
- Chhabra, R.P., Richardson, J.F., 2008. Non-Newtonian Flow and Applied Rheology: Engineering Applications. Butterworth-Heinemann, Elsevier, Linacre House, Jordan Hill, Oxford, UK, chap. 8.

- Dean, W.R., 1927. Note on the motion of the fluid in a curved pipe. Philos. Mag. 4, 208-223.
- Dean, W.R., 1928. The streamline motion of fluid in a curved pipe. Philos. Mag. 7, 673.
- Fogler, H.S., 2007. Elements of Chemical Reaction Engineering. Prentice-Hall Int. Inc., New Jersey, 955-961
- Jiang, F., Drese, K.S., Hardt, S., Kuipper, M., Schonfeld, F., 2004. Helical flows and chaotic mixing in curved micro channels. AIChE J. 50, 2297-2305.
- Kelkar, B.G., Phulgoankar, S.R., Shah, Y.T., 1983. The effect of electrolyte solution on hydrodynamics and back mixing characteristics in bubble column. Chem. Eng. Sci. 27, 125 –133.
- Koray, P.T., Sandeep, K.P., 2004. Effect of tube curvature ratio on the residence time distribution of multiple particles in helical tubes. LWT - Food Sci. and Technol. 37, 387-393.
- Kramers, H., Alberda, G., 1953. Frequency response analysis of continuous flow systems. Chem. Eng. Sci. 2, 173–181.
- Kumar, V., Aggarwal, M., Nigam, K.D.P., 2006. Mixing in curved tubes. Chem. Eng. Sci. 61, 5742-5753.
- Leclerc, D.F., Smith, C.J., Clifford, Toren, E.C., 1987.Axial dispersion in coiled tubular reactors: The effect of curvature at low Dean Numbers. Anal. Chim. Acta. 184, 173-185.
- Majumder, S.K., Kundu, G., Mukherjee, D., 2005. Mixing mechanism in a modified co-current down flow bubble column. Chem. Eng. J. l, 45–55.
- Saxena, A.K., Nigam, K.D.P., 1979. On RTD in coiled tube. Chem. Eng. Sci. 34, 425-426.

- Saxena, A.K., Nigam, K.D.P., 1981. Axial dispersion in laminar flow of polymer solutions through coiled tubes. J. Appl. Polym. Sci. 26, 3475-3486.
- Saxena, A.K., Nigam, K.D.P., 1983a. Effect of coil pitch and cross sectional ellipticity on RTD for diffusion-free laminar flow in coiled tubes. Chem. Eng. Commun. 23, 277-289.
- Saxena, A.K., Nigam, K.M., Nigam, K.D.P., 1983. RTD for diffusion free laminar flow of non-Newtonian fluids through coiled tubes. Can. J. Chem. Eng. 61, 50-52.
- Saxena, A.K., Nigam, K.D.P., 1983b. Laminar dispersion in helically coiled tubes of square cross section. Can. J. Chem. Eng. 61, 53-57.
- Schonfeld, F., Hardt, S., 2003. Simulation of helical flows in micro channels. AIChE J. 50, 771-778.
- Shah, Y.T., 1979. Gas-liquid-solid reactor design. McGraw-Hill. New York, 65–93.
- Trivedi, R.N., Vasudeva, K., 1975. Axial dispersion in laminar flow in helical coils. Chem. Eng. Sci. 30, 317-325.

CHAPTER-5

HEAT TRANSFER CHARACTERISTICS

In this chapter heat transfer characteristics of vertical helical coil tube with various dynamic and geometrical parameters are investigated. It is observed that adding SCMC to the base fluid shows a significant change in heat transfer. A correlation model is also developed to interpret the heat transfer performance in the helical coil.

5.1. Introduction

Heat transfer enhancement is one of the main topics in thermal engineering research. Helical coils, additives to fluids, swirl flow devices, rough and extended surfaces are known as passive enhancement techniques whereas application of electric, acoustic and magnetic fields and fluid /system vibration are called enhancement active techniques (Bergles, 2002). Passive methods were preferred due to their simplicity in manufacturing, lower cost and longer operating life. According to Ali (2006) and Devanahalli et al. (2004), the use of helical coiled tubes has spread in many engineering fields such as heating, refrigerating, ventilating, air conditioning and energy systems. They also brought into service for steam generator and condenser designs, in power and nuclear plants because of their large surface area per unit volume (Pimenta and Campos, 2013). In spite of this advantage, for different heat transfer devices such as evaporators, condensers and steam generators, helical pipes produces 16-26% of heat losses to the environment in heat pumps technology. Although curved pipes are used in a wide range of applications, flow in curved pipes is relatively less well known than that in straight ducts. Williams et al. (1902) observed that the location of the maximum axial velocity is shifted towards the outer wall of a curved pipe. Later, Eustice (1911) showed the existence of a secondary flow by injecting ink into water. Due to the imbalance between inertial and centrifugal forces, a secondary motion develops in the cross section of a curved pipe. In his pioneering work, Dean (1927, 1928) described the flow behaviour of secondary flow based on stream function of the secondary motion and for the axial velocity which influence the thermal boundary layer in the helical coil. A thorough literature review of flow in curved pipes has been presented by Berger et al. (1983). Germano (1982) presented for the first time an orthogonal reference system for helical pipes. His work prompted a number of asymptotic analyses in the laminar (low-Reynolds number) range, aimed to studying the effect of torsion on the flow. Within this strand, remarkable works has been done by Chen and Jan (1992), Kao (1987), Xie (1990), Jinsuo and Benzhao (1999). By their asymptotic approach, these authors concluded that torsion has a second order effect on the flow with respect to the first order effect of curvature. The effect of curvature is the occurrence of two counter rotating vortices in the cross section, while the effect of torsion is an azimuthal rotation of the centres of circulation. Enormous studies have been carried out related to heat transfer in helical coil system. Cumo (1971) investigated the burnout heat transfer comparatively in straight and coiled tubes both, in order to study the influence of the geometric parameter. An improved two-phase flow heat transfer has been discovered in coiled tube than in straight ducts and also seen that higher burn-out heat fluxes, smoother and lower wall temperature rises at the dry-out point. In post burnout heat transfer a wall temperature difference between the internal and the external side of the coil (with respect to the helix axis) is set up. This temperature difference remains almost constant with quality downward from the dry-out point, depends on flow centrifugal acceleration and pressure, and remains at moderate values up to supercritical pressures. Mitsunobu and Cheng (1971) presented a numerical solution using a combination of line iterative method and boundary vorticity method for the hydro dynamically and thermally fully developed laminar forced convection in curved pipes. They found that the numerical solution converges up to a reasonably high Dean number where the asymptotic behaviour for the flow and heat transfer. Further they compared the numerical results with the experimental and theoretical results. Janssen and Hoogendoorn (1978) experimentally and numerically, studied the convective heat transfer in coiled tubes. The experiments have been carried out for tube diameter/coil diameter ratios from l/100 to l/10, Prandtl number from l0 to 500 and Reynolds numbers from 20 to 4000. The heat transfer has been studied for two boundary conditions: for a uniform peripherally averaged heat flux and for a constant wall temperature. They paid sufficient attention to the heat transfer in the thermal entry region as well as in the fully developed thermal region. The results obtained and the relations proposed are based on the flow behaviour. Kalb and Seader (1982) studied experimentally the entrance region heat transfer to gases flowing in a uniform wall-temperature helical coil. A novel gradient method of heat transfer investigation was developed based on measurement of the wall internal and external surface-temperature distributions. Experiments were done in the range of Reynolds numbers where the flow is initially turbulent upon entering the coil, but laminar downstream where secondary flow develops. No prior measurements of local heat transfer coefficients have been reported for this flow regime or thermal boundary condition. The results indicate a rapid transition to laminar flow and are in satisfactory agreement with a numerical solution for fully developed heat transfer. Liu and Masliyah (1993) numerically studied the simultaneous development of laminar Newtonian flow and heat transfer in helical pipes. They fully parabolized the governing equation in the axial direction and wrote them in an orthogonal helical coordinate system. For the special case of a torus, the numerical results for Nusselt number agreed well with published data. The Nusselt number in the developing region is found to be oscillatory. The asymptotic Nusselt number was correlated with the fluid Prandtl number and the flow Dean Number, $De = Re\ \lambda^{1/2}$ where λ is the dimensionless curvature ratio. When torsion is dominant, the asymptotic Nusselt number decreases with λ. Lin and

Ebadian (1997) carried out a fully elliptic numerical study to investigate three-dimensional turbulent developing convective heat transfer in helical pipes. They solved the governing equation by a control-volume finite element method. The results presented by them cover a Reynolds number range of 2.5×10^4 to 1.0×10^5, a pitch range of 0.0 to 0.6 and a curvature ratio range of 0.025 to 0.050. It was found that the examined parameters exert complex effects on developing thermal fields and heat transfer in the helical pipes. The Nusselt numbers for the helical pipes were oscillatory before the flow was fully developed, especially for the case of relatively large curvature ratio. Guo et al. (2001) conducted the experiments for sub-cooled water flow and steam-water two phase flow to investigate the effects of pulsation upon transient heat transfer characteristics in a closed circulation helical coiled tubing steam generator. The secondary flow mechanism and the effect of interaction between the flow oscillation and secondary flow were analysed on the basis of experimental data. A series of correlations were proposed for the average and local heat transfer coefficients. The results showed that there exist considerable variations in local and peripherally time-average Nusselt numbers for pulsating flow in a wide range of parameters. Bahiraei et al. (2011) analysed the thermodynamic potential of improvement for steady, laminar, fully developed, forced convection in a helical coiled tube subjected to uniform wall temperature based on the concept of avoidable and unavoidable energy destruction. The influence of various parameters such as coil curvature ratio, dimensionless inlet temperature difference, dimensionless passage length of the coil, and fluid properties on avoidable energy destruction have been investigated for water as working fluid. Results showed considerable potential of thermodynamic optimization of helical coil tubes. In addition, a relation for determining the amount of optimum Dean Number was proposed for the range of Reynolds number less than its critical value i.e. $Re_{cr} = 2100$. Yang et al. (2011) experimentally investigated the heat transfer in convection cooling section of pressurized coal gasifier with the membrane helical coils and membrane serpentine tubes under high pressure. They used high pressure single gas (He or N_2) and their mixture (He + N_2) as the test media in the test with pressure range of 0.5 MPa to 3.0 MPa. From their results it was seen that the convective heat transfer coefficient of high pressure gas is influenced by the working pressure, gas composition and symmetry of flow around the coil, of which the working pressure is the most significant factor. The average convective heat transfer coefficients for various gases in heat exchangers are systematically analysed, and the correlations between Nu and Re for two kinds of membrane heat exchangers are obtained. Pimenta and Campos (2013) carried out experimental work to investigate the heat transfer coefficients, at constant wall temperature as boundary condition, in fully developed laminar flow inside a helical coil. Behabadi et al. (2012) experimentally investigated the heat transfer enhancement of a nano-fluid flow inside vertical helically coiled tubes in the thermal entrance region. The temperature of the tube wall was kept constant at around 95°C to have isothermal boundary condition. Experiments were conducted for fluid flow inside straight and helical tubes. In these experiments, the effects of wide range of different parameters such as Reynolds and Dean Number, geometrical parameters and nano-fluid weight fractions have been studied. In order to investigate the effect of the fluid type on the heat transfer, pure heat transfer oil and nano-fluids with concentrations of 0.1, 0.2 and 0.4 wt% were used as the working fluid. The thermo-physical properties of the working fluids were extremely temperature dependent. They reported that helical coiled tubes compared to straight tubes enhanced the heat transfer rate remarkably. Besides, nano-fluid flows showed much higher Nusselt numbers compared to the base fluid flow. Finally, it was observed that combination of the two enhancing methods had noticeably high capability to the heat transfer rate. A number of non-Newtonian fluids like starch, clay suspensions, polyox, carboxymethylcellulose and many polymer solutions in water are extensively used in industries. In addition to the above mention fluids nano particles added to any fluid also shows a non-Newtonian fluid. A colloidal mixture of nano-sized particles in a base fluid tremendously enhances the heat transfer characteristics of the original fluid, and is ideally suited for practical applications due to its marvellous characteristics. Scientists are trying their best to reduce the amount of energy consumption throughout the world. A reduction in energy consumption is possible by enhancing the performance of heat exchange systems. Even though an improvement in energy efficiency is possible from the topological and configuration points of view, yet much more is needed from the perspective of the heat transfer fluid. Further, enhancement in heat transfer is always in demand. Further research on convective heat transfer based on theoretical and experimental research is needed in order to clearly understand and accurately predict their hydrodynamic and thermal characteristics with non-Newtonian liquid (Godson, 2010) also. The summary of heat transfer in helical coil is shown in Table 5.1. From the literature, it is seen that considerable experimental data is very less in literature on heat transfer characteristics in helically coiled tubes with two-phase (gas-non-Newtonian liquid) flow systems. Hence in the present work, an attempt is made to investigate the effect of various dynamic and geometric variables on heat transfer characteristics in two-phase (gas- non-Newtonian liquid) flow systems in helically coiled tubes.

5.2. Theoretical background

The heat transfer in coiled tubes takes place not only by diffusion but also by convection. Heat energy transferred between a surface and a moving fluid at different temperatures is known as convection. In reality this is a combination of diffusion and bulk motion of molecules. Near the surface the fluid velocity is low, and diffusion dominates. Away from the surface, bulk motion increase the influence and dominates. The convective heat transfer coefficient (h) is defined as,

$$h = \frac{q}{T_w - T_{out}} \tag{5.1}$$

where, q is the heat flux, T_w is the measured wall temperature, T_{out} is the outlet fluid temperature. The equation for the outlet fluid temperature is given by

$$T_{out} = T_{in} + \frac{q.S.L}{\rho.C_p.u.A} \tag{5.2}$$

where, T_{in} is the inlet fluid temperature given by thermocouple , C_p is the heat capacity, ρ is the fluid density, A is the cross-sectional area of the tube, S is the perimeter of the tube, L is the total length of the tube, u is the actual average fluid velocity. Rearranging Eq. (5.2) one gets

$$q = \frac{[T_{out} - T_{in}].\rho.C_p.u.A}{S.L} \tag{5.3}$$

Thus, by putting the value of heat flux (q) in Eq. (5.1) the heat transfer coefficient (h) can be calculated. Using temperature measurements taken at several different locations within the fluid to estimate the unknown heat flux and temperature on the external surface of the circular pipe. These methods are based on a minimization of the errors between calculated and measured temperatures at given locations and times, where the calculated values being obtained from a numerical solution of the heat flow (Chen et al., 2006)

5.3. Experimental

The experimental system for measuring the convective heat transfer coefficient is shown schematically in Figure 1.

Table 5.1: Summary of heat transfer studies in helical coil.

Author	Parameters	Working Fluid	Correlation	Remarks
Ali et al. (1968)	L_t = 10ft. d_i = 0.492 d_o = 625 D_c = 9.86, 20.5in. Water feed rate = 77-306 lb/h Heat flux = 19000- 81000 Btu/h ft^2	Air and Water	$\phi_{gtt} = \frac{(dP/dL)_{TPF}}{(dP/dL)_g}$ g refers to gas, ϕ_{stt} = Lockhart-Martinelli parameter at turbulent – turbulent condition.	Studied pressure drop and heat transfer and modified Lockhart-Martinelli correlation. Departure from nucleate boiling was not studied
Rajasekharan et al. (1970)	D_i/D_c = 0.031-0.222 di = 0.6407-0.27cm n = 4.5-12.	Water, CMC: 0.5 - 1%. sodium silicate : 1%	$N_{Nu} = \left[1.98 + 1.8\left(\frac{D_i}{D_c}\right)\right]\left[\frac{3n+1}{4n}\right]^{0.7n} N_{GN}^{0.7}$	Studied with both Pseudoplastic and Dilatant(Non-Newtonian fluids)

Janssen and Hoogendoorn (1978)	d_i = 5x10^{-3} m Di = 5x10^{-1}-6.2x10^{-2} m L = 4.5-5.9 m d/D = 1x10^{-2}-8.3x10^{-2} m	Water glycerol mixtures.	$\langle Nu \rangle_{\log} = \frac{1}{4}\langle \mathrm{Re}\,\mathrm{Pr}\rangle \frac{d}{L}\frac{\langle T\rangle_1 - \langle T\rangle_0}{\langle \Delta T\rangle_{\log}}$	It has appeared that only for low values of the Dean number ($De < 20$)
Sethumadhavan and Rao (1983)	d_i = 2, 3 mm α = 30-75^0 p = 10,22,38 and 66 L = 1500mm	Water and glycerol	$G(h^+,\mathrm{Pr})(\tan\alpha)^{0.18}(\mathrm{Pr}^{-0.55}) = 8.6(h^+)^{0.13}$	Given a correlation for heat transfer.
Austen and Soliman (1988)	d_i = 4.37 d_o = 6.34 Dc/d = 29.1-56 h/d = 5,58,60 D/d = 29-532	Water	$f_C / f_S = 1 + 0.033(\log Dn_m)^4$	Done a pressure drop and heat transfer coefficient

Ghorbani et al. (2010)	*di* = 7.77,10.82 mm; *do* = 9.47, 12.59 mm; *Di* = 125.71,128.31 mm; *p* = 16.47, 23.57 mm; *N* = 23.25, 16.25.	water	$Nu_{Deq} = 0.0041 Ra_{Deq}^{0.4533} \mathrm{Re}_{Deq}^{0.2} \mathrm{Pr}_s^{0.3}$	Studied mixed convection heat transfer in helical coiled tube heat exchanger
Pawar and Sunnapwar (2012)	*di* = 15.6 mm; *Di* = (320, 280, 260, 220) mm; *L* = (2612, 2813, 3593, 3920, 3619) mm; *N* = 4.4, 4.2, 3.9, 3.6, 2.6	Oil & Nano fluids (weight concentrations of 0.1, 0.2 & 0.4%)	$Nu = 1.75[(3n+1)/4n]^{1/3} Gz^{1/3}$ where Gz is the Graetz number	Showed that overall heat transfer coefficient is higher for smaller helix diameter as compared to larger helix diameter due to significant effect of centrifugal force on secondary flow in coil

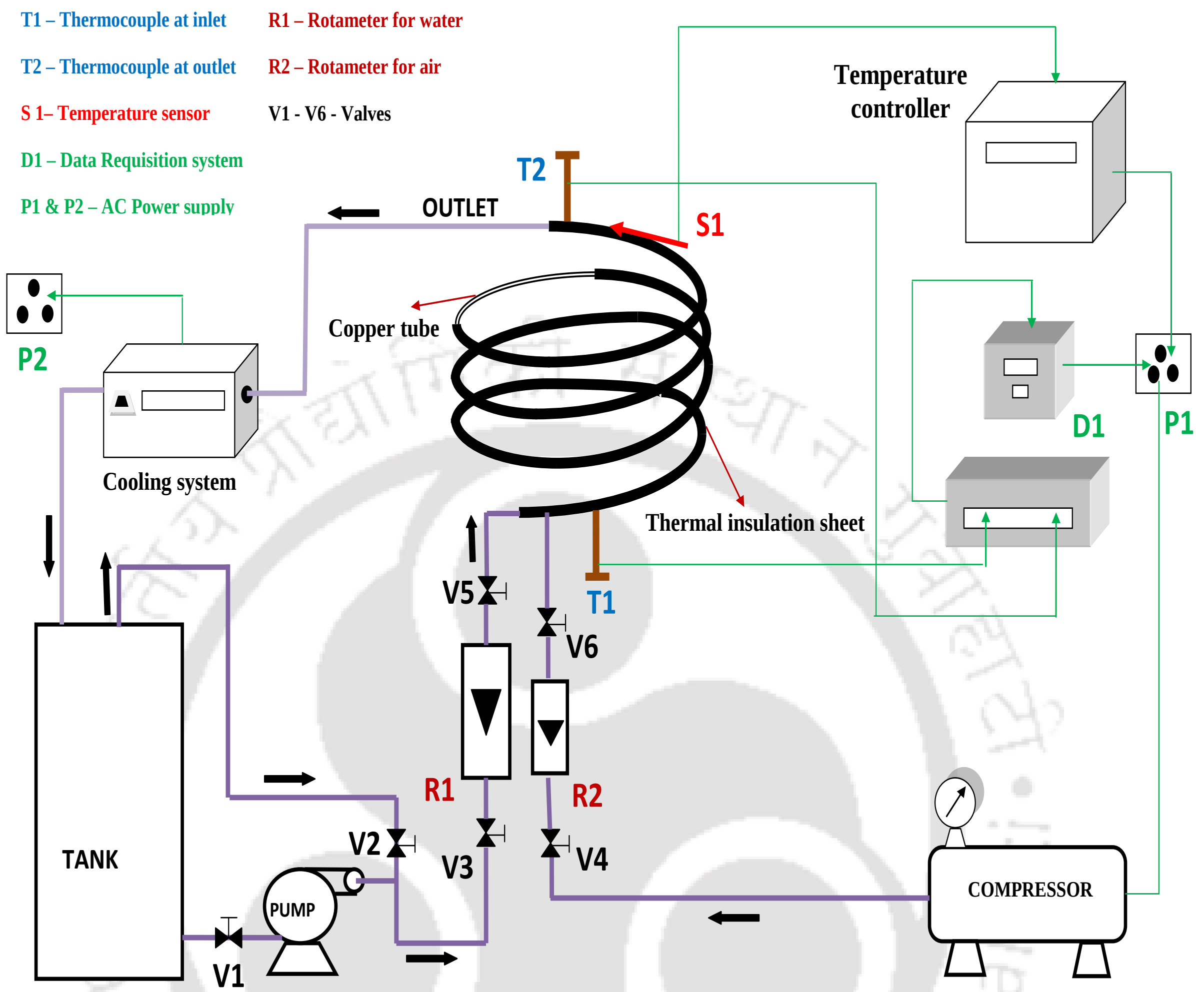

Figure 5.1: Schematic diagram of experimental set up.

It consists of a flow loop, a heating unit, a measuring unit and a control unit. The flow loop included a pump, two rotameters, a reservoir, and a test section. Three helical copper tube with 3500 mm length were used as the test section. Table 5.2 summarizes the geometrical specifications of the three coils tested in the present study. The whole test section was heated by a tape heater which is linked to an AC power supply. The maximum heating capacity of the tape heater was 500 W. There was a thick thermal insulating layer surrounding the heater to obtain a constant heat flux condition along the test section. Two K-type thermocouples were mounted on the test section, one at the inlet and other at the outlet of the helical coil.

The temperature readings from the thermocouples were registered by a digital data requisition system. The experiment was carried out for air-water system as well as air-SCMC system.

Table 5.2: Geometric specification of the different coils tested

Coil	D_c (m)	d_t (m)	N
Coil 1	0.2	0.01	4.5
Coil 2	0.15	0.01	6
Coil 3	0.2	0.015	4.5

The concentration of SCMC (Sodium Carboxy Methyl Cellulose) used were 1.0, 1.5 and 2.0 kg/m^3. The physical properties of water and SCMC solutions are shown in Table 5.3.

Table 5.3: Physical Properties of the SCMC solution

Fluid	Concentration kg/m^3	Flow behaviour index, n	Consistency index k,	Density, ρ_l, kg/m^3	Surface tension, σ_l, N/m
SCMC-1	1.0	0.9099	0.025516	1000.83	0.0721
SCMC-2	1.5	0.8701	0.036167	1001.69	0.0727
SCMC-3	2.0	0.8338	0.051265	1001.96	0.0732
Water	-	*	*	999.70	0.0710

* Viscosity of water : 0.797×10^{-3} kg/m.s

** Viscosity of air : 1.863×10^{-5} kg/m.s

For the specific heat capacity, the calculations of Semmar et al. (2004) has been referred, where they have calculated the specific heat of SCMC solution at different SCMC concentrations. The correlation that has been used to calculate the specific heat is given by

$$C_P(T) = A(T - T_0)^2 + B(T - T_0) + C \tag{5.4}$$

where, T_0 = 273.15^0, K and T is the wall temperature. The values of polynomial coefficients used in calculating the specific heat using Eq. (5.4) is shown in Table 5.4. Using these values a calibration curve is drawn from where a polynomial equation was developed which is related to specific heat (C_p) capacity with SCMC concentration.

Table 5.4: Values of polynomial coefficients at different SCMC concentrations

Coefficients	Pure water	SCMC (18 K/m^3)	SCMC (35 K/m^3)	SCMC (83 K/m^3)
A (Jkg^{-1} K^{-1})	0.015	-0.032	-0.015	0.0317
B (Jkg^{-1} K^{-1})	-1.145	6.953	5.441	-2.366
C (Jkg^{-1} K^{-1})	4215.6	4061.6	4231.2	4592

Thus a polynomial equation is obtained by fitting the experimental data of Semmar et al. (2004) can be represented by

$$C_P = -7\times10^{-5}C_{SCMC}{}^2 + 0.0099C_{SCMC} + 4.1895 \tag{5.5}$$

By putting the values of different SCMC concentration used in the experiment, C_p values of the solution were calculated from the fitted Eq. (5.5). The correlation coefficient for goodness of fit of Eq. (5.5) was found to be 0.9939. The thermal conductivity of the SCMC solution was calculated by the correlation developed from the experimental data of Carezzato et al. (2007). The correlation that has been developed can be expressed as

$$\kappa = 4\times10^{-5}C_{SCMC}^2 + 0.000C_{SCMC} + 0.643 \tag{5.6}$$

where 'κ' denotes thermal conductivity and 'C_{SCMC}' denotes SCMC concentration. By putting the values of different SCMC concentrations used in the experiment, the corresponding thermal conductivity values of the solution were calculated from the correlation. The uncertainty of the experimental data is shown in Table 5.5.

Table 5.5: Range of the Means, Standard Deviations, and Uncertainties of the heat transfer coefficient at constant tube diameter (d_t = 0.015 m), coil diameter (D_c = 0.20 m)

U_{sl} (m/s)	U_{sg} (m/s)	SCMC (kg/m^3)	Range of Mean* (w/m^2k)	N	Range of STDEV* ($\times 10^{-3}$)	Range of uncertainty* ($\times 10^{-3}$)	Range of relative uncertainty %
0.032-0.079	0.019	1.0	0.243-0.388	6.0	4.852-5.562	1.982-2.274	0.515-0.937
0.032-0.079	0.038	1.0	0.265-0.426	6.0	3.691-5.781	1.513-2.363	0.557-0.571
0.032-0.079	0.057	1.0	0.297-0.468	6.0	4.854-5.051	1.981-2.061	0.424-0.697
0.032-0.079	0.076	1.0	0.315-0.502	6.0	4.793-4.864	1.966-1.983	0.391-0.624
0.032-0.079	0.019	1.5	0.205-0.326	6.0	3.264-4.353	1.332-1.782	0.407-0.862
0.032-0.079	0.019	2.0	0.186-0.267	6.0	4.042-4.275	1.651-1.745	0.655-0.893

* The theory to calculate the values is given in chapter 2 in equations (2.10 – 2.12)

Each value of heat transfer coefficient in 4th column corresponds to the mean of 6 data points (i.e., N=6). Relative uncertainty is calculated from standard uncertainty and mean value of the corresponding data set.

5.4. Results and discussion

5.4.1. Variation of heat transfer coefficient with liquid flow rate

In Figure 5.2 the heat transfer coefficient has been plotted against the liquid flow rate for different SCMC concentrations. It was observed that the heat transfer coefficient depends on the liquid flow rate.

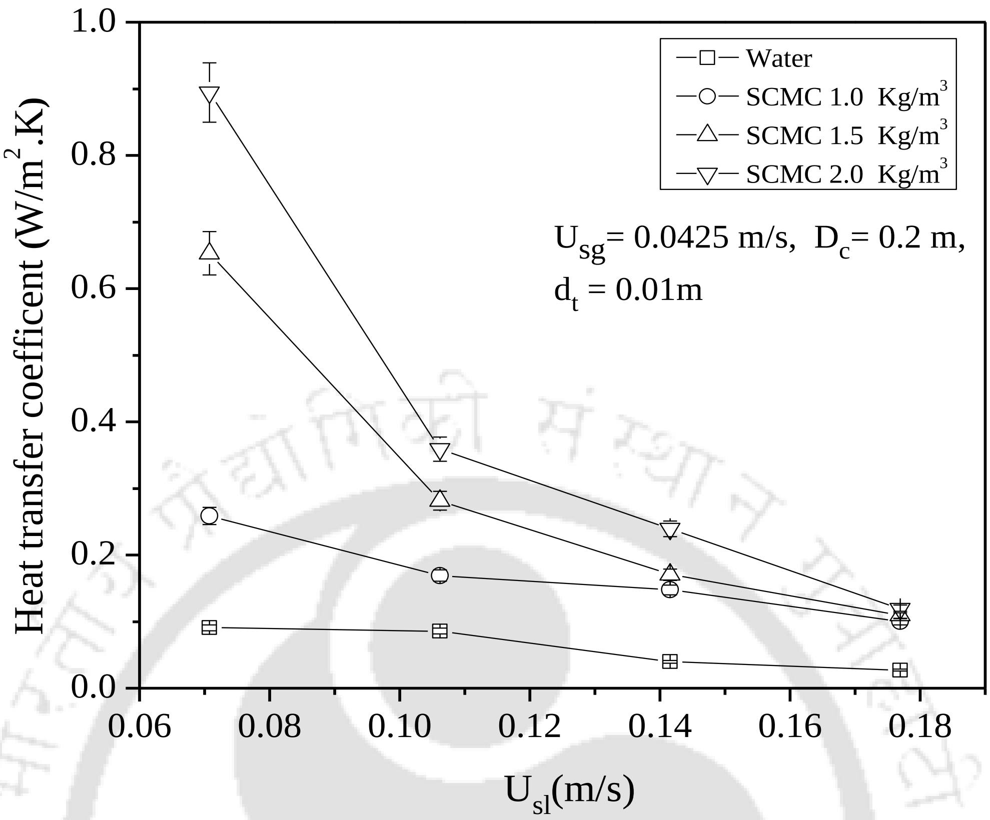

Figure 5.2: Heat transfer coefficient at different liquid flow rates.

As the liquid flow rate increased, the heat transfer coefficient starts to decrease. This is due to the fact that with higher liquid flow rate the residence time of the two phase gas-liquid mixture decreased in the helical coil. As a result the difference between the inlet and outlet temperature of the fluid decreases. Since the heat flux (*q*) is directly proportional to the inlet and outlet temperature difference, it will also decrease with the decrease in inlet and outlet temperature difference. Similar results of decreasing the heat transfer coeffiicient with an increase in liquid flow rate were shown by Yang (2003).

5.4.2. Variation of heat transfer coefficient with gas flow rate

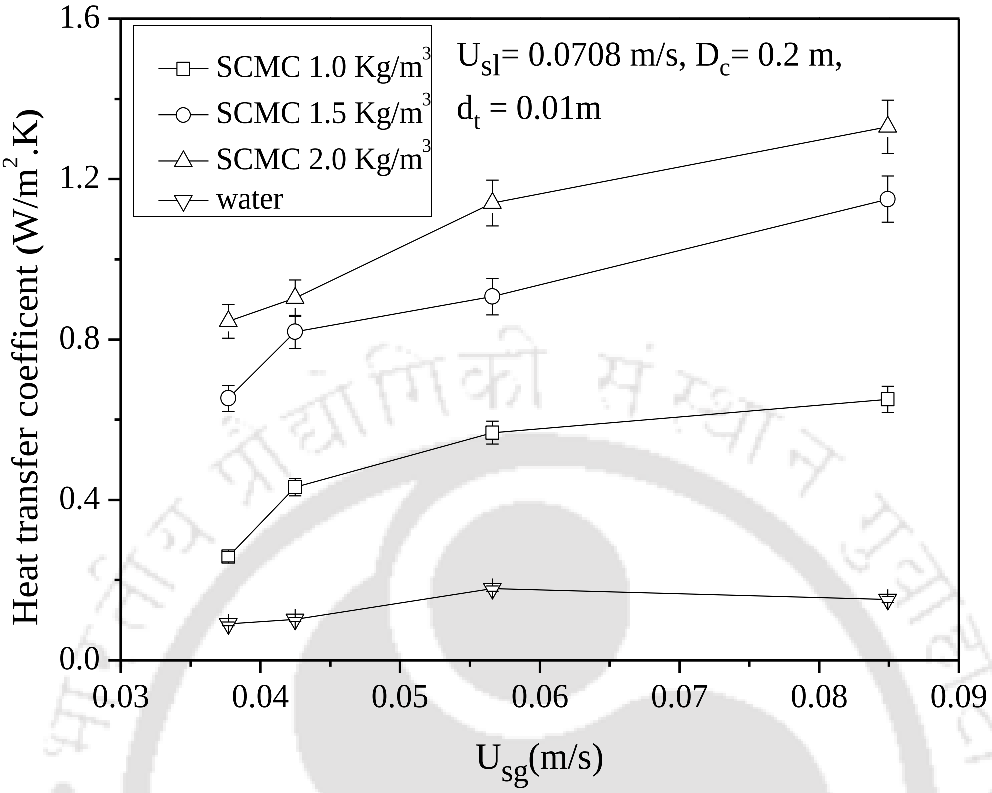

Figure 5.3: Heat Transfer coefficient at different gas flow rates.

It is observed that the heat transfer coefficient gradually increases as the gas flow rate is increased as shown in Figure 5.3. This is due to the reason that localized secondary flow is formed in a helical coil. When the gas flow rate is increased the turbulence inside the coil increases rapidly and as a result the secondary flow of the helical coil is increased. Higher the secondary flow higher will be the heat transfer coefficient. Similar results shown by Kim and Laurent (1991) that the heat transfer coefficient has found to increase with an increase in gas superficial velocity.

5.4.3. Variation of heat transfer coefficient with SCMC concentration

With increasing SCMC concentration the effective thermal conductivity of the fluid increases which results in the enhancement of heat transfer coefficient. Kumar et al. (2012) also mentioned the influence of effective thermal conductivity on heat transfer coefficient while studying the heat transfer and friction factor in helically coiled tube. The heat transfer coefficient increases with increase in SCMC concentration as shown in Figure 5.4.

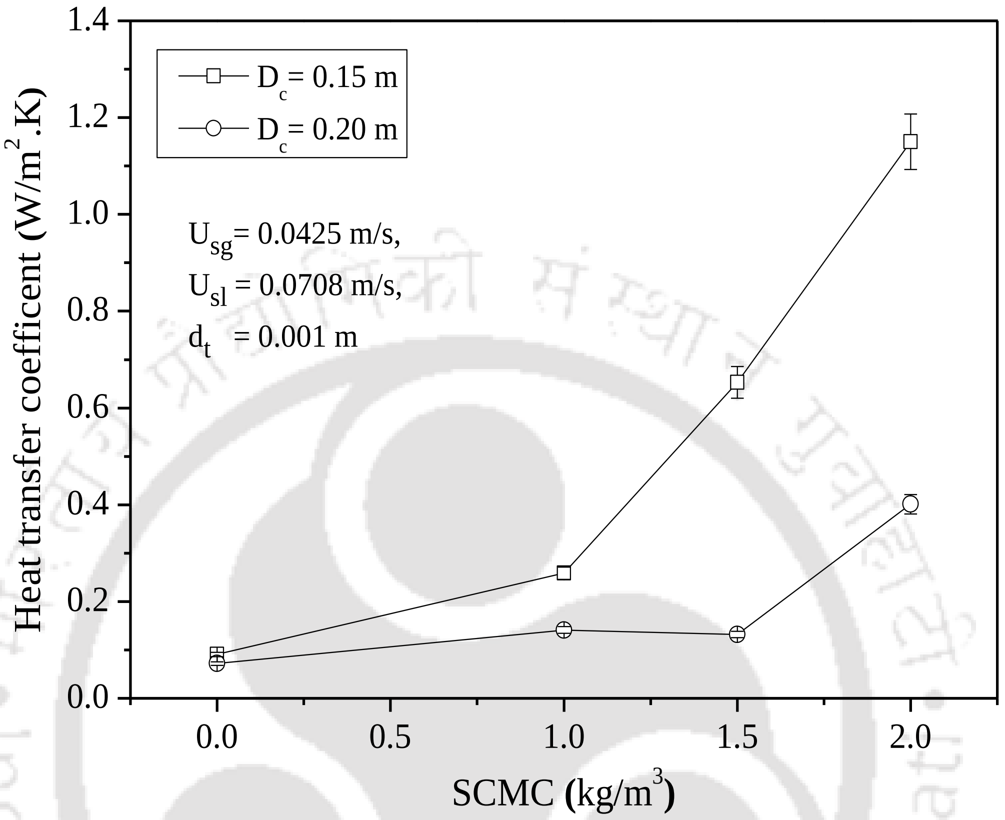

Figure 5.4: Heat transfer coefficient at different SCMC concentrations.

From the figure it is also observed that with decrease in coil diameter the heat transfer coefficient increases. With decreasing coil diameter, the change in flow pattern (as described in the chapter 2) result the change in heat transfer coefficient. Moreover decreasing the coil diameter provides more compactness to the helical coil system, which also results in heat transfer enhancement. From the figure (Figure 5.2 and Figure 5.3) it can be concluded that the heat transfer coefficient in the air-SCMC system gradually decreases with increase in liquid flow rate. Also with the increase in the air flow rate the heat transfer coefficient of the air-SCMC system increases gradually. Moreover addition of SCMC to the base fluid the heat transfer coefficient significantly increases. If the concentration of SCMC in the fluid is increased, the heat transfer coefficient increases to a large extent. This may happen due to the fact that the viscosity of the fluid gradually increases with the concentration of SCMC in the base fluid. More viscous fluid will spend comparatively more time inside the helical coil at a particular flow rate. This will result in an increase of outlet temperature and hence difference between the inlet and outlet temperature will increase. Since the heat flux is directly proportional to the temperature difference of the inlet and outlet fluid, therefore with increasing temperature difference the heat flux (q) increased and hence it resulted in an increase of the heat transfer coefficient. Ghorbani et al. (2010) shows the similar results that increasing the coil diameter resulted in the heat transfer coefficient reduction, and also observed that the convection heat transfer coefficient increases when the coil pitch increases.

5.4.4. Variation of heat transfer coefficient with tube diameter

It was also observed that with decrease in tube diameter the heat transfer coefficient increases at constant gas and liquid flow rates and at constant concentrations of SCMC as shown in Figure 5.5. Decreasing the tube diameter makes it confined with vapour bubbles which make the liquid film very thin which easily vanish at relatively high heat fluxes and causes early dry out. As the liquid film becomes thinner, more turbulent secondary flow is generated within the coil which results in the enhancement of heat transfer coefficient. Moreover coil surface area is one of the most influential geometric parameters on heat transfer coefficient. Surface and heat transfer coefficient are inversely related. With the increase of tube diameter the surface area of the coil increases and as a result the heat transfer coefficient decreases. Taherian and Allen (1998) studied the natural convection in shell-and-coil heat exchanger, also found that the heat transfer coefficient decreased as the surface area increased.

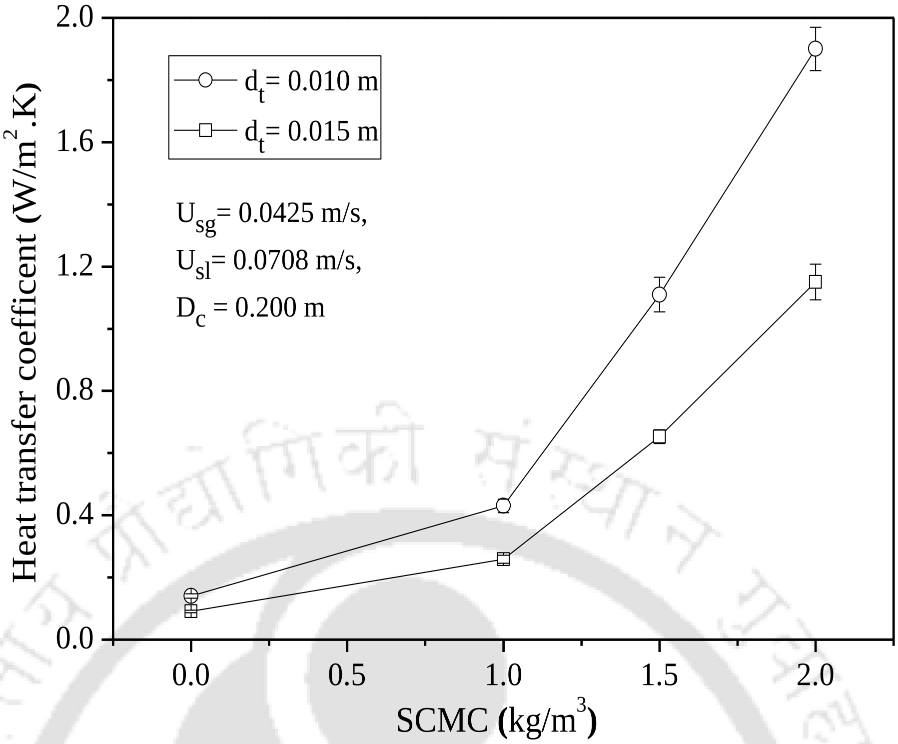

Figure 5.5: Heat transfer coefficient at different tube diameters.

5.4.5. Development of correlation model

A new correlation is introduced based on dimensional analysis using Pi-theorem. The heat transfer coefficient is a function of the following parameters including the thermo-physical properties, fluid properties, mass velocity and coil geometry.

$$h = f\,(C_p,\ \kappa,\ D_c,\ d_t,\ \rho_l\ ,\ \sigma_l,\ \mu_{eff},\ U_{slip},\ \Delta T_{(w\text{-}o)}) \tag{5.7}$$

The tube diameter, effective viscosity, liquid thermal conductivity and the slip velocity were selected as independence variables while the remaining were utilized to formulate the dimensionless groups. From the dimensional analysis the heat transfer coefficient may be correlated using the dimensionless groups as

$$Nu = \lambda\left[\frac{D_c}{d_t}\right]^a [\mathrm{Re}]^b [\mathrm{Pr}]^c \left[\frac{1}{Ca}\right]^d \left[\frac{1}{Br}\right]^e \tag{5.8}$$

The Eq. (5.8) has been fitted with experimental data using nonlinear multivariable regression analysis tool of Microsoft Excel 2013 software which is represented as follows

$$Nu = 2.35\times10^{-13}\frac{\mathrm{Re}^{1.507}\,\mathrm{Pr}^{4.11}\,Br^{1.415}}{Ca^{4.65}}\left[\frac{d_t}{D_c}\right]^{0.189} \tag{5.9}$$

Figure 5.6 shows the prediction of the experimental results using Eq. (5.9). The developed correlation is fitted well where 90% of data is predicted within ± 9.5% deviation. The convective heat transfer is dominating the conductive heat transfer due to the turbulence produced by the centrifugal force in the helical flow system.

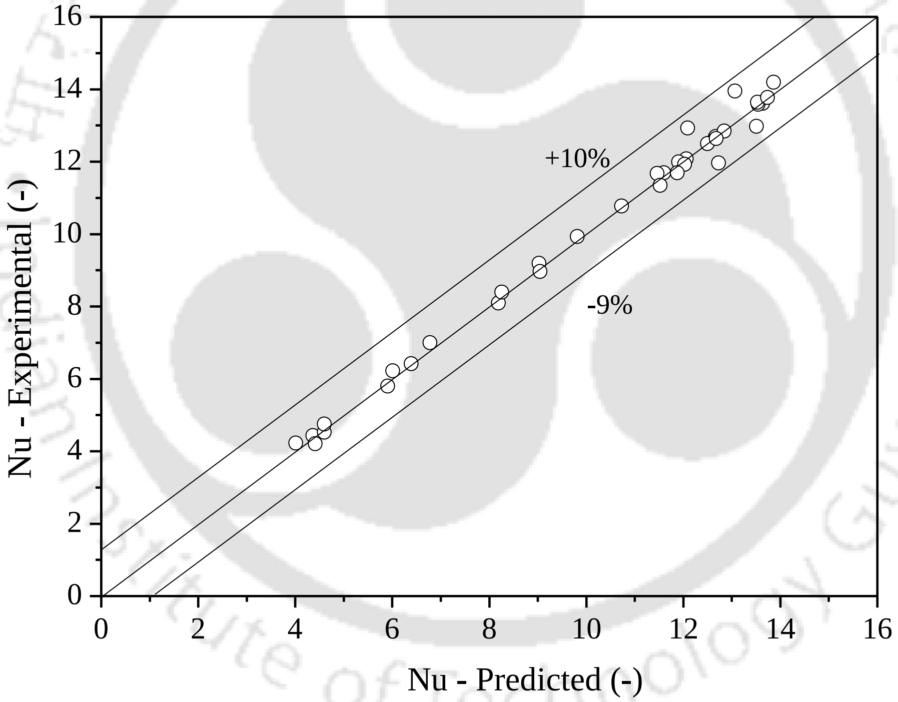

Figure 5.6: Parity plot of experimental Nusselt number to the predicted Nusselt number.

The viscous effect is controlled by the change in apparent viscosity by using different concentration of non-Newtonian liquid (SCMC) whereas the inertia force is controlled by changing both the gas and liquid velocities. It was seen that for a specific inertia force the viscous force dominating at laminar flow whereas at turbulent flow the inertia force dominating which gives higher heat transfer coefficient. At the laminar flow system where viscous force is dominating the heat transfer coefficient is decreasing due to its viscous effect. The Prandtl number shows the significance of the momentum diffusivity over thermal diffusivity. The present study resulted the dominate effect of momentum diffusivity over thermal diffusivity. This is due to the high momentum transfer of fluid surfaces caused by the inertia and the centrifugal force of the helical system. The larger the Prandtl number, the thicker will be the momentum boundary layer compared to the thermal boundary layer. Thus the physical significance of the Prandtl number is very strong in the present study. The Capillary number (Ca) represents the relative effect of viscous forces versus surface tension acting across an interface between a liquid and a gas, or between two immiscible liquids. For example an air bubble in a liquid flow tends to be deformed by the friction of the liquid flow due to viscosity effects but the surface tension forces tend to minimize the surface which may affect the change of heat transfer coefficient. From the correlation it is seen that the surface tension effect is predominant over the effect of viscous forces. This may be due to the formation of more bubble at higher surface tension and forms more interfacial area and increase the heat transfer coefficient. The Brinkman number (*Br*) is a dimensionless number related to heat conduction from a wall to a flowing viscous fluid. It is the ratio between heat produced by viscous dissipation and heat transported by molecular conduction or it is called the ratio of viscous heat generation to external heating. In the present study viscous heat generation by dissipation of energy due to friction of the interfacial surface may contribute more heat transfer in addition to the external heat. Overall it was seen that the heat transfer coefficient is increased as the viscous heat generation increased.

5.4.6. Comparison of heat transfer coefficient of helical coil with straight tube

After doing the experimental work it was seen that heat transfer coefficient significantly increased in helical coil system. To show the importance of using helical coil over straight tube it is required to show a comparison of helical coil system to the conventional straight tube. The results were compared with the predictions of the following well-known Shah's correlation for laminar flow under the constant heat flux boundary condition (Shah, 1975).

$$Nu = 1.953\left(\mathrm{Re}\,\mathrm{Pr}\frac{d_t}{L}\right)^{\frac{1}{3}} \qquad \text{When, } \left(\mathrm{Re}\,\mathrm{Pr}\frac{d_t}{L}\right) \geq 33.3 \tag{5.10}$$

$$Nu = 4.364 + 0.0722\left(\mathrm{Re}\,\mathrm{Pr}\frac{d_t}{L}\right) \qquad \text{When, } \left(\mathrm{Re}\,\mathrm{Pr}\frac{d_t}{L}\right) < 33.3 \tag{5.11}$$

In the present experimental study satisfied the condition $\left(\mathrm{Re}\,\mathrm{Pr}\frac{d_t}{L}\right) < 33.3$. Thus by using the Eq. (5.11) the Nusselt number for a conventional straight tube using the flow parameters and coil geometries used in the present work was calculated. The profiles of the Nusselt number for a helical coil and a straight tube are shown in Figure 5.7. From Figure 5.7 it is evident that the Nusselt number of a helical coil is higher at higher Reynolds number compared to that of a conventional straight tube. This is due to the fact that in the helical coils at higher Reynolds number the turbulence of the fluid inside the coil increases. Higher turbulence increases the intensity of secondary flow and hence the Nusselt number increases. In the helical coil, as the fluid flows through the coil, fluid particles undergo rotational motion. The fluid particles also undergo movement from inner side of the coil to the outer side and vice versa. It is to be noted that these fluid particles are taking various trajectories and also move with different velocities. This causes variations of Nusselt number and heat transfer coefficient inside the helical coil. The temperature drop for helical coiled tube is higher than the straight tube. This is due to the curvature effect of the helical coil, setting a secondary flow, results various flow patterns and enhance the heat transfer coefficient accordingly.

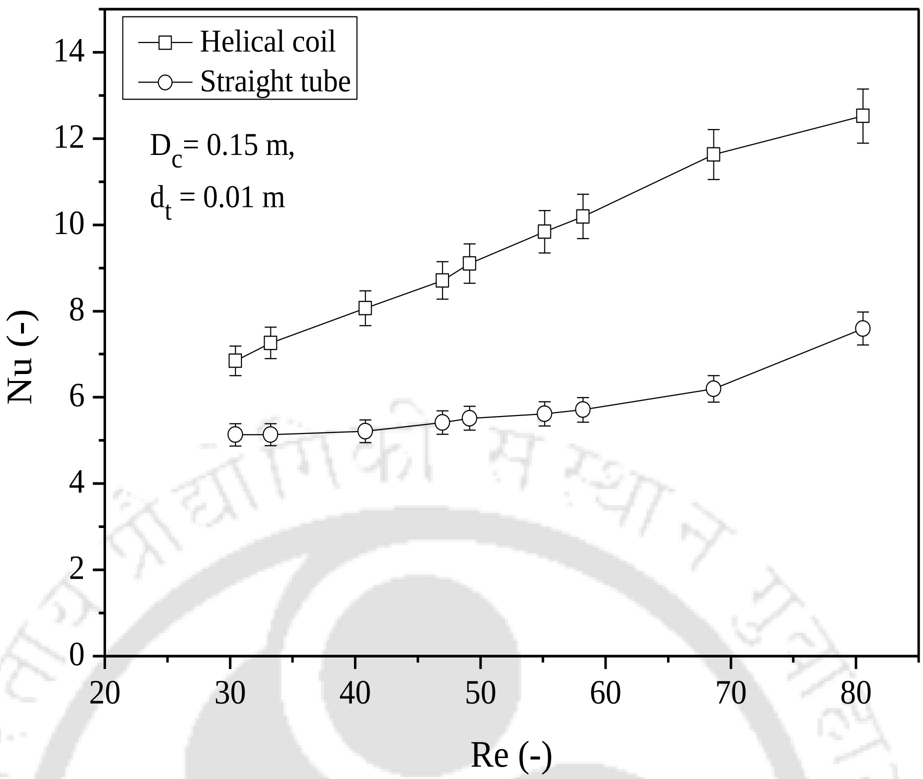

Figure 5.7: Comparison of Nusselt number of helical coil and conventional straight tube.

5.5. Conclusion

Understanding the heat transfer mechanism through helical coils is important to design efficient thermal system. The present study is an investigation of different strategies to enhance the heat transfer in helical coils. The heat transfer coefficient depends on various operating variables such as gas flow rate, liquid flow rate, density of liquid and gas, viscosity of liquid and gas, surface tension of liquid, heat capacity of the liquid, diameter of the tube, diameter of the coil and wall temperature. The heat transfer coefficient increases with increase in gas flow rate but it gradually decreases with the increase in liquid flow rate. Moreover with the increase of wall temperature the heat transfer coefficient increases. It was also observed that the coil geometry significantly affects the heat transfer coefficient. With the increase in coil diameter heat transfer coefficient decreases and with the decrease of tube diameter the heat transfer coefficient gradually increases. Various properties of the helical coil was observed in details and it was found that when a fluid is allowed to pass through a helical coil, the different forces acting on the fluid are viscous force, buoyancy force and centrifugal force. Among these the centrifugal force is predominant which acts normal direction to main flow and hence results in a secondary flow consequently the heat transfer is enhanced in a helical coil, compared to the straight tubes. It was also seen that a significant role has been played by the non-Newtonian (SCMC) fluids in enhancing the heat transfer. With increasing concentration of SCMC the heat transfer coefficient in the helical coil system increases significantly. A correlation has been developed to predict the heat transfer coefficient, the study may be useful for further understanding the two-phase heat transfer characteristics in helical coil system.

Nomenclature

C_p	Specific heat ($J/\ kg\ K$)
Ca	Capillary number ($\mu U/\gamma$) (-)
Br	Brinkham number ($\mu U^2/k\ (T^w\text{-}T_o)$ (-)
d_t	Tube diameter (m)
D_c	Coil diameter (m)
De	Dean Number ($Re\sqrt{\delta}$)
h	Heat transfer coefficient in (W/m^2K)
L	Length of the coil (m)
Nu	Nusselt number (hd_t / k) (-)
Pr	Prandtl number (v/α) (-)
q	Rate of heat transfer (watt)
q_w	Wall heat flux (W/m^2)

Ra	Rayleigh number ($g\beta\Delta TD^3/\alpha v$) (-)
Re	Reynolds number ($d_t v\rho/\mu$) (-)
Re_{cr}	Critical Reynolds number (-)
SCMC	Sodium Carboxy Methyl Cellulose
T_w	Temperature at the wall (K)
U_{sl}	Superficial liquid velocity (m/s)
U_{sg}	Superficial gas velocity (m/s)

Greek symbols

κ	Thermal conductivity (*W/m K*)
ρ	Fluid density (kg/m^3)
µ	Viscosity (*kg/m s)*
v	Kinematic viscosity of the fluid (m^2 /s)
σ	Surface tension (*N/m*)

Subscripts

b	Bulk
cr	Critical
in	inlet
out	outlet
w	Wall

Reference

- Ali, O., Kenneth, J.B., Crainjr, B., 1968. Forced convection boiling inside helically-coiled tubes. Int. J. Heat Mass Transfer 11, 1779-1793.
- Ali, M.E., 2006. Natural convection heat transfer from vertical helical coil in oil. Heat Transfer Eng. 27, 79–85.

- Austen, D.S., Soliman, H.M., 1988. Laminar flow and heat transfer in helically coiled tubes with substantial pitch. J. Exp. Therm. Fluid Sci. 1, 183-194.
- Bahiraei, F., Saray, R.K., Salehzadeh, A., 2011. Investigation of potential of improvement of helical coils based on avoidable and unavoidable exergy destruction concepts. Energy 36, 3113-3119.
- Behabadi, M.A.A., Pakdaman, M.F., Ghazvini, M., 2012. Experimental investigation on the convective heat transfer of nanofluid flow inside vertical helically coiled tubes under uniform wall temperature condition. Int. Commun. Heat and Mass 39, 556–564.
- Berger, S.A., Talbot, L., Yao, L.S., 1983. Flow in curved pipes. Annu. Rev. of Fluid Mech. 15, 461-512.
- Bergles, A.E., 2002. ExHFT for fourth generation heat transfer technology. Exp. Therm. Fluid Sci. 26, 355-344.
- Carezzato, A., Alcantara, M.R., Telis-Romero, J., Tadini, C.C., Gut, J.A.W., 2007. Non-Newtonian heat transfer on a plate heat exchanger with generalized configurations. Chem. Eng. Tech. 30, 21–26.
- Chen, C.K., Wu, Li-W., Yang, Y.T., 2006. Application of the inverse method to the estimation of heat flux and temperature on the external surface in laminar pipe flow. Appl. Therm. Eng. 26, 1714–1724.
- Chen, W.H., Jan, R., 1992. The characteristics of laminar flow in helical circular pipe. J. Fluid Mech. 244, 241-256.
- Cumo, M., 1971. The influence of curvature in post dry-out heat transfer. Int. J. Heat Mass Tran. 15, 2045-2062.
- Dean, W.R., 1927. Note on the motion of the fluid in a curved pipe. Philos. Mag. 4, 208-223.

- Dean, W.R., 1928. The streamline motion of fluid in a curved pipe. Philos. Mag. 7, 673.
- Devanahalli, G.P., Timothy, J.R., Vijaya Raghavan, G.S., 2004. Natural convection heat transfer from helical coiled tubes. Int. J. Therm. Sci. 43, 359–365.
- Eustice J., 1911. Experiment of streamline motion in curved pipes. Proceedings of the royal society A, Mathematical, Physical and Engineering 85, 119-131.
- Germano, M., 1982. On the effect of torsion in helical pipe flow. J. Fluid Mech.125, 1-8.
- Godson, L., 2010. Enhancement of heat transfer using nano-fluids-An overview. Renew. Sust. Energ. Rev. 14, 629–641.
- Ghorbani, N., Taherian, H., Gorji, H., Mirgolbabaei, H., 2010. Experimental study of mixed convection heat transfer in vertically coiled tube heat exchangers. Exp. Therm. Fluid Sci. 34, 900-905.
- Guo, L., Feng, Z., Chen, X., 2001. An experimental investigation of frictional pressure drop steam-water two-phase flow in helical coils. Int. J. Heat Mass Tran. 44, 2601-2610.
- Janssen, L.A.M., Hoogendoorn, C.J., 1978. Laminar convective heat transfer in helical coiled tubes. Int. J. Heat Mass Tran. 21, 1197-120.
- Jinsuo, Z., Benzhao, Z., 1999. Fluid flow in a helical pipe. Acta Mech. Sinica 15, 299-312.
- Kalb, C.E., Seader, J.D., 1982. Entrance region heat transfer in a uniform wall-temperature helical coil with transition from turbulent to laminar flow. Int. J. Heat and Mass Tran. 26, 582-589.
- Kao, H.C., 1987. Torsion effect on fully developed flow in a helical pipe. J. Fluid Mech.184, 335-356.

- Kim, S.D., Laurent, A., 1991. The state of Knowledge on heat transfer in three-phase fluidized beds. Int. Chem. Eng. 31, 284-302.
- Kumar, P.C.M., Kumar, J., Suresh, S., 2012. Heat transfer and friction factor studies in helically coiled tube using Al_2O_3/ water nanofluid. Eur. J. Scientific Res. 82, 161-172.
- Lin, C.X., Ebadian, M.A., 1997. Developing turbulent convective heat transfer in helical pipes. Appl. Therm. Eng. 47, 231-238.
- Liu, S., Masliyah, J.H., 1993. Axially invariant laminar flow in helical pipes with a finite pitch. J. Fluid Mech. 251, 315-353.
- Mitsunobu, A., Cheng, K.C., 1971. Boundary vorticity method for laminar forced convection heat transfer in curved pipes. Int. J. Heat Mass Tran. 14, 1659–1675.
- Pawar, S.S., Sunnapwar, V.K., 2012. Experimental studies on heat transfer to Newtonian and non-Newtonian fluids in helical coils with laminar and turbulent flow. Exp. Therm. Fluid Sci. 44, 792-804.
- Pimenta, T.A., Campos, J.B.L.M., 2013. Heat transfer coefficients from Newtonian and non-Newtonian fluids flowing in laminar regime in a helical coil. Int. J. Heat Mass Tran. 58, 676–690.
- Rajasekharan, S., Kubair, V.G., Kuloor, N.R., 1970. Heat transfer to Non-Newtonian fluids in coiled pipes in laminar flow. Int. J. Heat Mass Transfer 13, 1583-1594.
- Semmar, N., Tanguier, J.L., Rigo, M.O., 2004. Analytical expressions of specific heat capacities for aqueous solutions of SCMC and CPE. Thermochim. Acta 419, 51–58.
- Sethumadhavan, R., Rao, M.R., 1983. Turbulent Flow Heat Transfer and Fluid Friction in Helical-Wire-Coil-Inserted Tubes. Int. J. Heat mass Transfer 26, 12, 1833-1845.

- Shah, R.K., 1975. Thermal entry length solutions for the circular tube and parallel plates, In: Proc. 3rd National Heat and Mass Transfer Conference, IIT, Bombay, 1, 11- 75.
- Taherian, H., Peter, L., Allen, 1998. Experimental study of natural convection shell-and-coil heat exchanger. The American society of mechanical engineers, ASME, 357-2.
- Williams, G.S., Hubbell, C.W., Fenkell, G.H., 1902. On the effect of curvature upon the flow of water in pipes. Am. Soc. Civ. Eng. 47, 1-196.
- Xie, G.D., 1990. Torsion effect on secondary flow in helical pipes. Int. J. Heat Fluid Flow 11, 114-119.
- Yang, W.C., 2003. Handbook of fluidization and fluid-particle systems. Marcel Dekker, Inc. New York. Basel. 785.
- Yang, Z., Zhao, Z., Liu, Y., Chang, Y., Cao, Z., 2011. Convective heat transfer characteristics of high-pressure gas in heat exchanger with membrane helical coils and membrane serpentine tubes. Exp. Therm. Fluid Sci. 35, 1427 – 1434.

CHAPTER-6

MASS TRANSFER CHARACTERISTICS

This chapter investigates the two- and three-phase mass transfer phenomena with gas-Newtonian and non-Newtonian fluids in vertically helical coil reactor. The effects of various dynamic and geometric parameters on mass transfer coefficients in the helical coil reactor are examined. The flow pattern-based mass transfer phenomena in the helical coil reactor are ennuntiated at different operating conditions. Generalized correlation model for the mass transfer coefficient based on the flow pattern are developed.

6.1 Introduction

Helical coiled tubes are widely used for mass-transfer operations, e.g., membrane separation processes of reverse osmosis, ultra-microfiltration, gas permeation, and chromatography. The mass transfer improvement is induced by complex hydrodynamic phenomena involving the centrifugal force. Most of the reported studies in coiled flow were aimed at study the hydrodynamics (Banerjee et al., 1969; Awwad et al., 1995; Ali, 2001; Mandal and Das, 2002; Mandal and Das, 2003; Biswas and Das, 2006; Biswas and Das, 2007; Biswas and Das, 2008; Thandlam et al., 2015). Hameed and Muhammed (2003) experimentally determined the gas–liquid mass transfer in helical coiled tubes for absorption of carbon dioxide (CO_2) into liquid films of distilled water, ethyl alcohol and ethylene glycol. The mass transfer coefficient was found to higher for helical coiled tube than that of straight tube. Sujatha et al. (2003) developed mass transfer coefficient in the presence of spiral coil promoters in batch fluidized beds. Thandlam et al. (2009) studied wall-liquid mass transfer in helical coil tubes in the presence of fluidized solids and with two-phase gas-liquid flow. In their study the mass transfer coefficient found to be influenced by particle diameter and pitch difference (p/Dc). Kumar et al. (2011) studied the wall-liquid mass transfer in helical coil tubes with packing materials. The mass transfer found to be 115% over that of empty coil and higher magnitudes of augmentation in helical packed beds at higher liquid flowrates. A summary of correlations and related parameters observed from the literature review is shown in Table 6.1.

From the literature, it is seen that considerable experimental data is not available on flow pattern-based liquid phase controlled mass transfer in helically coiled tubes with two- and three-phase systems and with non-Newtonian liquid. Due to higher mass transfer in the helical coil, more studies on the same is required. Most of the chemical processes include the mass transfer with the non-Newtonian liquid. There is a lack of study on the mass transfer with non-Newtonian liquid in helical coil system. Hence in the present work, an attempt is made to investigate the effect of various dynamic and geometric variables on wall-liquid mass transfer in two-phase (gas-liquid) gas-non-Newtonian liquid and three-phase (gas-liquid-solid) flow systems in helically coiled tubes.

6.2 Experimental

6.2.1 Experimental setup and operating conditions

The schematic of the experimental setup used in the present investigation for mass transfer characteristics is shown in Figure 6.1(a). A photograph of the experimental setup with necessary accessories is also shown in Figure 6.1(b). The experimental unit essentially consists of a vertical helical coil (H), centrifugal pump (Pm) to deliver the electrolyte, one air compressor (C_o) to pumping the air to the helical system, re-circulating storage tank (St) for circulating the liquid.

Table 6.1: Summary of mass transfer studies in helical coils

Author	Parameters	Working Fluid	Correlation	Remarks
Sujatha et al. (2003)	*Dc* = 0.011, 0.041 m; *P* = 0.016,0.076 *dw* = 0.26,0.4; *dp* = 0.292,0.687; ε = 0.46,0.993; *Q* = 19.6,820; *Re* = 340-488857; *Sc* = 842-1171	Water, Mass transfer fluid	$K_L = \frac{I}{nAFC_i}$ $\varepsilon = 1 - \left\{ \frac{V_S}{V_f - V_p} \right\}$	Mass transfer coefficient increased with increase in diameter of the particle, coil diameter, and diameter of the coil wire
Thandlam et al. (2009)	*d* = 1.8, 2.3 cm; *P* = 0.5 - ∞; *Lc* = 1.56, 3.1 m; Electrode = 3.42mm	Air , water, Electrolyte solution	$k_L = 0.001213\, U_g$	Developed correlation for mass transfer coefficient
Abdel-Aziz et al. (2010)	*d* = 1, 1.4, 2 cm; Dc = 10, 15, 20, 25 cm; *P* = 3 cm; *Lc* = 1.56, 3.1 m Electrode = 3.42mm	Electrolyte solution	$j_H = 0.0255\,\mathrm{Re}^{-0.15}\left(\frac{d}{Dc}\right)^{0.1}$ $j_H = St\,\mathrm{Pr}^{0.66}$	Studied the rate of liquid–solid mass transfer controlled processes in helical tubes under turbulent flow conditions
Kumar et al. (2011)	*d = 1.8, 2.3 cm* *P* = 0.5 - ∞	Air (Nitrogen), Water, Electrolyte	$j_D = 0.34\mathrm{Re}^{-0.5}8\mathrm{Tn}^{0.17}$	Developed correlations for mass transfer coefficient

	Lc = 1.56, 3.1 m Electrode = 3.42mm	solution		in packed coil
Rao et al. (2013)	*Dc= 0.031 – 0.038 m; P =* 0.016 – 0.046; *Lc* = 0.05 – 0.16 m; Re = 1200 – 14500; Sc = 789-1132.	Electrolyte solution	$g(h) = 5369.5\,\mathrm{Re}_m^{0.19}\left(\frac{p_c}{d_e}\right)^{0.19}\left(\frac{L_c}{d_e}\right)^{0.30} \times\left(\frac{d_c}{d_e}\right)^{1.19}\left(\frac{d_w}{d_e}\right)^{0.21}$	Developed a correlation for mass transfer coefficient.
Abdel-Aziz (2013)	p = 0.01, 0.015, 0.02 m; d_t = 0.175 m; D_c = 0.01 m; L_c = 3.5 m; *Re* = 4705 – 52450; *Sc* = 1104-1506.	Electrolyte solution	$Sh = 0.023 Sc^{0.33}\,\mathrm{Re}^{0.59}\left(\frac{D_c}{S}\right)^{0.49}$ For 90° $Sh = 0.13 Sc^{0.33}\,\mathrm{Re}^{0.51}$ For 45°	Given a correlation of mass transfer coefficient for different pitch lengths.

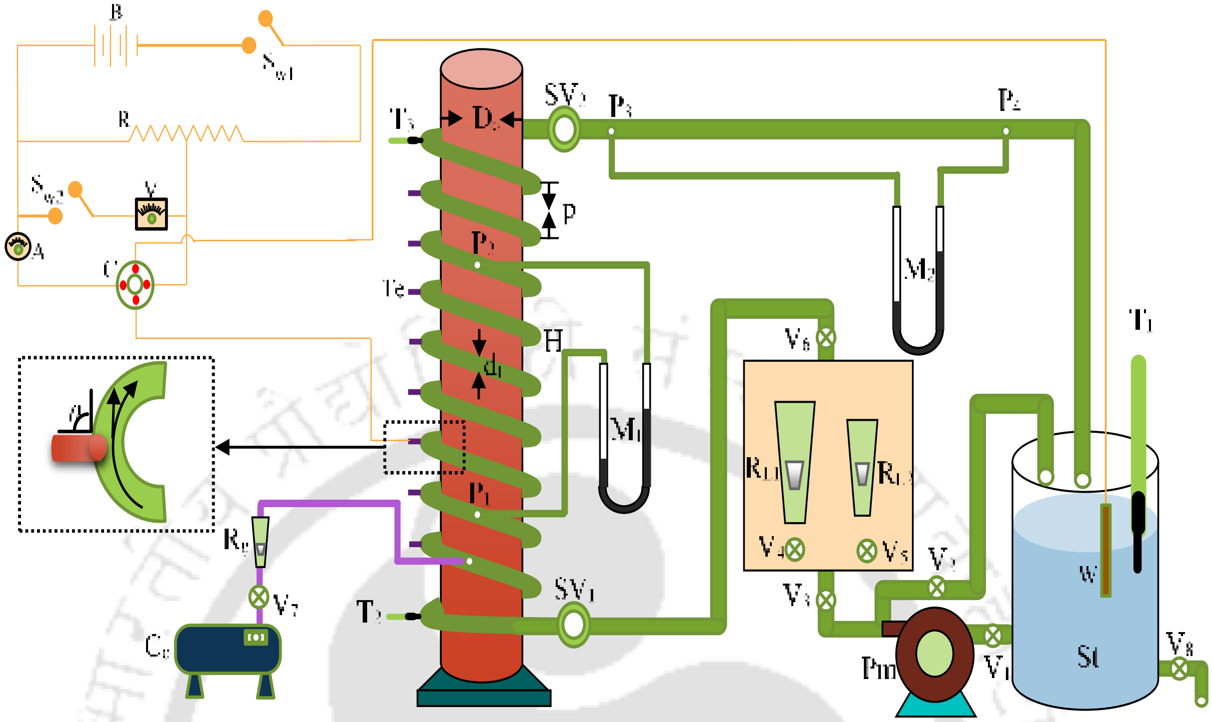

Figure 6.1 (a): Schematic diagram of the system

Legend- A: Milli ammeter, B: Battery, C: Commutator, Co: Compressor, d_t: Tube diameter, D_c: Coil diameter, H: Helical coil, M1, M2: U-tube Manometers, p: pitch, Pm: Pump, P_1 – P_4: Pressure taps, R: Rheostat, R_{L1}, R_{L2}:Liquid Rotameter, R_G: Gas Rotameter, SV_1, SV_2: Solenoid Valves, St: Storage tank, Sw_1 and Sw_2: Switches, T_1 and T_3: Thermometers, Te: Test electrodes, V: Volt meter, V_1 – V_8: Valves, W: Wall electrode.

The liquid was pumped through the pre-calibrated liquid rotameter, R_{L1} (range: 6.94×10^{-05} - 6.67×10^{-04} m^3/s) and R_{L2} (range: 1.67×10^{-05} - 3.33×10^{-04} m^3/s). Similarly air was pumped through the pre-calibrated gas rotameter, R_g (range: 1.67×10^{-05} to 1.67×10^{-04} m^3/s).

Two U-tube manometers (M_1 and M_2) were used for measuring the pressure difference in helical and horizontal parts of the tube. Valves (V_1 to V_4 and V_5) were used to control the flow rates of liquid and gas.

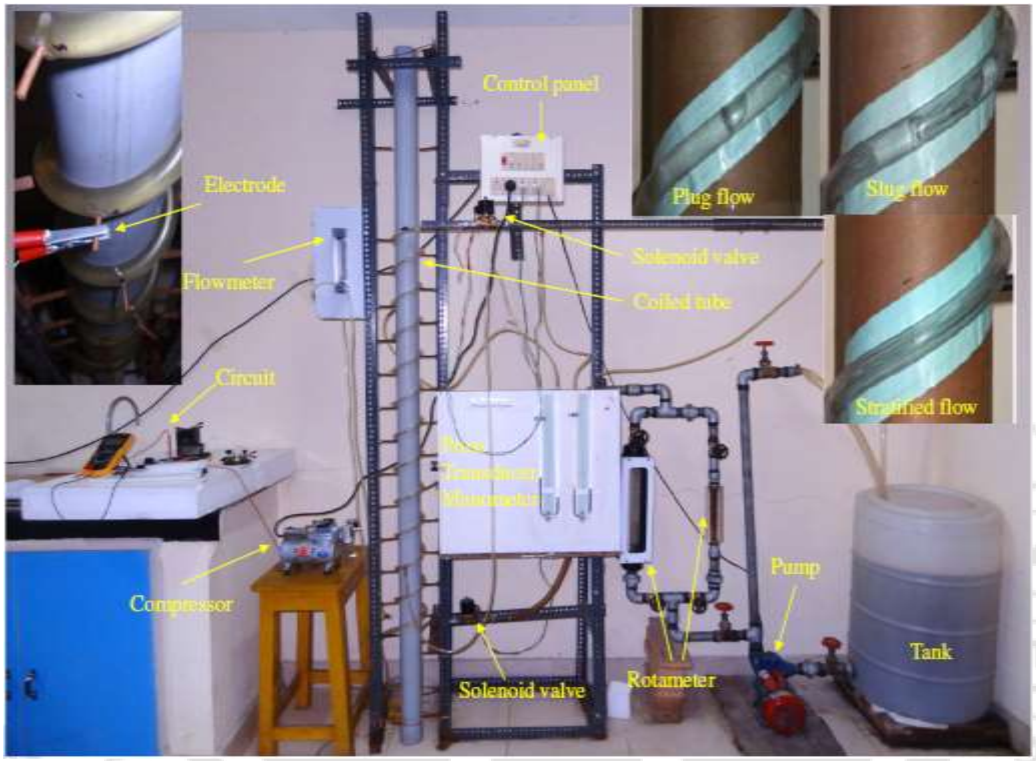

Figure 6.1 (b): Photograph of experimental setup for mass transfer with accessories.

The storage tank was of 100 liters capacity which is completely covered with an ebonite sheet in order to eliminate continuous contact with the surrounding air. The gas holdup is measured by phase isolation technique. Two solenoid valves SV_1 and SV_2 placed at the two ends of the coil system (Figure 6.1) are used to close the operation quickly, for measurement of gas holdup as described in chapter 3. Each set of helical coil are arranged in three different pitch differences (p/D_c: 0.5, 1.0 and 1.5) and three coil diameters (D_c: 0.075, 0.117 and 0.200 m). The minimum and maximum values of the operating conditions are shown in Table 6.1. The physical properties of the systems are shown in Table 2.1 and described in chapter 2.

6.2.2 Measurement of mass transfer coefficient

The mass transfer coefficient was estimated using limiting current technique as per Ramesh et al., 2009. The inner walls of the coils were provided with copper point electrodes of 3.024×10^{-3} m diameter to estimate the mass transfer coefficient. One end of these electrodes was very carefully fixed with the surface of the inner wall of the test section (coil tube), whereas the other end projected outward which was served as terminal for connecting the electrodes to the external circuit as shown in Figure 6.2.

Table 6.2: The range of variables covered in the present study

Parameter	**Minimum**	**Maximum**
Particle diameter, d_p (μm)	2.210	96.00
Slurry concentration, (wt %)	5.000	15.00
Liquid velocity, U_{sl} (m/s)	0.106	3.145
Gas velocity, U_{sg} (m/s)	0.053	1.048
Tube diameter, d_t (m)	0.009	0.020
Tube length, L_c (m)	4.940	5.400
Coil diameter, D_c (m)	0.075	0.200
Pitch difference (p/D_c)	0.500	2.000

Prior to the assembly of the helically coiled electrochemical cell, the surfaces of the point electrodes were polished with an emery paper and cleaned thoroughly. The electrical connectivity was checked using a digital multi-meter (Make: MAXX, Model: DT9205A). The current-potential measuring circuit (shown in Figure 6.1) consisted of a voltmeter (V), an ammeter (A), a rheostat, a commutator and a 6-V direct current source. The measurement were carried out for the case of an electrochemical redox system in the presence of an excess indifferent electrolyte (NaOH). The systems were chosen for these studies on (i) reduction of ferricyanide and (ii) oxidation of ferrocyanide, because the measurements by this method are relatively fast, accurate and reproducible. The electrode reactions involved are:

(i) Reduction of ferricyanide

$$[Fe(CN)_6]^{3-} + e \rightarrow [Fe(CN)_6]^{4-} \tag{6.1}$$

(ii) Oxidation of ferrocyanide

$$[Fe(CN)_6]^{4-} - e \rightarrow [Fe(CN)_6]^{3-} \tag{6.2}$$

About 80 liters of an equimolar solution of potassium ferrocyanide and potassium ferricyanide (0.01 kmol/m^3 each) and sodium hydroxide (0.5 kmol/m^3) were prepared from analytical grade reagents using distilled water of 5 μmho specification. These solutions were used as the electrolytes. The electrolyte from the storage tank was metered by two pre-calibrated rotameters and circulated through the helical coil tube. The flowrate was adjusted by using the control and by-pass valves. The temperature of the electrolyte was measured for each and every run with an accuracy ± 0.1 ^{0}C. When the liquid flow was stabilized, the limiting current was measured by applying an electric potential in small increment between the test electrode (Te) and the wall electrode (We). Initially the experiments were conducted with only indifferent electrolyte (sodium hydroxide). Since no appreciable currents were detected, the measured limiting currents obtained during redox process were essentially due to the potassium ferrocyanide or potassium ferricyanide. The measurement of limiting current was done as similar to earlier studies on ionic mass transfer (Lin et al., 1951; Raju and Rao, 1965; Ramesh et al., 2009). The ferrocyanide ion concentration was estimated by the permanganometric titration method (as per Lin et al., 1951), and the ferricyanide ion concentration was obtained by the iodometric titration method (as per Kolthoff and Furman, 1929; Sutton, 1935). In any electrochemical cell, the mass transfer between the bulk solution and the polarized surface takes place either by diffusion of ions due to concentration gradient or migration of ions due to potential difference. The emphasis is laid on the diffusion of the reacting material towards electrode surface and the reacted species to the bulk solution. This process is of the type steady state diffusion of solute in a dilute solution through a stagnant solvent. The transfer rate of diffusion of particular ionic species is written by using the Fick's first law of diffusion, which is governed by the following expression:

$$\frac{dS_i}{dt} = \frac{A_e D_L (C_i - C_s)}{\delta(1 - t_i^+)} \tag{6.3}$$

where, dS_i/dt is the transfer rate of ionic species (equivalents/s), A_e is the exposed area of the electrode surface, D_L is the diffusion coefficient of the ions, δ is the thickness of the hypothetical diffusion layer, C_i is the concentration of the ionic species in solution, C_s is the concentration of the ionic species at electrode surface and t_i^+ is the transport number of the reacting species. In the present study the concentration of indifferent electrolyte (0.5 kmol/m^3) is very high compared to the concentration (0.01 kmol/m^3) of the reacting ionic species. So the transport number of the discharge ions can be neglected. Therefore, Eq. (6.3) becomes

$$\frac{ds}{dt} = \frac{A_e D_L (C_i - C_s)}{\delta} \tag{6.4}$$

The rate of discharge of ions can be expressed as:

$$\frac{i_d}{zF} = \frac{D_L (C_i - C_s)}{\delta} \tag{6.5}$$

where i_d is the limiting current density (i_L/A_e), z is the number of electrons involved in the discharge process and F is the Faraday constant (96500 C/equivalent). The limiting current density represents the maximum rate at which the particular ion can be discharged under the given experimental conditions. At this current density, rapid increase of potential is observed. The value of the limiting current is obtained from the profile of current (i) and applied potential (E). The attainment of the limiting current is indicated by a sharp increase in potential for a marginal increase in the current. Figure 6.2 illustrates the graphical method of obtaining limiting current from voltage (E) vs. current (i) data. In the present study initially limiting currents were measured randomly at each of the 30 electrodes for different gas and liquid flow rates. From the experimental data it was observed that there was no longitudinal variation in the limiting current along the test section. Therefore 20 electrodes were shorted and then measured the limiting current data at this combined electrode for all subsequent runs. When the limiting current stage was reached on a polarized electrode, the concentration of the ionic species at the electrode surface (C_s) becomes zero. Then Eq. (6.5) can be written as

$$\frac{i_d}{zF} = \frac{D_L C_i}{\delta} \tag{6.6}$$

The mass transfer coefficient (k_L) is defined as the ratio of diffusion coefficient to the thickness of the diffusion layer (D_L/δ), which on substitution into Eq. (6.6) yields

$$k_L = \frac{i_d}{zFC_i} \tag{6.7}$$

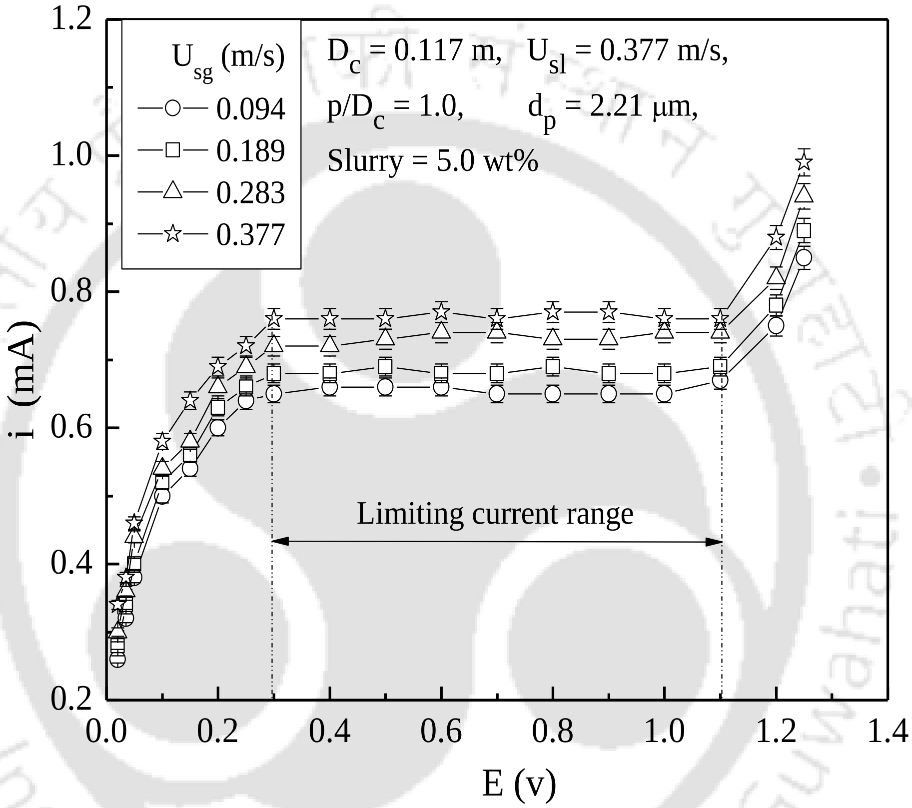

Figure 6.2: Polarization curve for limiting current estimation

In the present study the gas phase was used essentially to favor the hydrodynamic conditions at the reacting surface. A point electrode fixed at the inner wall of the coil was chosen as a reacting surface. The reacting ion in the continuous phase reaches the reacting surface under an electric potential by diffusion which depends on the polarity induced at the electrode surface. Reduction of ferricyanide ion was chosen for these studies which takes place at the electrode surface. For each run the limiting current for the case of reduction of ferricyanide was noted. However, at the end of each run the polarity was interchanged and few milliamperes of current were allowed to pass through the circuit for minimizing the concentration changes at the electrode surface. The limiting current data on oxidation were also obtained similarly as outlined above. The uncertainty of the experimental data is shown in Table 6.3.

Table 6.3: Range of the means, standard deviations, and uncertainties of the mass transfer (k_L) coefficient at constant tube diameter (d_t = 0.015 m), coil diameter (D_c = 0.075 m)

U_{sl} (m/s)	U_{sg} (m/s)	SCMC (kg/m^3)	wt %	Range of mean*, m/s (x10^4)	N	Range of STDEV* (× 10^{-3})	Range of uncertainty* (× 10^{-3})	Range of relative uncertainty %
0.189-1.132	0.000	0.0	0.0	0.301 - 0.524	12.0	4.294-4.901	1.24-1.40	0.406- 0.271
0.189-1.132	0.094	0.0	0.0	0.344 -1.069	12.0	2.121-3.705	0.61-1.07	0.136- 0.179
0.189-1.132	0.094	2.0	0.0	0.448 - 1.051	12.0	7.657-9.523	2.21-5.64	0.499- 0.739
0.189-1.132	0.094	0.0	5.0	0.384 - 0.793	12.0	3.392-3.582	0.98-1.03	0.254- 0.131

* The theory to calculate the values is given in chapter 2 in equations (2.10 – 2.12)

Each value of k_L in 5th column corresponds to the mean of 12 data points (i.e., N=12). Relative uncertainty is calculated from standard uncertainty and mean value of the corresponding data set.

6.3 Results and discussion

6.3.1 Variations of mass transfer coefficient with different variables

In the following sections, wall-liquid mass transfer at the confining wall of a helically coiled tube employing two-phase and three-phase flow is presented as a function of various operating variables. The phase velocities of liquid and gas exhibit strong influence on wall–liquid mass transfer. It is observed that the wall–liquid mass transfer coefficient was largely influenced by gas velocity and relatively less influenced by liquid velocity. The mass transfer increases with increasing superficial gas velocity as shown in Figure 6.3 due to increase in gas holdup with gas velocity (Thandlam et al., 2015). The gas holdup increases with the increase in gas velocity (Thandlam et al., 2015). It was also observed that in slurry system, for smaller particle size the gas holdup is higher compared to larger particles size as shown in Figure 6.4. Hence the mass transfer is increased with decrease in particle size. In case of catalyst solid particle where the reactive mass transfer happens on the surface of the solid, the mass transfer increases due to the same reason for increase in surface area with decreasing particle size. In this case it is to be noted that though the gas holdup is higher in case of the plug flow compared to the slug and stratified flow for which mass transfer to be higher, the overall effect of solute distribution in the plug flow decreases the mass transfer coefficient. For the same reason the overall mass transfer coefficient in the stratified flow is higher.

6.3.2 Variation of mass transfer coefficient with flow pattern

Based on the flow pattern at a constant geometry of the helical coil, it was seen that the mass transfer was higher in slug flows compared to plug flows (Figure 6.3 and 6.5). In slug flow higher mass transfer was observed because it is enhanced by the circulation flow inside a slug generated by the shear between fluid and the tube wall. Fluid flows forwards at the center of the tube and backwards near the tube wall and circulates inside a slug. The circulation flow enhances mixing inside a slug, making the concentration gradient gradual, improving the mass transfer rate through the interface. According to conventional theories, mass transfer depends on the mass transfer flux (the product of the mass transfer coefficient and the concentration gradient), the interfacial area, and residence time. The interfacial area for mass transfer depends on both the slug length and the thickness of liquid film formed between a slug and the tube wall. A narrow residence time distribution of fluid within each slug may result due to restricted mixing along the tube axis and the possibility of controlling residence time. The slug length varies with the change of the slug velocity or tube size.

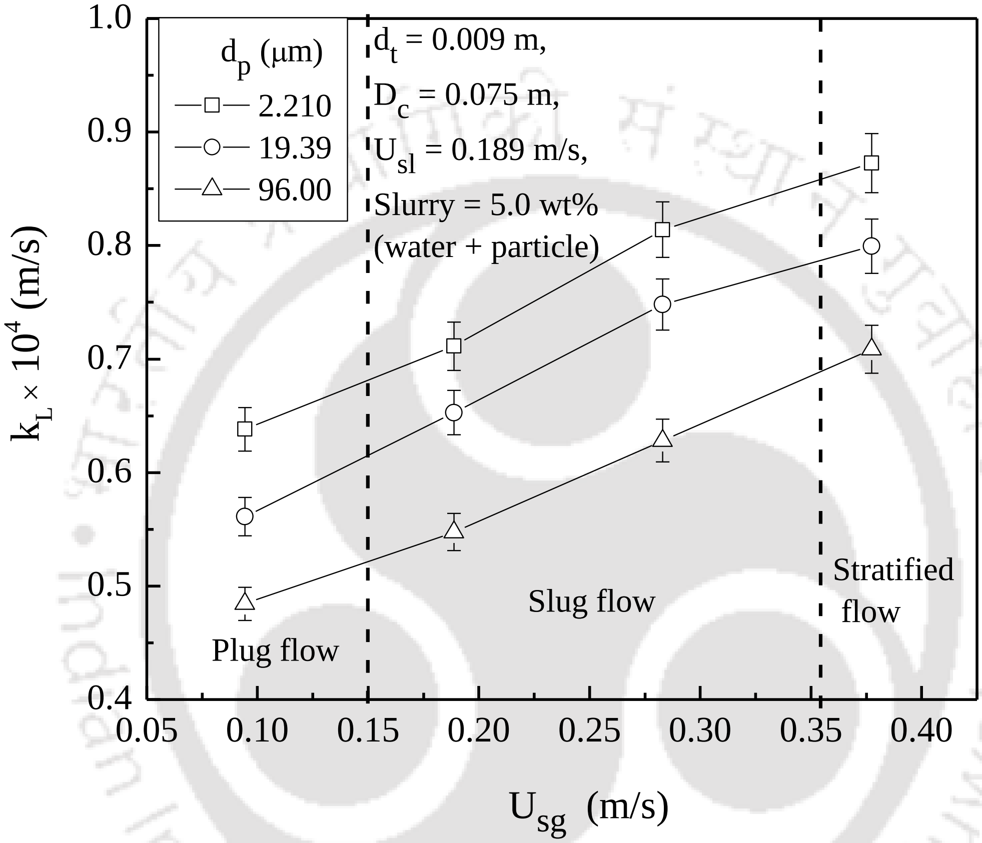

Figure 6.3: Effect of particle diameter on mass transfer coefficient in slurry system

An increase in liquid flowrate, increase in the value of mass transfer coefficient was observed because the flow getting twisted due to centrifugal action for curved structure of the helical tube and producing secondary flow pattern and induce more driving to the mass transfer of solute.

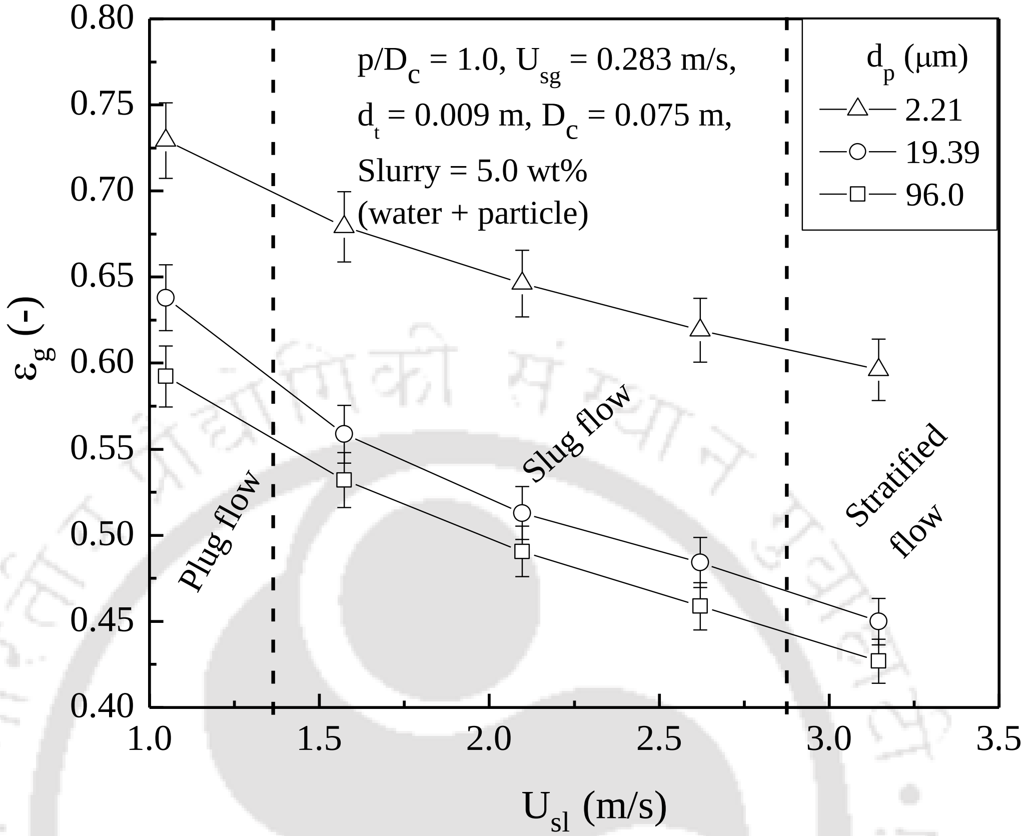

Figure 6.4: Effect of particle size on gas holdup in three-phase flow

6.3.3 Effect of physical properties

The liquid properties have a noticeable effect on mass transfer coefficient for the liquids investigated in the present study. The mass transfer coefficient decreases with increasing sodium carboxymethyl cellulose (SCMC) concentration in aqueous solution. This can be related to the increase of the liquid viscosity (shown in Table 2.1 in chapter 2), which resulted in a decrease of the diffusivity and consequently k_L at the higher concentration of the SCMC solution as shown in Figure 6.5. The efficiency of mass transfer is quietly controlled by transport mechanism of species in the liquid viscous boundary layer around the interface. The contact time between liquid particles active for the transfer result in variation of mass transfer efficiency with viscosity of liquid. Using the correlation of Haut and Cartage (2005), the expressions of volumetric mass transfer coefficient can be written as:

$$k_L \propto (\varepsilon_g / \sqrt{t_c})\sqrt{(D_L / \pi)} \tag{6.8}$$

Also within the liquid viscous boundary layer, the transport of solute in a direction normal to the interface is purely diffusional, while its transport in a direction tangential to the interface is purely convective (Haut and Cartage, 2005).

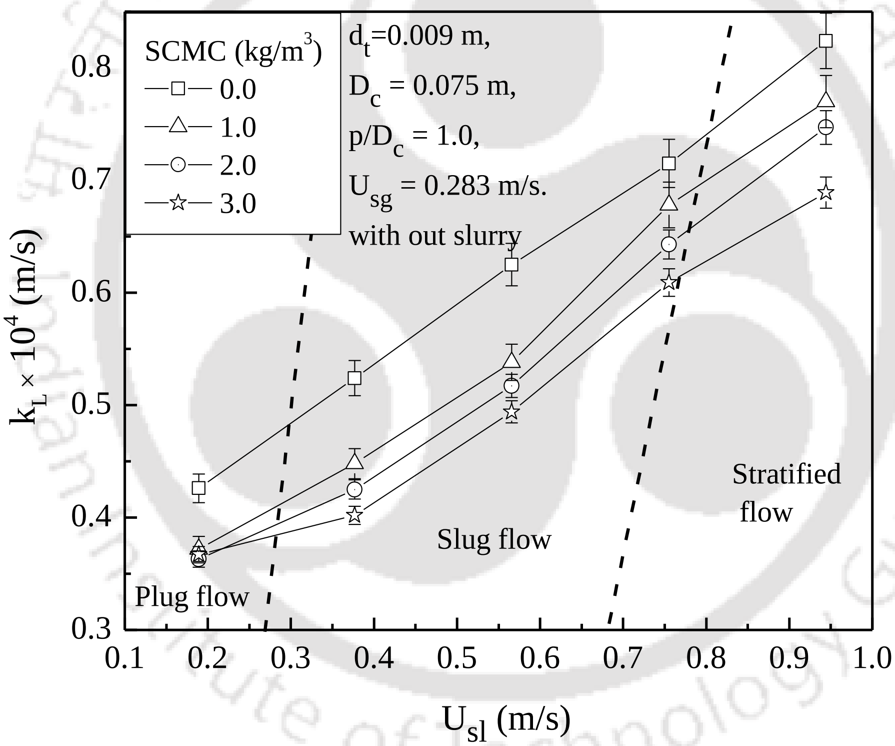

Figure 6.5: Variation of the mass transfer coefficient with the superficial velocities of the SCMC

A liquid element active for the transfer of solute enters the liquid boundary layer near the point of incidence and leaves it near the extreme point of the bubble. More viscous liquid resumes the more contact time between a solute and a liquid element active for the transfer of solute which may cause the decrease in mass transfer efficiency with increase in viscosity, as per Eq. (3.13).

6.3.4 Effect of geometrical variables

Figure 6.6 presents the mass transfer coefficient with liquid velocity for the three cases of pitch difference ratio (p/D_c) employed in the present experiment. It is observed that the increase in pitch difference, the mass transfer coefficient decreases. At lower pitch distance, the curvature effect increases. The centrifugal force increases with the increase in curvature. Also mass transfer coefficient depends on the particle size. The mass transfer coefficient increases with decreasing particle diameter. Coarser particle size decreases the mass transfer coefficient as shown in Figure 6.3, because the ability of the particle decreases the travel in radial direction. This can also be interpreted by gas holdup which is described in previous section. The effects of tube diameter on mass transfer coefficient are shown in Figure 6.7. The results show that the mass transfer coefficient increases with the decreasing tube diameter at constant liquid velocity. At a constant liquid flow rate, increasing the tube diameter the pressure decreases, which may increase the mass transfer. Coil diameter has strongly influence on mass transfer coefficient (k_L) as shown in Figure 6.8. It is observed that the mass transfer increases with increasing coil diameter. As the coil diameter increases the curvature effect decreases which results in decrease in mass transfer coefficient. By increasing coil diameter the number of turns decreases, which may also effect on mass transfer coefficient.

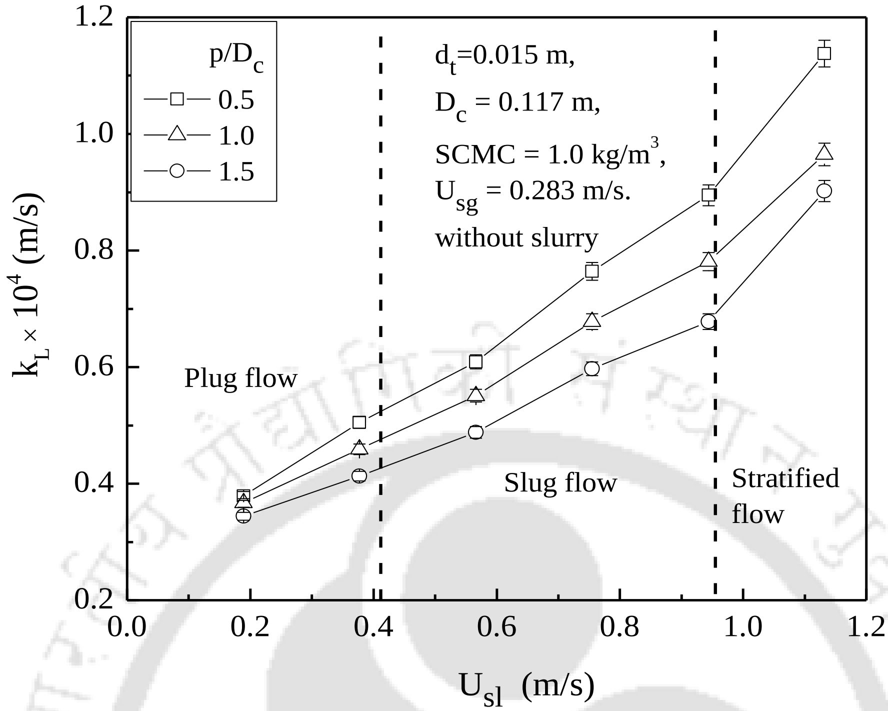

Figure 6.6: Effect of pitch difference (*p/D$_c$*) on mass transfer coefficient

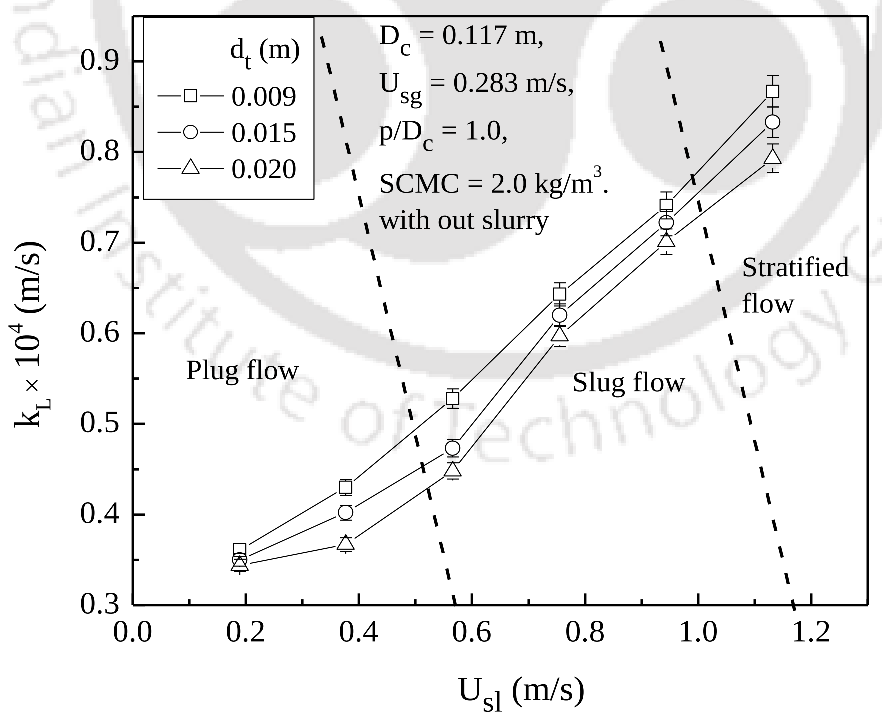

Figure 6.7: Effect of tube diameter on mass transfer coefficient

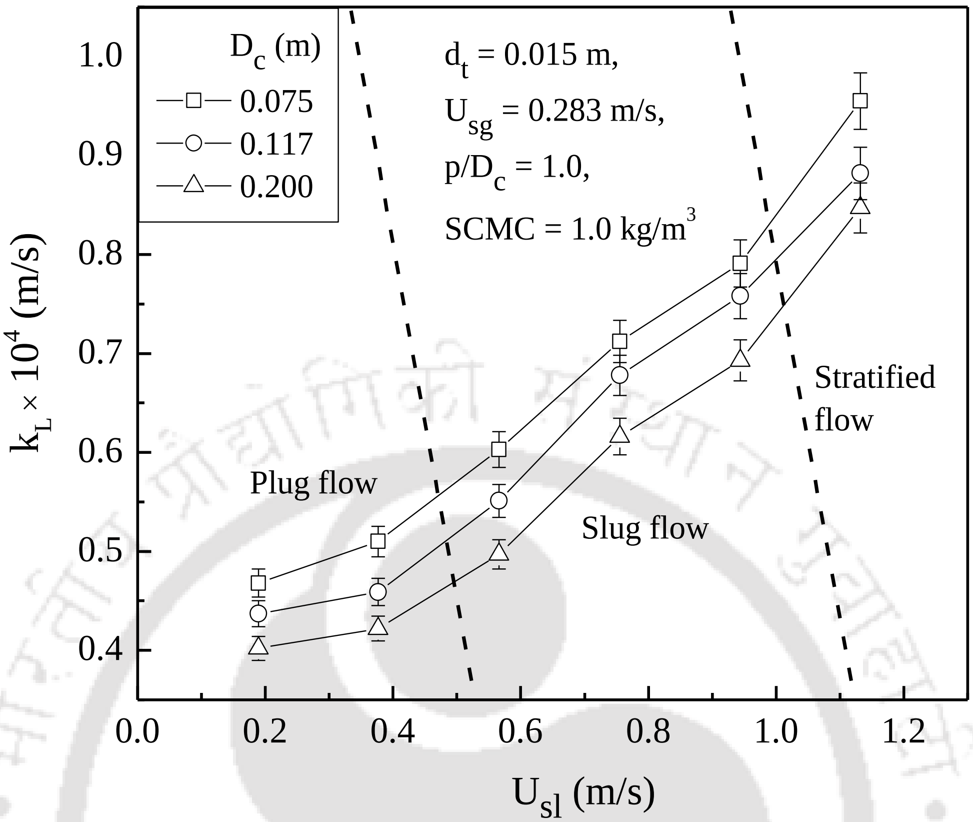

Figure 6.8: Effect of coil diameter on mass transfer coefficient

6.3.5 Comparison with straight tube

Experimental results show that higher mass transfer in the case of helically coiled tubes compared to straight tubes. This fact is expected to occur as a result of the difference in the hydrodynamic behavior between the two cases. Mass transfer coefficient in helical tube seems to decrease with decreasing tube curvature (increasing helical diameter) and eventually approaches that obtained for straight tube or minimum curvature, particularly in laminar region. Figure 6.9 shows that (k_L) values for straight tube vs. helical tube within laminar region while the two cases divert in values in turbulent region. In Figure 6.9 the mass transfer coefficient for straight tube represents the data from Lin et al. (1951). The higher k_L for helical tube may be due to increase in secondary flow in case of low curvature at high flow rate.

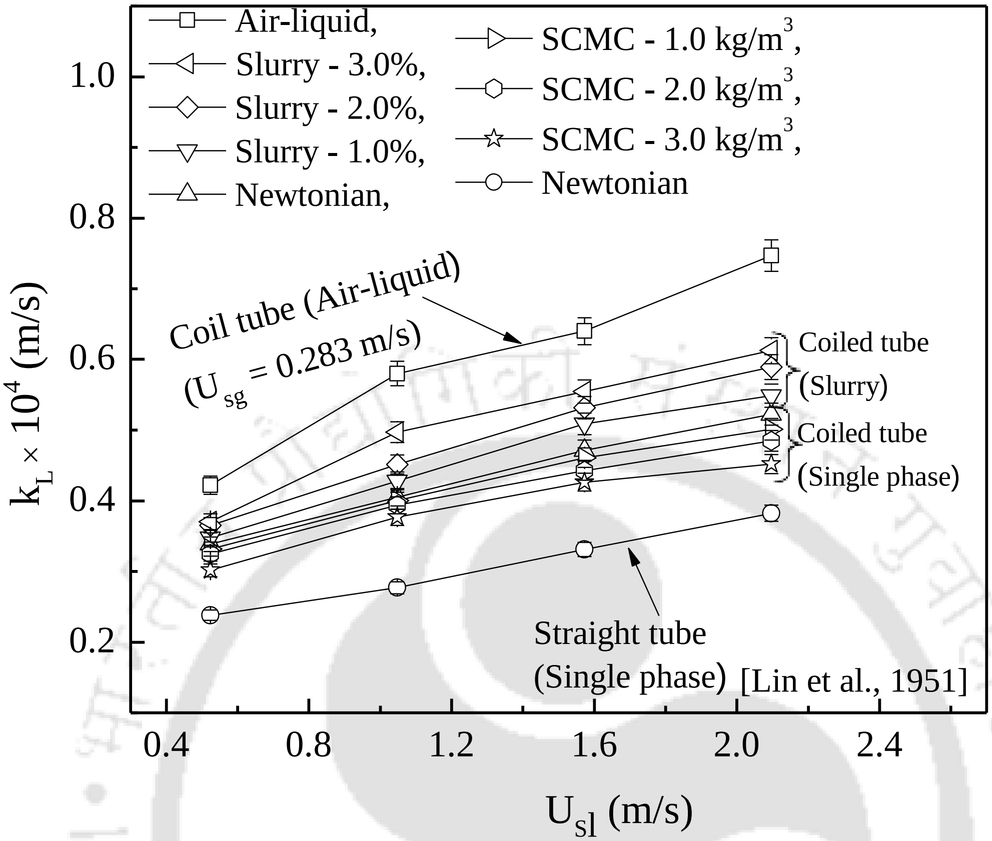

Figure 6.9: Augmentation of mass transfer coefficient with liquid velocity due to the presence of helical coiled tube (with d_t = 0.020 m, p/D_c = 1.0 and D_c = 0.20 m) in comparison with straight tube (with d_t = 0.020 m).

6.3.6 Flow pattern based correlations for mass transfer coefficient

The coil Reynolds number (Re_c) that is related to the flow change from laminar to turbulent can be represented to interpret the mass transfer coefficients. The onset of laminar and turbulent flow conditions in the helical coil tube (Thandlam et al., 2015) are respectfully as laminar if $Re \leq 2100 / (1-(8d_t/\pi D_c))$ and turbulent if $Re \geq 4000 / (1-(8d_t/\pi D_c))$. $Re\ (1-(8d_t/\pi D_c))$ is called the coil Reynolds number. This is an important criteria that concludes the momentum transfer behavior from mass transfer studies. The dimensionless groups affecting mass transfer has been recognized by assuming that the mass transfer coefficient is a function of the following parameters:

$$k_L = f(U, d_t, D_c, L_p, L_c, \rho_{l,} \mu_l, \sigma, D_L) \tag{6.9}$$

By using the dimensional analysis and incorporating the coil Reynolds number $Re_{cm} = Re(1-(8d_t/\pi D_c))$ instead of only Reynolds number ($Re = \rho U d_t/\mu$), the Stanton number in coil (St_c) was found to be a function of coil Reynolds number, capillary number, Bodenstein number and other ratios of coil length to tube diameter and coil pitch to tube diameter as given in the following equation:

$$St_c = \lambda(\mathrm{Re}_{cm})^a (Ca)^b (Bs)^c (D_{cR})^d (L_{pR})^e (L_{cR})^f \tag{6.10}$$

where $D_{cR} = D_c/d_t$, $L_{pR} = L_p/d_t$ and $L_{cR} = L_c/d_t$. By using the multiple regression analysis (Microsoft Excel, 2013) with the experimental data, the constants and powers of dimensionless groups are found which are shown in Table 6.4. The correlation can also be expressed by the Coulburn J-factor as

$$J_D = St_c Sc^{2/3} \tag{6.11}$$

Table 6.4: The parameters for the correlations (Eq. (6.10)) of mass transfer coefficient

Flow patterns	**λ**	**a**	**b**	**c**	**d**	**e**	**f**	**Re_{cm}×10^3**	**R^2**	**SE**
Plug	6.426	-0.134	0.222	0.166	-0.223	-0.158	-0.203	2.05-25.11	0.995	0.057
Slug	11.631	-0.089	0.149	0.267	0.187	-0.190	-0.524	1.15-7.95	0.991	0.062
Stratified	4.383	0.032	0.001	0.624	-0.090	-0.146	-0.280	2.23-8.50	0.993	0.052

The experimental data obtained in the present investigation have plotted in accordance with Eq. (6.11). A plot of experimental values of J_D and that of J_D calculated from the Eq. (6.11) is shown in Figure 6.10. The range of variables of the equation is $0.09 \leq J_D \leq 1.41$, $2.09\times10^2 \leq Re_{cm} \leq$

2.51×10^{4} , $47.26 \leq Ca \leq 9.078\times10^{4}$, $3.8\times10^{4} \leq Bs \leq 2.25 \times10^{2}$, $5 \leq (D_{cR}) \leq 13.33$, $3.9 \leq L_{pR} \leq 13.33$, $58.5 \leq L_{cR} \leq 275.55$.

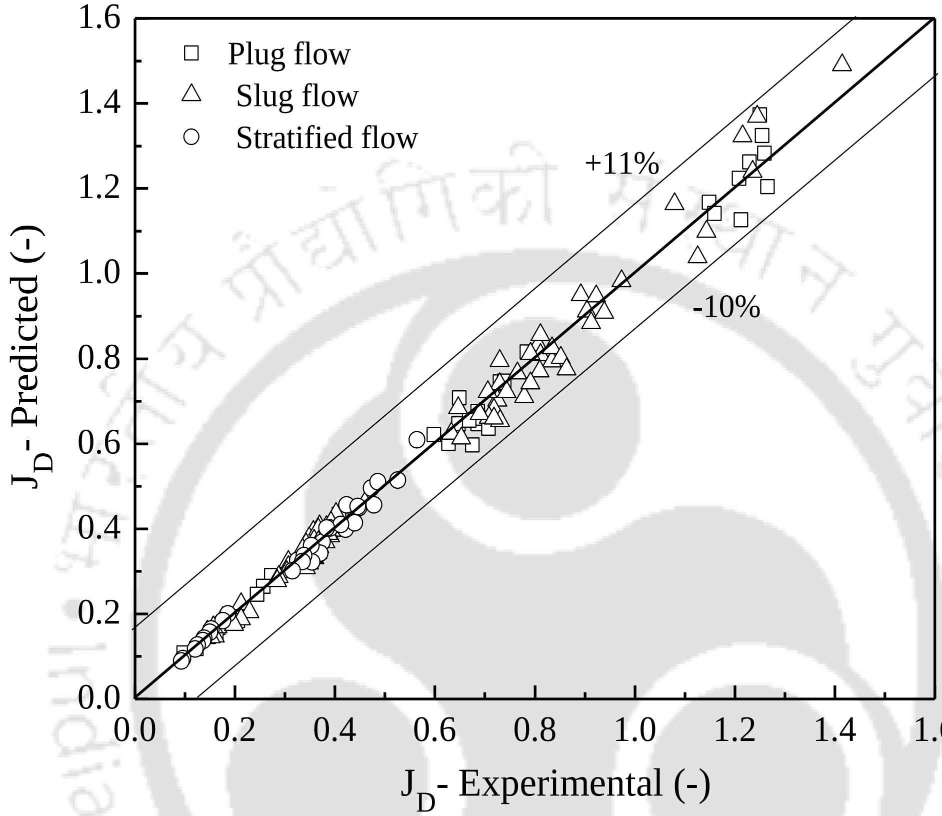

Figure 6.10: Parity plot of experimental J_D to the predicted J_D factor for different flow patterns

6.3.7 Analysis of frictional drag coefficient based on mass transfer coefficient

The time average of the apparent local mass transfer coefficient k_L, is related to the average velocity gradient at the wall (Reiss and Hanratty, 1963) as

$$k_L = 0.807\left(\left(D_L^2 S_p\right)/L_e\right)^{1/3} \tag{6.12}$$

D_L is the diffusion coefficient of the ions. The values of diffusion coefficients can be evaluated by Eq. (6.13) (Tonini et al., 1978) from the measured values of limiting current and superficial liquid velocity

$$D_L = \left(\left(i_L d_t L_e^{1/3}\right) / \left(1.614 zFC_i A_e u_{sl}^{1/3} d_t^{2/3}\right)\right)^{3/2} \tag{6.13}$$

The parameter, L_e, is the equivalent electrode length. For a circular electrode the equivalent electrode length is $L_e = 0.820 d_e$ where d_e is the electrode diameter. Eq. (6.13) is valid over a wide range of values of the shear stress both in laminar and turbulent flows. The local velocity gradient at the wall is related to the local stress. In this case, it is possible to calculate the frictional drag force acting on the spherical object, F_f, from the data of the local velocity gradient $s(\theta)$:

$$F_f = \iint_{sphere} \tau \sin(\theta) dS = 2\pi R^2 \int_0^{\theta} \tau \sin^2(\theta) d\theta \tag{6.14}$$

From Eq. (6.14) the frictional drag force exerted on electrode as per present experimental design can be estimated (Essadki et al., 2005) by

$$F_f = 2\pi R^2 \mu_{eff} \int_0^{\pi/2} S_p Sin^2\theta d\theta \tag{6.15}$$

So the frictional drag force is interrelated to the mass transfer coefficient by Eqs. (6.12-6.15) and can be expressed as

$$F_f = \lambda' k_L^3 \tag{6.16}$$

where,

$$\lambda' = 2.45\mu_{eff}\,\frac{d_e^3}{D_L^2}\int_0^{\pi/2} Sin^2\theta\, d\theta = 2.45\mu_{eff}\,\frac{d_e^3}{D_L^2}\left((\pi - 1)/4\right) \tag{6.17}$$

The frictional drag force on any surface is characterized by the frictional drag coefficient (C_f) as (Essadki et al., 2005)

$$C_f = \frac{F_f}{0.5\pi R^2 u_{sl}^2 \rho_l} \tag{6.18}$$

where R is the radius of the electrode and F_f is the frictional drag force related to the velocity gradient at the surface of the object (S_p). The velocity gradient at the surface of the particle can be calculated from the experimentally measured mass transfer coefficient by Eq. (6.19).

$$S_p = (1.24k_L)^3\,\frac{d_e}{D_L^2} \tag{6.19}$$

In the present study, in the helical upward flow, the angle (θ) between electrode position and the main liquid flow is $\pi/2$. The values of frictional drag coefficient can be calculated from Eq. (6.18) for different operating conditions by substituting the values of frictional drag force estimated by Eq. (6.16). The variation of frictional drag coefficient with Reynolds number is shown in Figure 6.11. A functional relationship has been developed based on present experimental data for frictional drag coefficient as a function of Reynolds number for different flow patterns as

$$C_f = \lambda(\mathrm{Re}_{cm})^a (Ca)^b (D_{cR})^c (L_{pR})^d (L_{cR})^e \tag{6.20}$$

For plug flow

$$C_f = 5.14 \times 10^{03} (\mathrm{Re}_{cm})^{-0.634} (Ca)^{-0.319} (D_{cR})^{0.144} (L_{pR})^{-0.164} (L_{cR})^{-0.453} \tag{6.21}$$

For slug flow

$$C_f = 5.21 \times 10^{03} (\mathrm{Re}_{cm})^{-0.626} (Ca)^{-0.333} (D_{cR})^{0.196} (L_{pR})^{-0.098} (L_{cR})^{-0.532} \tag{6.22}$$

For stratified flow

$$C_f = 1.75 \times 10^{02} (\mathrm{Re}_{cm})^{-0.717} (Ca)^{-0.270} (D_{cR})^{0.076} (L_{pR})^{-0.163} (L_{cR})^{0.148} \tag{6.23}$$

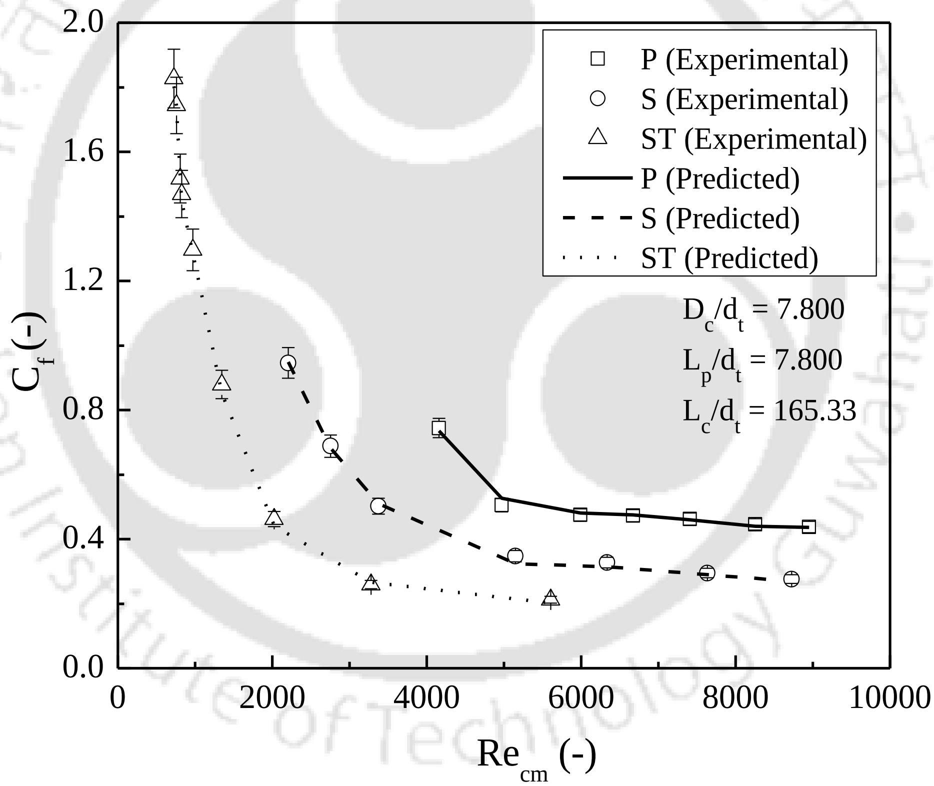

Figure 6.11: Variation of the frictional drag coefficient with the Reynolds number at different flow patterns with two-phase air-Newtonian fluids.

Figure 6.12 shows typical experimental and predicted data of drag coefficient for SCMC at different flow patterns.

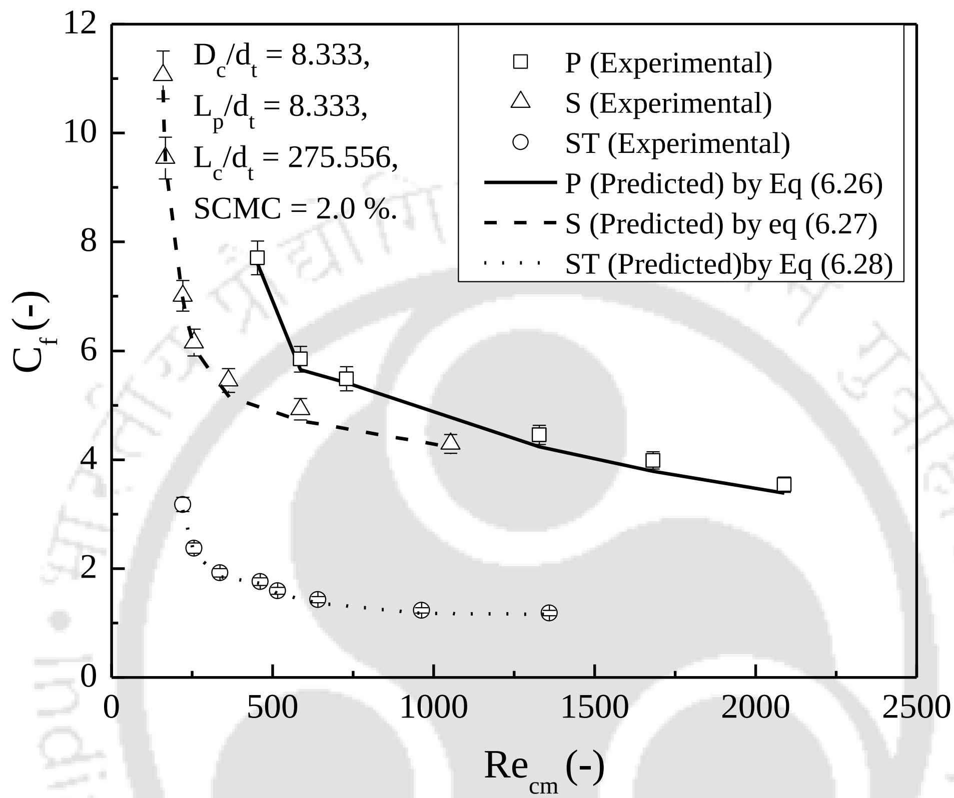

Figure 6.12: Variation of the frictional drag coefficient with the Reynolds number at different flow patterns with two-phase air-non-Newtonian fluids.

With increasing Reynolds number the drag coefficient decreases. Similarly with slurry system with different flow patterns it is shown in Figure 6.13. For slurry system, the developed correlations are:

For plug flow

$$C_f = 3.51\times10^{04}(\mathrm{Re}_{cm})^{0.118}(Ca)^{0.657}(D_{cR})^{-0.049}(L_{pR})^{0.189}(L_{cR})^{-0.994} \quad (6.24)$$

For slug flow

$$C_f = 2.33\times10^{06}(\mathrm{Re}_{cm})^{0.341}(Ca)^{0.771}(D_{cR})^{-0.068}(L_{pR})^{-0.125}(L_{cR})^{-1.471} \tag{6.25}$$

For stratified flow

$$C_f = 1.92\times10^{05}(\mathrm{Re}_{cm})^{-0.015}(Ca)^{-0.470}(D_{cR})^{0.684}(L_{pR})^{-0.095}(L_{cR})^{-1.307} \tag{6.26}$$

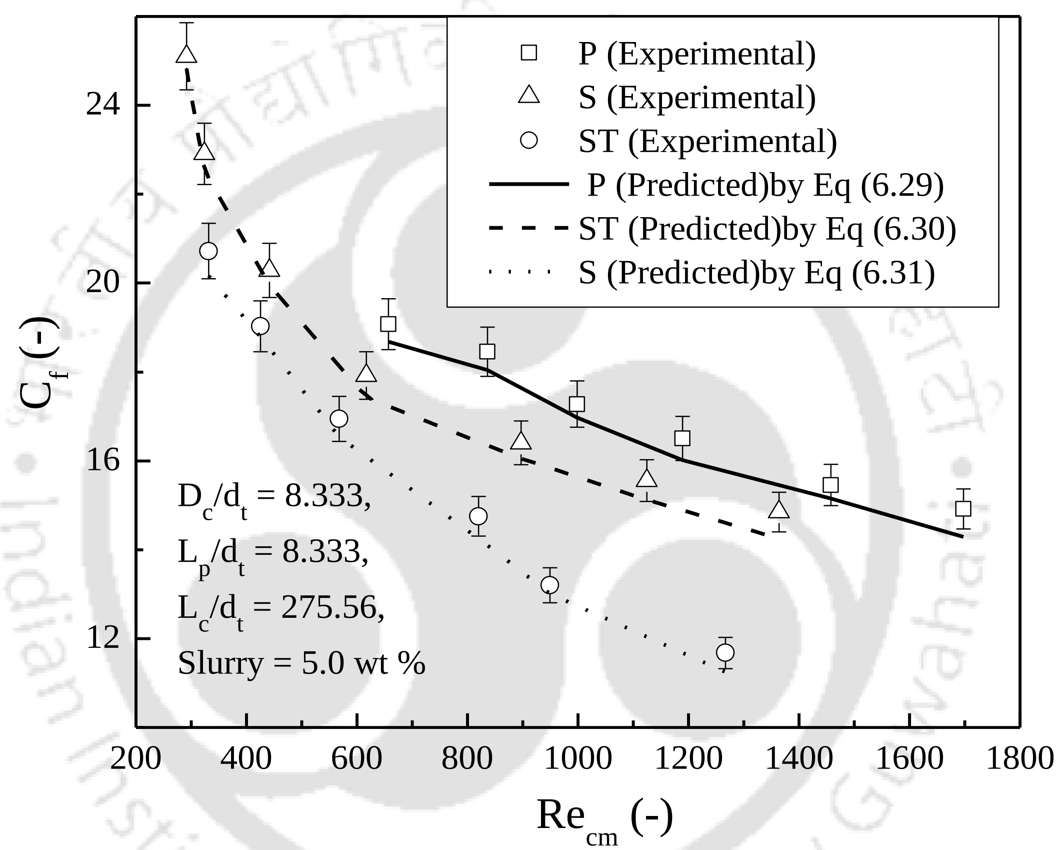

Figure 6.13: Variation of the frictional drag coefficient with the Reynolds number at different flow patterns with three phase air-slurry system.

6.3.8 Mass transfer based on mixing characteristics

As per the present experimental conditions, the mass transfer between the confined wall and the liquid occurring in the helical system depends on the dynamic and physical properties of the system and the dispersion of the phases. Figure 6.14 shows the present experimental data of dispersion coefficient with mass transfer coefficient for three different liquid concentrations (SCMC – 1.0, 2.0 and 3.0 kg/m^3) at constant tube diameter (d_t = 0.015 m), coil diameter (D_c = 0.117 m), pitch difference (L_p/D_c = 1.0) and gas superficial velocity (U_{sg} = 0.188 m/s). It is observed that the increase in dispersion coefficient, the mass transfer coefficient increases at constant two-phase upward flow. The variation of dispersion coefficient has been described in chapter 4 in details. Based on the flow patterns, slug flow getting higher mass transfer because of it is enhanced by the circulation flow inside a slug flow with the generation of a shear between fluid and the tube wall. The circulation flow improves mixing inside a slug by inducing concentration gradient gradually. As a results the mass transfer rate through the interface was improved. Further a correlation has been developed in order to relate the dispersion coefficient (E_z) and the mass transfer coefficient (k_L) which can be expressed by

$$k_L = \alpha + \frac{\beta}{1 + Z^2 + Z^4 + Z^6} \tag{6.27}$$

where

$$Z = \left[2\left(E_z - \gamma\right)/\varphi\right] \tag{6.28}$$

The parameters α, β, γ and φ are found to be dependent on the SCMC concentration (C_c) of the liquid and can be correlated as

$$\alpha = 0.0065{C_c}^2 - 0.0407C_c + 0.4019$$

(6.29)

$$\beta = 0.334e^{-0.077C_c} \tag{6.30}$$

$$\gamma = 0.0066C_c^{\ 2} - 0.0396C_c + 1.1143 \tag{6.31}$$

$$\varphi = 0.7568e^{-0.017C_c} \tag{6.32}$$

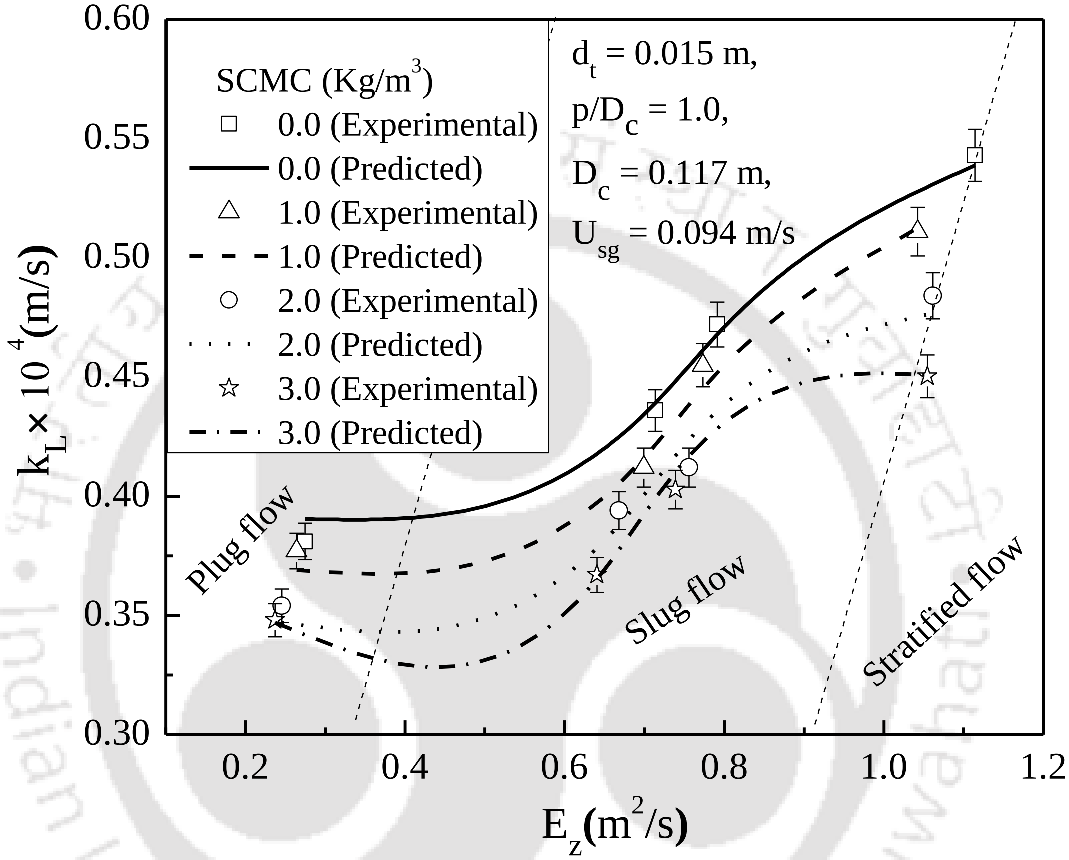

Figure 6.14: Effect of dispersion coefficient on mass transfer coefficient

The correlation is best suitable with ± 9% of error, Standard error is found to be 1.42 as per following equation

$$SE = S/\sqrt{N} \tag{6.33}$$

$$S = \sqrt{\frac{1}{(N-1)}\sum_{i=1}^{N}(x_i - x)^2} \tag{6.34}$$

where SE is the standard error, S is the standard deviation, $x_1, x_2, \ldots x_n$ is the sample data, x is the mean value of the sample data, N is the size of the sample data. A typical comparison between the predictions of the proposed correlation and the experimental data of the present system is shown in Figure 6.14.

6.4 Conclusions

The studies on flow pattern based mass transfer and drag phenomena of two-phase (gas-liquid) and three-phase (gas-liquid-solid) flow in vertical helically coiled tube with various geometrical conditions have experimentally been investigated. The mass transfer coefficient increases with liquid and gas velocities. It was observed that gas velocity have 7% more effect on mass transfer coefficient than the liquid velocity. Mass transfer coefficient has strongly influenced by gas holdup. With non-Newtonian fluid the mass transfer coefficient decreases with increasing the liquid viscosity (SCMC concentration). For a given set of conditions the rate of mass transfer coefficient in helical coil decreases with increasing pitch length (pitch difference, p/D_c). In three-phase flow system mass transfer coefficient increases with decreasing the particle diameter (d_p). It was also observed that the mass transfer coefficient increases with decreasing tube diameter (d_t) and coil diameter (D_c). Variations in mass transfer with gas and liquid flow rate are related to flow patterns. Based on flow patterns; the flow has been segregated into three regions as Plug flow ($1.21\times10^{03} \leq Re_{cm} \leq 2.51\times10^{04}$), Slug flow ($2.51\times10^{02} \leq Re_{cm} \leq 2.54\times10^{04}$), Stratified flow ($2.23\times10^{03} \leq Re_{cm} \leq 8.50\times10^{03}$). Plug flow results the lowest mass transfer coefficient ($0.344\times10^{4} \leq k_L \leq 1.312\times10^{4}$) and stratified flow provides the highest ($0.298\times10^{4} \leq k_L \leq 1.635\times10^{4}$), which increase constantly with gas superficial velocity. Slug flow results in mass transfer rates ($0.560\times10^{4} \leq k_L \leq 1.990\times10^{4}$) fairly independent of gas superficial velocity. Correlations developed based on the semi theoretical consideration. It was observed from the present study that the drag coefficient decreases with increase of Reynolds number with different flow patterns (plug, slug and stratified flow). For a fixed Reynolds number the value of frictional drag coefficients was highest in plug flow and least in stratified flow. In case of slug flow, the value of frictional drag found to be greater than plug flow and less than stratified flow. The dispersion of fluid changes the degree of mass transfer coefficient. A correlation has been developed for mass transfer coefficient based on the dispersion coefficient.

Nomenclature

A_e	Area of transfer surface of the electrode (m^2)
d_e	Electrode diameter (m)
d_t	Tube diameter (m)
d_p	Particle diameter (μm)
D_c	Coil diameter (m)
D_L	Diffusivity of reacting ion ($m^2 s^{-1}$)
E	Applied potential (V)
F	Faraday constant (96500 C/equivalent)
F_f	Frictional drag force (N)
g	Acceleration due to gravity ($m\ s^{-2}$)
i_d	Limiting current density ($A\ m^{-2}$)
i_L	Limiting current (A)
J_D	Mass transfer factor (-)
k_L	Mass transfer coefficient ($m\ s^{-1}$)
L_c	Length of coil (m)

L_e	Equivalent electrode length (m)
L_p	Pitch length (m)
n	Flow behavior index (-)
R	Radius of the electrode (m)
U_l	Superficial liquid velocity (m s^{-1})
U_g	Superficial gas velocity (m s^{-1})

Greek letters

p	Pitch (m)
ρ_l	Density of liquid (kg m^{-3})
ρ_m	Mixed density (kg m^{-3})
ρ_s	Density of solids (kg m^{-3})
μ_{eff}	Effective viscosity (kg m^{-1} s^{-1})
σ_l	Surface tension (N m^{-1})
ε_g	Gas holdup (-)

Dimensionless groups

Ca	Capillary Number ($U_{gl}\mu_{gl}/\sigma_l$) (-)
Bs	Bodestiein Number ($U_{gl}d_t/D_L$) (-)
Re	Reynolds Number ($d_tU\rho/\mu$) (-)
Re_{cm}	Coil Reynolds Number ($Re_{cm}=Re\ (1-(8d_t)/(\pi D_c))$) (-)
Sc	Schmidt number ($\mu/\rho D_L$) (-)
St	Stanton number (k_L/U) (-)

Reference

- Abdel-Aziz, M.H., Mansour, I.A.S., Sedahmed, G.H., 2010. Study of the rate of liquid–solid mass transfer controlled processes in helical tubes under turbulent flow conditions. Chem. Eng. Proc. 49, 643-648.
- Abdel-Aziz, M.H., 2013. Solid–liquid mass transfer in relation to diffusion controlled corrosion at the outer surface of helical coils immersed in agitated vessels. Chem. Eng. Res. Des. 91, 43-50.
- Ali, S., 2001. Pressure drop correlations for flow through regular helical coil tubes. Fluid Dyn. Res. 28, 295–310.
- Awwad, A., Xin, R.C., Dong, Z.F., 1995. Measurement and correlation of the pressure-drop in air-water two-phase flow in horizontal helicoidal pipes. Int. J. Multiphase Flow 21, 607-619.
- Banerjee, S., Rhodes, E., Scott, D.S., 1969. Studies on co-current gas-liquid flow in helically coiled tubes I. flow patterns, pressure drop and holdup. Can. J. Chem. Eng. 47, 445–453.
- Biswas, A.B., Das, S.K., 2006. Holdup characteristics of gas-non-Newtonian liquid flow through helical coils in vertical orientation. Ind. Eng. Chem. Res. 45, 7287-7292.
- Biswas, A.B., Das, S.K., 2007. Frictional pressure drop of air non-Newtonian liquid flow through helical coils in horizontal orientation. Can. J. Chem. Eng. 85, 129-136.
- Biswas, A.B., Das, S.K., 2008. Two-phase frictional pressure drop of gas–non-Newtonian liquid flow through helical coils in vertical orientation. Chem. Eng. Proc. 47, 816–826.

- Essadki, A.H., Nikov, I., Delmas, H., 2005. Local shear and skin friction on particles in three-phase fluidized beds. Chem. Eng. Sci. 60, 6034−6042.
- Hameed, M.S., Muhammed, S., 2003. Mass transfer into liquid falling film in straight and helically coiled tubes. Int. J. Heat Mass Transfer 46, 1715-1724.
- Haut, B., Cartage, T., 2005. Mathematical modeling of gas–liquid mass transfer rate in bubble columns operated in the heterogeneous regime. Chem. Eng. Sci. 60, 5937-5944.
- Kolthoff, I.M., Furman, N.H., 1929. Volumetric Analysis. J. Wiley & Sons Inc., New York.
- Kumar, R.H., Ramesh, K.V., Sarma, G.V.S., Raju, G.M.J., 2011. Mass transfer at the confining wall of helically coiled circular tubes in the absence and presence of packed solids, Int. Comm. Heat Mass Transfer 38, 319–323.
- Lin, C.S., Denton, E.B., Gaskill, H.S., Putan, C.L., 1951. Diffusion controlled electrode reactions. Ind. Eng. Chem. Res. 43, 2136–2143.
- Mandal, S.N., Das, S.K., 2002. Gas–Newtonian liquid flow through helical coils in horizontal orientation. Can. J. Chem. Eng. 80, 979–983.
- Mandal, S.N., Das, S.K., 2003. Gas-liquid flow through coils. Korean J. Chem. Eng. 20, 624-630.
- Mandal, S.N., Das, S.K., 2003. Gas–liquid flow through helical coils in vertical orientation. Ind. Eng. Chem. Res. 42, 3487–3494.
- Raju, J.G.J.V., Rao, V.C., 1965. Ionic mass transfer in the presence of fluidizing solids. Ind. J. Tech. 3, 201-205.

- Ramesh, K.V., Raju, G.M.J., Bhaskara Sarma, C., Subba Raju, R.V., 2008. Liquid–wall mass transfer in three-phase fluidized beds with cross-flow of electrolyte. Chem. Eng. J. 135: 234–241.
- Ramesh, K.V., Raju, G.M.J., Murthy, Ch.V.R., Bhaskara Sarma, C., 2009. Wall-to-bed mass transfer in three-phase fluidized beds in the absence and presence of a composite promoter. Chem. Eng. J. 152, 207–211.
- Rao, T.P., Prasad, P.R., Rao, G.Y., Sujatha, V., 2013. Studies on mass transfer in electrochemical cells with coaxially placed entry region coil as turbulence promoter in annular conduit in homogeneous flow. Int. J. Innov. Res. Sci. Eng. Tech. 2, 3521-3535.
- Reiss, L.P., Hanratty, T.J., 1963. An experimental study of the unsteady nature of the viscous sublayer. AIChE J. 9, 154-160.
- Sujatha, V., Rajendra Prasad, P., Bhaskara Sarma, C., Jagannadha Raju, G.J.V., 2003. Studies on ionic mass transfer with insert helical tape promoters in batch fluidized beds. Ind. J. Chem. Tech. 10, 694-700.
- Sutton, F., 1935. Volumetric Analysis. 12th ed., Blakiston & Co., Philadelphia.
- Thandlam A.K., Raju. G.M.J., Sarma, G.V.S., Ramesh, K.V., 2009. Mass transfer at the confining wall of helically coiled circular tubes with gas–liquid flow and fluidized beds. Chem. Eng. J. 153, 114–119.
- Thandlam, A.K., Mandal, T.K., Majumder, S.K., 2015. Flow pattern transition, frictional pressure drop, and holdup of gas non-Newtonian fluid flow in helical tube, Asia Pacific J. Chem. Eng. 10, 422-437.
- Tonini, R.D., Remorino, M.R., Brea, F.M., 1978. Determination of diffusion coefficients with a pipe wall electrode. Electrochimica Acta 23, 699−704.

- Vashisth, S., Kumar, V., Nigam, K.D.P., 2008. A review on potential applications of curved geometries in process industry. Ind. Eng. Chem. Res. 47, 3291–3337.

CHAPTER-7

OVERALL CONCLUSIONS AND RECOMMENDATIONS FOR FUTURE STUDY

This chapter summarizes conclusions made from the present research findings of the thesis, and also points out possible scope for future research work.

7.1. Overall conclusions

In this work, three different types of flow patterns namely plug, slug and stratified flow were observed. The flow patterns of two-phase air-non-Newtonian that were not similar compared to air-Newtonian at a particular conditions. In both cases slug flow appeared as intermittent region. With increasing coil diameter, plug and stratified flow are affected but there was no change in slug flow. When a small pitch difference increased, plug flow was resulted without any change in slug and stratified flow. It was noticed that the flow pattern transitions among the plug, slug and stratified pattern shifted by changing liquid concentrations at a particular geometrical variables. Probabilistic neural network (PNN) has successfully developed for two-phase helical coil system to predict the flow patterns and their transition boundaries. Correlation model was also proposed for flow pattern transitions of air-non-Newtonian fluids. The characteristics of gas holdup and the frictional pressure drop is investigated. Increase in liquid concentrations two-phase frictional pressure drop increased. Due to viscous effect of non-Newtonian liquid the changes of flow patterns and two-phase frictional pressure drop may occur. The two-phase pressure drop increased with the increase in ratio of the tube to coil diameter. The ratio of tube to coil diameter changed the generation of secondary flow. There was no change in two-phase pressure drop when increasing pitch difference. That means there was no pressure loss by increasing the pitch difference. The two-phase frictional pressure drop increased due to bubble formation and phase interaction which contributed to the total pressure drop for typical flow rates of the phases. The bubble-liquid interfacial shear stress increased with the increase in surface tension and decreased with increase in bubble diameter. The effect of gas holdup was more in non-Newtonian fluids when compared to Newtonian fluids. With decreasing liquid velocity at constant gas flow rate, the gas holdup increased in both Newtonian and non-Newtonian fluids. If coil diameter is increased the two-phase friction factor decreases. The energy loss due to wettability increased with the decrease in surface tension. The frictional two-phase pressure drop was analysed by a mechanistic model based on the plug/slug formation, drag at interface and wettability effect of the Newtonian and non-Newtonian fluids. Based on flow patterns, plug flow resulted the lower dispersion coefficient whereas stratified flow showed higher dispersion coefficient. Slug flow resulted in dispersion coefficient fairly independent of gas superficial velocity. The mean residence time of the fluid decreased when the gas flow rate (or) liquid flow rate was increased. The Peclet number of liquid decreased with increasing either gas velocity or liquid velocity. Similarly, the dispersion coefficient increased with increasing gas flow rate or liquid flow rate. It was observed that the dispersion coefficient increased with the decrease of tube diameter, coil diameter, liquid concentration (SCMC) and pitch difference. The correlation was developed for a Peclet number with different operating variables based on different flow patterns (plug flow, slug flow and stratified flow). It was observed that heat transfer coefficient increased with increase in gas flow rate but it gradually decreased with the increase in liquid flow rate. Moreover with the increase of wall temperature the heat transfer coefficient increased. With the increase in coil (or) tube diameter heat transfer coefficient decreased. With increasing concentration of SCMC the heat transfer coefficient in the helical coil system increased significantly. A correlation has been developed for the heat transfer coefficient. The mass transfer coefficient increased with liquid velocity and gas velocity. It has been observed that gas velocity had 7% more effect on mass transfer coefficient than the liquid velocity. Mass transfer coefficient was strongly influenced by gas holdup in two-phase gas-liquid up flow system. With non-Newtonian fluid the mass transfer coefficient decreased with increasing the liquid viscosity (SCMC concentration). For a given set of conditions the rate of mass transfer coefficient in helical coil decreased with increasing pitch length (pitch difference, p/D_c). In three-phase flow system mass transfer coefficient increased with decreasing the particle diameter (d_p). It was observed that the mass transfer coefficient increased with decreasing tube diameter (d_t) and coil diameter (D_c). Based on flow patterns; the two-phase flow has been segregated into three regions as Plug flow, Slug flow, Stratified flow. Plug flow resulted the lower mass transfer coefficient whereas stratified flow showed the highest, which increased constantly with gas superficial velocity. Slug flow resulted in mass transfer rates fairly independent of gas superficial velocity. Correlations developed based on the semi theoretical consideration. It was observed from the present study that the drag coefficient decreased with increase of Reynolds number with different flow patterns (plug, slug and stratified flow). For a fixed Reynolds number the value of frictional drag coefficients was highest in plug flow and least in stratified flow. In case of slug flow, the value of frictional drag found to be greater than plug flow and less than stratified flow. It is observed that the dispersion of fluid changes the degree of mass transfer coefficient. A correlation has also been developed for mass transfer coefficient based on the dispersion coefficient.

7.2. Recommendations for future study

This thesis has highlighted details of the flow patterns, gas holdup, pressure drop, mixing characteristics, heat transfer characteristics and mass transfer characteristics in non-

Newtonian liquid. However further work is required to have a complete idea in this field for proper design and scaling of helical coil. The possible recommendations for further research work in this field can be summarized as

- The rheological study of helical coil shown in the present study is limited to two-phase and three phase flow in up flow vertical helical coil system. The work can be extended to down flow helical coil system.
- The study of helical coil is considered with only one non-Newtonian fluid (SCMC), other different types of fluids may also be used to explore the research.
- The study of flow patterns in helical coil with different systems can be extended with various geometry.
- The effect of heat and mass transfer with nano-particles in helical coil can be studied.
- The work can be extended by comparing the experimental data with CFD simulation.

Appendix-I

Calculation Procedure for Typical Multiple Regression

[Equation (3.11)]

The regression equation is

$$\varepsilon_g/\psi = C_1\left(\frac{\mu_m}{\rho_m U_m d_t}\right)^{b_1}\left(\frac{\sigma_L}{\rho_m U_m d_t^2}\right)^{b_2}\left(\frac{D_c}{d_t}\right)^{b_3}\left(\frac{L_p}{d_t}\right)^{b_4}\left(\frac{L_t}{d_t}\right)^{b_5} \tag{A1}$$

Taking logarithm on both side of Equation A1, one get

$$\log(\varepsilon_g/\psi) = \log(C_1) + b_1\log\left(\frac{\mu_m}{\rho_m U_m d_t}\right) + b_2\log\left(\frac{\sigma_L}{\rho_m U_m d_t^2}\right) + b_3\log\left(\frac{D_c}{d_t}\right) + b_4\log\left(\frac{L_p}{d_t}\right) + b_5\log\left(\frac{L_t}{d_t}\right) \tag{A2}$$

The equation A2 can be written as

$$Y = b_0 + b_1X_1 + b_2X_2 + b_3X_3 + b_4X_4 + b_5X_5 + e \qquad + \tag{A3}$$

where Y = Log(ε_g/ψ), X_1 = Log($\mu_m/\rho_m U_m d_t$), X_2 = Log($\sigma_m/\rho_m U_m d_t^2$), X_3 = Log(D_c/d_t), X_4 = Log(L_p/d_t) and e is the error term which has to be minimized to estimate the regression model as

$$\hat{Y} = b_0 + b_1X_1 + b_2X_2 + b_3X_3 + b_4X_4 + b_5X_5 \tag{A4}$$

where $\hat{Y}$ is the predicted value of Y.

The intercept b_0 and the coefficients b_1, b_2, b_3, b_4 and b_5 have been estimated by multiple regression analysis by "Data Analysis Tool" of software "Microsoft Excel".

The software gives output on the basis of the following calculation

The Equation A3 can be written as matrix form for n (here n = 474) and k (here k = 5) variables as

$$\begin{bmatrix} Y_1 \\ Y_2 \\ \cdot \\ \cdot \\ Y_n \end{bmatrix} = \begin{bmatrix} 1 & X_{11} & \cdots & X_{1k} \\ 1 & X_{21} & & X_{2k} \\ \cdot & \cdot & \cdots & \cdot \\ \cdot & \cdot & \cdots & \cdot \\ 1 & X_{n1} & \cdots & X_{nk} \end{bmatrix} \times \begin{bmatrix} b_1 \\ b_2 \\ \cdot \\ \cdot \\ b_k \end{bmatrix} + \begin{bmatrix} e_1 \\ e_2 \\ \cdot \\ \cdot \\ e_n \end{bmatrix} \tag{A5}$$

$$\mathbf{Y} = \mathbf{X} \times \mathbf{B} + \mathbf{e}$$

Regression statistics

		Explanation
Multiple R	0.978	R = square root of R^2
R Square	0.957	R^2 = Coefficient of determination
Adjusted R Square	0.957	Adjusted R^2 used if more than one X variable
Standard Error	0.044	This is the estimate of the st. dev. of the error *e*
Observations	474	Number of observations used in the regression (n)

Analysis of variance

	Degrees of freedom	Sum of Square	Mean Sum of Square	F-stat
Regression	5	20.705	4.141	2122.012
Residual	468	0.913	0.002	
Residual	472	21.618		

Regression Sum of Square = $B'X'Y - n\bar{Y}^2$

Total Sum of Square = $Y'Y - n\bar{Y}^2$

Residual Sum of square = Total sum of square – Regression Sum of Square

$$R^2 = \frac{\text{Regression sum of square}}{\text{Residual sum of square}}$$

$$F-stat = \frac{R^2/(k-1)}{(1-R^2)/(n-k)}$$

$$Adjusted\ R^2 = 1 - \left(1 - R^2\right)\left(\frac{n-1}{n-k}\right)$$

$$\text{Standard Error} = \sqrt{\frac{\text{Residual Sum of Square}}{\text{n} - \text{k}}}$$

$$Y' = \begin{bmatrix} Y_1 & \text{Y}_2 & \text{Yn} \end{bmatrix}$$

$$B' = \begin{bmatrix} B_1 & \text{B}_2 & \text{B}_k \end{bmatrix}$$

The F-stat gives the overall F-test of null hypothesis H_0: $b_i = 0$. The F-stat gives the associated Probability value. Since it is greater than 0.05 at 5% significance level we do not reject null hypothesis for the goodness of fit.

Appendix-II

Definition of onset of laminar and turbulent flow conditions based on Reynolds number defined in the present study:

In helical coil, both the intertie and the centrifugal force are acting on the fluid during its flow. The ration of centrifugal force to the inertia fore is less than one if tube diameter is less than 39% of the coil diameter, which can be derived in the following way:

$$\frac{\text{Centrifugal force}}{\text{Inertia force}} = \frac{(2\rho u^2 d_t^3 / D_c)}{(\rho u^2)(\pi d_t^2 / 4)} < 2.55 d_t / D_c < 1; \quad \text{If } d_t / D_c < 0.39 \ (i.e. 1/2.55) \tag{A1}$$

So at this criterion, inertia force (F_i) is greater than centrifugal force (F_c) at a certain operating condition. The effective inertia force is then

$$F_{i,eff} = F_i - F_c = \frac{\pi}{4}\rho u^2 d_t^2 \left(1 - \frac{8d_t}{\pi D_c}\right) \tag{A2}$$

So coil Reynolds number can be defined as ratio of effective inertia force to shear force which can be mathematically represented as

$$\mathrm{Re}_c = \frac{\text{Effective inertia force } (\mathrm{F_{i,eff}})}{\text{Shear force}} = \frac{\frac{\pi}{4}\rho u^2 d_t^2 \left(1 - \frac{8d_t}{\pi D_c}\right)}{\left(\mu \frac{u}{d_t}\right)\left(\frac{\pi}{4} d_t^2\right)} \tag{A3}$$

$$\mathrm{Re}_c = \mathrm{Re}_s \left(1 - \frac{8d_t}{\pi D_C}\right) \tag{A4}$$

So the onset of laminar and turbulent flow conditions in the helical coil tube will be respectfully as $\mathrm{Re}_c = \mathrm{Re}_s \left(1 - \frac{8d_t}{\pi D_c}\right) \le 2100$ and $\mathrm{Re}_c = \mathrm{Re}_s \left(1 - \frac{8d_t}{\pi D_c}\right) \ge 4000$